THESIS ON INFORMATICS AND SYSTEM ENGINEERING C88

Robust Detectors for Cognitive Radio

IVO MÜÜRSEPP

TUT PRESS

TALLINN UNIVERSITY OF TECHNOLOGY
Faculty of Information Technology
Department of Radio and Communication Engineering

Dissertation was accepted for the defense of the degree of Doctor of Philosophy in Telecommunication on June 28, 2013.

Supervisors: Professor Tõnu Trump, Department of Radio and Communication Engineering, Tallinn University of Technology

Professor Andres Taklaja, Department of Radio and Communication Engineering, Tallinn University of Technology

Opponents: PhD Tommy Svensson, Former vice president, LM Ericsson AB, Älta, Sweden

Associate Professor Peep Miidla, Institute of Applied Mathematics, Tartu University, Estonia

Master Researcher Andres Reial, PhD, LM Ericsson AB, Lund, Sweden

Defence of the thesis: October 3, 2013

Declaration:
Hereby I declare that this doctoral thesis, my original investigation and achievement, submitted for the doctoral degree at Tallinn University of Technology has not been submitted for any academic degree.

/Ivo Müürsepp/

ISSN 1406-4731
ISBN 978-9949-23-515-5 (publication)
ISBN 978-9949-23-516-2 (PDF)

INFORMAATIKA JA SÜSTEEMITEHNIKA C88

Robustsed detektorid kognitiivsele raadiole

IVO MÜÜRSEPP

TTÜ
KIRJASTUS

Contents

Introduction

Today our lives are unimaginable without internet access and web based applications. Our everyday work, shopping, banking, social networking and many other daily activities are done online. Due to this the demand for wireless internet connections is growing. Wireless connections are mostly preferred due to comfort or low cost-efficiency. In rural areas wireless connection may be the only option.

Rapid increase in the use of smart phones and personal digital assistants places available wireless networks under increasing load. Relief is hard to find because the electromagnetic spectrum available is strictly licensed. Studies have shown that often those licensed spectrum parts are strongly underutilized. This means that in reality many bandwidths are physically available but legal restrictions make them unavailable. To overcome this restriction, the cognitive radio concept was proposed by Joseph Mitola III in 1998.

The basic idea of cognitive radio states that a licensed but unused spectrum resource should be used opportunistically on a need-to-use basis. When a licensed, or so called primary user, is not using its dedicated spectrum resources, then others may use it. Those others are called secondary users and they are always listening. When they need to transfer data, they find a channel unoccupied by the primary user and take it temporarily into use. When the primary user becomes active during the transfer, then the secondary user finds another unoccupied channel and continues communication over it. In such a manner, the primary user's right to its dedicated resources is not violated while others can still use its resources when they are currently available.

Cognitive radio is a complex device containing many vital sub-circuits necessary for its work. One of them is the detector – a device that can detect presence or absence of the primary user at some part of the frequency spectrum. As secondary users should not disturb the primary one, the correct detection of the primary signal is of high importance. On the other hand, for successful work the secondary user must be able for correct detection of the absence of the primary signal. Both of those decisions must be made correctly even at low signal-to-noise ratio. Thus, the detector is a vital part of a cognitive radio system. There are many known detector types that can be used in cognitive radio applications. Most popular and widely used amongst them are: an energy detector, a cyclostationary feature detector and a matched filter.

All of those detectors are derived on the basis of the assumption of Gaussian background noise. As usually background noise is influenced by numerous factors, due to the law of large numbers, this assumption is usually valid. But in urban areas this Gaussian background assumption is not valid anymore. Manmade

background noise is commonly impulsive in nature. For example, impulsive noise can be produced by electric motors, switches and fluorescent lamps.

An explanation here is that detectors designed for Gaussian background noise will suffer considerably from reduced performance under the influence of impulsive noise. Reduction in performance affects mostly secondary users. Detectors tend to interpret impulsive noise falsely as a signal from the primary user, telling the cognitive radio that the given channel is occupied and cannot be used. Such false alarms are thus reducing the throughput of the secondary system.

The aim of the present work is to deal with the described problem. A new mathematical model of impulsive noise is introduced. Effects of impulsive noise on ordinary detectors are studied, as results, three new detectors, robust to impulsive noise, were worked out.

Use of those new robust detectors allows more effective utilization of radio spectrum in urban areas where new spectrum resources are needed most. When the background noise is Gaussian only, the introduced detectors will work as well as conventional ones. But when the background noise contains also an impulsive component, robust detectors are outperforming others in many orders of magnitude.

On this basis, robustness use of the proposed detectors decreases false alarm rate and thus allows secondary users to utilize the spectrum to the full. Thus, the detector resulting from this thesis research is of high practical value.

Approbation

The results of the thesis have been presented at the following conferences and seminars:

1.) Tõnu Trump and *Ivo Müürsepp*. Robust spectrum sensing for Cognitive Radio. 19th European Signal Processing Conference EUSIPCO2011, Barcelona, Spain, August 29-September 2, 2011 [72].

2.) Tõnu Trump and *Ivo Müürsepp*. An Energy Detector for Spectrum Sensing in Impulsive Noise Environment. 22nd Annual IEEE International Symposium on Personal, Indoor and Mobile Radio Communications. Toronto, Canada, September 11-14, 2011[73].

3.) Julia Berdnikova, Toomas Ruuben, *Ivo Müürsepp*, Erik Lossmann. Resolution and Doppler Tolerance of Cognitive System Waveforms. 14th international conference ELECTRONICS' 2010. Kaunas, Lithuania, May 21.-23, 2010 [74]

4.) Tõnu Trump, *Ivo Müürsepp*. „Detection Speed of Responsive Communication Jamming Detectors.“ Presented at the 2nd International Conference on Circuits, Systems, Communications, Computers and Applications ,Dubrovnik, Croatia June 25-27, 2013

Author’s contribution to the presented articles is as follows:

1.) The author found threshold value and number of samples required for a specific point in the receiver operating characteristic. Also, computer simulations and their presentation were done by the author of the thesis.

2.) The author calculated maximum likelihood estimators for signal variance and impulse probability. Also, computer simulations and their presentation were done by the author of the thesis.

3.) The article is partially based on the author’s master’s thesis. Author’s contribution is linked to probe signals and their ambiguity functions.

4.) Fourth section about detection speed of feature detector is solely author’s contribution. This includes analytical results and computer simulations for the false detection probability, the correct detection probability and ROC curves of the feature detector.

Dedications

I dedicate my thesis to my father Toomas Müürsepp for inspiring me to take interest in science and technology.

Acknowledgements

First and foremost, I would like to thank my supervisor, Professor Tõnu Trump for the valuable guidance and advice and also my co-supervisor, Professor Andres Taklaja for his contribution. I also wish to thank all my colleagues for support and help. I am grateful to Avo Ots for all his help and support. Also, I would like to thank teaching assistant Kairi Kasemets and assistant professor Alar Leibak for consultations on mathematics. Special thanks are due to all my family for enabling me to study and work and for being a good example for me. And last but not least I wish to thank all my friends for being supportive and for listening to my endless moan and groan all over the years.

Abbreviations

ACF	Autocorrelation function
ACS	Almost-cyclostationary
CAF	cyclic autocorrelation function
CFAR	Constant false alarm probability
CDF	Cumulative distribution function
CLT	Central limit theorem
CR	Cognitive radio
ED	Energy detector
FFT	Fast Fourier transform
MC	Multicycle detector
ML	Maximum likelihood
IID	Independent and identically distributed
PDF	Probability density function
QoS	Quality of Service
ROC	Receiver operating curve
SC	Single-cycle detector
SCF	Spectral correlation function
SNR	Signal to noise ratio
SSS	Strict sense stationary
WSCS	Wide-sense cyclostationary
WSS	Weak-sense stationary

Symbols

*	complex conjugate
$\wedge$	logical conjunction
α	cycle frequency
β	Normalization coefficient
$\Gamma(\cdot)$	gamma function
$\gamma(\cdot,\cdot)$	lower incomplete gamma function
Δt	time duration of signal
$\delta(\cdot)$	Dirac delta function
ε	contamination factor
η_p	intersection border between Gaussian and impulsive noise
η_v	noise spectral density
λ	decision threshold
Λ	decision statistic
μ	mean
$\boldsymbol{\mu}$	mean vector

ρ	correlation coefficient
$\rho(\cdot,\cdot)$	distance function
σ	standard deviation
σ_s	rms value of signal
$\theta_{q,l}$	function tail
Θ	decision
$\Phi(\cdot)$	standard Gaussian CDF
ψ	noncentrality parameter
ω	angular frequency
a	lower limit of impulsive noise value
b	upper limit of impulsive noise value
B	bandwidth
c	probability of noise impulse
$\mathbf{C}$	covariance matrix
$\hat{\mathbf{C}}$	estimate of covariance matrix
$d_{i,j}$	element of inverse matrix of covariance matrix
e	error
E_s	energy of signal
$\mathbf{E}(\cdot)$	expected value
f	frequency
$f_v(x)$	probability density function of sum of Gaussian and impulsive noise
$fv_g(x)$	probability density function of Gaussian noise
$fv_i(x)$	probability density function of impulsive noise
$F(x)$	cumulative distribution function
$g(y)$	saturation nonlinearity
$h(t)$	impulse response
H_0	hypothesis corresponding to the absence of primary signal
H_1	hypothesis corresponding to the presence of primary signal
$H(\omega)$	frequency response
$I_0(\cdot)$	modified Bessel function of the first kind with order zero
$i(t)$	interference
$\mathbf{I}_n$	n^{th} order unity matrix
j	imaginary unit
k	sample number (in time)
l	index of hypothesis
$\mathrm{L}(\cdot)$	likelihood function, likelihood ratio
m	sample number (in frequency)
M_1,M_2	signal subsets
n	number of samples
N	length of FFT
O	Computational complexity
p	dimension of covariance matrix
P	probability
P_D	probability of detection

P_F	probability of false detection
P_M	probability of missed detection
q	index
$R_X(\tau)$	autocorrelation function
$R_x^{\alpha}(t,\tau)$	cyclic autocorrelation function
$\mathbf{R}$	correlation matrix
$R_x^{\alpha}(f)$	spectral correlation function
$s(t)$	signal of interest
$S_x(f)$	power spectral density
S_N	Fourier transform of signal
$\mathbf{S}$	scatter matrix
t	time
T	duration
T_0	signal period
$^{\mathrm{T}}$	matrix transpose
$\mathbf{v}$	noise vector
$v(t)$	noise
v_g	Gaussian noise
v_i	impulsive noise
w	parameter of PDF
$x(t)$	received waveform
x_k	discrete time waveform
$\overline{x}$	sample mean
$\overline{\mathbf{x}}$	sample mean vector
$\mathbf{X}$	random vector
y	output signal
$\mathbf{y}$	observation vector
z_q	saturated variable
w	weighted sum of saturated variables
$\mathbf{w}$	projection vector

1 The Problem and Task Statement

1.1 Overview of Cognitive Radio

The rapid growth in wireless communication has led us to problems with spectrum utilization. Usable frequency spectrum is a limited precious natural resource and its demand is increasing. The solution how to deal with this problem is to share available bandwidths between licensed users. But in practice this solution leads to significant underutilization, resulting in spectrum wastage. For example, studies by the Federal Communications Commission (FCC) show that the spectrum utilization in the 0–6 GHz band varies from 15% to 85% [1]. The same report states: "In many bands, spectrum access is a more significant problem than physical scarcity of spectrum, in large part due to legacy command-and-control regulation that limits the ability of potential spectrum users to obtain such access." In other words, there are users who have license for some frequency band but they do not use it. At the same time other users are in need for a bandwidth to use but none are available. Figure 1.1 illustrates density and strictness of modern day spectrum allocation.

75.200-87.500 MHz	Land mobile:
FIXED	75.20-77.70 MHz Du
MOBILE except aeronautical mobile	(+9.8 MHz)
5.175 Alternative allocation in Russia : 68-73 MHz	77.70-77.80 MHz Si
broadcasting on a primary basis. In Latvia: 68-73 broadcasting	77.80-79.00 MHz Du (-9.8 MHz)
and mobile, except aeronautical mobile on a primary basis	81.75-84.60 MHz Du (-9.8 MHz)
	84.60-85.00 MHz Si
5.179 Additional allocation: in Russia 75.2-75.4 MHz	85.00-87.50 MHz Du (-9.8 MHz)
also allocated to the aeronautical radio-navigation service on a	79.00-81.75 MHz
primary basis, for ground-based transmitters only (WRC-07)	Governmental use type 1
87.500-108.000 MHz	87.500-108.000 MHz
BROADCASTING	FM-broadcasting
	Wireless Audio Applications

Fig. 1.1 Example of Estonian radio frequency allocation plan [2]

Cognitive radio was born as the solution for such a contradiction. The concept was first proposed by Joseph Mitola III at a seminar at the Royal Institute of Technology in Stockholm in 1998 and published in an article by Mitola and Gerald Q. Maguire, Jr. in 1999 [3]. Cognitive radio is basically a software defined radio with a cognitive engine brain. Full cognitive radio or so called Mitola radio is observing and adjusting every possible parameter of a transceiver in order to maximize its performance. Those parameters include operating frequency, power, waveform, protocol and networking. Concept of full cognitive radio can be summarized as "reading the radio's meters and tuning the radio's knobs".

The first phone call over a cognitive-radio network was made on Monday, 11 January 2010 in the Centre for Wireless Communications at the University of Oulu using CWC's cognitive-radio network, CRAMNET (Cognitive Radio Assisted Mobile Ad Hoc Network), which was developed by CWC researchers [4].

Most of today's research, including the current thesis, is focused on spectrum-sensing cognitive radio, in which only the radio-frequency spectrum is considered [5]. This type of cognitive radio allows dynamic spectrum management on the following basis. When a licensed (primary) user is not using its allocated resources, then others – so called secondary users are allowed to use it. When a primary user starts to use its frequency band, a secondary user must be able to detect it and release the resource to its dedicated owner. The secondary user then has to find another unused part of the frequency spectrum, so called spectrum hole or white space, and continues the communication process there. In such a way primary user's rights to the licensed spectrum are not violated and also spectrum underutilization is reduced significantly.

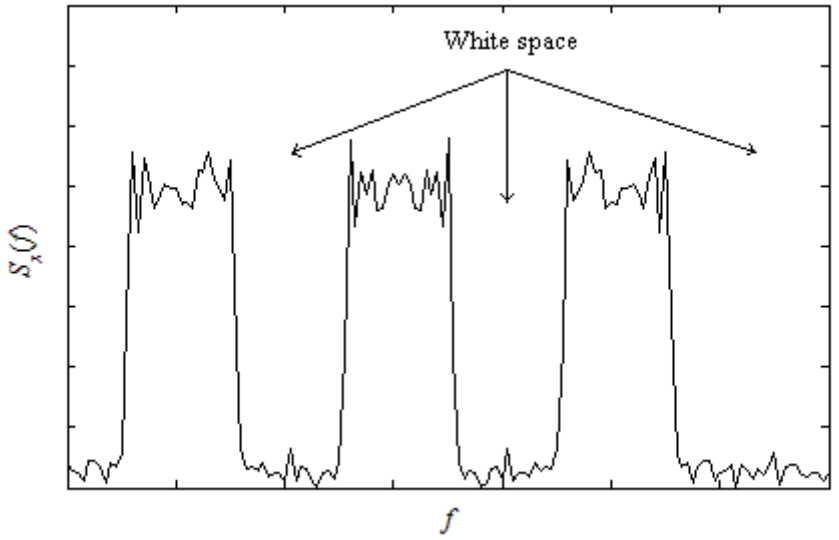

Fig. 1.2 Illustration of white space in spectrum

In the literature, the unused portions of the spectrum are often referred to as spectrum holes or white spaces. Those white spaces contain only white thermal noise and are free to be used for secondary user communication. In a similar fashion gray spaces are also occupied by interference but not by a primary user. They can additionally be used for secondary transmission only by reduced performance caused by interference. Areas that are fully utilized by primary or other secondary users are called black spaces that cannot be used.

White spaces can be divided into three categories. White space in the spectrum (Fig. 1.2) occurs when some parts of the spectrum are permanently unused. Figure 1.2 shows three occupied channels separated from each other by unused parts of the spectrum. Cognitive radio must be able to find those unused spectrum areas and use them for its own purposes. White space in time means that the part of the spectrum that is normally occupied is temporarily available for use (Fig. 1.3). Under such circumstances cognitive radio must be able to detect white space as quickly as possible. Additionally, it must continue spectrum monitoring to detect when the primary user comes back online in order to release an occupied resource and move on to some other currently available frequency band.

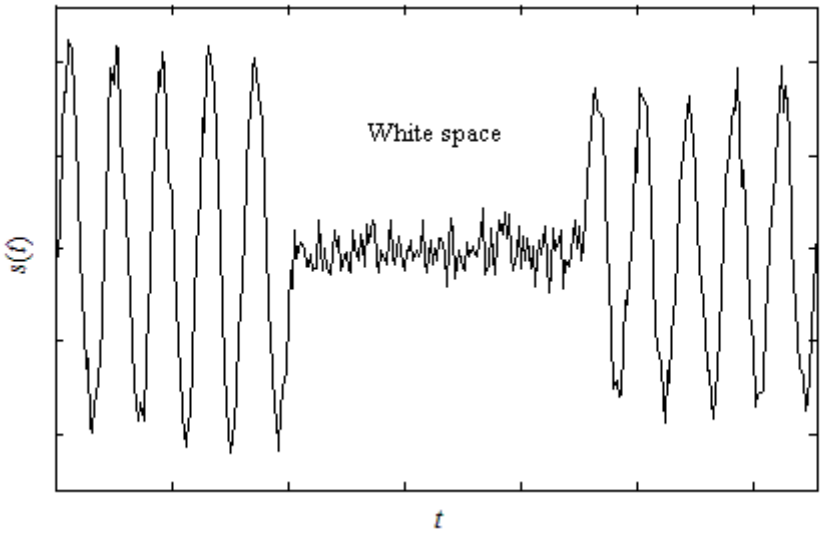

Fig. 1.3 Illustration of white space in time

Spatial white space means that some locations or areas are not reached by the primary signal. Simplified concept of a spatial white hole is demonstrated in Figure 1.4. Outside of the coverage area of primary transmitters is one form of the spatial white hole where other ones can be formed in the shadows of large obstacles. In the latter case a danger exists that the primary transmitter signal is not detected by a cognitive user due to shadowing. In that case the cognitive user may erroneously assume absence of a primary user and start to transmit, which will cause unwanted interference to primary receivers.

The idea of cognitive radio described in this section is simple and straightforward. However, to implement it in practice, many novel signal processing techniques need to be developed. According to [6] any cognitive radio (CR) network that can be deployed in practice must have the following minimal features:

• a unified cross-layer cognitive network architecture equipped to handle diverse QoS requirements;

• efficient spectrum sensing techniques that provide continuous monitoring of the presence of multicarriers in the CR network;

• dynamic spectrum access methods that adapt to the fluctuating nature of the CR network and allocate bandwidth accordingly;

• adaptive spectrum sculpting at the transmitter end that causes minimal or no interference to the primary users occupying adjacent bands.

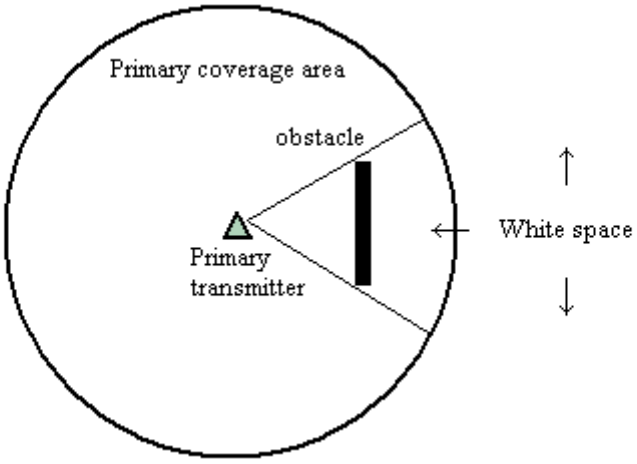

Fig. 1.4 Illustration of spatial white space

In order to work out necessary techniques, the IEEE has formed a working group (IEEE 802.22) to develop an air interface for opportunistic secondary access to the TV spectrum via the cognitive radio technology [6,7]. On July 1st, 2011, a standard for Cognitive Wireless Regional Area Networks (RAN) for Operation in TV Bands was published as an Official IEEE Standard (IEEE 802.22-2011(TM)).

One of those features mentioned above in this section was an efficient spectrum sensing technique. The secondary user of cognitive radio must be able to correctly detect the presence or the absence of a primary user. If the presence of a primary user is left undetected, then the primary user cannot access its own frequency resources and such scenarios have to be avoided at any cost. On the other hand, incorrect detection of the absence of a primary user decreases QoS for secondary users. Because of radio effects like shadowing and fading the signal of the primary user may be rather weak at the position of the secondary user. This leaves the secondary user with the requirement of detecting a potentially weak primary user signal in unknown noise. For instance, the IEEE 802.22 suggests that the cognitive radio needs to detect the primary signals with a probability P_D = 0.9 when the signal-to-noise ratio is -21dB [7].

1.2 Robust Detection

Several detectors have been proposed for this purpose [8, 9], the most popular probably being the energy detector. The reason is partly in the simplicity of the energy detector as well as in no need of any assumptions on the waveforms emitted by the primary users.

The noise is usually assumed to be white and Gaussian but in reality this is often not the case [71]. In particular, one has to consider the presence of impulsive noise, both man-made and natural. Non-Gaussian ambient noise is a major impairment to signal processing techniques that are based on a Gaussian assumption [10, 11]. The examples of the impulsive noise include man–made noise like car ignition, emissions from the microwave ovens or natural impulsive noise due to, e.g. lightning. Measurement results concentrating on impulsive noise are reported in [12, 13]. In brief, detection algorithms designed to work in the environment of Gaussian noise will perform poorly in urban environments where much impulsive noise is present. The main effect of noise impulses will be manifested in the increase of false detections, thus leading into the decrease of QoS for the secondary users.

A common approach to model the impulsive component of noise is to use some probability density functions with heavy "tails". Noise under such distributions has frequently a higher value than that in the Gaussian case. Those high values are taken as impulsive components. The model that is probably used most often is ε-Contaminated Gaussian Noise with PDF [54, 67, 70]

$$f_v(v) = \frac{1-\varepsilon}{\sqrt{2\pi}\sigma} e^{-\frac{v^2}{2\sigma^2}} + \varepsilon f(v), \qquad (1.1)$$

where ε is the contamination factor, σ is the standard deviation of Gaussian noise and $f(v)$ is some other PDF. Often the second PDF is also Gaussian but with higher standard deviation. Such models are known as the Contaminated Gaussian Noise. Other models containing weighted sum of more than two Gaussian distributed noises are known as the Gaussian Mixture Noise and the Generalized Gaussian noise [15]. Sometimes noise is also modeled as some single heavy "tailed" distribution. For example, as double exponential noise with PDF

$$f_v(v) = \frac{1}{2\sigma} e^{-\frac{|v|}{\sigma}}, \qquad (1.2)$$

or Cauchy noise with PDF[70]

$$f_v(v) = \frac{\sigma}{\pi\left(\sigma^2 + v^2\right)}. \tag{1.3}$$

The described impulsive noise has been studied in [10], [14], [15], [54], [67]-[70]. Focus is mainly on the so-called robust M-estimators proposed by J.P Huber in 1964 [11]. An M-estimator or a generalizing maximum likelihood estimator for a parameter **w** is obtained through the minimization

$$\sum_{k=1}^{n} \rho(x_k, \mathbf{w}), \tag{1.4}$$

where x_k are samples of observed waveform with length n and $\rho(\cdot,\cdot)$ is the distance function. Distance function must be a symmetric, positive-definite function with a unique minimum at zero, and it is chosen to be increasing less than square. The solutions

$$\hat{\mathbf{w}} = \arg\min_{\mathbf{w}} \left(\sum_{k=1}^{n} \rho(x_k, \mathbf{w}) \right) \tag{1.5}$$

are called *M* estimators [11]. Robustness of those estimators depends substantially on the chosen cost function. The Huber function is used in [10] to detect asynchronous multi-users in non-Gaussian noise. L_p-norm estimator is used in [15] for spectrum sensing in non-Gaussian noise. Among other methods, [54] proposes use of the M-estimator to estimate cyclic correlation. In [67] – [69] Huber's minimax estimator for the detection of signal in non-Gaussian noise is suggested.

Other approaches are available for robust detection. For example, in [14] the Kolmogorov-Smirnov test for robust spectrum sensing is used. In [54] a trimmed mean is suggested to guarantee robustness of a cyclic correlation estimator. In the final part of this thesis we will compare some of those proposed robust detectors with our obtained results.

As the author found none of the earlier models of impulsive noise intuitively satisfying, in the current thesis we model impulsive noise explicitly by a uniform distribution. We allow impulses to occur only with certain probability and preserve the usual Gaussian noise component for most of the time.

The uniform distribution is selected because of its maximum entropy property, i.e. nothing is assumed to be known about the origin of the impulses. This noise model takes into account that the impulses that disturb the detection based on Gaussian

assumption occur only with certain probability *c*. As such, the noise model is more intuitively satisfying than other popular models for impulsive noise like Laplacian or other ones mentioned above.

1.3 Task statement

The objective of the current thesis is to work out a set of three robust detectors for cognitive radio. This set includes a robust energy detector, a robust cyclostationary detector and a robust matched filter. An additional condition to those robust detectors is that in the case of Gaussian background noise singly, they must work almost as well as regular detectors. However, when impulsive noise is added to the scene, they must perform almost as well as before.

The following three considerations about the objective of the thesis must be taken into account:

1. Cognitive radio has strong potential for future, i.e. research work on the given topic is of high value.

2. In practical applications the impulsive nature of background noise must be considered.

3. As choice of a detector depends on a specific application, it is sensible to work out robust analogues to all three most common detectors. This allows future designers to choose the most suitable robust detector for their design.

In order to fulfill the given task the following work must be conducted.

Three most common detectors suitable for cognitive radio applications will be introduced in Chapter 2. An energy detector, a cyclostationary detector and a matched filter are introduced and their noise performance is analyzed. Theoretical results are confirmed by computer simulations.

Chapter 3 covers the derivation of the noise model under which our robust detectors must work. First, Gaussian noise will be briefly described. Our model of impulsive noise, briefly described before, will be introduced in detail. Focus is on the derivation of the sum of impulsive and Gaussian noise – both for one- and multidimensional cases.

As the robust detectors to be worked out need information about some parameters of background noise, Maximum Likelihood Estimators for those parameters will be derived in Chapter 4.

Chapter 5 will demonstrate clearly that impulsive noise has a strong effect on the performance of the detectors derived under the assumption of Gaussian background noise only.

Center of gravity of the current thesis will lies in Chapter 6 where robust analogues to all three detector types will be derived. For all three, the theoretical noise performance is analyzed and computer simulated. Good compliance between those results will indicate that proposed detectors are working well both under Gaussian only and also in additive impulsive noise conditions.

Chapter 7 analyzes the influence of estimation uncertainty of noise parameters on the performance of the derived robust detectors. The final chapter summarizes the results of the thesis research.

2 Known Detection Algorithms for Cognitive Radio

Spectrum sensing in cognitive radio involves deciding whether the primary signal is present or not from the observed signals. It can be formulated as the following hypotheses testing problem with [6]:

$$\begin{aligned} H_0 &: x(t) = v_g(t) + i(t) \\ H_1 &: x(t) = s(t) + v_g(t) + i(t) \end{aligned}, \tag{2.1}$$

where $x(t)$ is the received waveform, $s(t)$ is the primary signal, $i(t)$ is interference and $v_g(t)$ is additive white Gaussian noise (AWGN). To simplify the analysis, we assume from now on that the interference $i(t)$ is included in the noise as a part of it, if not stated otherwise. H_0 and H_1 denote the hypotheses corresponding to the absence and presence of the primary signal, respectively. Thus from the observation $x(t)$, the cognitive radio user needs to decide between H_0 and H_1[6]. To decide between the two hypothesis, the decision statistic Λ is calculated from the received waveform $x(t)$ and compared against a threshold λ. If the decision statistic Λ is above the threshold λ, we can decide in favor of the hypothesis H_1, the presence of the primary signal, and *vice versa*

$$\begin{aligned} \Lambda \geq \lambda &: H_1 - s(t) \text{ is present} \\ \Lambda < \lambda &: H_0 - s(t) \text{ is absent} \end{aligned}. \tag{2.2}$$

As the received waveform $x(t)$ is a random process, the decision statistic Λ is also a random variable which can be described with its conditional PDFs $f(\Lambda|H_0)$ and $f(\Lambda|H_1)$ (Fig 2.3). When the received waveform contains no primary signal but the decision device makes an incorrect decision in favor of the presence of such signal, then we have a false detection. Probability of false detection P_F is equal to the area of $f(\Lambda|H_0)$ from the decision threshold λ to infinity

$$P_F = \int_{\lambda}^{\infty} f\left(\Lambda \middle| H_0\right) d\Lambda = 1 - F\left(\Lambda \middle| H_0\right), \tag{2.3}$$

where $F(\Lambda|H_0)$ is a conditional cumulative distribution function of the decision statistic. A case where the primary signal is present and correctly detected is called detection. Probability of detection P_D is equal to the area of $f(\Lambda|H_1)$ from the decision threshold λ to infinity

$$P_D = \int_{\lambda}^{\infty} f\left(\Lambda \middle| H_1\right) d\Lambda = 1 - F\left(\Lambda \middle| H_1\right), \tag{2.4}$$

Receiver operating characteristic or ROC curve (Fig 2.1) illustrates the relationship between the probability of detection P_D and the probability of false detection P_F as the function of signal-to-noise ratio SNR.

$$P_D = \mathrm{f}(P_F) \tag{2.5}$$

The larger the area between the line $P_D = P_F$ and ROC, the better is the given decision device.

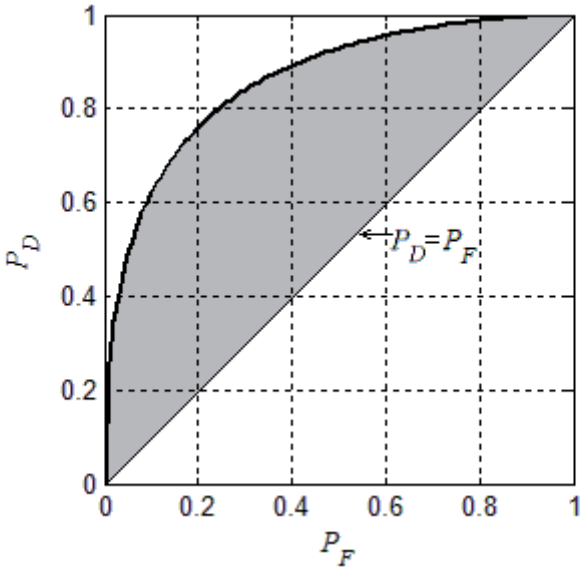

Fig. 2.1 Example of an ROC curve

Three common solutions to detect the presence of the primary signal are: an energy detector, a cyclostationary or feature detector and a matched filter detector. Each of the three will be analyzed briefly in the following chapter. Also, less common detection methods are reviewed at the end of the chapter.

The literature review in Chapter 1 covers the working principles of the mentioned detectors. Author's main contribution here is the derivation of correct detection probability for a specific case of a cyclostationary feature detector. The reason is lack of literature on this topic. The author also performed computer simulation of the performance of all three detector types.

2.1 Energy detector

Energy detection is the simplest spectrum sensing technology. An energy detector treats the primary signal simply as a random process and decides its presence or absence based on the energy of the received waveform. Since an energy detector needs no a *priori* knowledge of the primary signal, it makes energy detection robust to the parameters of the primary signal, which is beneficial for cognitive radio. Another advantage of energy detection is in its low complexity – no complicated signal processing is needed.

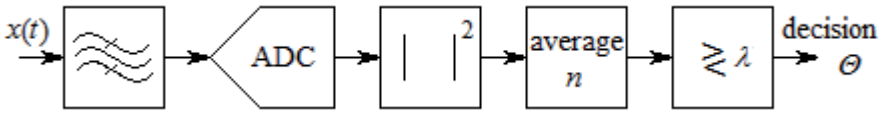

Fig. 2.2 Implementation of an energy detector in time domain

An implementation of an energy detector is depicted in Figure 2.2. The figure shows that for a given signal bandwidth B, a pre-filter matched to the bandwidth of the signal has to be applied. This implementation is quite inflexible, particularly at narrowband signals and sine waves. The decision statistic for an energy detector [16] is

$$\Lambda = \sum_{k=1}^{n} x_k^2 \tag{2.1.1}$$

Received waveform is the AWG noise $X \sim \mathbf{N}(0,\sigma)$ with PDF

$$f_x(x) = \frac{1}{\sqrt{2\pi}\sigma} e^{-\frac{x^2}{2\sigma^2}}, \tag{2.1.2}$$

And the decision statistic Λ has an unscaled central chi-square distribution with n degrees of freedom. The cumulative distribution function of unscaled central chi-square distribution with n degrees of freedom is [17]

$$F(\Lambda|H_0) = \frac{1}{\Gamma\left(\frac{n}{2}\right)} \gamma\left(\frac{n}{2}, \frac{\Lambda}{2\sigma^2}\right), \tag{2.1.3}$$

where $\Gamma(\cdot)$ and $\gamma(\cdot,\cdot)$ denote the gamma function and the lower incomplete gamma function, respectively. Probability of a false alarm P_F (2.3) of the energy detector in [18] is

$$P_F = 1 - \frac{1}{\Gamma\left(\frac{n}{2}\right)} \gamma\left(\frac{n}{2}, \frac{\lambda}{2\sigma^2}\right). \qquad (2.1.4)$$

When the primary signal is present, the probability of detection is

$$P_D = 1 - \frac{1}{\Gamma\left(\frac{n}{2}\right)} \gamma\left(\frac{n}{2}, \frac{\lambda}{2(\sigma^2 + \sigma_s^2)}\right). \qquad (2.1.5)$$

A two hypotheses case for an energy detector (2.1.1) is illustrated in Figure 2.3. Solid line shows the PDF of decision statistic Λ for the hypothesis H_0 where the signal $s(t)$ is absent. Dashed curve in the figure is the PDF of decision statistic Λ for the hypothesis H_1 where the signal $s(t)$ is present.

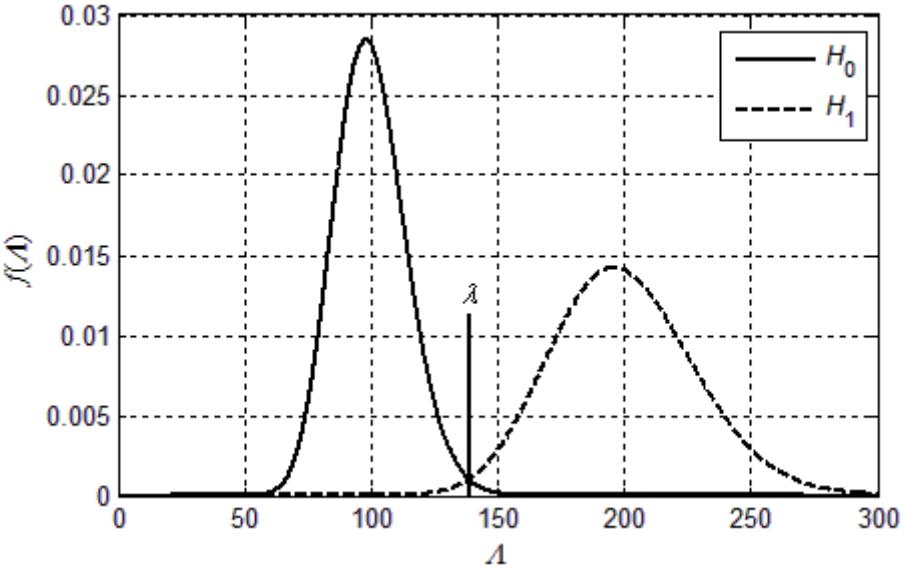

Fig. 2.3 PDFs of an energy detector for both hypotheses (σ_v =1,n=100, SNR = 0dB)

Since the number of required samples n is large, one can use the central limit theorem to approximate the test statistic Λ (2.1.1) as Gaussian [19]. In order to find the mean and the variance of this new Gaussian variable, we need the probability density function of variable $Y = X^2$. When no primary signal is present, $X \sim \mathbf{N}(0,\sigma_v)$, we can state that

$$F_y(y) = P(Y \le y) = P(X^2 \le y) = \\ = P(|X| \le \sqrt{y}) = F_x(\sqrt{y}) - F_x(-\sqrt{y}). \quad (2.1.6)$$

The probability density function is a derivate of the cumulative distribution function

$$f_y(y) = \frac{d}{dy} F_y(y) = \frac{d}{dy}\left[F_x(\sqrt{y}) - F_x(-\sqrt{y})\right] = \\ = \frac{1}{2\sqrt{y}}\left[f_x(\sqrt{y}) - f_x(-\sqrt{y})\right], \quad (2.1.7)$$

because the PDF of a variable X is an even function, we can write

$$f_y(y) = \frac{f_x(\sqrt{y})}{\sqrt{y}} = \frac{1}{\sqrt{2\pi y}\sigma} e^{-\frac{y}{2\sigma^2}}, y \ge 0. \quad (2.1.8)$$

The mean and variance of a variable Y can be calculated as

$$\mu_y = \frac{1}{\sqrt{2\pi}\sigma}\int_0^\infty \sqrt{y} e^{-\frac{y}{2\sigma^2}} dy = \sigma^2 \quad (2.1.9)$$

$$\sigma_y = \sqrt{\frac{1}{\sqrt{2\pi}\sigma^2}\int_0^\infty \frac{(y-\mu_y)^2}{\sqrt{y}} e^{-\frac{y}{2\sigma^2}} dy} = \sqrt{2}\sigma^2. \quad (2.1.10)$$

In a similar fashion, when the primary signal is present, we obtain $\mu_y = \sigma^2 + \sigma_s^2$ and $\sigma_y = \sqrt{2}\,(\sigma^2 + \sigma_s^2)$. Thus, at sufficiently large n, the test statistic Λ can be described as

$$H_0 : \Lambda \sim \mathbf{N}\left(n\sigma^2, \sqrt{2n}\sigma^2\right) \\ H_1 : \Lambda \sim \mathbf{N}\left(n\left(\sigma^2 + \sigma_s^2\right), \sqrt{2n}\left(\sigma^2 + \sigma_s^2\right)\right). \quad (2.1.11)$$

The probability of a false alarm and detection can be expressed through a complementary error function

$$P_F = \frac{1}{2}\mathrm{erfc}\left(\frac{\lambda - n\sigma^2}{2\sqrt{n\sigma^2}}\right); \quad P_D = \frac{1}{2}\mathrm{erfc}\left(\frac{\lambda - n\left(\sigma^2 + \sigma_s^2\right)}{2\sqrt{n\left(\sigma^2 + \sigma_s^2\right)}}\right). \quad (2.1.12)$$

In the low *SNR << 1* regime, the number of samples required for the detection that meets specified P_D and P_F, scales as $O(1/SNR^2)$. This inverse quadratic scaling is significantly inferior to the optimum matched filter detector whose sensing time scales as *O(1/SNR)* [20]. Threshold value can be evaluated as

$$\lambda = \sqrt{n}\sigma^2\left[2\,\mathrm{erfc}^{-1}\left(2P_F\right)+\sqrt{n}\right]. \qquad (2.1.14)$$

Time domain implementation of the energy detector is quite inflexible, particularly at narrowband signals and sine waves. An alternative approach could be devised by using a periodogram to estimate the spectrum via a squared magnitude of the FFT, as depicted in Figure 2.5 [19]. Our interest in the frequency domain energy detector results from the fact that the cyclostationary detector described in the next chapter is also based on FFT.

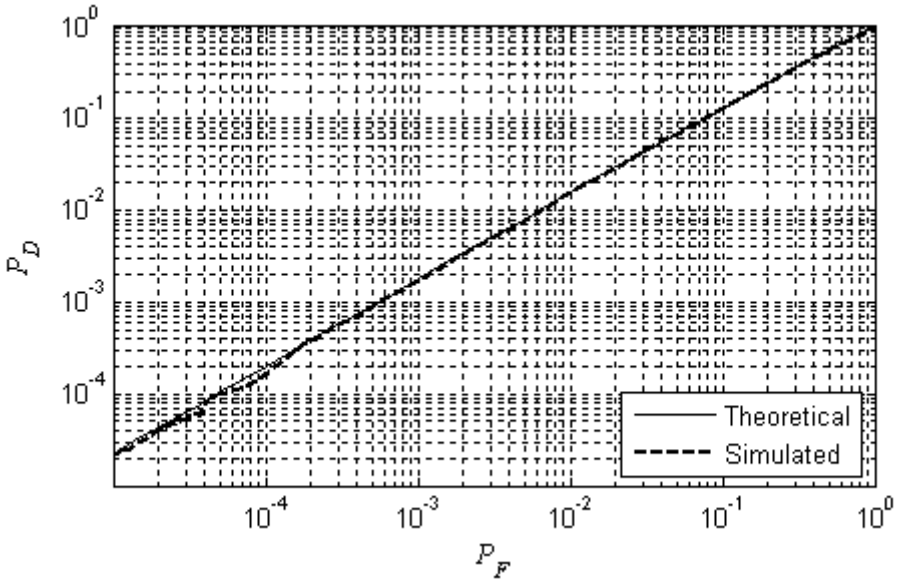

Fig. 2.4 Theoretical and simulated ROC of an energy detector (n=2080, SNR = -23dB)

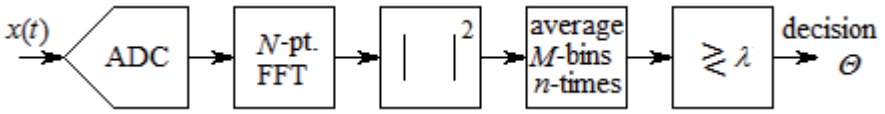

Fig. 2.5 Implementation of an energy detector using a periodogram

The decision statistic for an energy detector in the frequency domain is

$$\Lambda = \frac{1}{M}\sum_{n}\sum_{M}\left|X_m\right|^2, \tag{2.1.15}$$

where $X(m)$ is N-point FFT of x_k defined as

$$X_m = \sum_{k=0}^{N-1} x_k e^{\frac{-j2\pi mnk}{N}}. \tag{2.1.16}$$

If input is white noise with a uniform spectrum, its power will be equally distributed between all frequency bins in (2.1.16). As FFT is a complex transform, both real and imaginary parts of X_m will carry half of the energy of the input realization. Frequency bin with an index m is a weighted sum of N random Gaussian variables x_k. When only zero mean noise is present, all $\mu_k = 0$, thus also mean of frequency bin X_m equals zero. Variance of the m^{th} frequency bin by definition is

$$\begin{aligned}\mathbf{D}X_m &= \mathbf{E}\left[X_m X_m^*\right] = \mathbf{E}\left[\left(\sum_{k=0}^{N-1} x_k e^{\frac{-j2\pi mnk}{N}}\right)\left(\sum_{l=0}^{N-1} x_l e^{\frac{-j2\pi mnl}{N}}\right)^*\right] = \\ &= \mathbf{E}\left[\sum_{k=0}^{N-1}\sum_{l=0}^{N-1} x_k x_l^* e^{\frac{j2\pi m}{N}(k-l)}\right]\end{aligned} \tag{2.1.17}$$

Due to the assumption on uncorrelated white noise (2.1.17) is reduced into

$$\mathbf{D}X_m = \mathbf{E}\left[\sum_{k=0}^{N-1} x_k x_l^* e^{\frac{j2\pi m}{N}0}\right] = N\sigma_v^2. \tag{2.1.18}$$

Because the phase of noise $v(t)$ has uniform distribution, both the real and the imaginary parts of X_m have equal variance

$$\mathbf{D}\left(\operatorname{Re} X_m\right) = \mathbf{D}\left(\operatorname{Im} X_m\right) = \frac{N\sigma^2}{2}. \tag{2.1.19}$$

As both components have equal variances and zero mean, the square of the module X_m follows unscaled chi-squared distribution with two degrees of freedom. As we average n-times over M frequency bins, the decision statistic follows unscaled chi-

squared distribution with $2nM$ degrees of freedom. If nM is sufficiently large, we can approximate the PDF of the decision statistic Λ as normal

$$H_0 : \Lambda \sim \mathbf{N}\left(nN\sigma^2, \sqrt{\frac{2n}{M}} N\sigma^2 \right). \tag{2.1.20}$$

From here we obtain a probability of false detection as

$$P_F = \frac{1}{2} \operatorname{erfc}\left[\frac{\sqrt{M}\left(\lambda - nN\sigma^2\right)}{2\sqrt{n} N\sigma^2} \right]. \tag{2.1.21}$$

If the input of a FFT energy detector consists signal $s(t)$ too, the decision statistic Λ follows unscaled noncentral chi-squared distribution with $2nM$ degrees of freedom [6,21]

$$\Lambda \sim \frac{2M}{N\sigma^2} \chi^2_{2Mn}\left(\frac{2n\psi}{N\sigma^2}, \frac{2M\Lambda}{N\sigma^2} \right). \tag{2.1.22}$$

Noncentrality parameter ψ is defined as

$$\psi = \sum_{m=1}^{M} \left| S_m \right|^2 , \tag{2.1.23}$$

where $|S_m|^2$ is the power of the m^{th} spectral line of the primary signal. One can see that the noncentrality parameter is actually the signal power σ_s^2 within the given bandwidth M. Probability of correct detection can be found by the Marcum Q function $Q_M(\cdot,\cdot)$

$$P_D = Q_{nM}\left(\sqrt{\frac{2n\psi}{N\sigma^2}}, \sqrt{\frac{2M\lambda}{N\sigma^2}} \right). \tag{2.1.24}$$

When nM is large enough, we can also here approximate the PDF of the decision statistic as Gaussian. However, it is worth mentioning that noncentral chi-square distribution converges into Gaussian distribution much slower than central chi-square distribution. Thus, at large nM, the test statistic Λ can be described as

$$H_0 : \Lambda \sim \mathbf{N}\left(nN\sigma^2, \sqrt{\frac{2n}{M}} N\sigma^2 \right)$$
$$H_1 : \Lambda \sim \mathbf{N}\left[n\left(N\sigma^2 + \frac{\psi}{M} \right), \frac{N\sigma^2}{M} \sqrt{nM + \frac{2\psi}{N\sigma^2}} \right]. \qquad (2.1.25)$$

Threshold value can be evaluated as

$$\lambda = 2\sqrt{\frac{n}{M}} N\sigma^2 \operatorname{erfc}^{-1}(2P_F) + nN\sigma^2 . \qquad (2.1.26)$$

Figure 2.6 compares time and frequency domain energy detectors having the same parameters. At first glimpse it seems that a time-domain detector has slightly better performance than a frequency domain detector. Comparison of the theoretical and experimental performance of a frequency domain energy detector in Figure 2.7 shows that experimental results indicate a better performance than expected by theoretical approximation (2.1.25). Thus, the performance of both detectors is practically equal and differences witnessed here are caused by slow convergence of noncentral chi-square distribution into Gaussian.

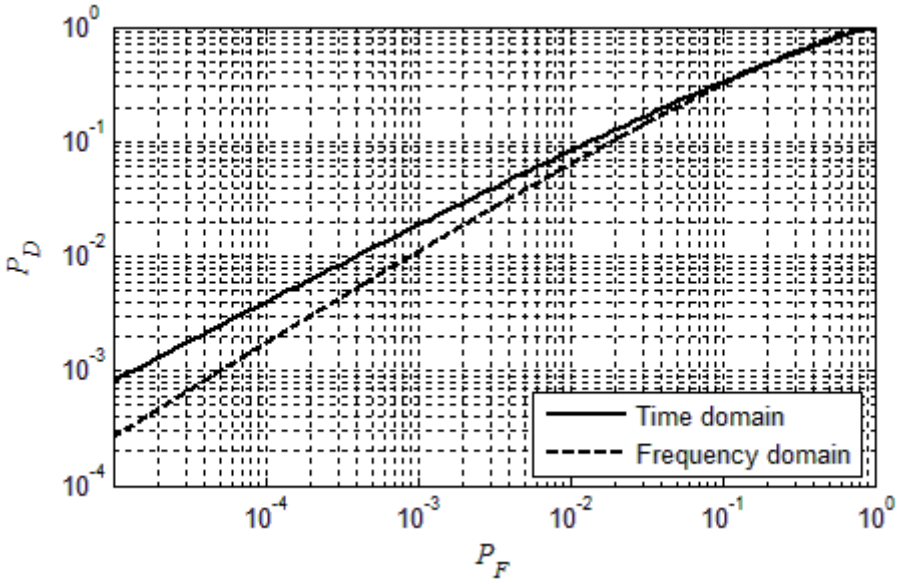

Fig. 2.6 Comparison of time and frequency domain energy detectors

Increased sensing time mentioned above is not the only disadvantage of an energy detector. Previous derivations are based on two assumptions. Firstly, we assume that additive noise is white and Gaussian and secondly, we assumed that

the exact value of noise variance σ^2 is known. Neither of those assumptions is true in real life situations – noise variance is not constant in time and its value is not known exactly but only with some uncertainty x. Thus, the real value of noise variance σ^2 lies inside the interval $[\sigma_L^2, \sigma_H^2]$ where

$$\sigma_H^2 = \sigma_L^2 10^{\frac{x}{10}}. \tag{2.1.27}$$

If now the power of our primary signal σ_s^2 is smaller than noise uncertainty

$$\sigma_H^2 \geq \sigma_L^2 + \sigma_s^2, \tag{2.1.28}$$

then the primary signal remains undetected. If there is noise uncertainty x dB, the detection is impossible below [6, 12]

$$SNR_{wall} = 10\log\left(10^{\frac{x}{10}} - 1\right). \tag{2.1.29}$$

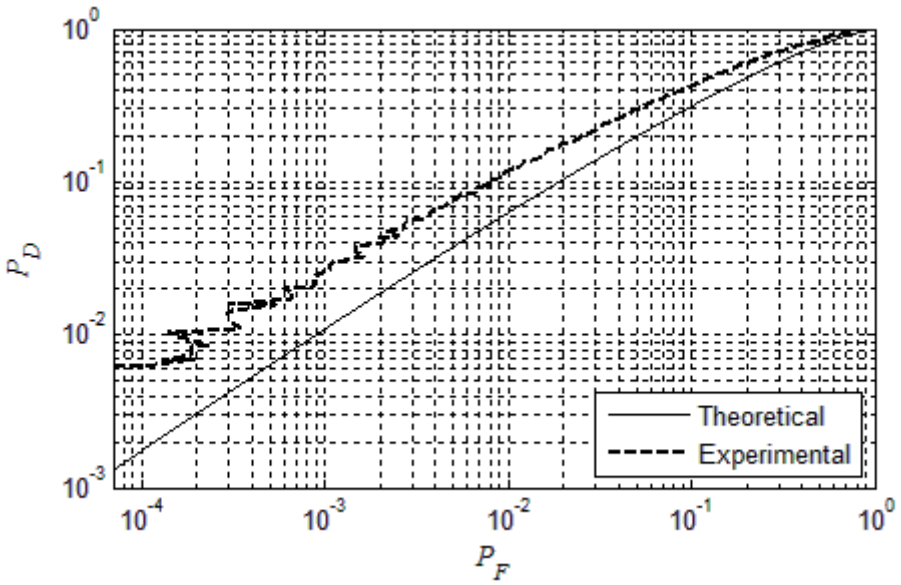

Fig. 2.7 ROC of the FFT energy detector (N = 128, M = 2, n=128, SNR = -10dB)

2.2 Cyclostationary feature detector

A random process $\{X_t\}$ is stationary in strict sense (SSS) if its cumulative distribution function of joint distribution of $\{X_t\}$ at time instances $t_1+\tau,\ldots, t_k+\tau$ satisfies

$$F_X\left(x_{t_1+\tau}, x_{t_2+\tau}, \ldots, x_{t_k+\tau}\right) = F_X\left(x_{t_1}, x_{t_2}, \ldots, x_{t_k}\right), \tag{2.2.1}$$

for all t_1, t_2, ...t_k, k and τ. Since τ does not affect $F_X(\cdot)$, it is not a function of time. In signal processing it is often satisfactory if only 1st and 2nd moments of random process do not vary in time. Such processes are called weak-sense stationary (WSS). A WSS continuous-time random process has time invariant mean

$$\mathbf{E}\{x(t)\} = \mu_X(t) = \mu_X(t+\tau), \quad \tau \in R \tag{2.2.2}$$

and autocorrelation function

$$\begin{aligned} &E\{x(t_1)x(t_2)\} = R_x(t_1,t_2) = \\ &= R_x(t_1 - t_2) = R_x(\tau) \quad \tau \in R \end{aligned}. \tag{2.2.3}$$

Common analyses of a WSS random signal are based on the autocorrelation function and power spectral density [22]. Two of them are related through Wiener-Khinchin theorem which states that the power spectral density of the WSS random process is the Fourier transform of the corresponding autocorrelation function

$$S_x(f) = \int_{-\infty}^{\infty} R_x(\tau) e^{-j2\pi f\tau} d\tau\,. \tag{2.2.4}$$

Function $x(t)$ is periodic with period T_0 if

$$x(t) = x(t+T_0), \quad \forall t\,. \tag{2.2.5}$$

Periodic functions can be represented as Fourier series

$$x(t) = \sum_{k=-\infty}^{\infty} a_k e^{jk\omega_0 t}\,, \tag{2.2.6}$$

where ω_0 is angular frequency of a periodic signal $x(t)$

$$\omega_0 = \frac{2\pi}{T_0} \tag{2.2.7}$$

and a_k are Fourier coefficients

$$a_k = \frac{1}{T_0}\int_{T_0} x(t)e^{-jk\omega_0 t}dt\,. \tag{2.2.8}$$

Many processes encountered in nature arise from periodic phenomena. These processes, although not periodic functions in time, give rise to random data whose statistical characteristics vary periodically with time and are called a cyclostationary process [23]. Causes of periodicity in telecommunications are sampling, coding, modulation and multiplexing operations. Random process is wide-sense cyclostationary (WSCS) if there is a period T_0 that satisfies both

$$\mu_X(t) = \mu_X(t+T_0) \tag{2.2.9}$$

$$R_x(t,\tau) = R_x(t+T_0,\tau)\,. \tag{2.2.10}$$

Thus, the autocorrelation function of a cyclostationary process is periodic in nature. It is important to notice that the autocorrelation function is periodic in time t not in lag τ. As mentioned above (2.2.5), any periodic function can be represented as a Fourier series. Thus, also our periodic autocorrelation function (2.2.10) can be represented as

$$R_x(t,\tau) = \sum_{k=-\infty}^{\infty} R_x^{\frac{k}{T_0}}(\tau)e^{\frac{j2\pi kt}{T_0}}\,, \tag{2.2.11}$$

where the Fourier coefficients

$$R_x^{\alpha}(\tau) \equiv \frac{1}{T_0}\int_{-\frac{T_0}{2}}^{\frac{T_0}{2}} R_x(t,\tau)e^{-j2\pi\alpha t}dt \tag{2.2.12}$$

are referred to as cyclic autocorrelation functions and the frequencies $\alpha = k/T_0$ are called cycle frequencies. A more general class of stochastic processes is obtained if the autocorrelation function $R_x(t,\tau)$ is almost periodic in t for each τ. A continuous-time real-valued stochastic process $x(t)$ is said to be almost-cyclostationary (ACS) in the wide sense if its autocorrelation function $R_x(t,\tau)$ is almost periodic function of t [24]. Autocorrelation function $R_x(t,\tau)$ is almost periodic if it is the limit of a uniformly convergent sequence of trigonometric polynomials in t [25]:

$$R_x(t,\tau) = \sum_{\alpha \in A} R_x^{\alpha}(\tau) e^{j2\pi\alpha t} \,, \tag{2.2.13}$$

where A is a countable set, the frequencies α are possibly incommensurate, and the coefficients are given by

$$R_x^{\alpha}(\tau) \equiv \lim_{T\to\infty} \frac{1}{T} \int_{-\frac{T}{2}}^{\frac{T}{2}} R_x(t,\tau) e^{-j2\pi\alpha t} dt \,. \tag{2.2.14}$$

The last equation is usually a basis for practical implementations of a cyclostationary detector and for practical use it can be written as

$$R_x^{\alpha}(\tau) = \lim_{T\to\infty} \frac{1}{T} \int_{-\frac{T}{2}}^{\frac{T}{2}} x\left(t+\frac{\tau}{2}\right) x^*\left(t-\frac{\tau}{2}\right) e^{-j2\pi\alpha t} dt \,. \tag{2.2.15}$$

If $x(t)$ is cyclostationary with period T_0, then the cycle autocorrelation has a component at $\alpha = 1/T_0$. Wiener-Khinchin theorem can be applied also for cyclostationary processes resulting in a spectral correlation function (SCF) or simply a cyclic spectrum

$$S_x^{\alpha}(f) = \int_{-\infty}^{\infty} R_x^{\alpha}(\tau) e^{-j2\pi f\tau} d\tau \,. \tag{2.2.16}$$

Substituting (2.2.15) into (2.2.16) will result in

$$S_x^{\alpha}(f) = \lim_{\Delta t\to\infty} \lim_{T\to\infty} \frac{1}{\Delta t} \frac{1}{T} \int_{-\frac{\Delta t}{2}}^{\frac{\Delta t}{2}} X_T(t, f+\frac{\alpha}{2}) X_T^*(t, f-\frac{\alpha}{2}) dt \,, \tag{2.2.17}$$

where Δt is the duration of the whole analyzed waveform and

$$X_T(t,f) = \int_{t-\frac{T}{2}}^{t+\frac{T}{2}} x(u) e^{-j2\pi f u} du \tag{2.2.18}$$

is the spectral component of $x(t)$ at frequency f with the bandwidth $B = 1/T$. The spectral correlation function is a two dimensional complex transform on a support set (f,α). SCF can be used for feature detection. Power spectral density (2.2.4) is a

special case of a SCF for $\alpha = 0$. To illustrate the concept we have plotted the cyclic spectrum of the 4-FSK modulated signal in Figure 2.8.

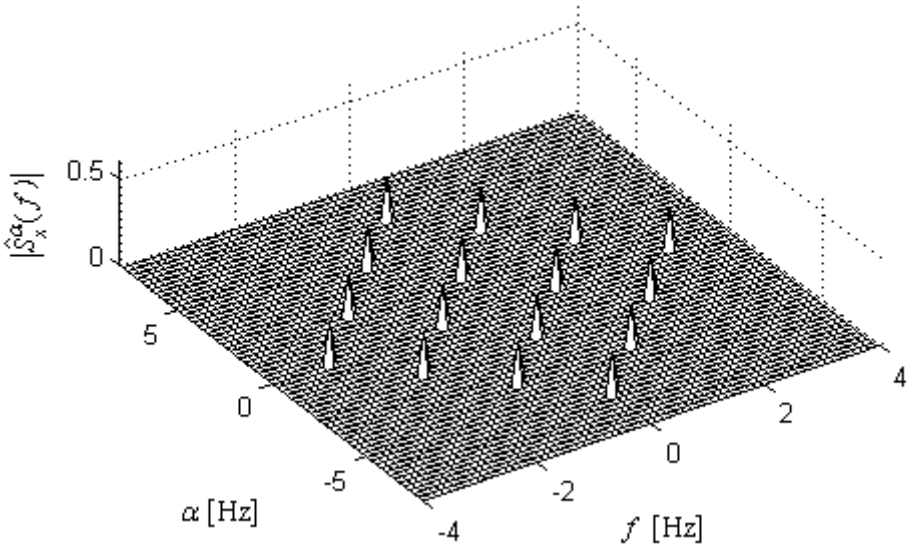

Fig. 2.8 Cyclic spectrum of the 4-FSK modulated signal

Signal analysis in the cyclic spectrum domain preserves phase and frequency information related to timing parameters in modulated signals. As a result, overlapping features in the power spectrum density are non-overlapping features in the cyclic spectrum. Different types of modulated signals that have identical power spectral density functions can have highly distinct SCFs. Furthermore, a stationary white noise exhibits no spectral correlation [26].This statement is well illustrated by comparing Figures 2.8 and 2.9. AWG has influence only where $\alpha = 0$, anywhere else features of the 4-FSK signal are still easily distinguishable. Due to its noise rejection property, cyclostationary detection works even in very low SNR region where the traditional signal detection method such as the energy detector fails [6].

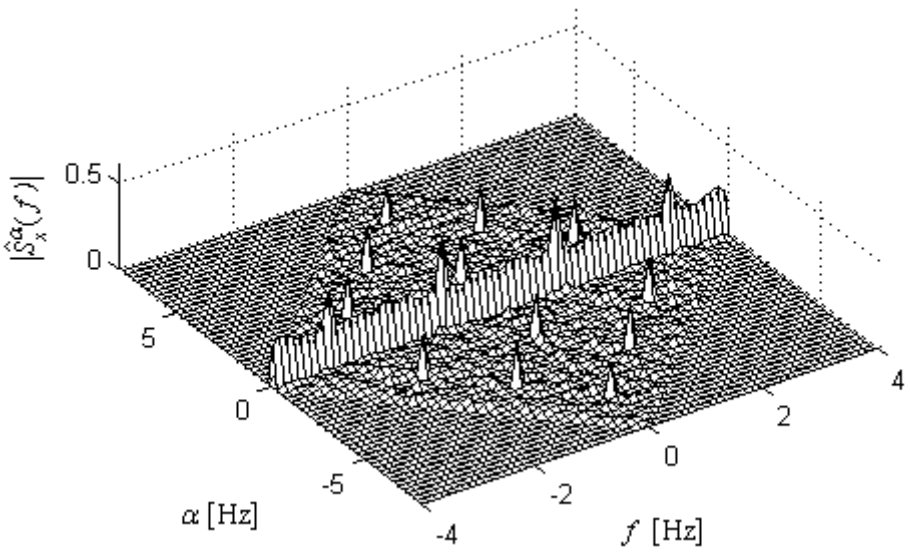

Fig. 2.9 Cyclic spectrum of the 4-FSK modulated signal in AWG noise

A spectral correlation receiver can be realized (Fig. 2.10) by correlating two frequency components of signal $x(t)$ separated in frequency by α. The final result is obtained by averaging correlation over time. When the correlation time T approaches to infinity and the bandwidth B to zero, we obtain SCF (2.2.17) [24].

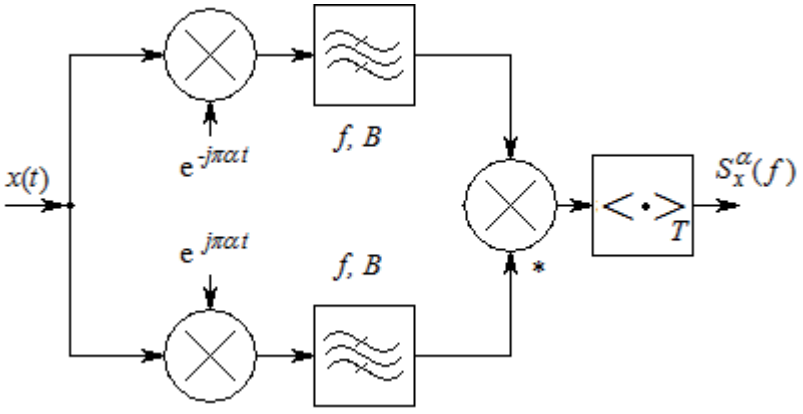

Fig. 2.10 Spectral correlation analyzer

Most attractive implementation solutions for a spectral correlation analyzer are digital frequency smoothing algorithms. Given n samples divided in blocks of N samples, SCF is estimated as

$$\hat{S}_x^{\alpha}(f) = \frac{1}{n}\frac{1}{N}\sum_{k=1}^{n} X_N(k, f + \frac{\alpha}{2}) X_N^*(k, f - \frac{\alpha}{2}), \qquad (2.2.19)$$

where $X_N(k,f)$ is (2.1.16) the N point FFT around sample k [22]. Direct algorithms first compute the spectral components of the data through FFT and then perform the spectral correlation directly on the spectral components (Fig. 2.9).

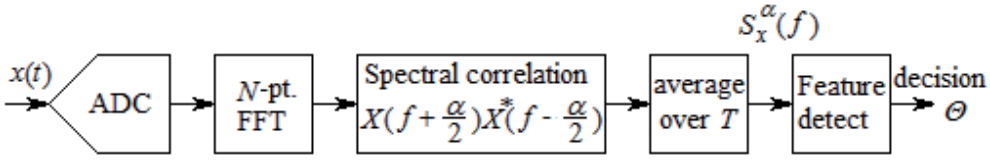

Fig. 2.11 Implementation of a cyclostationary feature detector [22]

Estimates can be improved by applying windows for smoothing at the cost of additional processing. The computational complexity of a SCF estimator is easily estimated. For a stream of N samples, it requires a computation of N point FFT, which requires O(Nlog$N$) multiplications, and O(N^2) multiplications for cross multiplications. This algorithm is extremely parallel so that the computation of the SCF can be organized across the frequency or across the cycle plane independently. Also, this method could be employed to compute SCF for smaller parts of bi-frequency plane and save the area and power [22].

When the spectral correlation function has been obtained, the last step towards a cyclostationary detector is detection of features. Features at zero cycle frequency are corrupted by noncyclical noise and interference making feature detection hard especially at low SNR regime. To detect a feature at (nonzero) cycle frequency α, the optimal processing is the projection of the estimated SCF onto the ideal SCF of a known primary user signal [22, 26]

$$y_{SC}(t) = \frac{1}{T}\int_{-\infty}^{\infty} S_x^{\alpha}(f)^* \hat{S}_x^{\alpha}(t, f) df \, . \qquad (2.2.20)$$

The detector (2.2.20) is referred to as a single-cycle detector (SC) or just a cycle detector [26, 27]. Single-cycle detectors are able to detect the presence of cyclostationarity at only one cyclic frequency at a time. They partly ignore the rich information present in the signals [27]. The device that takes into account all available information at different cyclic frequencies is known as a multicycle detector (MC) [26]

$$y_{MC}(t) = \frac{1}{TN_{\alpha}^2}\sum_{\alpha}\int_{-\infty}^{\infty} S_x^{\alpha}(f)^* \hat{S}_x^{\alpha}(t, f) df \, . \qquad (2.2.21)$$

The two detectors above are in the frequency domain, i.e. based on the cyclic spectrum. It is also possible to realize single- or multicycle detectors in the time domain, based on the cyclic autocorrelation function.

Comparison of the energy detector in Figure 2.2 to the cyclostationary feature detector in Figure 2.6 shows clearly that both of them start processing by finding an N point FFT of the input waveform $x(t)$. While the energy detector finds only the estimate of power spectral density, the cyclostationary feature detector finds correlation between separated frequencies. While calculating probabilities of false detection and detection in the case of the energy detector, we are dealing with a square of normally distributed random variables. In the case of the cyclostationary feature detector we are dealing with the product of two normally distributed random variables.

Next, we derive the probability of false detection for a single cycle detector for fixed α and f. Our decision statistic will be

$$\Lambda = \left| \hat{S}_x^{\alpha}(f) \right| \tag{2.2.22}$$

Our derivation is based on the FFT implementation depicted in Figure 2.11. When the input waveform $x(t)$ is AWGN noise only, each frequency bin $X_N(k,f)$ contains zero mean Gaussian noise with variances (2.1.19), as demonstrated in the previous section. The next step in the calculation of SCF is the multiplication of two frequency bins separated in frequency by α

$$X_N(k, f + \frac{\alpha}{2}) X_N^*(k, f - \frac{\alpha}{2}). \tag{2.2.23}$$

As both multiplicands are complex, the result of (2.2.23) is

$$\begin{aligned} &\left\{ \mathrm{Re}\left[X_N\left(k, f + \frac{\alpha}{2} \right) \right] \mathrm{Re}\left[X_N\left(k, f - \frac{\alpha}{2} \right) \right] + \right. \\ &\left. + \mathrm{Im}\left[X_N\left(k, f + \frac{\alpha}{2} \right) \right] \mathrm{Im}\left[X_N\left(k, f - \frac{\alpha}{2} \right) \right] \right\} + \\ &+ j \left\{ \mathrm{Im}\left[X_N\left(k, f + \frac{\alpha}{2} \right) \right] \mathrm{Re}\left[X_N\left(k, f - \frac{\alpha}{2} \right) \right] - \right. \\ &\left. - \mathrm{Re}\left[X_N\left(k, f + \frac{\alpha}{2} \right) \right] \mathrm{Im}\left[X_N\left(k, f - \frac{\alpha}{2} \right) \right] \right\} \end{aligned} . \tag{2.2.24}$$

Thus, both real and imaginary parts of (2.2.23) contain the products of two zero mean Gaussian variables. From [28] it is known that the PDF of the product of two Gaussian variables can be described by the second kind zero-order Bessel function. As the multiplication (2.2.24) is followed by averaging over n sample, the exact shape of the resulting PDF is actually unimportant because the PDF of the averaging filter output is Gaussian anyway. We only need to know the mean and standard deviation of the product of two random variables with zero mean Gaussian PDF. If two variables X and Y are independent, the variance of their product is given by [29]

$$\mathbf{D}(XY) = (\mathbf{E}X)^2 \mathbf{D}(Y) + (\mathbf{E}Y)^2 \mathbf{D}(X) + \mathbf{D}(X)\mathbf{D}(Y). \quad (2.2.25)$$

As the mean of both multiplicands is zero, $\mathbf{D}(XY) = \mathbf{D}(X)\mathbf{D}(Y)$. From (2.1.20) we obtain that a standard deviation of every single product in (2.2.24) is

$$\sigma_1 = \frac{N\sigma^2}{2}. \quad (2.2.26)$$

As we are averaging (2.2.23) $2n$ times according to (2.2.19), the resulting PDF of both imaginary and real parts at the output is Gaussian when n is sufficiently large. Standard deviation of both real and imaginary parts of the output PDF is

$$\sigma_0 = \frac{\sigma^2}{\sqrt{n}}. \quad (2.2.27)$$

Non-multiplicativity property of the expected value states that the mean of the product of two random variables is

$$\mathbf{E}(XY) = \mathbf{E}X\mathbf{E}Y + \mathrm{cov}(X,Y). \quad (2.2.28)$$

As we assume our random variables to be independent and with zero mean, then according to the last equation the mean of the product is zero.

To decide if the primary signal is present or absent, the detector compares the module of the SCF estimate (2.2.19) against the decision threshold λ. It is well known that with random complex numbers whose real and imaginary components are Gaussian, the module of the complex number is Rayleigh-distributed. Thus, in the case of noise only, the decision statistic Λ (2.2.22) follows the Rayleigh distribution

$$f_\Lambda(\Lambda|H_0) = \frac{n\Lambda}{\sigma^4} e^{-\frac{n\Lambda^2}{2\sigma^4}}, \quad \Lambda \geq 0. \quad (2.2.29)$$

From the CDF of the Rayleigh distribution it is easy to derive that the probability of false detection equals the probability of Λ being larger than λ

$$P_F = \int_{\lambda}^{\infty} f_{\Lambda}(\Lambda|H_0)d\Lambda = e^{-\frac{n\lambda^2}{2\sigma^4}} \tag{2.2.30}$$

and from it a threshold value for desired P_F must be

$$\lambda = \sigma^2 \sqrt{\frac{-2\ln P_F}{n}}\,. \tag{2.2.31}$$

When the primary user signal is present, the means of multiplicities (2.2.23) are not zero anymore. They depend on the amplitude and the initial phase of signal and noise. When we square such a signal, there is an analytical solution for the PDF of the result (2.1.23). But there is no known analytical solution for the PDF of the product of two Gaussian variables if one or both of them have nonzero mean. In literature [30] a moment generating function for such a product is given. Thus known expressions for the mean and variance of such a product exist. But a problem arises when a signal is also present, and then the distribution of the frequency bin corresponding to the signal frequency is usually not Gaussian. In such cases no known analytical solutions either for the PDF or values of parameters are available. Thus, no closed-form expressions of correct detection P_D for a cyclostationary detector exist [30, 31]. Therefore, an approach should be used where the threshold value (2.2.31) for a given false alarm probability is calculated and ROC curves are found experimentally.

However, in some specific cases it is possible to find an analytical expression for the probability of detection P_D. For example, when a pair $(\alpha, f) = (2f_s,0)$, where f_s is the signal frequency and if FFT is done coherently - with constant initial phase φ of signal $s(t)$. The mean value of $X_N(k,f \pm \alpha/2)$ in the given case is determined by the Fourier transform S_N of signal $s(t)$ and it can be expressed as

$$\begin{aligned}
\mathbf{E}\left[X_N\left(k, f+\frac{\alpha}{2}\right)\right] &= S_N\left(k, f+\frac{\alpha}{2}\right) = \frac{AN}{2}\left(\cos\varphi + j\sin\varphi\right) \\
\mathbf{E}\left[X_N\left(k, f-\frac{\alpha}{2}\right)\right] &= S_N\left(k, f-\frac{\alpha}{2}\right) = \frac{AN}{2}\left(\cos\varphi - j\sin\varphi\right)
\end{aligned} \tag{2.2.32}$$

If no spectral leak occurs, the means of all other spectrum bins are zero. Variances of all spectrum bins are still determined by Gaussian noise at the input and they are equal to (2.1.19)

$$\mathbf{D}\left\{\mathrm{Re}\left[X_N\left(k, f \pm \frac{\alpha}{2}\right)\right]\right\} = \mathbf{D}\left\{\mathrm{Im}\left[X_N\left(k, f \pm \frac{\alpha}{2}\right)\right]\right\} = \frac{N\sigma^2}{2}$$

Thus, in our case output signals at the spectrum bins under interest are Gaussian random processes with the mean determined by the signal $s(t)$ (2.2.32) and variance determined by the noise $v(t)$ (2.1.19). In our case, the multiplication of two frequency bins separated in frequency by α is equal to the square of one multiplicand. This results from the fact that bins at frequencies f_s and $-f_s$ are complex conjugates of each other, thus (2.2.23) becomes

$$Y_N = X_N(k, f_s)X_N^*(k, -f_s) = \left[X_N(k, f_s)\right]^2. \qquad (2.2.33)$$

As both multiplicands are complex, expanding the square in (2.2.33) results in

$$\begin{aligned} Y_N = &\left\{\mathrm{Re}\left[X_N(k, f_s)\right]\right\}^2 - \left\{\mathrm{Im}\left[X_N(k, f_s)\right]\right\}^2 + \\ &+ 2j\,\mathrm{Re}\left[X_N(k, f_s)\right]\mathrm{Im}\left[X_N(k, f_s)\right] \end{aligned}. \qquad (2.2.34)$$

Both summands in the real part of the product are following noncentral chi square distribution with one degree of freedom. PDF of the imaginary part has no analytical form, as mentioned above. But the moment-generating function of the two correlated normally distributed variables is known [30] and it can be used to calculate the mean and variance of products. If we have two correlated Gaussian variables with means μ_1, μ_2 standard deviations σ_1, σ_2 and with correlation ρ, then the mean and variance of their product are accordingly [30]

$$\begin{aligned} &\mathbf{E}(X_1X_2) = \mu_1\mu_2 + \rho\sigma_1\sigma_2 \\ &\mathbf{D}(X_1X_2) = \mu_1^2\sigma_2^2 + \mu_2^2\sigma_1^2 + (1+\rho^2)\sigma_1^2\sigma_2^2 + 2\mu_1\mu_2\sigma_1\sigma_2 \end{aligned}. \qquad (2.2.35)$$

As imaginary and real parts are by definition orthogonal, correlation between them is zero. Thus, the imaginary part of our product Y_N has the mean

$$\mathbf{E}(\mathrm{Im}\,Y_N) = \left(\frac{AN}{2}\right)^2 \sin(2\varphi) \qquad (2.2.36)$$

and the variance

$$\mathbf{D}(\mathrm{Im}\,Y_N) = \frac{A^2N^3\sigma^2}{2} + N^2\sigma^4. \qquad (2.2.37)$$

The square of a random Gaussian variable can be viewed as the product of this variable with itself. Correlation between the multiplicands in this case is 1. The means of squares of the real and the imaginary part of X_N are accordingly

$$\begin{aligned}\mathbf{E}\left[\left(\mathrm{Re}\,X_N\right)^2\right] &= \left(\frac{AN}{2}\right)^2\cos^2\varphi + \frac{N}{2}\sigma^2 \\ \mathbf{E}\left[\left(\mathrm{Im}\,X_N\right)^2\right] &= \left(\frac{AN}{2}\right)^2\sin^2\varphi + \frac{N}{2}\sigma^2\end{aligned}. \qquad (2.2.38)$$

As the real part of product Y_N is equal to the difference between the square of real and imaginary parts of X_N (2.2.34), due to the linearity of an expectation operator, the mean of the real part of Y_N is equal to the difference between the means of squares (2.2.38)

$$\mathbf{E}\left(\mathrm{Re}\,Y_N\right) = \left(\frac{AN}{2}\right)^2\left(\cos^2\varphi - \sin^2\varphi\right) = \left(\frac{AN}{2}\right)^2\cos 2\varphi\,. \qquad (2.2.39)$$

Variances of squares of the real and the imaginary part of X_N according to (2.2.35) are

$$\begin{aligned}\mathbf{D}\left[\left(\mathrm{Re}\,X_N\right)^2\right] &= \frac{A^2N^3\sigma^2}{2}\cos^2\varphi + \frac{N^2\sigma 4}{2} \\ \mathbf{D}\left[\left(\mathrm{Im}\,X_N\right)^2\right] &= \frac{A^2N^3\sigma^2}{2}\sin^2\varphi + \frac{N^2\sigma 4}{2}\end{aligned}. \qquad (2.2.40)$$

Variance of the real part of product Y_N is equal to the sum of previously found variances

$$\mathbf{D}\left(\mathrm{Re}\,Y_N\right) = \frac{A^2N^3\sigma^2}{2} + N^2\sigma^4\,. \qquad (2.2.41)$$

Now the final step in the calculation of the estimate of the cyclic spectrum (2.2.19) is averaging n times and dividing the result with N. If n is sufficiently large, the real and imaginary parts of the estimate (2.2.19) are following Gaussian distribution with parameters

$$\mathbf{E}\left[\operatorname{Im}\hat{S}_x^{\alpha}(f)\right]=\frac{A^2N}{4}\sin(2\varphi)$$
$$\mathbf{E}\left[\operatorname{Re}\hat{S}_x^{\alpha}(f)\right]=\frac{A^2N}{4}\cos(2\varphi) \tag{2.2.42}$$

and

$$\mathbf{D}\left[\operatorname{Im}\hat{S}_x^{\alpha}(f)\right]=\mathbf{D}\left[\operatorname{Im}\hat{S}_x^{\alpha}(f)\right]=\frac{A^2N\sigma^2}{2n}+\frac{\sigma^4}{n}. \tag{2.2.43}$$

Thus, under the given conditions our decision statistic Λ (2.2.22) will follow the Rice distribution $\Lambda\sim\mathbf{Ric}(\sigma_\Lambda,\psi)$ with parameters

$$\sigma_\Lambda=\sqrt{\frac{A^2N\sigma^2}{2n}+\frac{\sigma^4}{n}},\quad \psi=\frac{NA^2}{4}. \tag{2.2.44}$$

The cumulative distribution function of the Rice distribution is [17]

$$F(\Lambda)=1-Q_1\left(\frac{\psi}{\sigma_\Lambda},\frac{\Lambda}{\sigma_\Lambda}\right), \tag{2.2.45}$$

where $Q_1(\cdot,\cdot)$ is the Marcum Q function. Through identity (2.4) we can now find the probability of correct detection

$$P_D=1-F(\lambda)=Q_1\left(\frac{\psi}{\sigma_\Lambda},\frac{\lambda}{\sigma_\Lambda}\right). \tag{2.2.46}$$

Figure 2.12 shows the comparison between the theoretical PDF of the Rice distribution [17]

$$f\left(\Lambda|\psi,\sigma_\Lambda\right)=\frac{\Lambda}{\sigma_\Lambda^2}e^{-\frac{\Lambda^2+\psi^2}{2\sigma_\Lambda^2}}I_0\left(\frac{\Lambda\psi}{\sigma_\Lambda^2}\right) \tag{2.2.47}$$

and the simulated histogram, where $I_0(\cdot)$ is the modified Bessel function of the first kind with order zero. Simulation was carried out with N = 64 point FFT and averaging over n =32 samples. Signal-to-noise ratio at the detector's input was 17dB. Simulation was repeated for million times in order to construct the histogram shown in Figure 2.12. We can easily see that compliance between the

theoretical and simulated curves is very good. ROC curves in Figure 2.13 were obtained for the same values of parameters. The theoretical and experimental curves are fitting well around high P_F values. When P_F decreases, the difference between the two lines increases. The reason probably is that the value $n = 32$ is not large enough to the tail of averaged realizations PDF to follow normal distribution precisely.

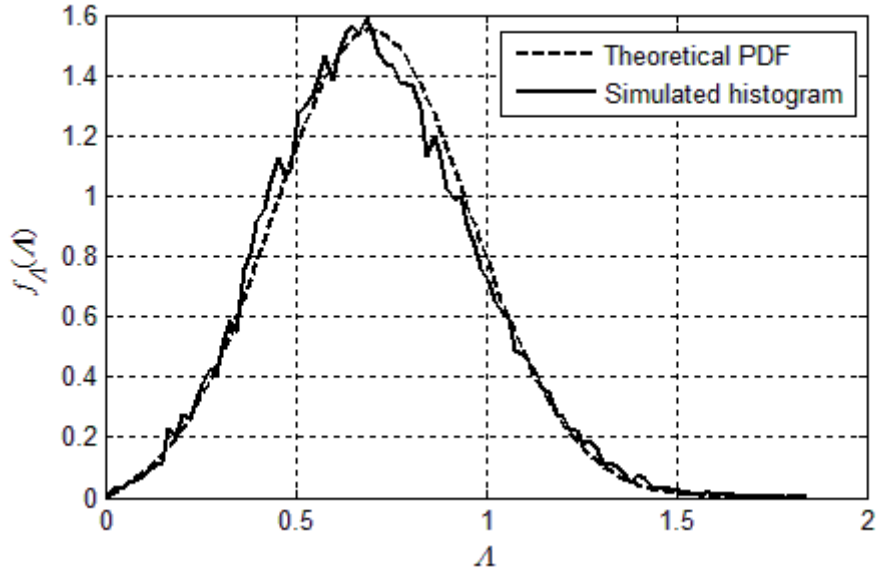

Fig. 2.12 Comparison of theoretical PDF and simulation results

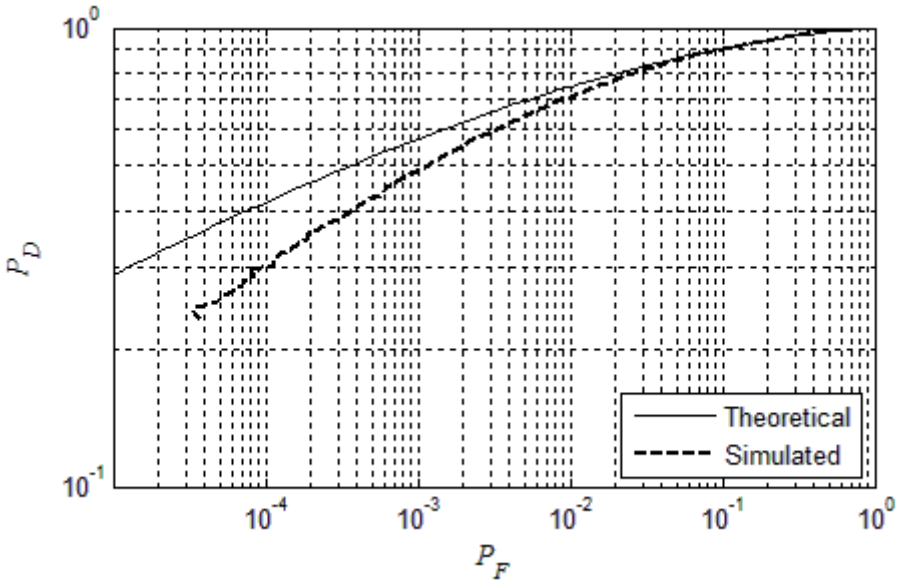

Fig. 2.13 Theoretical and simulated ROC of a cyclostationary detector

In order to calculate the necessary values of the number of samples n and threshold λ for a given operating point (P_F, P_D) at ROC we need to know the inverse function of the Marcum's Q function. To the best of the author's knowledge no direct solution to the inverse problem exists. However, in [32] the Newton-Raphson iteration algorithm is described for numerical solution of the inverse of the Marcum's Q function. Furthermore, for the constant false alarm probability (CFAR), the threshold λ can be set without description of the solution.

2.3 Matched filter

Matched filter is an optimal coherent detection method for cognitive radio. An input signal given,

$$x(t) = s(t) + v(t), \tag{2.3.1}$$

where $s(t)$ is the known primary user signal and $v(t)$ is additive stationary noise, the matched filter $h(t)$ (Fig. 2.14) is designed to maximize the peak SNR at its output.

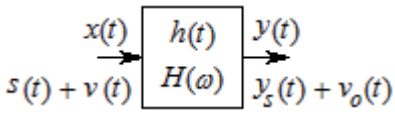

Fig. 2.14 Matched filter

Output of the matched filter is a convolution of the input signal $x(t)$ and filter's impulse response $h(t)$

$$y(t) = x(t) * h(t). \tag{2.3.2}$$

Because the matched filter is linear, we can regard its response to signal and noise as two additive components $y_s(t)$ and $v_o(t)$ at the filter's output

$$y(t) = y_s(t) + v_o(t) = s(t) * h(t) + v(t) * h(t). \tag{2.3.3}$$

Output signal-to-noise ratio at the time instant T is defined here as the peak signal power to the average noise power

$$SNR_0 = \frac{|y_s(T)|^2}{\overline{|v_0|^2}}. \tag{2.3.4}$$

It is well-known that convolution in the time domain is multiplication in the frequency domain, thus we can write the output signal also as

$$y_s(t) = s(t) * h(t) = \frac{1}{2\pi}\int_{-\infty}^{\infty} S(\omega)H(\omega)e^{j\omega t}d\omega\,, \qquad (2.3.5)$$

where $S(\omega)$ is the spectrum of the primary user signal and $H(\omega)$ is the frequency response of the matched filter.

Peak output power at the time instant T then is

$$\left|y_s(T)\right|^2 = \left|\frac{1}{2\pi}\int_{-\infty}^{\infty} S(\omega)H(\omega)e^{j\omega T}d\omega\right|^2. \qquad (2.3.6)$$

Average noise power at the filter output is

$$\overline{\left|v_0\right|^2} = \frac{1}{2\pi}\int_{-\infty}^{\infty} V_o(\omega)d\omega = \frac{1}{2\pi}\int_{-\infty}^{\infty} V(\omega)\left|H(\omega)\right|^2 d\omega\,, \qquad (2.3.7)$$

where $V_o(\omega)$ and $V(\omega)$ are spectra of the output and input noise, respectively. Now we can write signal-to-noise ratio (2.3.4) through (2.3.6) and (2.3.7) as

$$SNR_0 = \frac{\left|\frac{1}{2\pi}\int_{-\infty}^{\infty} S(\omega)H(\omega)e^{j\omega T}d\omega\right|^2}{\frac{1}{2\pi}\int_{-\infty}^{\infty} V(\omega)\left|H(\omega)\right|^2 d\omega}. \qquad (2.3.8)$$

Cauchy–Schwartz inequality for integrals [25] states that for two complex functions $f(x)$ and $g(x)$ integrable over $[a,b]$

$$\left|\int_a^b f(x)g(x)dx\right|^2 \le \int_a^b \left|f(x)\right|^2 dx \int_a^b \left|g(x)\right|^2 dx\,. \qquad (2.3.9)$$

Two sides of (2.3.9) are equal if and only if $g(x) = k f^*(x)$, where k is an arbitrary real constant. If $g(x) \neq k f^*(x)$, then the left side of inequality is smaller than the right side. For further derivation, we will use the following notations:

$$f(x) \equiv \frac{S(\omega)}{\sqrt{V(\omega)}} \quad g(x) \equiv \sqrt{V(\omega)}H(\omega)e^{j\omega T}\,. \qquad (2.3.10)$$

We write SNR (2.3.8) using the above notations for $f(x)$ and $g(x)$

$$SNR_0 = \frac{\left| \frac{1}{2\pi} \int_{-\infty}^{\infty} \left[\frac{S(\omega)}{\sqrt{V(\omega)}} \right] \left[\sqrt{V(\omega)} H(\omega) e^{j\omega T} \right] d\omega \right|^2}{\frac{1}{2\pi} \int_{-\infty}^{\infty} \left| \sqrt{V(\omega)} H(\omega) e^{j\omega T} \right|^2 d\omega}. \qquad (2.3.11)$$

For the next step, the numerator of the last result will be written in the form of Cauchy–Schwartz inequality, resulting in

$$SNR_0 \le \frac{\frac{1}{2\pi} \int_{-\infty}^{\infty} \left| \frac{S(\omega)}{\sqrt{V(\omega)}} \right|^2 d\omega \frac{1}{2\pi} \int_{-\infty}^{\infty} \left| \sqrt{V(\omega)} H(\omega) e^{j\omega T} \right|^2 d\omega}{\frac{1}{2\pi} \int_{-\infty}^{\infty} \left| \sqrt{V(\omega)} H(\omega) e^{j\omega T} \right|^2 d\omega}. \qquad (2.3.12)$$

The right term of the numerator cancels out with the denominator, leaving only

$$SNR_0 \le \frac{1}{2\pi} \int_{-\infty}^{\infty} \frac{|S(\omega)|^2}{V(\omega)} d\omega. \qquad (2.3.13)$$

The resulting inequality (2.3.13) is maximized if $g(x) = k f^*(x)$

$$\sqrt{V(\omega)} H(\omega) e^{j\omega T} = \left[\frac{S(\omega)}{\sqrt{V(\omega)}} \right]^*. \qquad (2.3.14)$$

Thus, the filter that maximizes the signal-to-noise ratio at its output on the time instance T has the frequency response

$$H(\omega) = k \frac{S^*(\omega)}{V(\omega)} e^{-j\omega T}. \qquad (2.3.15)$$

Impulse response $h(t)$ can be derived through an inverse Fourier transform. In the case of white noise with the constant $V(\omega) = \eta_v/2$

$$H(\omega) = \frac{2k}{\eta_v} S^*(\omega) e^{-j\omega T}. \qquad (2.3.16)$$

The inverse transform gives an impulse response

$$h(t) = \frac{2k}{\eta_v} s^*(T - t). \tag{2.3.17}$$

Thus, in the case of white noise, impulse response of the matched filter is a time inversed complex conjugate of the primary user signal $s(t)$.

The main advantage of the matched filter is that due to coherency, it requires minimal time to achieve high processing gain, since only ~ O(1/*SNR*) samples are needed to meet a given probability of detection constraint. However, a matched filter effectively requires demodulation of a primary user signal. This means that the CR has *a priori* knowledge of the primary user signal at both physical layer (PHY) and MAC layers, e.g., modulation type and order, pulse shaping, packet format, etc. Such information might be stored in a memory, but the cumbersome part is that for demodulation the CR has to achieve coherency with the primary user signal by performing timing and carrier synchronization, even channel equalization. This is still possible, since most primary users have pilots, preambles, synchronization words, or spreading codes that can be used for coherent detection [22].

Next, we derive the probability of detection and false detection for a discrete time real system with a discrete impulse response

$$h(k) = s(n - k). \tag{2.3.18}$$

When the input waveform of the matched filter is Gaussian noise, only then the output of the filter is also Gaussian noise with mean and standard deviation

$$\mu_y = \mu_v \sum_{k=1}^{n} h(k) \quad \sigma_y = \sigma \sqrt{\sum_{k=1}^{n} h^2(k)} = \sigma \sqrt{n\sigma_s^2}, \tag{2.3.19}$$

where σ_s^2 is the power of the signal. Generally, the mean of the input noise is zero and thus the output noise of the matched filter is also zero. When a signal $s(n)$ is also present in the input waveform, the standard deviation remains the same as in the previous case but the mean of output is

$$\mu_y = [s * h](n) = n\sigma_s^2. \tag{2.3.20}$$

Thus, the test statistic for the matched filter case can be described as

$$\begin{aligned} H_0 &: \Lambda \sim \mathbf{N}\left(0, \sqrt{n}\sigma\sigma_s\right) \\ H_1 &: \Lambda \sim \mathbf{N}\left(n\sigma_s^2, \sqrt{n}\sigma\sigma_s\right). \end{aligned} \tag{2.3.21}$$

Probability of false detection and detection can be expressed through the complementary error function

$$P_F = \frac{1}{2}\operatorname{erfc}\left(\frac{\lambda}{\sqrt{2n}\sigma\sigma_s}\right); \quad P_D = \frac{1}{2}\operatorname{erfc}\left(\frac{\lambda - n\sigma_s^2}{\sqrt{2n}\sigma\sigma_s}\right). \qquad (2.3.22)$$

The number of samples n necessary to reach the given operating point (P_F, P_D) at ROC can be found from (2.3.22) and it is

$$n = 2SNR^{-1}\left[\operatorname{erfc}^{-1}(2P_F) - \operatorname{erfc}^{-1}(2P_D)\right]^2, \qquad (2.3.23)$$

where SNR is signal-to-noise ratio σ_s^2/σ^2. Threshold value can be evaluated as

$$\lambda = 2\sigma^2 \operatorname{erfc}^{-1}(2P_F)\left[\operatorname{erfc}^{-1}(2P_F) - \operatorname{erfc}^{-1}(2P_D)\right]. \qquad (2.3.24)$$

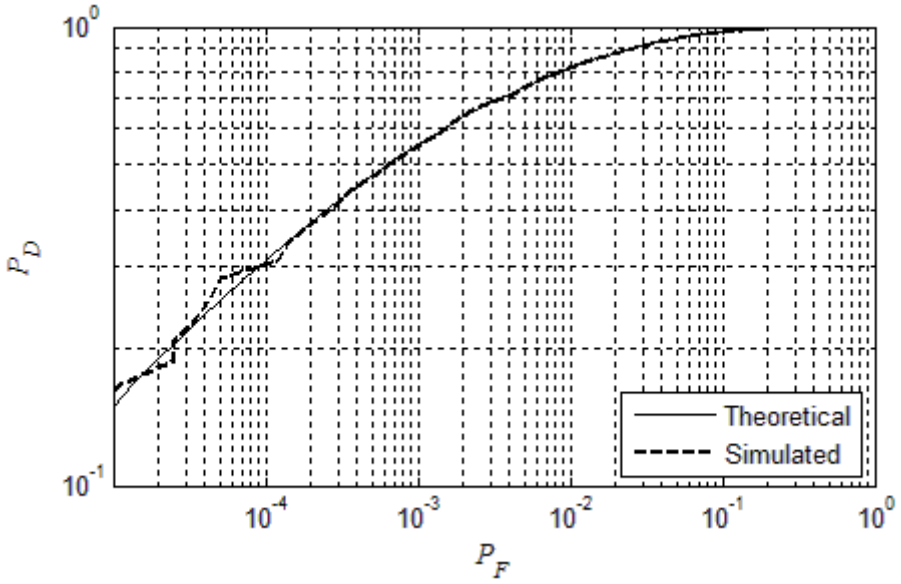

Fig. 2.15 Theoretical and simulated ROC of the matched filter (n=2080, SNR =-23dB)

2.4 Other detection methods

Besides energy and feature detector and matched filter, some other possible detectors are described in literature. Jun, Geofrey and Biing [6] have introduced a method based on covariance.

The key idea behind the covariance-based primary signal detection is that the primary signal received at the CR user is usually correlated because of the dispersive channels, the utility of multiple receive antennas, or even oversampling. Such correlation can be utilized by the CR user to differentiate the primary signal from white noise. Specifically, covariance-based detector determines the presence or absence of the primary signal based on the covariance matrix of the received signal [6]. Based on the sample covariance matrix of the received signal, various test statistics have been developed to detect the primary signal, including the ratio of its maximum and minimum eigenvalues [14, 33], the ratio of its diagonal and off-diagonal elements [34], and its maximum eigenvalue [35].

Moghimi, Nasri and Schober have proposed the so-called L_p–norm spectrum sensing for cognitive radio [15]. Suboptimal decision statistic for L diversity branches is

$$\Lambda_{SO} = \frac{1}{NL} \sum_{l=1}^{L} \sigma_{h_l}^2 \sum_{k=1}^{N} \left| x_{lk} \right|^{p_l}, \qquad (2.4.1)$$

where p_l ,$1 \le l \le L$, are tunable parameters and σ_h is the standard deviation of channel gain. If $p_l = 2$,$1 \le l \le L$, we obtain an energy detector (2.1.3).

This thesis concentrates on three main detector types and thus the other detector types are not analyzed here in detail.

2.5 Comparison of detectors

This chapter introduced three main types of detectors used to determine the presence or the absence of the primary user signal in cognitive radio applications.

An energy detector is easy to implement and it needs a minimal amount of *a priori* information about the primary user signal. Basically, only knowledge of energy and approximate frequency of the primary signal is required. An energy detector can be implemented both in the time and frequency domain. A frequency domain energy detector has some common basis with a cyclostationary feature detector. This was the reason here to take some interest in the topic. As both energy detectors had similar performance but the time domain detector is easier to implement, from now on it is sufficient to proceed with the time domain detector only.

If the number of samples n used in sensing is not limited, an energy detector can theoretically meet any desired P_D and P_F simultaneously. In practice we may never

know the exact value of noise variance σ^2 and this noise uncertainty sets limits to the lowest value of SNR under which correct detection is still possible.

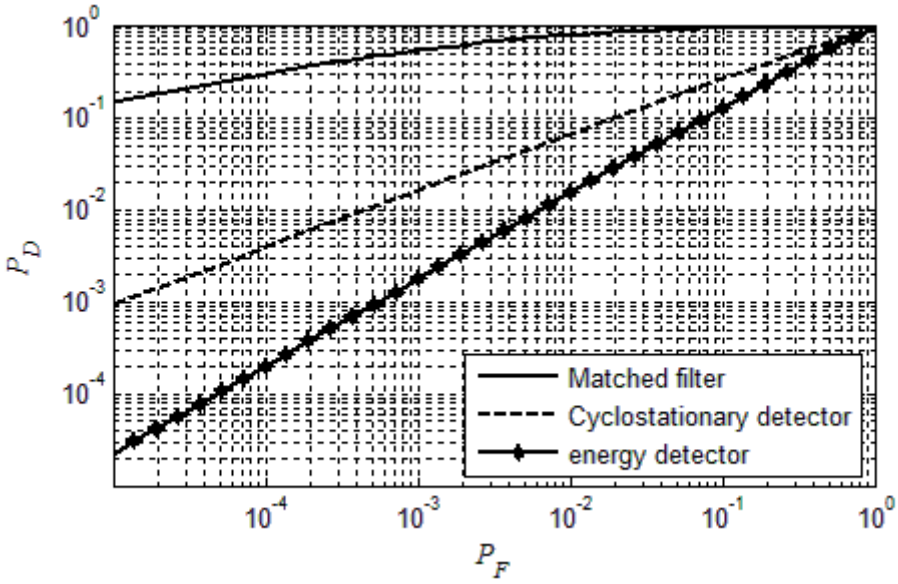

Fig. 2.16 Comparison of the presented detectors' performance (SNR =-23dB)

A cyclostationary feature detector uses periodicities hidden into the primary user signal for detection. In contrast to the energy detector, we need more information about the primary user signal. We need to know some or all periodicities in this signal, for example, carrier, synchronization or pilot frequencies, symbol or coding rates. Implementation and analysis of a cyclostationary detector is more complex than it was in the previous case. It was found that there is no closed-form expression of correct detection P_D for a cyclostationary detector [30, 31]. Therefore, CFAR approach is commonly used where we calculate threshold value for a given false alarm probability and find ROC curves experimentally.

Fortunately, we can take advantage of some special cases and find analytical expressions of P_D and ROC curves. One of those cases was analyzed in section 2.3.

The third option, a matched filter, is an optimal coherent detection method for cognitive radio. The main advantage of a matched filter is that due to coherency, it requires minimal time to achieve high processing gain. However, an effectively matched filter requires demodulation of a primary user signal. This means that the CR needs all information about the primary user, e.g., modulation type and order, pulse shaping, packet format. Also, CR has to achieve coherency with the primary user signal by performing timing and carrier synchronization, even channel

equalization. This means that practical implementation of a matched filter is a complicated task.

Figure 2.16 compares the performance of those three filter types. Curves in the figure are based on the theoretical results derived earlier in this chapter. Length of the input waveform, 2080 samples, is the same for all three. The primary user signal is modeled as a sine wave and signal-to-noise ratio is -23dB. The figure illustrates a well known fact that under the same circumstances a matched filter has the best performance and an energy detector has the worst one. On the other hand, the energy detector is the simplest to build and it needs only minimal *a priori* information about the primary user signal. Choice of the detector depends on three aspects: amount of information known about the primary signal, desired performance and complexity of the receiver.

3. Noise Model

This chapter presents the derivation of our noise model. The same model will be used in the following chapters. The first part introduces the Gaussian noise model. In the second part the one-dimensional impulsive noise model (3.2.1) [45] is extended into the *p*-dimensional form. The third part presents the calculation of the one- and two-dimensional joint PDF of the Gaussian and impulsive noise component. The author shows that in theory we can calculate such a joint PDF for an arbitrary number of dimensions. But the complexity of the solution and the length of the result grow exponentially with the number of dimensions. To overcome this problem the author has suggested a satisfactory approximation for the *p*-dimensional joint PDF of Gaussian and impulsive noise.

3.1 Multivariate Gaussian noise

Most common model for noise in telecommunication systems is an additive white Gaussian noise v_g with the probability density function (PDF) in the form of

$$f_{v_g}(v) = \frac{1}{(2\pi)^{\frac{1}{2}}\sigma} e^{-\frac{(v-\mu)^2}{2\sigma^2}}, \qquad (3.1.1)$$

where σ is standard deviation and μ is the mean of the distribution. For further simplification we assume that the mean μ is equal to zero if not stated else way.

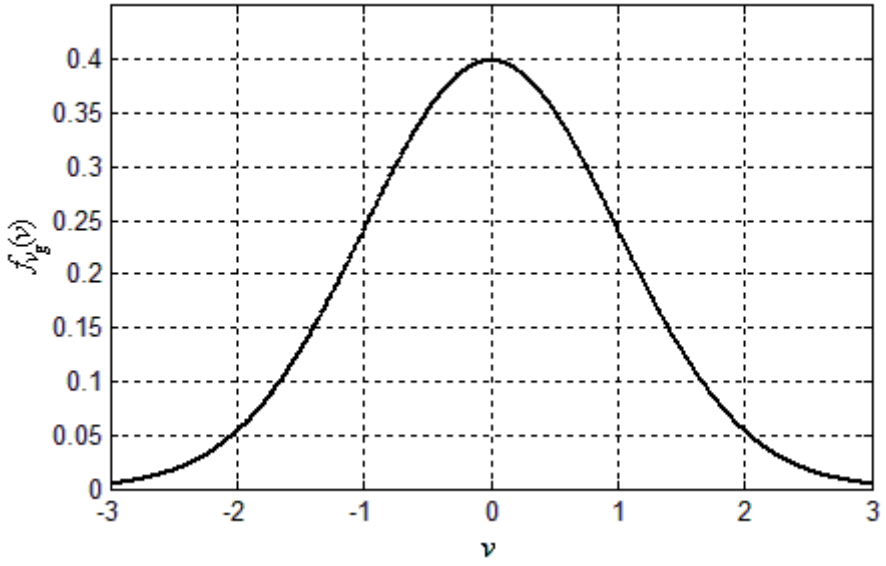

Fig. 3.1 Probability density function of zero-mean normal distribution

For several reasons, Gaussian distribution is one of the most suitable techniques for modeling real life signals. First, the reason is that normal distribution arises as the outcome of the central limit theorem. CLT states that under mild conditions the sum of a large number of random variables is distributed approximately normally, even if different variables have different distribution functions. Gaussian distribution is also very tractable analytically, allowing results involving this distribution to be derived in explicit form. Equation (3.1.1) describes the simplest one-dimensional case of uncorrelated (white) Gaussian noise. During future work we need to handle random noise vectors **v** described by multivariate Gaussian noise with PDF

$$f_{v_g}(\mathbf{v}) = \frac{1}{(2\pi)^{\frac{p}{2}}\sqrt{|\mathbf{C}|}} \exp\left[-\frac{1}{2}(\mathbf{v}-\boldsymbol{\mu})^T \mathbf{C}^{-1}(\mathbf{v}-\boldsymbol{\mu})\right], \qquad (3.1.2)$$

where **v** is a *p*-dimensional vector

$$\mathbf{v} = [v_1, v_2, ..., v_p]^{\mathrm{T}}, \qquad (3.1.3)$$

μ is the mean vector, assumed to be a zero vector if not stated anyway else

$$\boldsymbol{\mu} = [\mu_1, \mu_2, ..., \mu_p]^{\mathrm{T}} \qquad (3.1.4)$$

and **C** is a nonsingular covariance matrix

$$\mathbf{C} = \begin{bmatrix} \mathrm{cov}_{1,1} & \mathrm{cov}_{1,2} & \cdots & \mathrm{cov}_{1,p} \\ \mathrm{cov}_{2,1} & \mathrm{cov}_{2,2} & \cdots & \mathrm{cov}_{2,p} \\ \cdots & \cdots & \cdots & \cdots \\ \mathrm{cov}_{p,1} & \mathrm{cov}_{p,2} & \cdots & \mathrm{cov}_{p,p} \end{bmatrix}. \qquad (3.1.5)$$

Covariance between the two vectors $\mathbf{v}_i$ and $\mathbf{v}_j$ is defined as

$$\mathrm{cov}_{i,j} = \mathbf{E}\left[\left(\mathbf{v}_i - \mu_i\right)^{\mathrm{T}}\left(\mathbf{v}_j - \mu_j\right)\right] = \sigma_i \sigma_j \rho_{i,j}, \qquad (3.1.6)$$

where σ_i and σ_j are standard deviations of vectors $\mathbf{v}_i$ and $\mathbf{v}_j$ accordingly and $\rho_{i,j}$ is the correlation coefficient between those vectors

$$\rho_{i,j} = \frac{\mathrm{cov}_{i,j}}{\sigma_i \sigma_j}. \qquad (3.1.7)$$

We note here that covariance matrix is symmetric by the definition $\rho_{i,j} = \rho_{j,i}$.

For example, in the two-dimensional case ($p = 2$) mean and covariance matrixes are defined as

$$\boldsymbol{\mu} = \begin{bmatrix} \mu_1 \\ \mu_2 \end{bmatrix} \quad \mathbf{C} = \begin{bmatrix} \sigma_1^2 & \rho\sigma_1\sigma_2 \\ \rho\sigma_2\sigma_1 & \sigma_2^2 \end{bmatrix}. \tag{3.1.8}$$

In order to evaluate the PDF (3.1.2), we first find the determinant of the covariance matrix

$$|\mathbf{C}| = \begin{vmatrix} \sigma_1^2 & \rho\sigma_1\sigma_2 \\ \rho\sigma_2\sigma_1 & \sigma_2^2 \end{vmatrix} = \sigma_1^2\sigma_2^2 - \rho^2\sigma_1^2\sigma_2^2 = \sigma_1^2\sigma_2^2(1-\rho^2) \tag{3.1.9}$$

thus

$$\frac{1}{(2\pi)^{\frac{p}{2}}\sqrt{|\mathbf{C}|}} = \frac{1}{2\pi\sigma_1\sigma_2\sqrt{1-\rho^2}}. \tag{3.1.10}$$

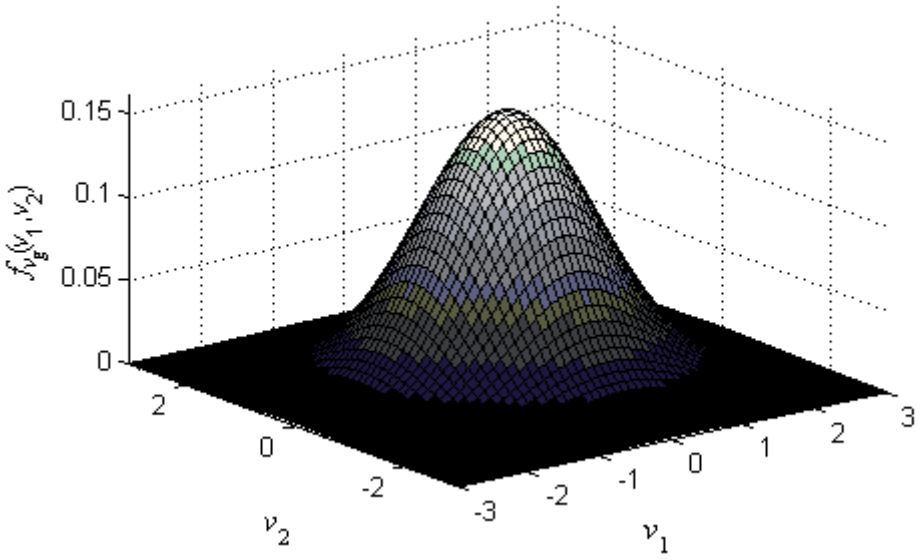

Fig. 3.2 Probability density function of zero-mean bi-variate normal distribution (ρ=0)

Next, we need to find a matrix inverse for **C**, the task that is easy for 2x2 matrixes

$$\mathbf{C}^{-1} = \frac{1}{|\mathbf{C}|}\begin{bmatrix} \sigma_2^2 & -\rho\sigma_1\sigma_2 \\ -\rho\sigma_2\sigma_1 & \sigma_1^2 \end{bmatrix} = \\ = \frac{1}{\sigma_1^2\sigma_2^2(1-\rho^2)}\begin{bmatrix} \sigma_2^2 & -\rho\sigma_1\sigma_2 \\ -\rho\sigma_2\sigma_1 & \sigma_1^2 \end{bmatrix}. \qquad (3.1.11)$$

Now we can calculate the argument of the exponent for equation (3.1.2)

$$-\frac{1}{2}\begin{bmatrix} v_1-\mu_1 & v_2-\mu_2 \end{bmatrix}\frac{1}{\sigma_1^2\sigma_2^2(1-\rho^2)}\begin{bmatrix} \sigma_2^2 & -\rho\sigma_1\sigma_2 \\ -\rho\sigma_2\sigma_1 & \sigma_1^2 \end{bmatrix}\begin{bmatrix} v_1-\mu_1 \\ v_2-\mu_2 \end{bmatrix} = \\ = -\frac{1}{2(1-\rho^2)}\left[\frac{(v_1-\mu_1)^2}{\sigma_1^2} - \frac{2\rho(v_1-\mu_1)(v_2-\mu_2)}{\sigma_1\sigma_2} + \frac{(v_2-\mu_2)^2}{\sigma_2^2}\right] \qquad (3.1.12)$$

Substituting (3.1.10) and (3.1.12) into (3.1.2) we obtain PDF for bi-variate (p = 2) normal distribution

$$f_{v_g}(\mathbf{v}) = \frac{1}{2\pi\sigma_1\sigma_2\sqrt{1-\rho^2}}\, e^{-\frac{1}{2(1-\rho^2)}\left[\frac{(v_1-\mu_1)^2}{\sigma_1^2} - \frac{2\rho(v_1-\mu_1)(v_2-\mu_2)}{\sigma_1\sigma_2} + \frac{(v_2-\mu_2)^2}{\sigma_2^2}\right]}. \qquad (3.1.13)$$

The shape of this distribution for an uncorrelated case can be seen above in Figure 3.2.

Let us now consider the three-dimensional case (p = 3). To simplify the matter we assume that the mean vector is a zero vector **μ** = 0. According to (3.1.6) covariance matrix is

$$\mathbf{C} = \begin{bmatrix} \sigma_1^2 & \sigma_1\sigma_2\rho_{1,2} & \sigma_1\sigma_3\rho_{1,3} \\ \sigma_2\sigma_1\rho_{2,1} & \sigma_2^2 & \sigma_2\sigma_3\rho_{2,3} \\ \sigma_3\sigma_1\rho_{3,1} & \sigma_3\sigma_2\rho_{3,2} & \sigma_3^2 \end{bmatrix}. \qquad (3.1.14)$$

Due to the symmetric nature of covariance (3.1.6) $\rho_{1,2} = \rho_{2,1}$, $\rho_{2,3} = \rho_{3,2}$ and $\rho_{1,3} = \rho_{3,1}$ thus, the determinant of the three-dimensional covariance matrix (3.1.14) is

$$|\mathbf{C}| = \sigma_1^2\sigma_2^2\sigma_3^2\left(1-\rho_{1,2}^2-\rho_{2,3}^2-\rho_{1,3}^2+2\rho_{1,2}\rho_{2,3}\rho_{1,3}\right). \qquad (3.1.15)$$

Matrix inverse for **C** equals

$$\mathbf{C}^{-1} = \frac{1}{|\mathbf{C}|}\begin{bmatrix} \sigma_2^2\sigma_3^2(1-\rho_{2,3}^2) & \sigma_1\sigma_2\sigma_3^2(\rho_{2,3}\rho_{1,3}-\rho_{1,2}) & \sigma_1\sigma_2^2\sigma_3(\rho_{1,2}\rho_{2,3}-\rho_{1,3}) \\ \sigma_1\sigma_2\sigma_3^2(\rho_{2,3}\rho_{1,3}-\rho_{1,2}) & \sigma_1^2\sigma_3^2(1-\rho_{1,3}^2) & \sigma_1^2\sigma_2\sigma_3(\rho_{1,3}\rho_{1,2}-\rho_{2,3}) \\ \sigma_1\sigma_2^2\sigma_3(\rho_{1,2}\rho_{2,3}-\rho_{1,3}) & \sigma_1^2\sigma_2\sigma_3(\rho_{1,3}\rho_{1,2}-\rho_{2,3}) & \sigma_1^2\sigma_2^2(1-\rho_{1,2}^2) \end{bmatrix}$$

Now we can calculate the argument of the exponent for equation (3.1.2) as

$$-\frac{1}{2}\mathbf{v}^{\mathrm{T}}\mathbf{C}^{-1}\mathbf{v} = \frac{-w}{2\sigma_1^2\sigma_2^2\sigma_3^2\left(1-\rho_{1,2}^2-\rho_{2,3}^2-\rho_{1,3}^2+2\rho_{1,2}\rho_{2,3}\rho_{1,3}\right)}, \quad (3.1.17)$$

where

$$\begin{aligned} w = {} & v_1^2\sigma_2^2\sigma_3^2(1-\rho_{2,3}^2)+v_2^2\sigma_1^2\sigma_3^2(1-\rho_{1,3}^2)+v_3^2\sigma_1^2\sigma_2^2(1-\rho_{1,2}^2)+ \\ & +2\sigma_1\sigma_2\sigma_3\left[v_1v_2\sigma_3(\rho_{2,3}\rho_{1,3}-\rho_{1,2})+v_1v_3\sigma_2(\rho_{1,2}\rho_{2,3}-\rho_{1,3})+\right. \\ & \left.+v_2v_3\sigma_1(\rho_{1,3}\rho_{1,2}-\rho_{2,3})\right] \end{aligned} \quad . (3.1.18)$$

Thus, PDF for tri-variate ($p = 3$) centralized normal distribution can be written as

$$f_g(\mathbf{v}) = \frac{e^{\frac{-w}{2\sigma_1^2\sigma_2^2\sigma_3^2\left(1-\rho_{1,2}^2-\rho_{2,3}^2-\rho_{1,3}^2+2\rho_{1,2}\rho_{2,3}\rho_{1,3}\right)}}}{(2\pi)^{\frac{3}{2}}\sigma_1\sigma_2\sigma_3\sqrt{1-\rho_{1,2}^2-\rho_{2,3}^2-\rho_{1,3}^2+2\rho_{1,2}\rho_{2,3}\rho_{1,3}}}. \quad (3.1.19)$$

The given examples show that a general expression for the p-variate normal distribution can be expanded analytically for any value of p. But it is also clear that the complexity of those expressions increases rapidly with p.

3.2 Multivariate impulsive noise

By far the most important artificial source of noise in mobile communications is man-made noise, which is radiated by different kinds of electrical equipment across a frequency band extending from about 2 to about 500 MHz [36]. Unlike thermal noise, man-made noise is impulsive in nature; hence the reference to it as impulsive noise. In urban areas, the impulsive noise generated by motor vehicles is a major source of interference to mobile communications. [8]

As the main focus of the present dissertation is on spectrum sensing algorithms robust against impulsive noise, it is essential to describe our model of impulsive

noise here. We start with one-dimensional impulsive noise and then progress to a p-dimensional case as we did with Gaussian noise above.

The impulsive noise component v_i is assumed not to be present most of the time but appears with a certain probability c so that the impulsive component obeys the PDF

$$f_{v_i}(v) = \frac{c}{b-a} + (1-c)\delta(v), \tag{3.2.1}$$

with $0 < c < 1$ and a and b being the lower and upper limits on the values that the impulsive noise can take and $\delta(\cdot)$ denotes the Dirac delta function. In practice, a and b may, for instance, be the smallest and largest numbers that can be represented at the output of analogue to digital (A/D) converter. In the following we assume that $a = -b$ if not stated otherwise, so (3.2.1) is simplified to

$$f_{v_i}(v) = \frac{c}{2b} + (1-c)\delta(v). \tag{3.2.2}$$

The uniform distribution is selected because of its maximum entropy property, i.e. there is nothing assumed to be known about the origin of the impulses. For instance, the impulses may be due to failures of the A/D converter or some interferences that are not well modeled by a Gaussian noise process [72].

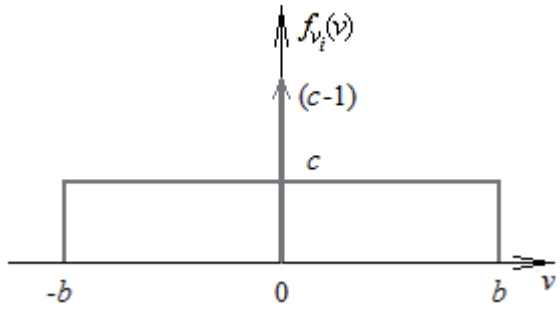

Fig. 3.3 Probability density function of one-dimensional impulsive noise

We can assume that values of impulsive noise are uncorrelated, so the probability density function of multivariate impulsive noise can be written as

$$f_{v_i}(\mathbf{v}) = \prod_{k=1}^{p} f_{v_i}(v_k) = \prod_{k=1}^{p} \left[\frac{c}{2b} + (1-c)\delta(v_k) \right]. \tag{3.2.3}$$

For a bi-variate case ($p = 2$) we can write (3.2.3)

$$f_{v_i}(v_1,v_2)=\left[\frac{c}{2b}+(1-c)\delta(v_1)\right]\left[\frac{c}{2b}+(1-c)\delta(v_2)\right]= \\ \left(\frac{c}{2b}\right)^2+\frac{c(1-c)}{2b}\left[\delta(v_1)+\delta(v_2)\right]+(1-c)^2\delta(v_1)\delta(v_2) \quad . \quad (3.2.4)$$

The given two-dimensional PDF is shown in Figure 3.4. As indicated by equation (3.2.4) and depicted in the figure, the PDF of 2D impulsive noise contains four parts. The first plane is with width 2*b* times 2*b* and with weight c^2. This plane is divided into four equal parts by two "walls" with length 2*b* and weight *c*(1-*c*), with the Dirac delta pulse with weight$(1-c)^2$ in the centre.

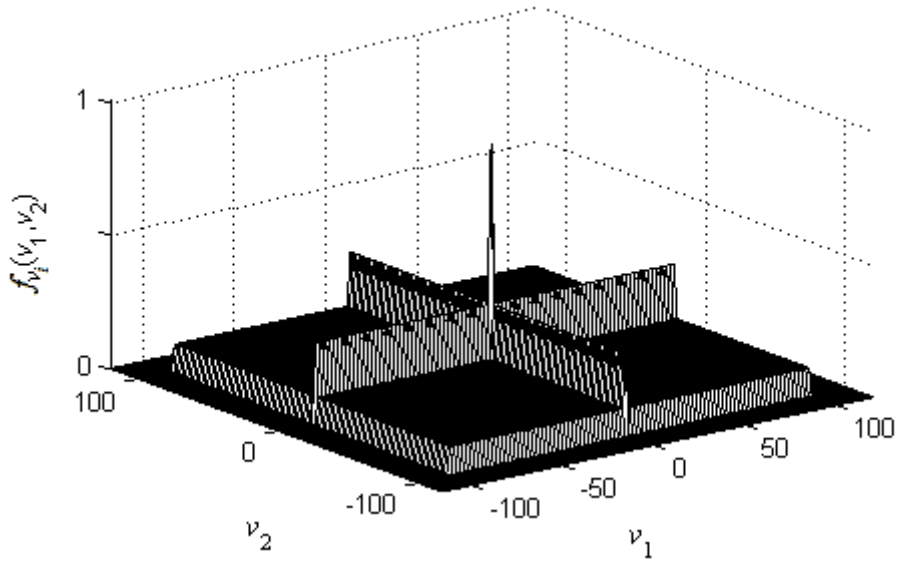

Fig. 3.4 Probability density function of two-dimensional impulsive noise

An example of impulsive noise realization is depicted in Figure 3.5. Most of the time the value of the noise there is equal to zero and with probability *c*, pulses with larger values appear.

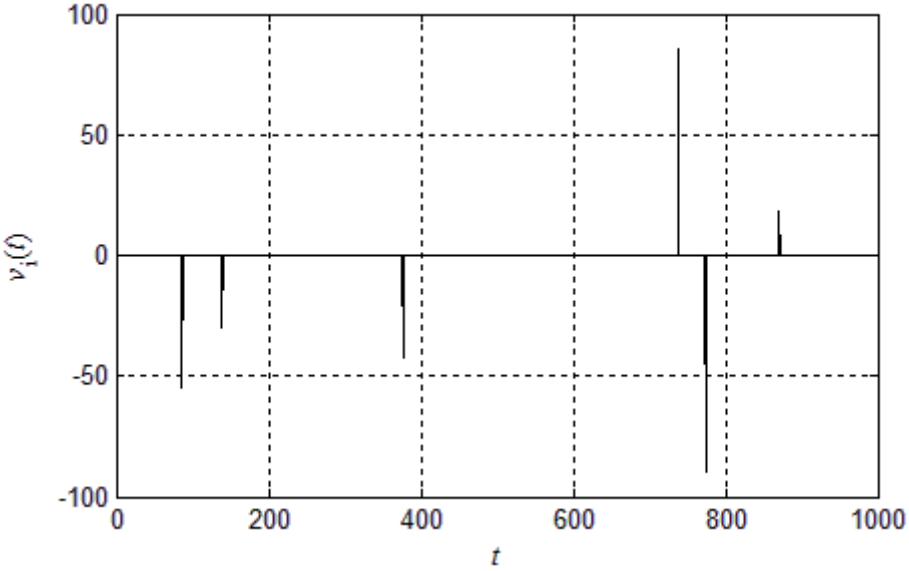

Fig. 3.5 Example of impulsive noise realization ($b = 100$, $c = 5 \cdot 10^{-2}$)

3.3 Gaussian noise with additive impulsive component

Next, two previously viewed noise models will be combined. From now on we assume that the noise $v(t)$ comprises a sum of zero mean additive Gaussian noise process $v_g(t)$ and an additional impulsive noise component $v_i(t)$ [73]

$$v(t) = v_g(t) + v_i(t). \tag{3.3.1}$$

It is well known that the probability density function of the sum of two independent random variables is the convolution of their respective density functions [17: 358]. In our case we can calculate the PDF of the sum (3.3.1) as the convolution

$$f_v(v) = \int_{-\infty}^{\infty} f_g(\tau) f_i(v-\tau) d\tau. \tag{3.3.2}$$

The PDF of the centered normal distribution is (3.1.1) with condition $\mu = 0$, and the PDF of impulsive noise is described by (3.2.2), thus, our convolution according to the above is

$$f_v(v) = \frac{1}{(2\pi)^{\frac{1}{2}}\sigma}\int_{-\infty}^{\infty} e^{-\frac{\tau^2}{2\sigma^2}}\left\{\frac{c}{2b}\left[\Theta(v-\tau+b)-\Theta(v-\tau-b)\right]+(1-c)\delta(v-\tau)\right\}d\tau$$

Due to the linearity property of the integral we can divide the previous equation into two parts

$$\begin{aligned} f_v(v) = &\frac{c}{2b(2\pi)^{\frac{1}{2}}\sigma}\int_{v-b}^{v+b} e^{-\frac{\tau^2}{2\sigma^2}}d\tau + \\ &+\frac{1-c}{(2\pi)^{\frac{1}{2}}\sigma}\int_{-\infty}^{\infty} e^{-\frac{\tau^2}{2\sigma^2}}\delta(v-\tau)d\tau \end{aligned}, \tag{3.3.4}$$

both of which can be solved separately. Using properties of the Dirac delta function, we can solve the second part of equation (3.3.4) as

$$\int_{-\infty}^{\infty} e^{-\frac{\tau^2}{2\sigma^2}}\delta(v-\tau)d\tau = e^{-\frac{v^2}{2\sigma^2}}. \tag{3.3.5}$$

The first part can be solved using the definition of the error function

$$\operatorname{erf}(x) = \frac{2}{\sqrt{\pi}}\int_0^x e^{-t^2}dt \tag{3.3.6}$$

which gives

$$\frac{1}{(2\pi)^{\frac{1}{2}}\sigma}\int_{v-b}^{v+b} e^{-\frac{\tau^2}{2\sigma^2}}d\tau = \frac{1}{2}\left[\operatorname{erf}\left(\frac{v+b}{\sqrt{2}\sigma}\right)-\operatorname{erf}\left(\frac{v-b}{\sqrt{2}\sigma}\right)\right]. \tag{3.3.7}$$

Thus, the PDF of the sum (3.3.1) is

$$f_v(v) = \frac{c}{4b}\left[\operatorname{erf}\left(\frac{v+b}{\sqrt{2}\sigma}\right)-\operatorname{erf}\left(\frac{v-b}{\sqrt{2}\sigma}\right)\right]+\frac{1-c}{(2\pi)^{\frac{1}{2}}\sigma}e^{-\frac{v^2}{2\sigma^2}}. \tag{3.3.8}$$

The shape of the probability density function of the sum of Gaussian and impulsive random variables is depicted in Figure 3.6. We have selected the difference between b and σ to be small and the probability of impulses c unrealistically high to make the shape of the achieved PDF clearly visible. In real life, scenario b is in the order of hundreds or thousands and c is at least thousands

of times smaller. In such cases, the shape of the PDF would resemble a narrow peak at $v = 0$ and equals almost zero all around the rest of abscissa.

It is also important to note that the first part of (3.3.8) changes its value only around ±b and is practically constant, with its value c/2b between those limits.

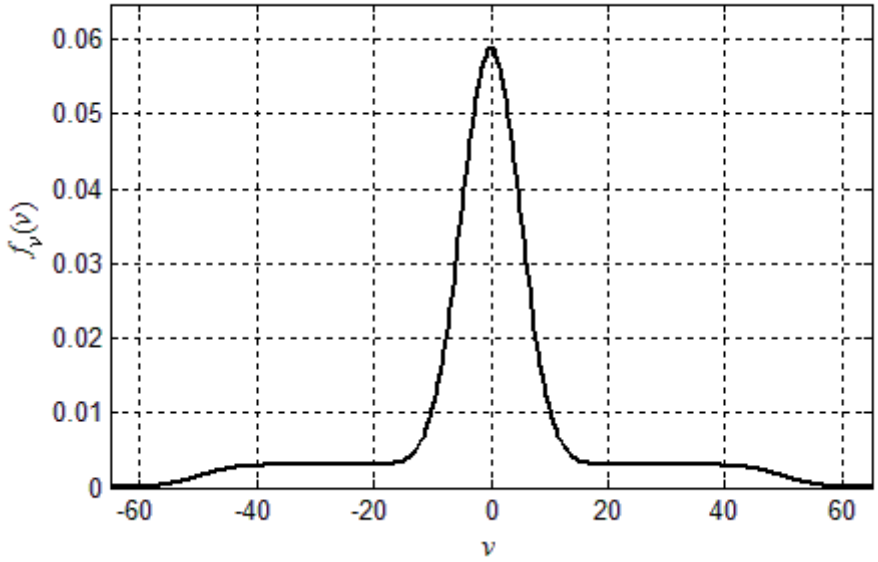

Fig. 3.6 PDF of the sum of Gaussian and impulsive noise (b = 50, c = 0.3, σ = 5)

To be exact, we must note that (3.3.8) corresponds to a case where the amplitude of impulsive noise only is limited within a range [-*b*,*b*]. In real systems it is logical to assume that the sum of Gaussian and impulsive noise (3.3.1) is limited to the interval [-*b*,*b*]. In such a case (3.3.8) it is valid only in the range [-*b*,*b*] and limiting adds two delta impulses with amplitudes

$$\int_{-\infty}^{-b} f_v(v)dv = \int_{b}^{\infty} f_v(v)dv \qquad (3.3.9)$$

to the positions $v = -b$ and $v = b$, as depicted in Figure 3.7.

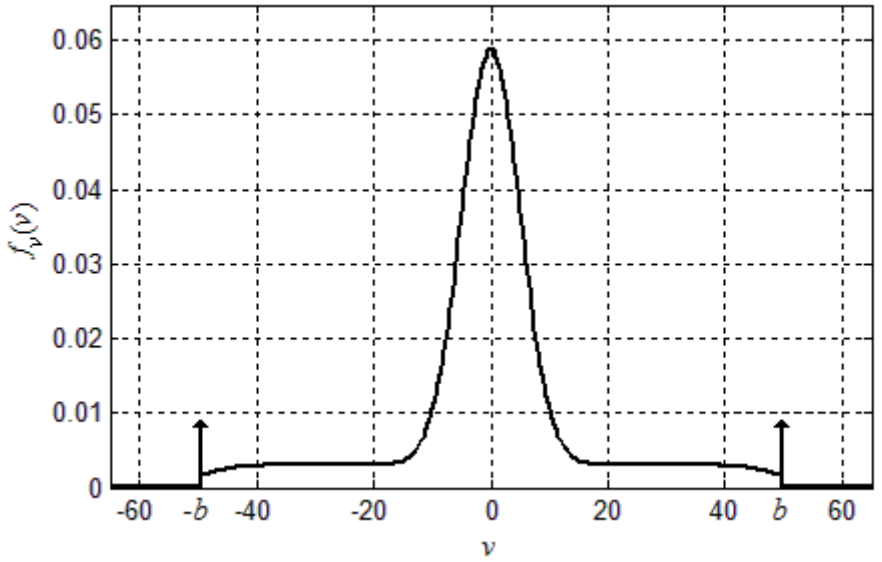

Fig. 3.7 PDF of a limited sum of Gaussian and impulsive noise (b = 50, c = 0.3, σ = 5)

From the exact solution in the one-dimensional case, we can move to cases with more dimensions. In a two-dimensional case, we need to calculate convolution also in two dimensions

$$f_v(v_1, v_2) = \int_{-\infty}^{\infty}\int_{-\infty}^{\infty} f_g(v_1 - \tau_1, v_2 - \tau_2) f_i(\tau_1, \tau_2) d\tau_1 d\tau_2 . \qquad (3.3.10)$$

Before going further, we should make one additional assumption to help simplify further derivations. We are assuming that random variables v_1 and v_2 have zero mean $\boldsymbol{\mu} = \mathbf{0}$ and their standard deviations of the Gaussian components are equal to $\sigma_1 = \sigma_2 = \sigma$. Both assumptions are realistic taking into account our signal model. For a simpler case of white Gaussian noise, when the two variables are uncorrelated ($\rho = 0$), we need to calculate the following convolution integral:

$$f_v(\mathbf{v}) = \frac{1}{2\pi\sigma^2}\int_{-\infty}^{\infty}\int_{-\infty}^{\infty} e^{-\frac{(v_1-\tau_1)^2+(v_2-\tau_2)^2}{2\sigma^2}} \left\{\frac{c}{2b}\left[\Theta(\tau_1+b)-\Theta(\tau_1-b)\right]+ \right.$$
$$\left. +(1-c)\delta(\tau_1)\right\}\cdot\left\{\frac{c}{2b}\left[\Theta(\tau_2+b)-\Theta(\tau_2-b)\right]+(1-c)\delta(\tau_2)\right\} d\tau_1 d\tau_2 \qquad (3.3.11)$$

Let us group the terms depending on τ_1 and τ_2 of equation (3.3.11) leading to

$$f_v(\mathbf{v}) = \frac{1}{2\pi\sigma^2}\int_{-\infty}^{\infty} e^{-\frac{(v_2-\tau_2)^2}{2\sigma^2}}\left\{\frac{c}{2b}\left[\Theta(\tau_2+b)-\Theta(\tau_2-b)\right]+(1-c)\delta(\tau_2)\right\}d\tau_2 \cdot \int_{-\infty}^{\infty} e^{-\frac{(v_1-\tau_1)^2}{2\sigma^2}}\left\{\frac{c}{2b}\left[\Theta(\tau_1+b)-\Theta(\tau_1-b)\right]+(1-c)\delta(\tau_1)\right\}d\tau_1 \quad . \quad (3.3.12)$$

Now we can calculate both of the one-dimensional multiplicands similarly to equation (3.3.3), resulting in

$$f_v(\mathbf{v}) = \left\{\frac{c}{4b}\left[\operatorname{erf}\left(\frac{v_1+b}{\sqrt{2}\sigma}\right)-\operatorname{erf}\left(\frac{v_1-b}{\sqrt{2}\sigma}\right)\right]+\frac{1-c}{(2\pi)^{\frac{1}{2}}\sigma}e^{-\frac{v_1^2}{2\sigma^2}}\right\}\cdot \left\{\frac{c}{4b}\left[\operatorname{erf}\left(\frac{v_2+b}{\sqrt{2}\sigma}\right)-\operatorname{erf}\left(\frac{v_2-b}{\sqrt{2}\sigma}\right)\right]+\frac{1-c}{(2\pi)^{\frac{1}{2}}\sigma}e^{-\frac{v_2^2}{2\sigma^2}}\right\} \quad . \quad (3.3.13)$$

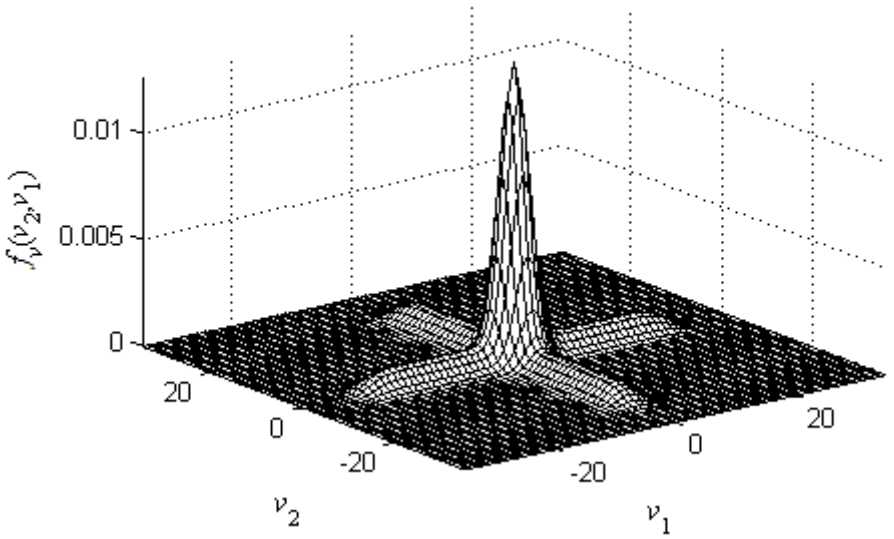

Fig. 3.8 PDF of 2D the sum of uncorrelated Gaussian and impulsive noise

The result is shown in Figure 3.8 for the following values of parameters: b = 25, c = 0.45 and σ = 2. Again, parameter values are chosen to be unrealistic in order to enhance details in the figure.

In a more general case of colored noise, Gaussian variables v_1 and v_1 may be correlated. In such a case, the two-dimensional PDF of a centralized normal distribution (3.1.12) is

$$f_{v_g}(\mathbf{v}) = \frac{1}{2\pi\sigma^2\sqrt{1-\rho^2}} e^{-\frac{v_1^2 - 2\rho v_1 v_2 + v_2^2}{2\sigma^2(1-\rho^2)}} . \qquad (3.3.14)$$

Further, we use the commutative property of the convolution, thus (3.3.10) can be also expressed in a more suitable form for future derivations

$$f_v(v_1, v_2) = \int_{-\infty}^{\infty}\int_{-\infty}^{\infty} f_g(\tau_1, \tau_2) f_i(v_1 - \tau_1, v_2 - \tau_2) d\tau_1 d\tau_2 . \qquad (3.3.15)$$

Thus, the convolution integral for a bi-variate case becomes

$$\begin{aligned} f_v(\mathbf{v}) = \frac{1}{2\pi\sigma^2\sqrt{1-\rho^2}} \int_{-\infty}^{\infty}\int_{-\infty}^{\infty} e^{-\frac{\tau_1^2 - 2\rho\tau_1\tau_2 + \tau_2^2}{2\sigma^2(1-\rho^2)}} \left\{ \frac{c}{2b}\left[\Theta(v_1 - \tau_1 + b) - \right.\right. \\ \left. - \Theta(v_1 - \tau_1 - b)\right] + (1-c)\delta(v_1 - \tau_1)\Big\} \Big\{ \frac{c}{2b}\left[\Theta(v_2 - \tau_2 + b) - . \\ \left. - \Theta(v_2 - \tau_2 - b)\right] + (1-c)\delta(v_2 - \tau_2)\right\} d\tau_1 d\tau_2 \end{aligned} \qquad (3.3.16)$$

We can rearrange the last equation to obtain

$$\begin{aligned} f_v(\mathbf{v}) = \frac{1}{2\pi\sigma^2\sqrt{1-\rho^2}} \int_{-\infty}^{\infty} e^{-\frac{\tau_2^2}{2\sigma^2(1-\rho^2)}} \left\{ \frac{c}{2b}\left[\Theta(v_2 - \tau_2 + b) - \right.\right. \\ \left. - \Theta(v_2 - \tau_2 - b)\right] + (1-c)\delta(v_2 - \tau_2)\Big\} \int_{-\infty}^{\infty} e^{-\frac{\tau_1^2 - 2\rho\tau_1\tau_2}{2\sigma^2(1-\rho^2)}} \cdot \\ \cdot \left\{ \frac{c}{2b}\left[\Theta(v_1 - \tau_1 + b) - \Theta(v_1 - \tau_1 - b)\right] + (1-c)\delta(v_1 - \tau_1) \right\} d\tau_1 d\tau_2 \end{aligned} \qquad . (3.3.17)$$

In order to calculate (3.3.17), we start from solving the inner integral

$$\begin{aligned} \int_{-\infty}^{\infty} e^{-\frac{\tau_1^2 - 2\rho\tau_1\tau_2}{2\sigma^2(1-\rho^2)}} \left\{ \frac{c}{2b}\left[\Theta(v_1 - \tau_1 + b) - \Theta(v_1 - \tau_1 - b)\right] + (1-c)\delta(v_1 - \tau_1) \right\} d\tau_1 = \\ = \frac{c}{2b} \int_{v_1 - b}^{v_1 + b} e^{-\frac{\tau_1^2 - 2\rho\tau_1\tau_2}{2\sigma^2(1-\rho^2)}} d\tau_1 + (1-c) \int_{-\infty}^{\infty} e^{-\frac{\tau_1^2 - 2\rho\tau_1\tau_2}{2\sigma^2(1-\rho^2)}} \delta(v_1 - \tau_1) d\tau_1 \end{aligned} \qquad . (3.3.18)$$

The first half of it is

$$\frac{c}{2b}\int_{v_1-b}^{v_1+b} e^{-\frac{\tau_1^2-2\rho\tau_1\tau_2}{2\sigma^2(1-\rho^2)}}d\tau_1 = \frac{c\sqrt{2\pi\sigma^2(1-\rho^2)}}{4b}e^{\frac{\rho^2\tau_2^2}{2\sigma^2(1-\rho^2)}}\cdot$$
$$\cdot\left[\operatorname{erf}\left(\frac{v_1+b-\rho\tau_2}{\sqrt{2\sigma^2(1-\rho^2)}}\right)-\operatorname{erf}\left(\frac{v_1-b-\rho\tau_2}{\sqrt{2\sigma^2(1-\rho^2)}}\right)\right] \qquad (3.3.19)$$

and the second half is

$$(1-c)\int_{-\infty}^{\infty} e^{-\frac{\tau_1^2-2\rho\tau_1\tau_2}{2\sigma^2(1-\rho^2)}}\delta(v_1-\tau_1)d\tau_1 = (1-c)e^{-\frac{v_1^2-2\rho v_1\tau_2}{2\sigma^2(1-\rho^2)}}. \qquad (3.3.20)$$

Now our two-dimensional convolution obtains the following form:

$$f_v(\mathbf{v}) = \frac{1}{2\pi\sigma^2\sqrt{1-\rho^2}}\int_{-\infty}^{\infty}\left\{\frac{c}{2b}e^{-\frac{\tau_2^2}{2\sigma^2(1-\rho^2)}}\left[\Theta(v_2-\tau_2+b)-\Theta(v_2-\tau_2-b)\right]+\right.$$
$$\left.+(1-c)e^{-\frac{\tau_2^2}{2\sigma^2(1-\rho^2)}}\delta(v_2-\tau_2)\right\}\left\{(1-c)e^{-\frac{v_1^2-2\rho v_1\tau_2}{2\sigma^2(1-\rho^2)}}+\frac{c\sqrt{2\pi\sigma^2(1-\rho^2)}}{4b}e^{\frac{\rho^2\tau_2^2}{2\sigma^2(1-\rho^2)}}\cdot\right. \qquad (3.3.21)$$
$$\left.\cdot\left[\operatorname{erf}\left(\frac{v_1+b-\rho\tau_2}{\sqrt{2\sigma^2(1-\rho^2)}}\right)-\operatorname{erf}\left(\frac{v_1-b-\rho\tau_2}{\sqrt{2\sigma^2(1-\rho^2)}}\right)\right]\right\}d\tau_2$$

The result can be divided into six parts; each solved separately and then the results are added back together afterwards. The first out of the six parts is the following equation:

$$\frac{c}{4\pi\sigma^2\sqrt{1-\rho^2}\,b}\int_{v_2-b}^{v_2+b} e^{-\frac{\tau_2^2}{2\sigma^2(1-\rho^2)}}\frac{c\sqrt{2\pi\sigma^2(1-\rho^2)}}{4b}e^{\frac{\rho^2\tau_2^2}{2\sigma^2(1-\rho^2)}}\cdot$$
$$\cdot\operatorname{erf}\left(\frac{v_1+b-\rho\tau_2}{\sqrt{2\sigma^2(1-\rho^2)}}\right)d\tau_2 = \frac{c^2}{8\sqrt{2\pi\sigma^2}b^2}\int_{v_2-b}^{v_2+b} e^{-\frac{\tau_2^2}{2\sigma^2}}\operatorname{erf}\left(\frac{v_1+b-\rho\tau_2}{\sqrt{2\sigma^2(1-\rho^2)}}\right)d\tau_2 \qquad (3.3.22)$$

As it can be seen, this part has no result in terms of standard mathematical functions, but the result can be easily computed numerically. Very close solution is achieved also for the second part – and here no result in terms of standard mathematical functions is available

$$\frac{-c}{4\pi\sigma^2\sqrt{1-\rho^2}\,b}\int_{v_2-b}^{v_2+b} e^{-\frac{\tau_2^2}{2\sigma^2(1-\rho^2)}}\frac{c\sqrt{2\pi\sigma^2(1-\rho^2)}}{4b}e^{\frac{\rho^2\tau_2^2}{2\sigma^2(1-\rho^2)}}\cdot$$
$$\cdot\operatorname{erf}\left(\frac{v_1-b-\rho\tau_2}{\sqrt{2\sigma^2(1-\rho^2)}}\right)d\tau_2=\frac{-c^2}{8\sqrt{2\pi\sigma^2}b^2}\int_{v_2-b}^{v_2+b} e^{-\frac{\tau_2^2}{2\sigma^2}}\operatorname{erf}\left(\frac{v_1-b-\rho\tau_2}{\sqrt{2\sigma^2(1-\rho^2)}}\right)d\tau_2 \quad . \text{(3.3.23)}$$

Due to linearity of the integral we can take the first two parts (3.3.22) and (3.3.23) together into one more compact form

$$\frac{c^2}{8\sqrt{2\pi\sigma^2}b^2}\int_{v_2-b}^{v_2+b} e^{-\frac{\tau_2^2}{2\sigma^2}}\left[\operatorname{erf}\left(\frac{v_1+b-\rho\tau_2}{\sqrt{2\sigma^2(1-\rho^2)}}\right)-\operatorname{erf}\left(\frac{v_1-b-\rho\tau_2}{\sqrt{2\sigma^2(1-\rho^2)}}\right)\right]d\tau_2 \,. \text{(3.3.24)}$$

This sum is also solvable numerically, and the result is shown in Figure 3.9 for values $b = 25$, $c = 0.45$, $\sigma = 2$ and $\rho = 0.6$. The result is approximately shaped as a rectangular prism with sides $2b$ times $2b$.

The third part of (3.3.21) has more compact solution than the two previous ones

$$\frac{c}{4\pi\sigma^2\sqrt{1-\rho^2}\,b}\int_{v_2-b}^{v_2+b} e^{-\frac{\tau_2^2}{2\sigma^2(1-\rho^2)}}(1-c)e^{-\frac{v_1^2-2\rho v_1\tau_2}{2\sigma^2(1-\rho^2)}}d\tau_2=$$
$$=\frac{c(1-c)}{4\sqrt{2\pi\sigma^2}b}e^{-\frac{v_1^2}{2\sigma^2}}\left[\operatorname{erf}\left(\frac{v_2+b-\rho v_1}{\sqrt{2\sigma^2(1-\rho^2)}}\right)-\operatorname{erf}\left(\frac{v_2-b-\rho v_1}{\sqrt{2\sigma^2(1-\rho^2)}}\right)\right]. \quad \text{(3.3.24)}$$

Graphical representation of (3.3.24) is shown in Figure 3.10. The equation describes a wall with a length $2b$ along the v_1 axis The height of the wall is about three orders larger than that of the rectangular prism (3.3.23) shown in the previous figure.

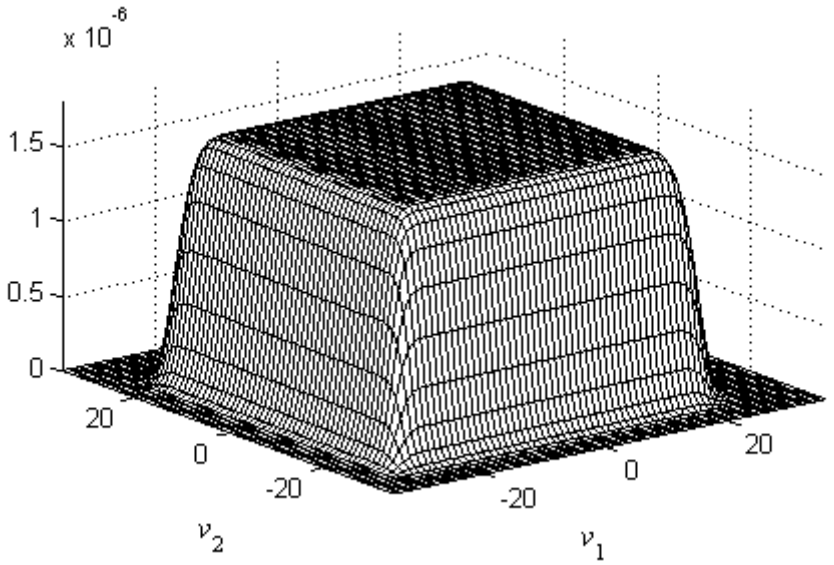

Fig. 3.9 Graphical representations of the first two summands of the 2D convolution

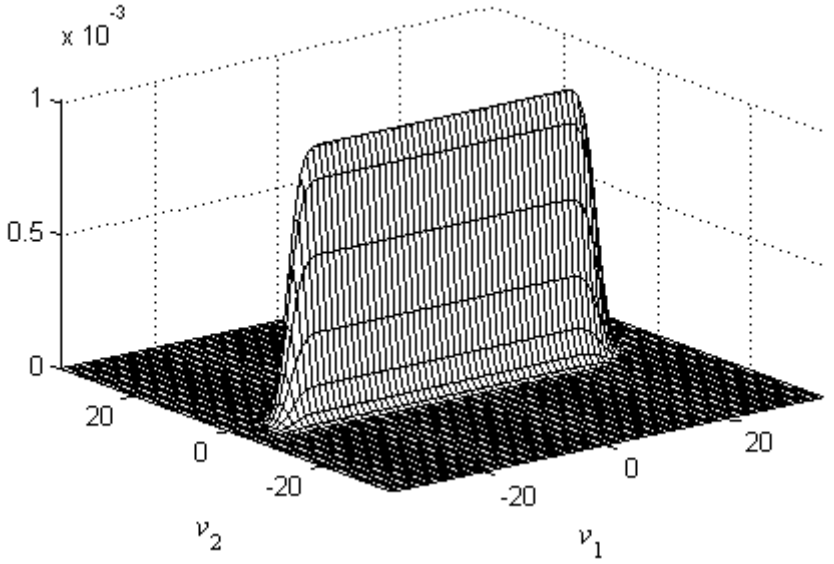

Fig. 3.10 Graphical representations of the third summand of the 2D convolution

The fourth part equals

$$\frac{c(1-c)}{4\sqrt{2\pi\sigma^2 b}}\int_{-\infty}^{\infty} e^{-\frac{\tau_2^2}{2\sigma^2}}\,\mathrm{erf}\left(\frac{v_1+b-\rho\tau_2}{\sqrt{2\sigma^2(1-\rho^2)}}\right)\delta(v_2-\tau_2)d\tau_2 = \\ =\frac{c(1-c)}{4\sqrt{2\pi\sigma^2 b}}e^{-\frac{v_2^2}{2\sigma^2}}\,\mathrm{erf}\left(\frac{v_1+b-\rho v_2}{\sqrt{2\sigma^2(1-\rho^2)}}\right) \qquad (3.3.25)$$

and in a similar fashion also the fifth part can be solved

$$\frac{-c(1-c)}{4\sqrt{2\pi\sigma^2 b}}\int_{-\infty}^{\infty} e^{-\frac{\tau_2^2}{2\sigma^2}}\,\mathrm{erf}\left(\frac{v_1-b-\rho\tau_2}{\sqrt{2\sigma^2(1-\rho^2)}}\right)\delta(v_2-\tau_2)d\tau_2 = \\ =\frac{-c(1-c)}{4\sqrt{2\pi\sigma^2 b}}e^{-\frac{v_2^2}{2\sigma^2}}\,\mathrm{erf}\left(\frac{v_1-b-\rho v_2}{\sqrt{2\sigma^2(1-\rho^2)}}\right) \qquad . (3.3.26)$$

The last two parts can be combined

$$\frac{c(1-c)}{4\sqrt{2\pi\sigma^2 b}}e^{-\frac{v_2^2}{2\sigma^2}}\left[\mathrm{erf}\left(\frac{v_1+b-\rho v_2}{\sqrt{2\sigma^2(1-\rho^2)}}\right)-\mathrm{erf}\left(\frac{v_1-b-\rho v_2}{\sqrt{2\sigma^2(1-\rho^2)}}\right)\right]. \qquad (3.3.27)$$

When comparing the result obtained with the third part (3.3.24) of the convolution integral, the results are exactly the same except the places of v_1 and v_2 are switched. Thus, (3.3.27) has the same shape as in Figure 3.10 only turned π/2 radians around the origin. Sum of those two walls forms a cross-shaped body shown in Figure 3.11.

The final sixth part of our long equation gives the following result:

$$\frac{(1-c)^2}{2\pi\sigma^2\sqrt{1-\rho^2}}\int_{-\infty}^{\infty} e^{-\frac{\tau_2^2-2\rho v_1\tau_2+v_1^2}{2\sigma^2(1-\rho^2)}}\,\delta(v_2-\tau_2)d\tau_2 = \frac{(1-c)^2}{2\pi\sigma^2\sqrt{1-\rho^2}}e^{-\frac{v_1^1-2\rho v_1 v_2+v_2^2}{2\sigma^2(1-\rho^2)}} \quad . \qquad (3.3.28)$$

This final result is scaled PDF of a two-dimensional correlated normal distribution (3.1.12) the shape of which is similar to that represented in Figure 3.2. Putting together all six parts of (3.3.21), we finally obtain the two-dimensional PDF of the sum of Gaussian and impulsive random variables

$$f_v(\mathbf{v}) = \frac{(1-c)^2}{2\pi\sigma^2\sqrt{1-\rho^2}} e^{-\frac{v_1^2-2\rho v_1 v_2+v_2^2}{2\sigma^2(1-\rho^2)}} + \frac{c^2}{8\sqrt{2\pi\sigma^2 b^2}} \int_{v_2-b}^{v_2+b} e^{-\frac{\tau_2^2}{2\sigma^2}} \cdot$$
$$\cdot \left[\operatorname{erf}\left(\frac{v_1+b-\rho\tau_2}{\sqrt{2\sigma^2(1-\rho^2)}} \right) - \operatorname{erf}\left(\frac{v_1-b-\rho\tau_2}{\sqrt{2\sigma^2(1-\rho^2)}} \right) \right] d\tau_2 +$$
$$+ \frac{c(1-c)}{4\sqrt{2\pi\sigma^2 b}} e^{-\frac{v_1^2}{2\sigma^2}} \left[\operatorname{erf}\left(\frac{v_2+b-\rho v_1}{\sqrt{2\sigma^2(1-\rho^2)}} \right) - \operatorname{erf}\left(\frac{v_2-b-\rho v_1}{\sqrt{2\sigma^2(1-\rho^2)}} \right) \right] + \quad (3.3.29)$$
$$+ \frac{c(1-c)}{4\sqrt{2\pi\sigma^2 b}} e^{-\frac{v_2^2}{2\sigma^2}} \left[\operatorname{erf}\left(\frac{v_1+b-\rho v_2}{\sqrt{2\sigma^2(1-\rho^2)}} \right) - \operatorname{erf}\left(\frac{v_1-b-\rho v_2}{\sqrt{2\sigma^2(1-\rho^2)}} \right) \right]$$

The two-dimensional PDF described by the last equation looks almost as that for a non-correlated case shown in Figure 3.8. Difference between those two is illustrated by contour plots in Figure 3.12 When the correlation between the random variables is zero, the PDF is symmetric across both axes, as shown on the left. On the right side, the correlation ρ = 0.6 and the distribution have lost its symmetry.

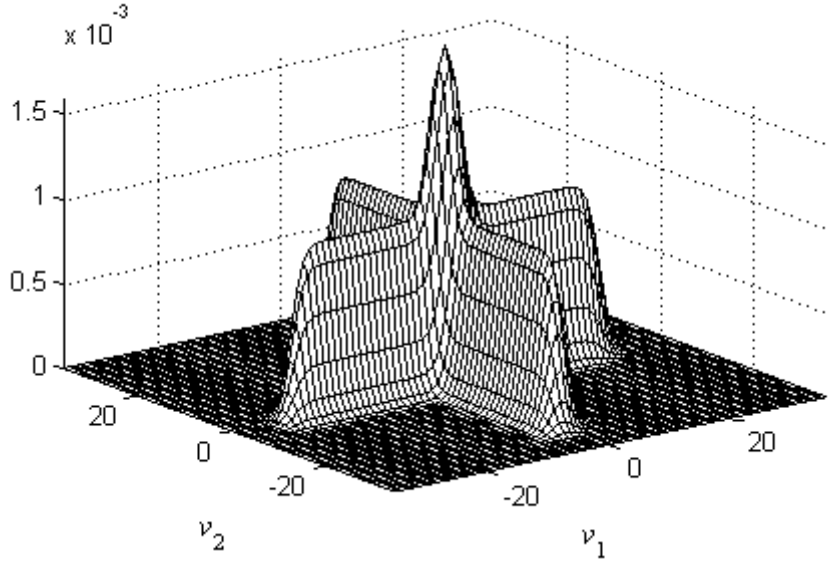

Fig. 3.11 Graphical representations of summands 3-5 of the 2D convolution

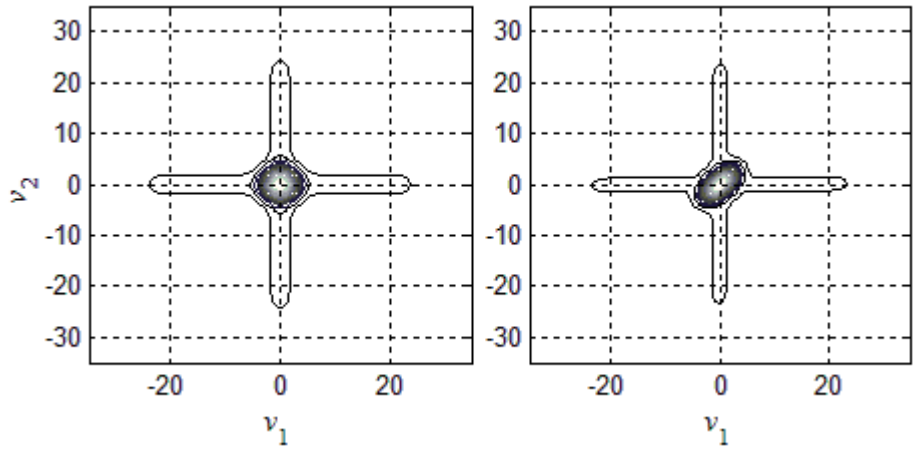

Fig. 3.12 Comparison of the 2D PDF for an uncorrelated (left) and a correlated case (right)

We would obtain similar solutions also for a higher number of dimensions p. It can be seen that even in the 2D case, our result is too complicated for practical use, thus further simplification is required in order to progress with work. Thus, the next question that arises is how to approximate the sum (3.3.1) to enable further analysis to be done without a major loss of accuracy.

Impulses occur only seldom, so most of the time a small-amplitude Gaussian noise has much higher value. On the other hand, when an impulse appears, it has usually much larger value than Gaussian noise samples, so in both cases one noise component is much larger than the other. Therefore, noise $v(t)$ can be modeled such that the largest component out of the two determines the outcome at each time instant.

$$v(t) = v_g(t) + v_i(t) \approx \max[v_g(t), v_i(t)]. \qquad (3.3.30)$$

The probability density function of noise $v(t)$ for the one-dimensional case ($p = 1$) can be approximated as

$$f_v(v) = \begin{cases} \beta \max\left[\dfrac{1-c}{(2\pi)^{\frac{1}{2}}\sigma} e^{\frac{-v^2}{2\sigma^2}}, \max\left(\dfrac{c}{2b}, \dfrac{c}{(2\pi)^{\frac{1}{2}}\sigma} e^{\frac{-v^2}{2\sigma^2}}\right)\right] & -b < v < b \\ 0, & \text{otherwise} \end{cases} . \qquad (3.3.31)$$

If there is no noise impulse which happens with a probability 1-c, then the PDF of noise is fully determined by Gaussian noise. In the case of impulsive noise, with a probability c, the outcome is determined by the larger of the two distributions (3.3.30). If the amplitude of the impulse is larger than the value of Gaussian noise,

the PDF is determined by uniform distribution and by Gaussian distribution otherwise. For further simplification, we consider the fact that impulsive noise with low amplitude is undistinguishable from Gaussian noise (Figures 3.13 and 3.14). Thus, we can simplify (3.3.31) into the following form:

$$f_v(v) = \begin{cases} \beta \max\left(\frac{1-c}{(2\pi)^{\frac{1}{2}}\sigma} e^{\frac{-v^2}{2\sigma^2}}, \frac{c}{2b} \right) & -b < v < b \\ 0, & \text{else} \end{cases} . \qquad (3.3.32)$$

Strictly speaking, a variable c in equation (3.3.32) is not the probability of the impulse anymore but instead, the probability of the impulsive noise having larger value than Gaussian one

$$c^* = P[v_i(t) > v_g(t)] . \qquad (3.3.33)$$

For practical considerations, c^* is smaller than c by amount of σ/b. In real life scenarios it means that difference is in order of one tenth of percent.

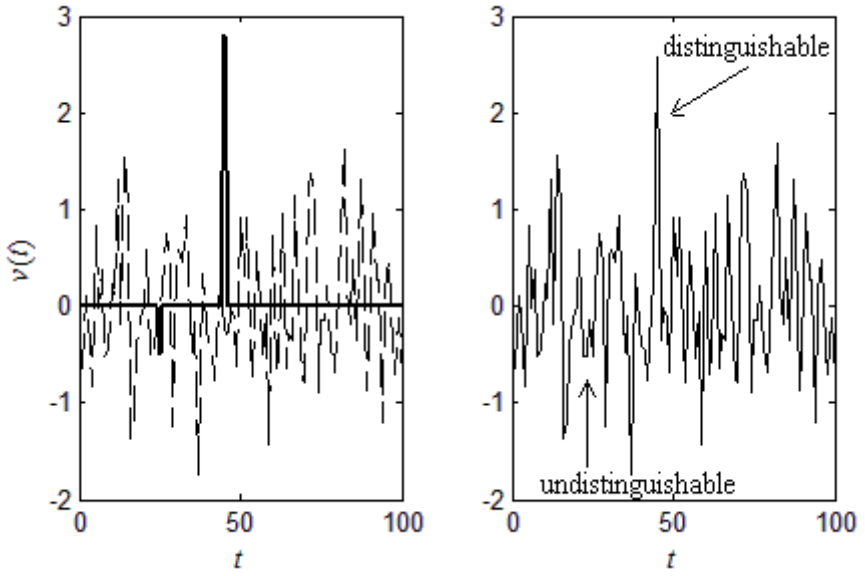

Fig. 3.13 Example of mutual masking of Gaussian and impulsive noise

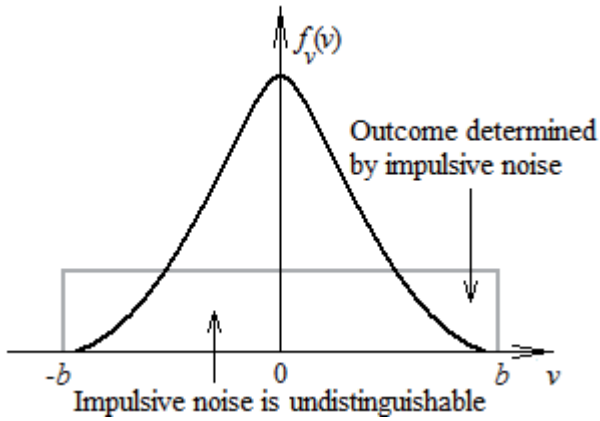

Fig. 3.14 Explanation of masking impulsive noise by Gaussian noise

The normalization factor β can be found by solving

$$\int_{-b}^{b} f_v(v)dv = 1, \tag{3.3.34}$$

this results in

$$\beta_1 = \left[(1-c)\,\mathrm{erf}\left(\frac{\eta_1}{\sqrt{2}\sigma}\right) + c\left(1-\frac{\eta_1}{b}\right)\right]^{-1} \tag{3.3.35}$$

and

$$\eta_1 = \sqrt{-2\sigma^2 \ln\left(\frac{c}{1-c}\frac{\sqrt{2\pi}\sigma}{2b}\right)} \tag{3.3.36}$$

is the intersection point of the Gaussian and uniform distributions [72]. In practice, the value of β_1 is very close to 1.

The PDF of v (3.3.32) in the interval [$-b$,b] can be given a more convenient form for the future derivation [73]

$$f_v(v) = \frac{\beta_1(1-c)}{(2\pi)^{\frac{1}{2}}\sigma} e^{\frac{-1}{2\sigma^2}\min\left(v^2,\eta_1^2\right)} . \tag{3.3.37}$$

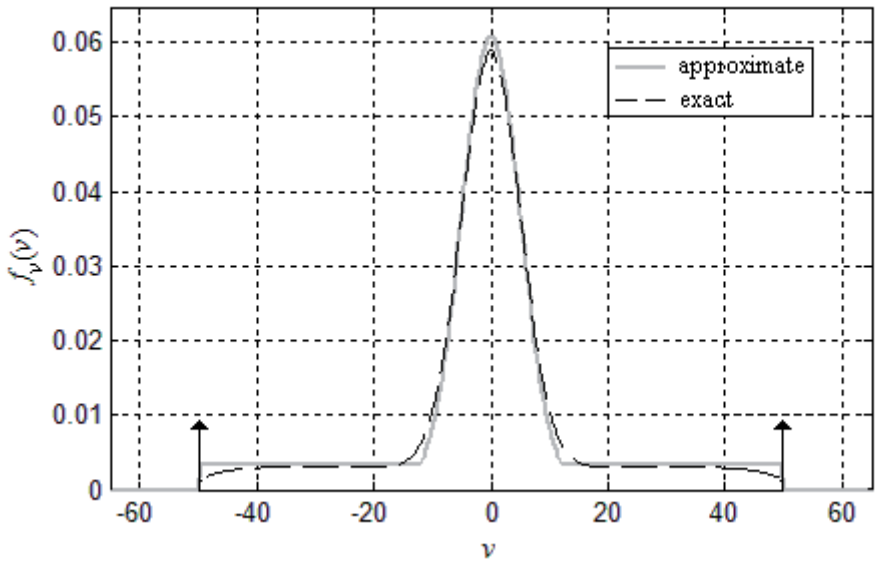

Fig. 3.15 Comparison of the exact PDF and its approximation

The approximation is illustrated in Figure 3.15 with $b = 50$, $c = 0.3$, $\sigma = 5$. Note that we have selected difference between b and σ to be small and the probability of impulses unrealistically high to make the difference between the lines clearly visible. It can be seen that the approximation is very close to the true probability density function. The differences appear in the area where the Gaussian PDF goes over to the uniform tail and at the ends of the interval $[-b,b]$. The larger the difference between the standard deviation of Gaussian noise from one side and the impulsive noise interval from the other side, the better is the invoked approximation. The main benefit from the approximation is that it leads to tractable mathematics.

In a similar fashion we need to find suitable approximation for the p – dimensional sum of Gaussian and impulsive noise. In order to find out which parts of the complete model are important and which ones can be discarded, we must analyze each part separately. The first summand in our model (3.3.29) corresponds to Gaussian noise and this is definitely an important one. The second part has the largest area but also the smallest magnitude in order of $(c/b)^2$. In order to our noise vector $\mathbf{v}$ to be placed on this plane we need that two succeeding noise samples v_1 and v_2 both be corrupted with impulsive noise with values larger than Gaussian. In our model we assume impulsive noise not to be correlated, so the probability of such an event is very small. This is well illustrated by the fact that even with parameter values $b = 25$ and $c = 0.45$ we cannot see the second part of our noise model in Figure 3.8.

Additionally, we can see that if a dimension p increases, the influence of the second part of our noise model decreases rapidly. Thus, we can discard the second summand from our noise model without suffering a great loss of accuracy.

Two last parts of the noise model (3.3.29) are two "walls" that are forming cross the shape at the base of Gaussian "bell" in Figure 3.8. Although at first glimpse it seems that the magnitude of those walls is much smaller than the Gaussian part and thus we can discard them as well, this is not the case. Let us look at the PDF of one dimensional sum of Gaussian and impulsive noise (3.3.8). As mentioned earlier it changes its value only around $\pm b$ and is practically constant, with the value $c/2b$ between those limits.

At a closer look at the "wall" (3.3.24) now, we can also observe similar facts. Along the v_2 axis, the value of the function is mostly constant and only decreases near the values $\pm b$. The cross-section of the function is shaped as a centered Gaussian curve with its shape and magnitude not depending on the correlation ρ except again near the maximal values $\pm b$. As we are actually only interested in the area where the Gaussian PDF has higher values than impulsive ones, we are not interested in what happens at the far ends around $\pm b$. Thus, we will consider the following simplification for the two last parts of our noise model inside the interval $-b < v_1 < b$:

$$\frac{c(1-c)}{2\sqrt{2\pi\sigma^2}b} e^{-\frac{v_2^2}{2\sigma^2}} \quad . \tag{3.3.38}$$

and in a similar fashion for v_1 inside the interval $-b < v_2 < b$:

$$\frac{c(1-c)}{2\sqrt{2\pi\sigma^2}b} e^{-\frac{v_1^2}{2\sigma^2}} \quad . \tag{3.3.39}$$

Thus, the first step of our simplification was to discard the second summand from the noise model (3.3.29). The second step was the simplification of the two last summands. Next, we should also replace here the sum of Gaussian and impulsive noise components with the larger of the two as we did in the one- dimensional case (3.3.30). Thus, our approximate model of two-dimensional noise is (inside square - $b \leq v_{1,2} \leq b$)

$$f_v(\mathbf{v}) = \frac{\beta_2(1-c)}{\sqrt{2\pi\sigma^2}} \max\left[\frac{(1-c)e^{-\frac{v_1^2 - 2\rho v_1 v_2 + v_2^2}{2\sigma^2(1-\rho^2)}}}{\sqrt{2\pi\sigma^2\left(1-\rho^2\right)}}, \frac{c}{2b}\left(e^{-\frac{v_1^2}{2\sigma^2}} + e^{-\frac{v_2^2}{2\sigma^2}} \right) \right] \tag{3.3.40}$$

Further, we will obtain the p-dimensional model of the sum of Gaussian and impulsive noise. The model will be defined as the maximum of p-dimensional hyper cross and p-dimensional Gaussian noise multiplied by the factor $(1\text{-}c)^p$. Correctness of this model is demonstrated by the results obtained in the following chapters. An exact and an approximate PDF for a two-dimensional case are illustrated in Figure 3.16.

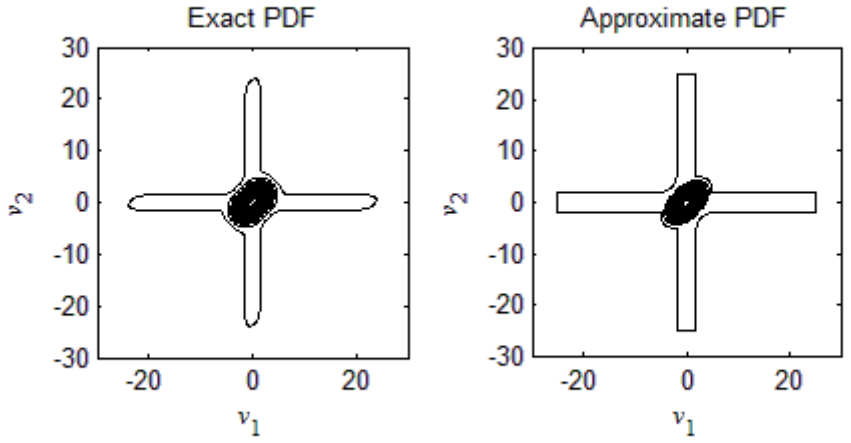

Fig. 3.16 Comparison of an exact PDF and its approximation in a 2D case

3.4 Conclusion

Current mathematical models used to describe impulsive noise [10, 14, 15] are intuitively unsatisfactory. Based on impulsive noise measurements [12, 13] a new mathematical model for impulsive noise is introduced (3.2.3).

As noise at the input of the detector is an additive sum of Gaussian and impulsive noise, joint PDF was found for both one- and two-dimensional noise. It was shown that theoretically we can find an analytical PDF for the sum of Gaussian- and impulsive noise for any number of dimensions p. But such tasks are time-consuming. For example, calculations for a one-dimensional joint PDF (3.3.8) takes one and half pages but for a two-dimensional case (3.3.29) seven pages are needed to write down the derivation. Also, the number of the components in the resulting p- dimensional joint PDF is increasing with p.

Clearly, for practical use some approximations must be made. First, the sum operator was replaced by the maximum operator under assumptions that the sum of two noises is mostly determined by the value of the larger of the two. Secondly, we eliminated the components of the joint PDF that were too small to have any real influence. Due to those simplifications we obtained a noise model suitable for further use.

4. Maximum Likelihood Estimators of Noise Parameters

This chapter covers the derivation of the maximum likelihood estimator (MLE) for Gaussian noise with an additive impulsive component. First, the concept of MLE is introduced, demonstrated on the example of p-dimensional Gaussian noise. Next, a likelihood function for the p-dimensional sum of Gaussian and impulsive noise is derived. The nose model derived in the previous chapter is used here. ML estimators are found both for the impulse probability c and the covariance matrix $\mathbf{C}$.

4.1 Maximum Likelihood Estimator

Suppose that we have a sample of n independent and identically distributed (IID) observations v_1, v_2, …, v_n of some ergodic random process with an unknown PDF $f_0(\cdot)$. However, it is surmised that the function f_0 belongs to a certain family of distributions

$$\{f(\cdot|w), w \in W\}, \tag{4.1.1}$$

called the parametric model, so that $f_0 = f(\cdot|)$. The true value of the parameter w_0 is unknown and so it is desirable to find the estimator $\hat{w}$ as close to the true value w_0 as possible. Both the observed variables v_k and the parameter w can be either scalars or vectors.

To use the maximum likelihood (ML) method, first, the joint probability density function must be specified for all observations. For an IID sample, this joint PDF is

$$f_{\mathbf{v}}(v_1, v_2, \ldots, v_n|\mathbf{w}) = f_{v_1}(v_1|\mathbf{w}) \cdot f_{v_2}(v_2|\mathbf{w}) \cdot \ldots f_{v_n}(v_n|\mathbf{w}). \tag{4.1.2}$$

If the described joint PDF parameter $\mathbf{w}$ is fixed and $v_1 \ldots v_n$ are variables, thus (4.1.2) is a function of the data given a particular set of parameter values defined on the data scale [37]. We can look at this function from a different perspective considering the observed values $v_1 \ldots v_n$ to be fixed parameters of this function whereas $\mathbf{w}$ will be a variable allowed to vary freely. This function is called likelihood

$$L(\mathbf{w}|v_1, v_2, \ldots, v_n) = f_{\mathbf{v}}(v_1, v_2, \ldots, v_n|\mathbf{w}) = \prod_{k=1}^{n} f_{v_k}(v_k|\mathbf{w}). \tag{4.1.3}$$

The likelihood function is a function of the parameter given a particular set of observed data defined on the parameter scale [37]. The logarithm of likelihood is

monotonically related to the likelihood function itself. Because that it is often more convenient to work with a so-called log-likelihood

$$\ln L\left(\mathbf{w}|v_1, v_2, \ldots, v_n\right) = \sum_{k=1}^{n} \ln f_{v_k}\left(v_k|\mathbf{w}\right). \qquad (4.1.4)$$

The principle of maximum likelihood estimation (MLE) states that the desired probability distribution is the one that makes the observed data ‘‘most likely,’’ which means that one must seek the value of the parameter ***w*** that maximizes the likelihood function $L(\mathbf{w}|\mathbf{v})$ [37]. For the sake of compactness, we will use from now on vector **v** instead of notation $v_1, v_2 \ldots v_n$. Assuming that the log/likelihood function $\ln L(\mathbf{w}|\mathbf{v})$ is differentiable and the ML estimator exists, it must satisfy the following partial differential equation known as the likelihood equation [37]

$$\frac{\partial \ln L\left(\mathbf{w}|\mathbf{v}\right)}{\partial w_k} = 0\,. \qquad (4.1.5)$$

The likelihood equation represents a necessary condition for the existence of the MLE estimate. An additional condition must also be satisfied to ensure that $\ln L(\mathbf{w}|\mathbf{v})$ is a maximum and not a minimum, since the first derivative cannot reveal this. To be a maximum, the shape of the log-likelihood function should be convex (it must represent a peak, not a valley) in the neighborhood of the estimate. This can be checked by calculating the second derivatives of the log-likelihoods and showing whether they are all negative [37]

$$\frac{\partial^2 \ln L\left(\mathbf{w}|\mathbf{v}\right)}{\partial w_k^2} < 0\,. \qquad (4.1.6)$$

In the above exposition it is assumed that the data is IID, but the method can be applied in a broader setting as long as it is possible to write the joint PDF $f(\mathbf{v}|\mathbf{w})$ and its parameter **w** has a finite dimension which does not depend on the sample size *n*.

For some cases, MLE can be found as an explicit function of the observed data **v**, but in many cases no closed-form solution to the maximization problem is known or available. In such cases MLE has to be found by numerical optimization methods. For some problems there may be many estimates that maximize likelihood and for some cases no maximum likelihood function exists at all.

4.2 ML estimator for Gaussian noise

Parameter vector for a normal family of distributions contains two elements $\mathbf{w} = \{\boldsymbol{\mu}, \mathbf{C}\}$. Likelihood function for the p-variate normal distribution (3.1.2) is

$$L(\boldsymbol{\mu}, \mathbf{C}|\mathbf{v}) = \prod_{k=1}^{n} \frac{1}{(2\pi)^{\frac{p}{2}}\sqrt{|\mathbf{C}|}} \exp\left[-\frac{1}{2}(\mathbf{v}_k - \boldsymbol{\mu})^T \mathbf{C}^{-1}(\mathbf{v}_k - \boldsymbol{\mu})\right]. \quad (4.2.1)$$

The previous equation can be simplified into the following form:

$$L(\boldsymbol{\mu}, \mathbf{C}|\mathbf{v}) = (2\pi)^{-\frac{np}{2}} |\mathbf{C}|^{-\frac{n}{2}} \exp\left[-\frac{1}{2}\sum_{k=1}^{n}(\mathbf{v}_k - \boldsymbol{\mu})^T \mathbf{C}^{-1}(\mathbf{v}_k - \boldsymbol{\mu})\right]. \quad (4.2.2)$$

Log-likelihood for the p-variate normal distribution is

$$\ln L(\boldsymbol{\mu}, \mathbf{C}|\mathbf{v}) = -\frac{np\ln(2\pi)}{2} - \frac{n}{2}\ln|\mathbf{C}| - \frac{1}{2}\sum_{k=1}^{n}(\mathbf{v}_k - \boldsymbol{\mu})^T \mathbf{C}^{-1}(\mathbf{v}_k - \boldsymbol{\mu}). \quad (4.2.3)$$

Maximum likelihood estimate of $\boldsymbol{\mu}$ is obtained by computing the derivate of log-likelihood with respect to $\boldsymbol{\mu}$. Using equation (11.6) from [38] we obtain

$$\frac{\partial \ln L(\boldsymbol{\mu}, \mathbf{C}|\mathbf{v})}{\partial \boldsymbol{\mu}} = -\frac{1}{2}\sum_{k=1}^{n}\left[-2\mathbf{C}^{-1}(\mathbf{v}_k - \boldsymbol{\mu})\right] = \mathbf{C}^{-1}\sum_{k=1}^{n}(\mathbf{v}_k - \boldsymbol{\mu}). \quad (4.2.4)$$

From the above we obtain that the ML estimator of the mean vector $\boldsymbol{\mu}$ is the sample mean vector

$$\hat{\boldsymbol{\mu}} = \frac{1}{n}\sum_{k=1}^{n}\mathbf{v}_k = \overline{\mathbf{v}}. \quad (4.2.5)$$

Using (11.7) and (11.8) from [38] we can compute the ML estimate for the covariance matrix $\mathbf{C}$

$$\frac{\partial \ln L(\boldsymbol{\mu}, \mathbf{C}|\mathbf{v})}{\partial \mathbf{C}} = -\frac{n}{2}\mathbf{C}^{-1} + \frac{1}{2}\mathbf{C}^{-1}\sum_{k=1}^{n}(\mathbf{v}_k - \boldsymbol{\mu})(\mathbf{v}_k - \boldsymbol{\mu})^T \mathbf{C}^{-1}. \quad (4.2.6)$$

Substituting $\boldsymbol{\mu} = \overline{\mathbf{v}}$, we obtain the ML estimator

$$\hat{\mathbf{C}} = \frac{\sum_{k=1}^{n} (\mathbf{v}_k - \overline{\mathbf{v}})(\mathbf{v}_k - \overline{\mathbf{v}})^T}{n} = \frac{\mathbf{S}}{n}, \tag{4.2.7}$$

where **S** is the scatter matrix

$$\mathbf{S} = \sum_{k=1}^{n} (\mathbf{v}_k - \overline{\mathbf{v}})(\mathbf{v}_k - \overline{\mathbf{v}})^T \in \mathbf{R}^{pxp}. \tag{4.2.8}$$

4.3 MLE estimator for Gaussian noise with an additive impulsive component

Development of robust detectors in the following chapters requires knowledge about the parameters of noise. Thus, we will find maximum likelihood estimators for additive Gaussian and impulsive noise parameters needed in the chapters below. Noise models derived in section 3.3 are used for the analysis.

For energy and matched filter detectors, it is sufficient to look at our noise as a one-dimensional process. The probability density function for a one- dimensional case was (3.3.37)

$$f_v(v) = \frac{\beta(1-c)}{(2\pi)^{\frac{1}{2}}\sigma} e^{\frac{-1}{2\sigma^2}\min\left(v^2, \eta_1^2\right)},$$

where β is the normalization coefficient (3.3.35), c is the probability of impulse, σ is standard deviation for the Gaussian process and η_1 is (3.3.36) the intersection point of the Gaussian and uniform distributions

$$\eta_1 = \sqrt{-2\sigma^2 \ln\left(\frac{c}{1-c}\frac{(2\pi)^{\frac{1}{2}}\sigma}{2b}\right)}.$$

To find the ML estimator for $\mathbf{w} = \{\sigma^2, c\}$, we must first find the likelihood function (4.1.3). In order to make our work easier we can assume to have n IID variables, thus likelihood can be written as

$$L(\sigma^2, c|\mathbf{v}) = \prod_{k=1}^{n} \frac{\beta(1-c)}{(2\pi)^{\frac{1}{2}}\sigma} e^{\frac{-1}{2\sigma^2}\min\left(v_k^2, \eta_1^2\right)}. \tag{4.3.1}$$

For the log-likelihood we obtain then

$$\ln L(\sigma^2, c|\mathbf{v}) = \sum_{k=1}^{n} \left[\ln \frac{\beta(1-c)}{(2\pi)^{\frac{1}{2}}} - \ln \sigma - \frac{1}{2\sigma^2} \min\left(v_k^2, \eta_1^2\right) \right]. \quad (4.3.2)$$

The above can be rewritten as

$$\ln L(\sigma^2, c|\mathbf{v}) = n \ln \frac{\beta(1-c)}{(2\pi)^{\frac{1}{2}}} - n \ln \sigma - \frac{1}{2\sigma^2} \sum_{M_1} v_k^2 + \sum_{M_2} \ln \left(\frac{c}{1-c} \frac{(2\pi)^{\frac{1}{2}} \sigma}{2b} \right), \quad (4.3.3)$$

where M_1 and M_2 are subsets that contain all noise samples that satisfy accordingly

$$\begin{aligned} M_1 &: v_k^2 < \eta_1^2 \\ M_2 &: v_k^2 \geq \eta_1^2 \end{aligned}. \quad (4.3.4)$$

The derivative of the log-likelihood function with respect to σ^2 is

$$\frac{\partial \ln L(\sigma^2, c|\mathbf{v})}{\partial \sigma^2} = -\frac{n}{2\sigma^2} + \frac{1}{2\sigma^4} \sum_{M_1} v_k^2 + \frac{n_2}{2\sigma^2}, \quad (4.3.5)$$

where n_2 is the number of elements in the subset M_2. Equating (4.3.5) to zero, the ML estimator for variance results

$$\hat{\sigma}^2 = \frac{1}{n_1} \sum_{M_1} v_k^2, \quad (4.3.6)$$

where n_1 is the number of elements in the subset M_1 and $n_1 + n_2 = n$. The result (4.3.6) shows that the ML estimator of variance can be calculated similarly to that in case of only Gaussian noise by (4.2.7), using only samples uncorrupted by the impulsive noise v_i.

Let us take the derivative of the log-likelihood function (4.3.3) with respect to c

$$\frac{\partial \ln L(\sigma^2, c|\mathbf{v})}{\partial c} = \frac{n}{c-1} - \frac{n_2}{c(c-1)}. \quad (4.3.7)$$

Equating (4.3.7) to zero yields the ML estimator for the probability of an impulse

$$\hat{c} = \frac{n_2}{n}. \tag{4.3.8}$$

The result is intuitively satisfying, as it shows that in order to estimate the probability of impulses c one must count how many noise samples n_2 out of all n samples cross the intersection point η_1 (3.3.36) between the Gaussian and the impulsive noise distributions. A problem with the estimate (4.3.8) lies in the fact that at small probability c the number of noise samples n must be very large in order to obtain a precise estimation.

Our future approach to a cyclostationary feature detector requires that input noise has to be handled as p-dimensional. To calculate the cyclic spectrum we need an estimate of the covariance matrix **C,** thus in the following sections we will find the ML estimator for this matrix, first in two-dimensions and then in a general p-dimensional case.

A starting point for the bi-variate analysis would be a general PDF (3.3.40) for the case $p = 2$ viewed only inside the square $-b \le v_{1,2} \le b$

$$f_v(\mathbf{v}) = \frac{\beta_2(1-c)}{\sqrt{2\pi\sigma^2}} \max\left[\frac{(1-c)e^{-\frac{v_1^2 - 2\rho v_1 v_2 + v_2^2}{2\sigma^2(1-\rho^2)}}}{\sqrt{2\pi\sigma^2(1-\rho^2)}}, \frac{c}{2b}\left(e^{-\frac{v_1^2}{2\sigma^2}} + e^{-\frac{v_2^2}{2\sigma^2}} \right) \right]$$

As the aim is to find the estimate of the covariance matrix **C**, we should rewrite (3.3.40)

$$f_v(\mathbf{v}) = \frac{\beta_2(1-c)}{\sqrt{2\pi\sigma^2}} \max\left[\frac{(1-c)e^{-\frac{1}{2}\mathbf{v}^T\mathbf{C}^{-1}\mathbf{v}}}{\sqrt{2\pi|\mathbf{C}|}}, \frac{c}{2b}\left(e^{-\frac{v_1^2}{2\sigma^2}} + e^{-\frac{v_2^2}{2\sigma^2}} \right) \right] \tag{4.3.9}$$

Having n IID observations of **v** we can write the likelihood function as

$$L(\mathbf{C}, c|\mathbf{v}) = \prod_{k=1}^{n} \frac{\beta_2(1-c)}{\sqrt{2\pi\sigma^2}} \cdot$$
$$\cdot \max\left[\frac{(1-c)e^{-\frac{1}{2}\mathbf{v}_k^T\mathbf{C}^{-1}\mathbf{v}_k}}{\sqrt{2\pi|\mathbf{C}|}}, \frac{c}{2b}\left(e^{-\frac{v_{k1}^2}{2\sigma^2}} + e^{-\frac{v_{k2}^2}{2\sigma^2}} \right) \right]. \tag{4.3.10}$$

Next, we move the common multiplier $(1\text{-}c)(2\pi|\mathbf{C}|)^{-½}$ out of brackets and then the multiplicand from the previous equation can be rewritten as

$$\frac{\beta_2(1-c)^2}{2\pi\sigma\sqrt{|\mathbf{C}|}}\max\left[e^{-\frac{1}{2}\mathbf{v}_k^{\mathrm{T}}\mathbf{C}^{-1}\mathbf{v}_k},\frac{c\sqrt{2\pi|\mathbf{C}|}}{(1-c)2b}\left(e^{-\frac{v_{k1}^2}{2\sigma^2}}+e^{-\frac{v_{k2}^2}{2\sigma^2}}\right)\right] \quad (4.3.11)$$

In view of the geometry of our PDF, we should be able to divide our problem into two separate parts – along v_1 and v_2 axes. First, we look along v_2 axis. By use of the identity $e^{\ln(x)} = x$, we obtain

$$\max\left[e^{-\frac{1}{2}\mathbf{v}_k^{\mathrm{T}}\mathbf{C}^{-1}\mathbf{v}_k},e^{\ln\frac{c\sqrt{2\pi|\mathbf{C}|}}{(1-c)2b}-\frac{v_{k1}^2}{2\sigma^2}}\right]=e^{-\frac{1}{2}\min\left[\mathbf{v}_k^{\mathrm{T}}\mathbf{C}^{-1}\mathbf{v}_k,-2\ln\frac{c\sqrt{2\pi|\mathbf{C}|}}{(1-c)2b}+\frac{v_{k1}^2}{\sigma^2}\right]}. \quad (4.3.12)$$

Thus, the likelihood (4.3.10) along the v_2 axis can now be written as

$$L(\mathbf{C},c|\mathbf{v})=\left[\frac{\beta_2(1-c)^2}{2\pi\sigma}\right]^n|\mathbf{C}|^{-\frac{n}{2}}\prod_{k=1}^{n}e^{-\frac{1}{2}\min\left[\mathbf{v}_k^{\mathrm{T}}\mathbf{C}^{-1}\mathbf{v}_k,-2\ln\frac{c\sqrt{2\pi}|\mathbf{C}|^{\frac{1}{2}}}{(1-c)2b}+\frac{v_{k1}^2}{\sigma^2}\right]}, \quad (4.3.13)$$

from which we can derive the log-likelihood

$$\ln L(\mathbf{C},c|\mathbf{v})=n\ln\left[\frac{\beta_2(1-c)^2}{2\pi\sigma}\right]-\frac{n}{2}\ln|\mathbf{C}|-$$
$$-\frac{1}{2}\sum_{k=1}^{n}\min\left[\mathbf{v}_k^{\mathrm{T}}\mathbf{C}^{-1}\mathbf{v}_k,-2\ln\frac{c\sqrt{2\pi}|\mathbf{C}|^{\frac{1}{2}}}{(1-c)2b}+\frac{v_{k1}^2}{\sigma^2}\right]. \quad (4.3.14)$$

Let us define again the two subsets M_1 and M_2 containing all noise samples that satisfy

$$M_1:\mathbf{v}_k^T\mathbf{C}^{-1}\mathbf{v}_k<-2\ln\frac{c\sqrt{2\pi}|\mathbf{C}|^{\frac{1}{2}}}{(1-c)2b}+\frac{v_{k1}^2}{\sigma^2}$$
$$M_2:\mathbf{v}_k^T\mathbf{C}^{-1}\mathbf{v}_k\geq-2\ln\frac{c\sqrt{2\pi}|\mathbf{C}|^{\frac{1}{2}}}{(1-c)2b}+\frac{v_{k1}^2}{\sigma^2} \quad (4.3.15)$$

and use them to rewrite the log-likelihood function

$$\ln L(\mathbf{C}, c|\mathbf{v}) = n \ln\left[\frac{\beta_2 (1-c)^2}{2\pi\sigma}\right] - \frac{n}{2}\ln|\mathbf{C}| - \\ -\frac{1}{2}\sum_{M_1} \mathbf{v}_k^T \mathbf{C}^{-1} \mathbf{v}_k + \sum_{M_2}\left[\ln\frac{c\sqrt{2\pi}|\mathbf{C}|^{\frac{1}{2}}}{(1-c)2b} - \frac{v_{k1}^2}{2\sigma^2}\right]. \quad (4.3.16)$$

The maximum likelihood estimate of **C** can now be found through the derivative of the obtained log-likelihood. It is useful to remind that the covariance matrix **C** is symmetric, so $\mathbf{C}^T = \mathbf{C}$ and the inverse of the transposed covariance matrix is the same as the transpose of the inverse matrix

$$\left(\mathbf{C}^T\right)^{-1} = \left(\mathbf{C}^{-1}\right)^T. \quad (4.3.17)$$

The two properties above show that in the case of symmetric matrix **C**

$$\mathbf{C}^{-T} = \left(\mathbf{C}^T\right)^{-1} = \left(\mathbf{C}^{-1}\right)^T = \mathbf{C}^{-1}. \quad (4.3.18)$$

According to [39], the derivative of the matrix determinant with respect to the same matrix is

$$\frac{\partial|\mathbf{C}|}{\partial\mathbf{C}} = |\mathbf{C}|\left(\mathbf{C}^{-1}\right)^T = |\mathbf{C}|\mathbf{C}^{-1}. \quad (4.3.19)$$

We are now ready to find the derivate of the log-likelihood (4.3.16). Using (4.3.19) we can find the derivative of the second summand of log-likelihood as

$$\frac{\partial}{\partial\mathbf{C}}\left(-\frac{n}{2}\ln|\mathbf{C}|\right) = -\frac{n}{2}\frac{1}{|\mathbf{C}|}|\mathbf{C}|\mathbf{C}^{-1} = -\frac{n}{2}\mathbf{C}^{-1}. \quad (4.3.20)$$

Equation (55) from [39] and (4.3.18) can be used to find the derivatives

$$\frac{\partial}{\partial\mathbf{C}}\left(\mathbf{v}_k^T\mathbf{C}^{-1}\mathbf{v}_k\right) = -\mathbf{C}^{-T}\mathbf{v}_k\mathbf{v}_k^T\mathbf{C}^{-T} = -\mathbf{C}^{-1}\mathbf{v}_k\mathbf{v}_k^T\mathbf{C}^{-1} \quad (4.3.21)$$

and

$$\frac{\partial}{\partial \mathbf{C}}\left[\ln\frac{c\sqrt{2\pi}|\mathbf{C}|^{\frac{1}{2}}}{(1-c)2b}-\frac{v_{k1}^2}{2\sigma^2}\right]=\frac{1}{2}\mathbf{C}^{-1}. \tag{4.3.22}$$

Derivative of the log-likelihood function in respect to the covariance matrix **C** along the v_2 axis then is

$$\frac{\partial \ln L(\mathbf{C},c|\mathbf{v})}{\partial \mathbf{C}}=-\frac{n}{2}\mathbf{C}^{-1}+\frac{1}{2}\sum_{M_1}\mathbf{C}^{-1}\mathbf{v}_k\mathbf{v}_k^T\mathbf{C}^{-1}+\frac{1}{2}\sum_{M_2}\mathbf{C}^{-1}, \tag{4.3.23}$$

from which we obtain the ML estimator

$$\hat{\mathbf{C}}=\frac{1}{n_1}\sum_{M_1}\mathbf{v}_k\mathbf{v}_k^T. \tag{4.3.24}$$

Next, let us take the derivative of the log-likelihood function (4.3.16) with respect to the impulse probability c

$$\frac{\partial \ln L(\mathbf{C},c|\mathbf{v})}{\partial c}=\frac{2n}{c-1}-\frac{n_2}{c(c-1)}. \tag{4.3.25}$$

Equating (4.3.25) to zero yields the ML estimator for the probability of impulse

$$\hat{c}=\frac{n_2}{2n}. \tag{4.3.26}$$

A value reduced by one half to be compared with the one dimensional case (4.3.8) results from looking only at the direction of v_2 axes. If we have the probability of impulse c, then about half times the first element of the vector is corrupted by the impulsive noise and the other half times the second element is the one that is corrupted.

To obtain a complete solution to (4.3.11), we also need to analyze this equation along the v_1 axes in a similar way as we did before along the v_2 axes. First, as another half of the ML estimator of the impulse probability c, this gives

$$\hat{c}=\frac{n_2}{2n}+\frac{n_2}{2n}=\frac{n_2}{n}, \tag{4.3.27}$$

it is now compatible with the result (4.3.8) for p =1.

Secondly, if values of $\boldsymbol{v}_k$ are also limited along the v_1 axis

$$\begin{aligned} M_1 &: \mathbf{v}_k^T \mathbf{C}^{-1} \mathbf{v}_k < -2 \ln \frac{c\sqrt{2\pi}|\mathbf{C}|^{\frac{1}{2}}}{(1-c)2b} + \frac{v_{k2}^2}{\sigma^2} \\ M_2 &: \mathbf{v}_k^T \mathbf{C}^{-1} \mathbf{v}_k \geq -2 \ln \frac{c\sqrt{2\pi}|\mathbf{C}|^{\frac{1}{2}}}{(1-c)2b} + \frac{v_{k2}^2}{\sigma^2} \end{aligned} \tag{4.3.28}$$

Then the final result shows again that the ML estimator of the covariance matrix can be calculated in the same way as in the case of only Gaussian noise by (4.2.7) using only samples uncorrupted by the impulsive noise v_i. To determine which noise sample belongs to the subset M_1 and which does not, we need to find intersection borders between the Gaussian and the impulsive region

$$\begin{cases} \mathbf{v}_k^T \mathbf{C}^{-1} \mathbf{v}_k = -2 \ln \frac{c\sqrt{2\pi}|\mathbf{C}|^{\frac{1}{2}}}{(1-c)2b} + \frac{v_{k1}^2}{\sigma^2} \\ \mathbf{v}_k^T \mathbf{C}^{-1} \mathbf{v}_k = -2 \ln \frac{c\sqrt{2\pi}|\mathbf{C}|^{\frac{1}{2}}}{(1-c)2b} + \frac{v_{k2}^2}{\sigma^2} \end{cases} . \tag{4.3.29}$$

First, we find this border again along the v_2 axis by solving the first equation in (4.3.29) that results in

$$-|\mathbf{C}| \ln \left[\frac{c\sqrt{2\pi}|\mathbf{C}|^{\frac{1}{2}}}{(1-c)2b} \right] = \rho^2 v_1^2 - 2\rho v_1 v_2 + v_2^2 . \tag{4.3.30}$$

Expressing in (6.11) v_2 as roots of the quadratic equation, we obtain

$$v_2 = \rho v_1 \pm \sqrt{-2|\mathbf{C}| \ln \left[\frac{c\sqrt{2\pi}|\mathbf{C}|^{\frac{1}{2}}}{(1-c)2b} \right]} . \tag{4.3.31}$$

Comparing the result with (3.3.36) shows that in the case of zero correlation both one- and two-dimensional cases have exactly the same intersection point as expected. Also, in case $p = 2$, intersection borders are a straight line. When we solve the second equation of (4.3.29), we obtain a similar result for variable v_1.

Thus, noise samples $\mathbf{v} = (v_1,v_2)$ should be used to estimate the covariance of Gaussian noise according to (4.3.24) if

$$(v_2 < \rho v_1 + \eta_2) \wedge (v_2 > \rho v_1 - \eta_2) \wedge (v_1 < \rho v_2 + \eta_2) \wedge (v_1 > \rho v_2 - \eta_2), \quad (4.3.32)$$

where

$$\eta_2 = \sqrt{-2|\mathbf{C}| \ln \left[\frac{c\sqrt{2\pi}|\mathbf{C}|^{\frac{1}{2}}}{(1-c)2b} \right]}. \quad (4.3.33)$$

Derived intersection border (4.3.31) between the impulsive and the Gaussian noise is depicted in Figure 4.1.

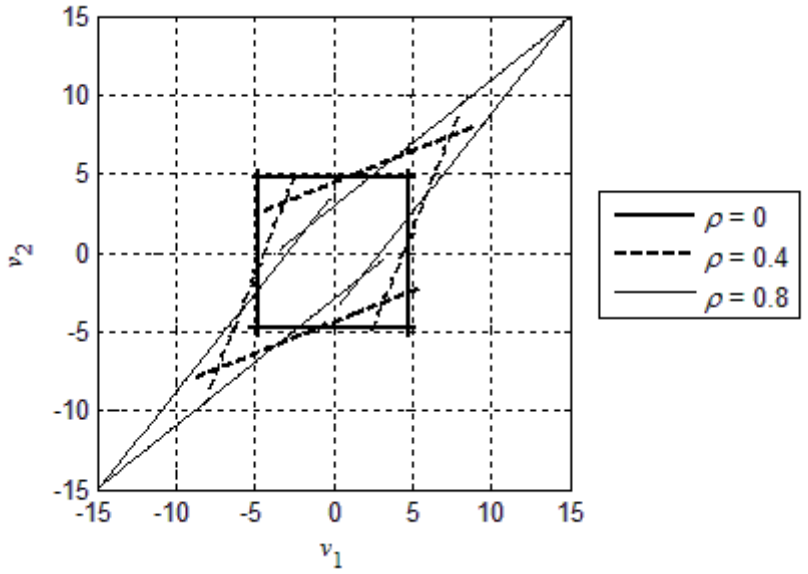

Fig. 4.1 Intersection borders ($c = 10^{-3}$, $b = 128$, $\sigma = 1$)

The figure shows that the intersection border between the Gaussian and the impulsive noise forms a rhombus which at zero correlation decays into a square. If vector $\mathbf{v} = (v_1,v_2)$ falls inside the rhombus, we can assume that we deal with the Gaussian noise and if it falls outside it, then we have impulsive noise included.

In order to induce the PDF for a general p dimensional case, we should have some idea about a look of 3D PDF of the sum of impulsive and Gaussian noise. According to (3.2.3), a three-dimensional impulsive noise is

$$f_{v_i}(v_1,v_2,v_3)=\left(\frac{c}{2b}\right)^3+\left(\frac{c}{2b}\right)^2(1-c)\sum_{k=1}^{3}\delta(v_k)+\frac{c(1-c)^2}{2b}\cdot$$
$$\cdot\left[\delta(v_1)\delta(v_2)+\delta(v_1)\delta(v_3)+\delta(v_2)\delta(v_3)\right]+(1-c)^3\delta(v_1)\delta(v_2)\delta(v_3) \quad (4.3.34)$$

A three-dimensional Gaussian PDF in the form suitable for the calculation of 3D convolution is as follows:

$$f_g(\mathbf{v})=\frac{e^{-\frac{v_1^2(1-\rho_{23}^2)+v_2^2(1-\rho_{13}^2)+v_3^2(1-\rho_{12}^2)+2\left[v_1v_2(\rho_{23}\rho_{13}-\rho_{12})+v_1v_3(\rho_{12}\rho_{23}-\rho_{13})+v_2v_3(\rho_{13}\rho_{12}-\rho_{23})\right]}{2\sigma^2\left[1-\rho_{12}^2-\rho_{23}^2-\rho_{13}^2+2\rho_{12}\rho_{23}\rho_{13}\right]}}}{(2\pi)^{\frac{3}{2}}\sigma^3\sqrt{1-\rho_{12}^2-\rho_{23}^2-\rho_{13}^2+2\rho_{12}\rho_{23}\rho_{13}}}. \quad (4.3.35)$$

Now we can calculate the PDF of the three-dimensional sum by the convolution

$$f_v(v_1,v_2,v_3)=\int_{-\infty}^{\infty}\int_{-\infty}^{\infty}\int_{-\infty}^{\infty}f_g(v_1,v_2,v_3)f_i(v_1-\tau_1,v_2-\tau_2,v_3-\tau_3)d\tau_1d\tau_2d\tau_3 \quad .(4.3.36)$$

Actual computation of such an integral is a time-consuming task, therefore we should seek ways to make things simpler. First, we can leave out two first summands in the impulsive noise PDF because both of them have very small influence. Last summand in the impulsive noise PDF provides the PDF of the Gaussian noise multiplied by the coefficient $(1-c)^3$, as it did in one- and two-dimensional cases before. Thus, it is necessary to calculate only the convolution of the Gaussian and the third summand of the impulsive noise PDF. The third summand is composed of three parts, each of them similar to other parts but centered on another axis. Thus, we can only calculate the result for one of the three and other ones can be found through switching of variables, as we did already in the 2D case. Thus, the convolution to be calculated is as follows:

$$\frac{c(1-c)^2}{2b(2\pi)^{\frac{3}{2}}\sigma^3\sqrt{1-\rho_{12}^2-\rho_{23}^2-\rho_{13}^2+2\rho_{12}\rho_{23}\rho_{13}}}\cdot$$
$$\cdot\int_{-\infty}^{\infty}\int_{-\infty}^{\infty}\int_{-\infty}^{\infty}e^{-\frac{v_1^2(1-\rho_{23}^2)+v_2^2(1-\rho_{13}^2)+v_3^2(1-\rho_{12}^2)+2\left[v_1v_2(\rho_{23}\rho_{13}-\rho_{12})+v_1v_3(\rho_{12}\rho_{23}-\rho_{13})+v_2v_3(\rho_{13}\rho_{12}-\rho_{23})\right]}{2\sigma^2\left[1-\rho_{12}^2-\rho_{23}^2-\rho_{13}^2+2\rho_{12}\rho_{23}\rho_{13}\right]}}\cdot \quad (4.3.37)$$
$$\cdot\delta(v_1-\tau_1)\delta(v_2-\tau_2)d\tau_1d\tau_2d\tau_3$$

The part under the integrals can be rearranged similarly to the two-dimensional case in Chapter 3

$$\int_{-\infty}^{\infty} e^{-\frac{\tau_3^2(1-\rho_{12}^2)}{2\sigma^2\left[1-\rho_{12}^2-\rho_{23}^2-\rho_{13}^2+2\rho_{12}\rho_{23}\rho_{13}\right]}} \int_{-\infty}^{\infty} e^{-\frac{\tau_2^2(1-\rho_{13}^2)+2\tau_2\tau_3(\rho_{13}\rho_{12}-\rho_{23})}{2\sigma^2\left[1-\rho_{12}^2-\rho_{23}^2-\rho_{13}^2+2\rho_{12}\rho_{23}\rho_{13}\right]}} \delta(v_2-\tau_2)\cdot$$
$$\cdot \int_{-\infty}^{\infty} e^{-\frac{\tau_1^2(1-\rho_{23}^2)+2\left[\tau_1\tau_3(\rho_{12}\rho_{23}-\rho_{13})+\tau_1\tau_2(\rho_{23}\rho_{13}-\rho_{12})\right]}{2\sigma^2\left[1-\rho_{12}^2-\rho_{23}^2-\rho_{13}^2+2\rho_{12}\rho_{23}\rho_{13}\right]}} \delta(v_1-\tau_1)d\tau_1 d\tau_2 d\tau_3 \quad .(4.3.38)$$

The innermost integral equals

$$\int_{-\infty}^{\infty} e^{-\frac{\tau_1^2(1-\rho_{23}^2)+2\left[\tau_1\tau_3(\rho_{12}\rho_{23}-\rho_{13})+\tau_1\tau_2(\rho_{23}\rho_{13}-\rho_{12})\right]}{2\sigma^2\left[1-\rho_{12}^2-\rho_{23}^2-\rho_{13}^2+2\rho_{12}\rho_{23}\rho_{13}\right]}} \delta(v_1-\tau_1)d\tau_1 =$$
$$e^{-\frac{v_1^2(1-\rho_{23}^2)+v_1 2\left[\tau_3(\rho_{12}\rho_{23}-\rho_{13})+\tau_2(\rho_{23}\rho_{13}-\rho_{12})\right]}{2\sigma^2\left[1-\rho_{12}^2-\rho_{23}^2-\rho_{13}^2+2\rho_{12}\rho_{23}\rho_{13}\right]}} = \quad (4.3.39)$$
$$= e^{-\frac{v_1^2(1-\rho_{23}^2)}{2\sigma^2\left[1-\rho_{12}^2-\rho_{23}^2-\rho_{13}^2+2\rho_{12}\rho_{23}\rho_{13}\right]}} e^{-\frac{v_1 2\left[\tau_3(\rho_{12}\rho_{23}-\rho_{13})+\tau_2(\rho_{23}\rho_{13}-\rho_{12})\right]}{2\sigma^2\left[1-\rho_{12}^2-\rho_{23}^2-\rho_{13}^2+2\rho_{12}\rho_{23}\rho_{13}\right]}}$$

Taking the second integral, we obtain

$$\int_{-\infty}^{\infty} e^{-\frac{\tau_2^2(1-\rho_{13}^2)+2\tau_2\tau_3(\rho_{13}\rho_{12}-\rho_{23})}{2\sigma^2\left[1-\rho_{12}^2-\rho_{23}^2-\rho_{13}^2+2\rho_{12}\rho_{23}\rho_{13}\right]}} \delta(v_2-\tau_2) e^{-\frac{v_1 2\left[\tau_3(\rho_{12}\rho_{23}-\rho_{13})+\tau_2(\rho_{23}\rho_{13}-\rho_{12})\right]}{2\sigma^2\left[1-\rho_{12}^2-\rho_{23}^2-\rho_{13}^2+2\rho_{12}\rho_{23}\rho_{13}\right]}} d\tau_2 =$$
$$= e^{-\frac{v_1 2\tau_3(\rho_{12}\rho_{23}-\rho_{13})}{2\sigma^2\left[1-\rho_{12}^2-\rho_{23}^2-\rho_{13}^2+2\rho_{12}\rho_{23}\rho_{13}\right]}} \int_{-\infty}^{\infty} e^{-\frac{\tau_2^2(1-\rho_{13}^2)+2\tau_2\tau_3(\rho_{13}\rho_{12}-\rho_{23})+v_1 2\tau_2(\rho_{23}\rho_{13}-\rho_{12})}{2\sigma^2\left[1-\rho_{12}^2-\rho_{23}^2-\rho_{13}^2+2\rho_{12}\rho_{23}\rho_{13}\right]}} \quad (4.3.40)$$
$$\delta(v_2-\tau_2)d\tau_2 = e^{-\frac{v_2^2(1-\rho_{13}^2)+v_1 2v_2(\rho_{23}\rho_{13}-\rho_{12})}{2\sigma^2\left[1-\rho_{12}^2-\rho_{23}^2-\rho_{13}^2+2\rho_{12}\rho_{23}\rho_{13}\right]}} e^{-\frac{\tau_3 2\left[v_1(\rho_{12}\rho_{23}-\rho_{13})+v_2(\rho_{13}\rho_{12}-\rho_{23})\right]}{2\sigma^2\left[1-\rho_{12}^2-\rho_{23}^2-\rho_{13}^2+2\rho_{12}\rho_{23}\rho_{13}\right]}}$$

Then we can calculate the third, the final integral:

$$\int_{-\infty}^{\infty} e^{-\frac{\tau_3^2(1-\rho_{12}^2)+\tau_3 2\left[v_1(\rho_{12}\rho_{23}-\rho_{13})+v_2(\rho_{13}\rho_{12}-\rho_{23})\right]}{2\sigma^2\left[1-\rho_{12}^2-\rho_{23}^2-\rho_{13}^2+2\rho_{12}\rho_{23}\rho_{13}\right]}} d\tau_3 =$$
$$= \sqrt{\frac{2\pi\sigma^2\left[1-\rho_{12}^2-\rho_{23}^2-\rho_{13}^2+2\rho_{12}\rho_{23}\rho_{13}\right]}{4(1-\rho_{12}^2)}} \cdot e^{\frac{\left[v_1(\rho_{12}\rho_{23}-\rho_{13})+v_2(\rho_{13}\rho_{12}-\rho_{23})\right]^2}{(1-\rho_{12}^2)2\sigma^2\left[1-\rho_{12}^2-\rho_{23}^2-\rho_{13}^2+2\rho_{12}\rho_{23}\rho_{13}\right]}} \cdot (4.3.41)$$
$$\cdot \operatorname{erf}\left(\frac{(1-\rho_{12}^2)\tau_3 + v_1(\rho_{12}\rho_{23}-\rho_{13}) + v_2(\rho_{13}\rho_{12}-\rho_{23})}{\sigma\sqrt{(1-\rho_{12}^2)2\left[1-\rho_{12}^2-\rho_{23}^2-\rho_{13}^2+2\rho_{12}\rho_{23}\rho_{13}\right]}} \right)\Bigg|_{-\infty}^{\infty}$$

If the interval of the last integral really were [-∞,∞], then the error function in (4.3.41) would decay into constant 2. But in our case the interval is limited [v_3+b, v_3-b]. We have now reached a complete solution for (4.3.37)

$$\frac{c(1-c)^2 e^{-\frac{(1-\rho_{12}^2)\left[v_1^2(1-\rho_{23}^2)+v_2^2(1-\rho_{13}^2)+2v_1v_2(\rho_{23}\rho_{13}-\rho_{12})\right]+\left[v_1(\rho_{12}\rho_{23}-\rho_{13})+v_2(\rho_{13}\rho_{12}-\rho_{23})\right]^2}{(1-\rho_{12}^2)2\sigma^2\left[1-\rho_{12}^2-\rho_{23}^2-\rho_{13}^2+2\rho_{12}\rho_{23}\rho_{13}\right]}}}{4\pi\sigma^2\sqrt{1-\rho_{12}^2}\,2b}\cdot$$

$$\cdot\left[\operatorname{erf}\left(\frac{(1-\rho_{12}^2)(v_3+b)+v_1(\rho_{12}\rho_{23}-\rho_{13})+v_2(\rho_{13}\rho_{12}-\rho_{23})}{\sigma\sqrt{(1-\rho_{12}^2)2\left[1-\rho_{12}^2-\rho_{23}^2-\rho_{13}^2+2\rho_{12}\rho_{23}\rho_{13}\right]}}\right)-\right. \qquad (4.3.42)$$

$$\left.-\operatorname{erf}\left(\frac{(1-\rho_{12}^2)(v_3-b)+v_1(\rho_{12}\rho_{23}-\rho_{13})+v_2(\rho_{13}\rho_{12}-\rho_{23})}{\sigma\sqrt{(1-\rho_{12}^2)2\left[1-\rho_{12}^2-\rho_{23}^2-\rho_{13}^2+2\rho_{12}\rho_{23}\rho_{13}\right]}}\right)\right]$$

To find the intersection border between the Gaussian bell and the impulsive "wall", we need to solve

$$\frac{c(1-c)^3 e^{-\frac{v_1^2(1-\rho_{23}^2)+v_2^2(1-\rho_{13}^2)+v_3^2(1-\rho_{12}^2)+2\left[v_1v_2(\rho_{23}\rho_{13}-\rho_{12})+v_1v_3(\rho_{12}\rho_{23}-\rho_{13})+v_2v_3(\rho_{13}\rho_{12}-\rho_{23})\right]}{2\sigma^2\left[1-\rho_{12}^2-\rho_{23}^2-\rho_{13}^2+2\rho_{12}\rho_{23}\rho_{13}\right]}}}{(2\pi)^{\frac{3}{2}}\sigma^3\sqrt{1-\rho_{12}^2-\rho_{23}^2-\rho_{13}^2+2\rho_{12}\rho_{23}\rho_{13}}}=$$

$$=\frac{c(1-c)^2 e^{-\frac{(1-\rho_{12}^2)\left[v_1^2(1-\rho_{23}^2)+v_2^2(1-\rho_{13}^2)+2v_1v_2(\rho_{23}\rho_{13}-\rho_{12})\right]+\left[v_1(\rho_{12}\rho_{23}-\rho_{13})+v_2(\rho_{13}\rho_{12}-\rho_{23})\right]^2}{(1-\rho_{12}^2)2\sigma^2\left[1-\rho_{12}^2-\rho_{23}^2-\rho_{13}^2+2\rho_{12}\rho_{23}\rho_{13}\right]}}}{2\pi\sigma^2\sqrt{1-\rho_{12}^2}\,2b} \qquad (4.3.43)$$

After canceling out common terms in (4.3.43), we take logarithm from both sides of the equation and the result is

$$\begin{aligned}
&(1-\rho_{12}^2)\left[v_1^2(1-\rho_{23}^2)+v_2^2(1-\rho_{13}^2)+2v_1v_2(\rho_{23}\rho_{13}-\rho_{12})\right]+\\
&+(1-\rho_{12}^2)\left\{v_3^2(1-\rho_{12}^2)+2v_3\left[v_1(\rho_{12}\rho_{23}-\rho_{13})+v_2(\rho_{13}\rho_{12}-\rho_{23})\right]\right\}=\\
&=(1-\rho_{12}^2)\left[v_1^2(1-\rho_{23}^2)+v_2^2(1-\rho_{13}^2)+2v_1v_2(\rho_{23}\rho_{13}-\rho_{12})\right]+\\
&+\left[v_1(\rho_{12}\rho_{23}-\rho_{13})+v_2(\rho_{13}\rho_{12}-\rho_{23})\right]^2- \qquad (4.3.44)\\
&-2\sigma^2\left[1-\rho_{12}^2-\rho_{23}^2-\rho_{13}^2+2\rho_{12}\rho_{23}\rho_{13}\right]\cdot\\
&\cdot\ln\frac{c\sqrt{2\pi}\sigma\sqrt{1-\rho_{12}^2-\rho_{23}^2-\rho_{13}^2+2\rho_{12}\rho_{23}\rho_{13}}}{(1-c)\sqrt{1-\rho_{12}^2}\,2b}
\end{aligned}$$

The first summand from both sides of the equation is the same, so we can cancel them out. The result is a quadratic equation of variable v_3

$$
\begin{aligned}
& v_3^2(1-\rho_{12}^2)^2 + v_3 2(1-\rho_{12}^2)\left[v_1(\rho_{12}\rho_{23}-\rho_{13}) + v_2(\rho_{13}\rho_{12}-\rho_{23})\right] + \\
& + 2\sigma^2\left[1-\rho_{12}^2-\rho_{23}^2-\rho_{13}^2+2\rho_{12}\rho_{23}\rho_{13}\right]\cdot \\
& \cdot \ln\frac{c\sqrt{2\pi}\sigma\sqrt{1-\rho_{12}^2-\rho_{23}^2-\rho_{13}^2+2\rho_{12}\rho_{23}\rho_{13}}}{(1-c)\sqrt{1-\rho_{12}^2}\,2b} - \\
& -\left[v_1(\rho_{12}\rho_{23}-\rho_{13}) + v_2(\rho_{13}\rho_{12}-\rho_{23})\right]^2
\end{aligned}
\quad . \qquad (4.3.45)
$$

Expressing in it v_3 as the roots of a quadratic equation, we obtain limits for it as

$$
v_3 = \frac{v_1(\rho_{12}\rho_{23}-\rho_{13}) + v_2(\rho_{13}\rho_{12}-\rho_{23})}{\rho_{12}^2-1} \pm \eta_{33}, \qquad (4.3.46)
$$

where

$$
\eta_{33} = \sqrt{\frac{-2|\mathbf{C}|^{\frac{1}{2}}}{(1-\rho_{12}^2)^2}\ln\frac{c\sqrt{2\pi}|\mathbf{C}|^{\frac{1}{2}}}{(1-c)\sqrt{1-\rho_{12}^2}\,2b}} \qquad (4.3.47)
$$

Thus, the threshold value is independent of dimension p and when the variables are uncorrelated $\rho_{12} = \rho_{23} = \rho_{13} = 0$, the result (4.3.47) is the same as for a one- or two-dimensional case. Equation (4.3.46) states that the values of variable v_3 must lie between two planes. Similarly, we can find interception borders for variables v_1 and v_2. Thus, to be used to estimate covariance, our three-dimensional sample vector $\mathbf{v} = \{v_1, v_2, v_3\}$ must satisfy all the following conditions:

$$\begin{cases} v_1 < \dfrac{v_2(\rho_{23}\rho_{13}-\rho_{12})+v_3(\rho_{12}\rho_{23}-\rho_{13})}{\rho_{23}^2-1}+\eta_{31} \\ v_1 > \dfrac{v_2(\rho_{23}\rho_{13}-\rho_{12})+v_3(\rho_{12}\rho_{23}-\rho_{13})}{\rho_{23}^2-1}-\eta_{31} \\ v_2 < \dfrac{v_1(\rho_{23}\rho_{13}-\rho_{12})+v_3(\rho_{13}\rho_{12}-\rho_{23})}{\rho_{13}^2-1}+\eta_{32} \\ v_2 > \dfrac{v_1(\rho_{23}\rho_{13}-\rho_{12})+v_3(\rho_{13}\rho_{12}-\rho_{23})}{\rho_{13}^2-1}-\eta_{32} \\ v_3 < \dfrac{v_1(\rho_{12}\rho_{23}-\rho_{13})+v_2(\rho_{13}\rho_{12}-\rho_{23})}{\rho_{12}^2-1}+\eta_{33} \\ v_3 > \dfrac{v_1(\rho_{12}\rho_{23}-\rho_{13})+v_2(\rho_{13}\rho_{12}-\rho_{23})}{\rho_{12}^2-1}-\eta_{33} \end{cases}, \qquad (4.3.48)$$

where η_{31} and η_{32} are calculated as η_{31} (4.3.47) only (1- ρ_{12}^2) is replaced with (1- ρ_{23}^2) or (1- ρ_{13}^2) accordingly.

We could continue in a similar fashion with higher dimensions. Results would be p-1 dimensional hyper plains forming 2p sided hyper rhomboids. But it is clear that computing those results will be increasingly complex. In general, an ML estimator of the p-dimensional covariance matrix is

$$\hat{\mathbf{C}} = \frac{1}{n_1}\sum_{M_1}\mathbf{v}_k\mathbf{v}_k^T, \qquad (4.3.49)$$

where $\mathbf{v}_k$ is the sample vector with length p and subset M_1 contains samples not contaminated by the impulsive noise. In a special case when noise samples are uncorrelated, the p-dimensional intersection border is p-dimensional hyper cube with a side length of $2\sqrt{\eta_1}$. The ML estimator for impulse probability is always the same as in a one-dimensional case (4.3.8).

5 Performance of known detection algorithms in the presence of impulsive noise

This chapter presents the results of computer simulations to show that all three main types of detectors described in Chapter 2 are sensitive to the impulsive noise.

Three common detection algorithms for cognitive radio were described in Chapter 2. This chapter studies the effects of the impulsive noise v_i (3.2.2) on those detectors.

To estimate the influence of impulsive noise v_i on different detectors, computer simulation is used. First, operating curves of the simulated receiver for different values of impulsive noise parameters are found and the results are compared. The comparison involves also the theoretical ROC for a case of Gaussian noise only. The following set of parameters was used for all the following simulations: length of input waveform n = 2080 samples; primary user signal modeled as a sine wave; signal-to-(Gaussian)-noise ratio -23dB and the amplitude of impulsive noise limited by b = 128. Thus, all the results are comparable with the theoretical curves in Figure 2.13.

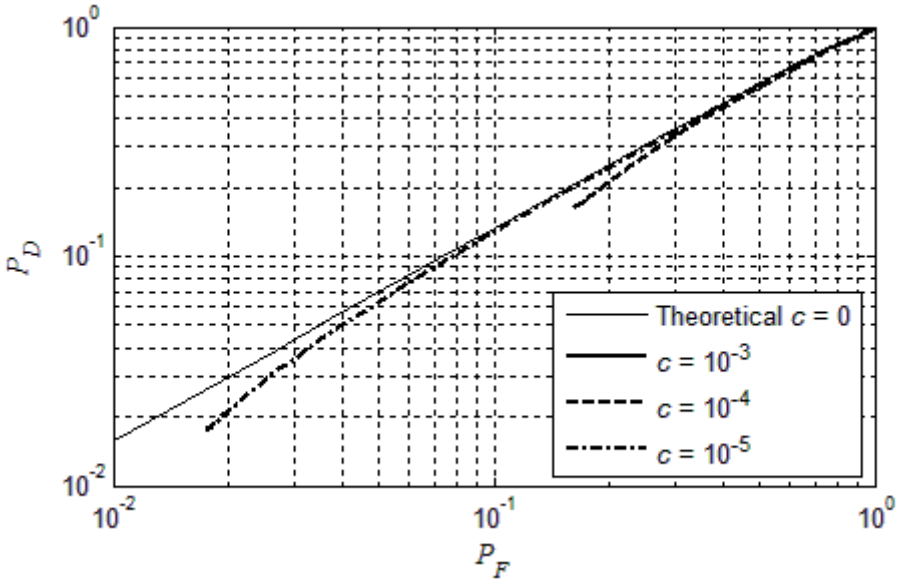

Fig. 5.1 Experimental ROC of an energy detector

The thick line in the figure is the theoretical ROC of the time domain energy detector (2.1.1) with the length n = 128, noise power σ_v^2 = 1 and signal-to-noise ratio SNR = -10dB. Experimental curves in the same figure are obtained when the impulsive noise has a maximum value of b = 64 with different probabilities of

impulse c. As expected, an additional impulsive noise decreases the performance of the energy detectors. The smaller the impulse probability c, the more close is the experimental ROC to the theoretical value.

The second measure of performance is the experimental curve of $P_F = f(c)$ for the fixed threshold value λ. The threshold value λ is computed for a fixed false detection probability P_F in the case of Gaussian noise only. In Figure 5.2 this *a priori* probability is marked with a dashed line.

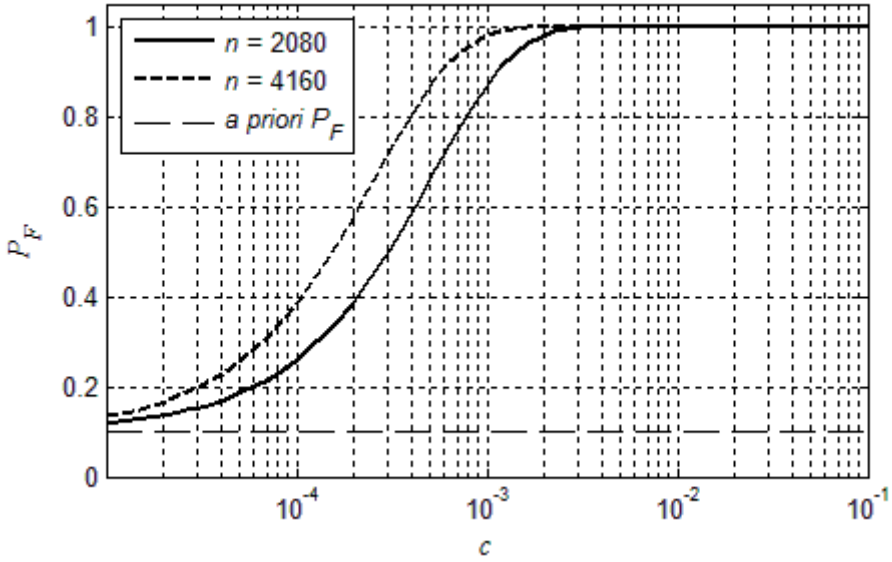

Fig. 5.2 Experimental curve PF = f(c) for a time domain energy detector

Results in Figure 5.2 show that a false detection rate climbs quickly with the probability of an impulse. Comparison of the two curves in the figure shows that the longer the detector, the more sensitive it is to the impulsive noise. Figure 5.3 shows that the rate of false detection increases monotonically with the length n. When the length of the receiver grows, the probability of an impulse appearing inside the input waveform increases also.

Simulations indicated that the value of b had almost no effect on the shape of the curves presented. As we assumed b to be much larger than the variance of Gaussian noise, the appearance of a noise impulse always causes false detection. There is little difference if the decision threshold λ is surpassed with the decision statistic two or ten times. In both cases false detection is still made.

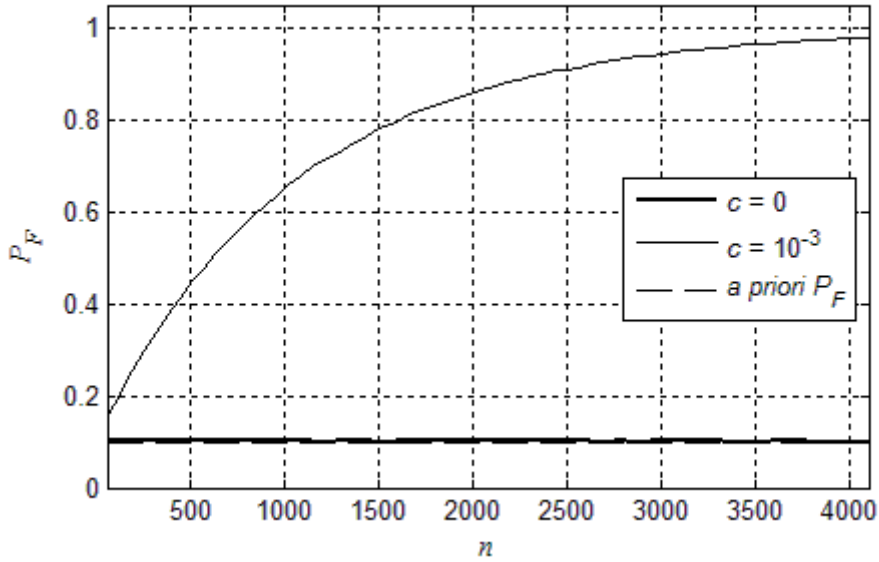

Fig. 5.3 Probability of false detection as a function of detector length

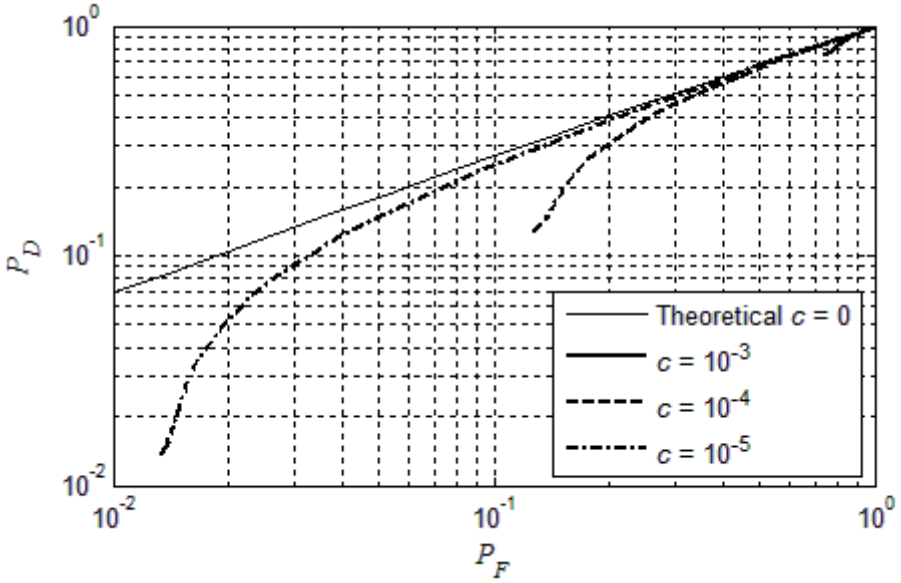

Fig. 5.4 Experimental ROC of a cyclostationary detector

The next three figures illustrate the performance of a cyclostationary detector under the influence of impulsive noise. As illustrated, the influence of impulsive noise is only slightly smaller than it was in the case of an energy detector where all of the energy from impulses is consumed in decision statistic Λ. A cyclostationary detector spreads this energy all along the spectrum, thus only part of it influences

the decision statistic. This is the reason why the influence of impulsive noise on a cyclostationary detector is lower.

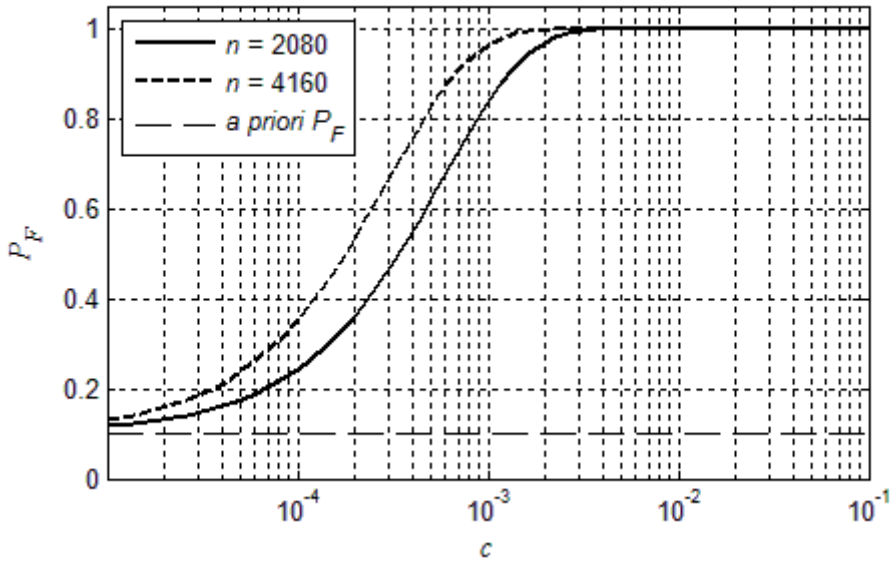

Fig. 5.5 Experimental curve PF = f(c) for a cyclostationary detector

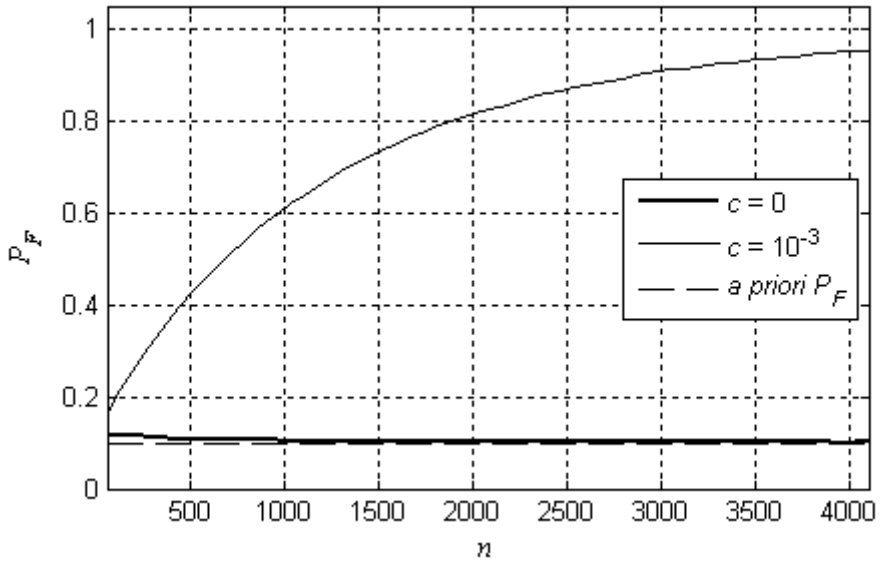

Fig. 5.6 Probability of false detection as a function of detector length

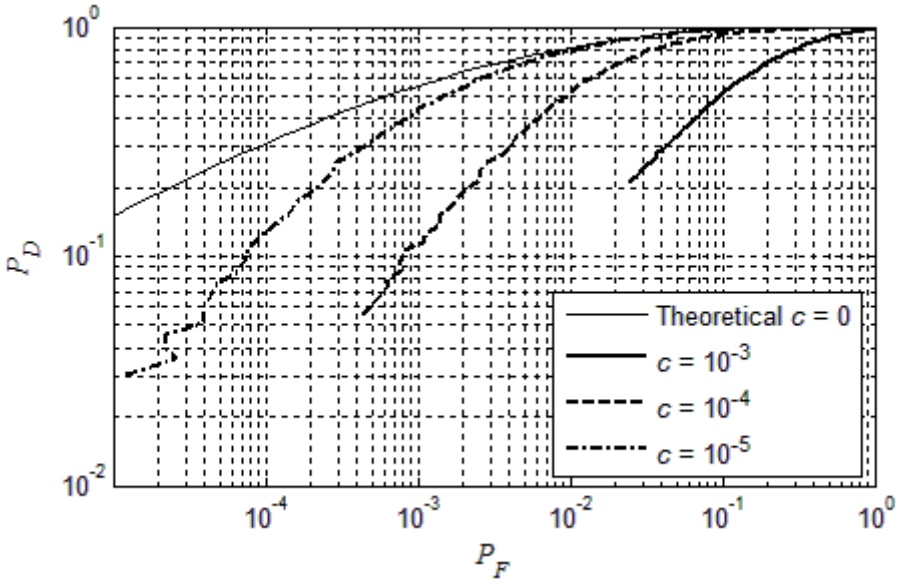

Fig. 5.7 Experimental ROC of a matched filter

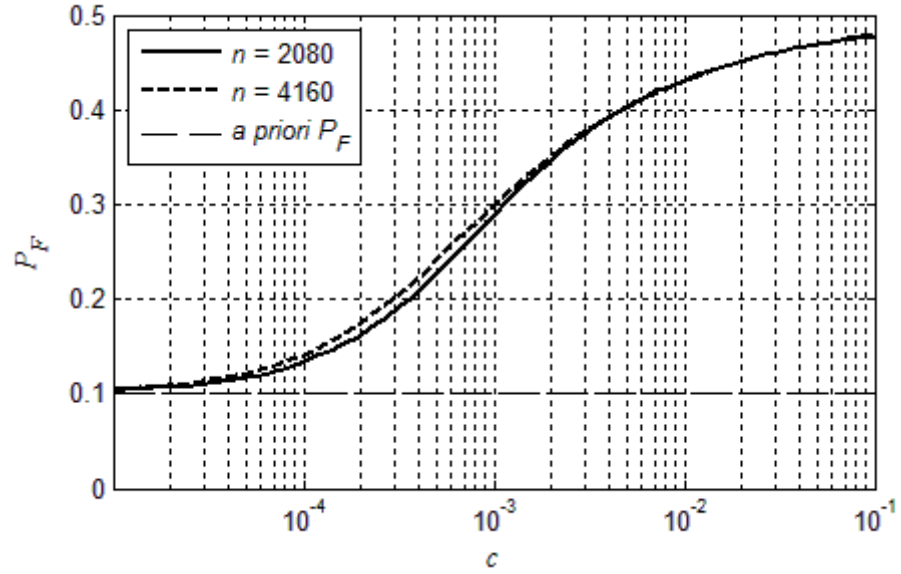

Fig. 5.8 Experimental curve PF = f(c) for a matched filter

The last three figures clearly show that the influence of impulsive noise on a matched filter is smaller than on previously viewed filters. Figures 5.8 and 5.9 illustrate an interesting fact that at first the probability of false detection P_F increases with a length n of the filter. The reason here is basically the same as described under the energy detector. On the other hand, the longer the filter, the more it averages the impulsive noise out. As shown clearly in Figure 5.9, those

two effects tend to cancel each other out, thus from some point further an increase of n has almost no influence on a false detection probability P_F. For this reason, both curves in Figure 5.8 are almost totally covering each other.

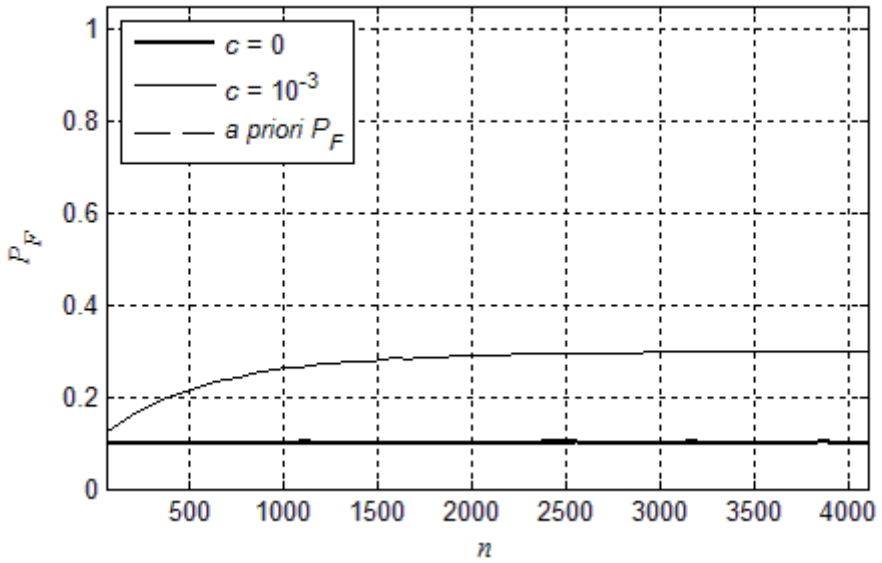

Fig. 5.9 Probability of false detection as a function of matched filter length

In conclusion, first, it is clear that impulsive noise has a strong influence on the detectors based on the assumption of Gaussian background noise. An energy detector is the most sensitive and a matched filter is less sensitive. This is explained by the circumstance that the more we know about the received signal, the easier it is to distinguish noise from this signal. In all three cases, false detection rate increases together with the probability of impulse appearance c.

When the signal-to-noise ratio decreases, then in order to maintain the probability of correct detection, detectors must use more samples for decision making. Increase in a detector length n increases its sensitivity to the impulsive noise. This means that the more sensitive the detector meant to work in Gaussian background, the more sensitive it is also to the influence of the impulsive noise.

Results obtained here clearly suggest that robust detectors are needed to make cognitive radio work under the influence of impulsive noise. Therefore, in the next chapter robust detectors for all three cases are introduced.

6 Robust detectors

In this chapter three robust detectors are derived. A robust energy detector is a robust analogue to a regular energy detector. A robust feature detector is similarly a robust analogue to a cyclostationary detector and a robust detector for a known primary signal can be viewed as a robust matched filter.

The noise model and estimators for its parameters used in this chapter were derived in Chapters 3 and 4. Some results from Chapter 2 are used to derive a robust feature detector.

Derivation of each detector is divided largely into two parts. The first part is detector derivation and the second contains asymptotic performance analysis. Obtained results are compared against regular detectors and between robust detectors themselves.

The results obtained are also compared with other robust detection methods proposed in various articles.

Author's contribution in this chapter is as follows. The first subdivision is based on the work presented in articles [45], [72] and [73]. Author's main contribution: derivation of expressions for parameters n and λ, derivation of a theoretical expression for the ROC curve and computer simulations, including comparison with other robust detection methods.

The whole second subdivision of this chapter is author's work, both theoretical analysis and computer simulations.

In the third subdivision, computer simulations and comparison with Huber sense Neyman-Pearson detector is purely the contribution of the author. Naturally comparison of detectors and the conclusion were written by the author.

6.1 Robust Energy Detector

Robust energy detector considers the problem of detecting the presence of primary users in a given frequency band without any prior knowledge of primary transmissions and in the presence of impulsive noise. The detection problem we need to solve is similar to (2.1)

$$\begin{aligned} H_0 &: x(t) = v(t) \\ H_1 &: x(t) = s(t) + v(t) \end{aligned} . \qquad (6.1.1)$$

Received waveform $x(t)$ may be noise $v(t)$ only or it may also consist of a signal of interest $s(t)$. The detector has to decide which of the hypotheses is more likely given the received waveform $x(t)$. We assume that noise $v(t)$ comprises a sum of zero mean additive white Gaussian noise v_g and additional impulsive noise component v_i (3.3.1)

$$v(t) = v_g(t) + v_i(t) .$$

The impulsive noise component v_i is assumed to obey PDF (3.2.2)

$$f_i(v) = \frac{c}{2b} + (1-c)\delta(v) .$$

As explained in section 3.3, noise $v(t)$ can be modeled as consisting of two components with the largest component determining the outcome entirely at each time instant (3.3.30)

$$v(t) = v_g(t) + v_i(t) \approx \max[v_g(t), v_i(t)] .$$

As we have no prior information about the primary signal $s(t)$, we regard it as a noise with a standard deviation σ_s . Let us also denote a common variance as

$$\sigma_l^2 = \begin{cases} \sigma^2 & l = 0 \\ \sigma^2 + \sigma_s^2 & l = 1 \end{cases}, \qquad (6.1.2)$$

where σ is the standard deviation of Gaussian noise. With this notation we can express the conditional PDFs corresponding to our two hypotheses H_l for l = 0,1. From (3.3.32) we obtain

$$f_x(x|H_l) = \begin{cases} \beta_l \max\left(\frac{1-c}{\sqrt{2\pi}\sigma_l} e^{\frac{-x^2}{2\sigma_l^2}}, \frac{c}{2b} \right), & |x| < b \\ 0, & \text{otherwise} \end{cases} \qquad (6.1.3)$$

The normalization factors β_l can be found by solving (3.3.34) for previous

$$\int_{-b}^{b} f_x(x|H_l)dx = 1, \qquad (6.1.4)$$

this results in

$$\beta = \left[(1-c)\,\mathrm{erf}\left(\frac{\eta_{1l}}{\sqrt{2\sigma_l^2}} \right) + c\left(1 - \frac{\eta_{1l}}{b} \right) \right]^{-1} \tag{6.1.5}$$

where

$$\eta_{1l} = \sqrt{-2\sigma_l^2 \ln\left(\frac{c}{1-c} \frac{\sqrt{2\pi}\sigma_l}{2b} \right)} \tag{6.1.6}$$

is the intersection point of the Gaussian and uniform distributions [66]. In practice the value of β_l is very close to 1. As shown in section 3.3, we can give PDF (6.1.3) of x in the interval [-b,b] a more convenient form (3.3.37) for further derivation

$$f_x(x|H_l) = \frac{\beta_l(1-c)}{\sqrt{2\pi}\sigma_l} e^{\frac{-1}{2\sigma_l^2}\min\left(x^2,\eta_{1l}^2\right)} \quad . \tag{6.1.7}$$

As focus is on the energy detector here, we need the probability density function of variable $Y = X^2$ as in Chapter 2. Our PDF is not Gaussian anymore but a mixture of Gaussian and impulsive instead. Using equations (2.1.6)-(2.1.8) we obtain

$$f_y(y|H_l) = \frac{\beta_l(1-c)}{\sqrt{2\pi y}\sigma_l} e^{\frac{-1}{2\sigma_l^2}\min\left(y,\eta_{1l}^2\right)} \quad . \tag{6.1.8}$$

Suppose that we have made n observations of the variable y and have collected these observations into a vector **y**. Also, assume that the observations at different time instances are statistically independent of each other. Then the joint probability density function (4.1.2) is a product of the individual probability densities

$$f_{\mathbf{y}}(\mathbf{y}|H_l) = \prod_{k=1}^{n} f(y_k|H_l), \quad l = 0,1 \,. \tag{6.1.9}$$

Likelihood ratio for the above hypothesis (6.1.1) reads

$$L(y) = \prod_{k=1}^{n} \frac{\beta_1\sigma_0}{\beta_0\sigma_1} \frac{e^{\frac{-1}{2\sigma_1^2}\min\left(y_k,\eta_{11}^2\right)}}{e^{\frac{-1}{2\sigma_0^2}\min\left(y_k,\eta_{10}^2\right)}} . \tag{6.1.10}$$

Taking the logarithm of both sides of (6.1.10) and simplifying it, we readily obtain the log-likelihood ratio

$$\ln L = n \ln\left(\frac{\beta_1 \sigma_0}{\beta_0 \sigma_1}\right) - \frac{1}{2\sigma_1^2}\sum_{k=1}^{n} \min(y_k, \eta_{11}^2) + \frac{1}{2\sigma_0^2}\sum_{k=1}^{n} \min(y_k, \eta_{10}^2). \qquad (6.1.11)$$

Our detector thus needs to decide in favor of H_1 if the log-likelihood ratio is larger than threshold. Otherwise, the hypothesis H_0 is selected.

If there is no impulsive noise, i.e. $c \to 0$, we have

$$\lim_{c\to 0} \eta_{1l} = -2\sigma_l^2 \ln(0) = \infty$$
$$\lim_{c\to 0} \beta_l = 1$$
$$\lim_{c\to 0}\left[n \ln\left(\frac{\beta_1 \sigma_0}{\beta_0 \sigma_1}\right)\right] = n \ln\left(\frac{\sigma_0}{\sigma_1}\right)$$

and the test is reduced to an ordinary energy detector [66].

Parameter η_l (6.1.6) depends on the Gaussian noise variance σ^2, signal variance σ_s^2 and the impulse probability c. Those parameters may not be known in advance and if they are not, they must be estimated from the input signal $x(t)$. In some applications it is known for certain that during some time the primary user is silent and during some other time it is working. The question is about all the other times. In Chapter 4 we have derived maximum likelihood estimators for σ (4.3.6) and c (4.3.8). Now we only need an MLE estimator for signal variance σ_s^2. If the signal of interest $s(t)$ is also present, then the log-likelihood function (4.3.3) can be written as

$$\ln L(\sigma_s^2|\mathbf{x}) = n \ln \frac{\beta(1-c)}{\sqrt{2\pi}} - n \ln \sqrt{\sigma_s^2 + \sigma^2} - \\ - \frac{1}{2(\sigma_s^2 + \sigma^2)}\left(\sum_{M_1} x_k^2 + n_2 \eta_{11}^2\right). \qquad (6.1.12)$$

The derivative of the log-likelihood function with respect to σ_s^2 equals

$$\frac{\partial \ln L(\sigma_s^2|\mathbf{x})}{\partial \sigma_s^2} = \frac{-n}{2(\sigma_s^2 + \sigma^2)} + \frac{1}{2(\sigma_s^2 + \sigma^2)^2}\sum_{M_1} x_k^2 + \frac{n_2}{2(\sigma_s^2 + \sigma^2)}. \qquad (6.1.13)$$

Equating (6.1.13) to zero results in an estimator

$$\hat{\sigma}_s^2 = \frac{1}{n_1}\sum_{M_1} x_k^2 - \hat{\sigma}^2 . \qquad (6.1.14)$$

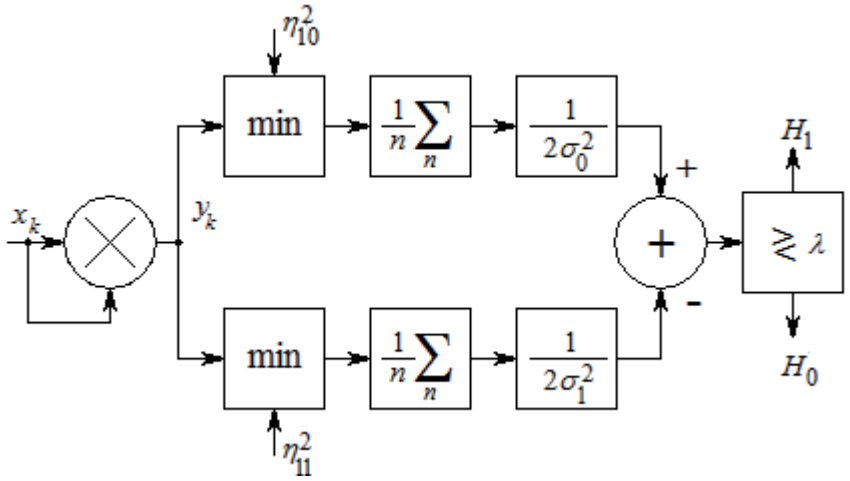

Fig. 6.1 Proposed structure of a robust energy detector

Next we perform the asymptotic analysis of the detector at large *n*. We first note that the detector computes if

$$\frac{1}{2\sigma_0^2}\frac{1}{n}\sum_{k=1}^{n}\min(y_k,\eta_{10}^2) - \frac{1}{2\sigma_1^2}\frac{1}{n}\sum_{k=1}^{n}\min(y_k,\eta_{11}^2) > \lambda , \quad (6.1.15)$$

where

$$\lambda = \frac{\ln L}{n} - \ln\left(\frac{\beta_1\sigma_0}{\beta_0\sigma_1}\right). \qquad (6.1.16)$$

We thus need to find a difference between weighted arithmetical means of saturated variables and compare the result to a threshold in order to perform the detections. Proposed structure of a robust energy detector (6.1.15) is depicted in Figure 6.1.

Let us concentrate on the variables under the summations in (6.1.15) and define a new variable z_q as

$$z_q = g(y) = \min(y,\eta_{1q}^2), \quad q = 0,1. \qquad (6.1.17)$$

The function $g(y)$ is saturation nonlinearity. The probability density function of the output of $z_q = g(y)$ is given by [40]

$$f_z(z_k) = \left.\frac{f_y(y)}{\frac{dz_k}{dy}}\right|_{y=g^{-1}(z_k)} . \qquad (6.1.18)$$

We need to investigate this PDF for four different cases – for both sums in (6.1.15), q = 0,1 for both hypotheses l = 0,1. Substituting (6.1.8) into the above for those four cases, we obtain the following four PDFs:

$$\begin{aligned} f_z(z_0|H_0) = {} & \frac{\beta_0(1-c)}{\sqrt{2\pi z_0}\sigma_0} e^{-\frac{z_0}{2\sigma_0^2}} \left[\Theta(z_0) - \Theta(z_0 - \eta_{10}^2)\right] + \\ & + c\beta_0 \left(1 - \frac{\eta_{10}}{b}\right) \delta(z_0 - \eta_{10}^2) \end{aligned} \qquad (6.1.19)$$

if l = 0 and q = 0,

$$\begin{aligned} f_z(z_1|H_0) = {} & \frac{\beta_0(1-c)}{\sqrt{2\pi z_1}\sigma_0} e^{-\frac{z_1}{2\sigma_0^2}} \left[\Theta(z_1) - \Theta(z_1 - \eta_{10}^2)\right] + \\ & + \frac{c\beta_0}{2b\sqrt{z_1}} \left[\Theta(z_1 - \eta_{10}^2) - \Theta(z_1 - \eta_{11}^2)\right] + c\beta_0 \left(1 - \frac{\eta_{11}}{b}\right) \delta(z_1 - \eta_{11}^2) \end{aligned} \qquad (6.1.20)$$

if l = 0 and q = 1,

$$\begin{aligned} f_z(z_0|H_1) = {} & \frac{\beta_1(1-c)}{\sqrt{2\pi z_0}\sigma_1} e^{-\frac{z_0}{2\sigma_1^2}} \left[\Theta(z_0) - \Theta(z_0 - \eta_{10}^2)\right] + \\ & + \left[\beta_1(1-c) \left(\operatorname{erf} \frac{\eta_{11}}{\sqrt{2}\sigma_1} - \operatorname{erf} \frac{\eta_{10}}{\sqrt{2}\sigma_1} \right) + \right. \\ & \left. + c\beta_1 \left(1 - \frac{\eta_{11}}{b}\right) \right] \delta(z_0 - \eta_{10}^2) \end{aligned} \qquad (6.1.21)$$

if l = 1 and q = 0 and

$$\begin{aligned} f_z(z_1|H_1) = {} & \frac{\beta_1(1-c)}{\sqrt{2\pi z_1}\sigma_1} e^{-\frac{z_1}{2\sigma_1^2}} \left[\Theta(z_1) - \Theta(z_1 - \eta_{11}^2)\right] + \\ & + c\beta_1 \left(1 - \frac{\eta_{11}}{b}\right) \delta(z_1 - \eta_{11}^2) \end{aligned} \qquad (6.1.22)$$

if $l = 1$ and $q = 1$. The cases are illustrated in Figures 6.2 and 6.3.

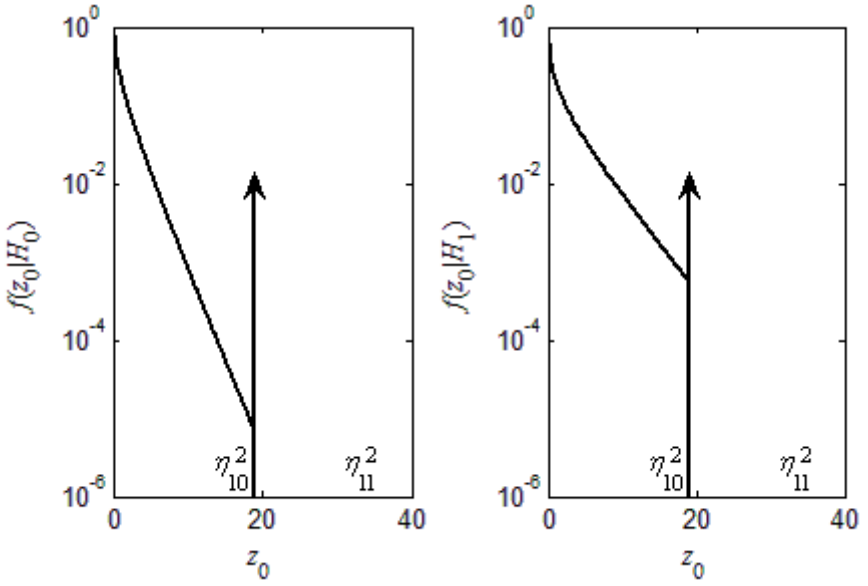

Fig. 6.2 Conditional PDFs for variable z_0

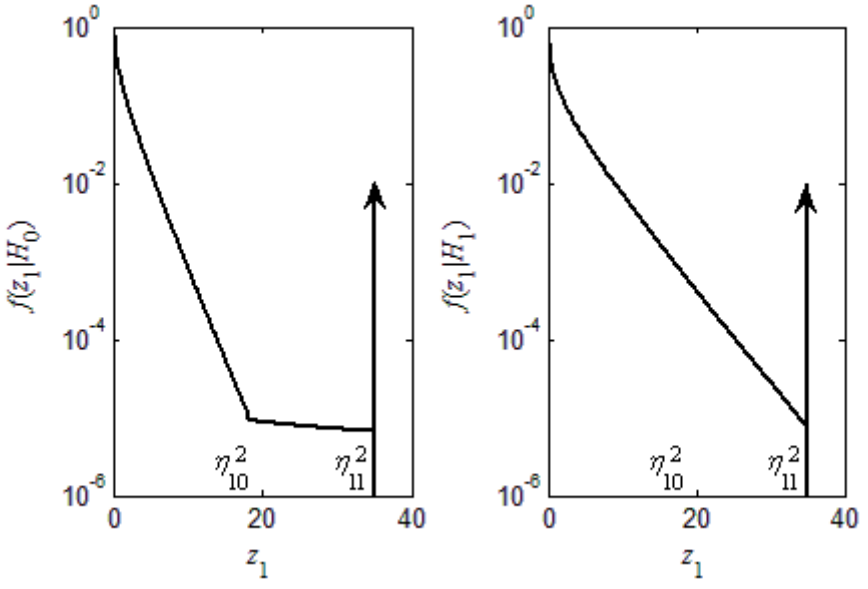

Fig. 6.3 Conditional PDFs for variable z_1

Combining results (6.1.19)-(6.1.22) we can reach a somewhat more compact common expression covering all the four cases as

$$f_z(z_q|H_l) = \frac{\beta_l(1-c)}{\sqrt{2\pi z_q}\sigma_l} e^{-\frac{z_q}{2\sigma_l^2}} \left[\Theta(z_q) - \Theta(z_q - \eta_{1m_1}^2)\right] + \\ + \frac{m_2 c\beta_0}{2b\sqrt{z_q}} \left[\Theta(z_q - \eta_{10}^2) - \Theta(z_q - \eta_{11}^2)\right] + \delta(z_q - \eta_q)\theta_{q,l} \quad , (6.1.23)$$

where functions tail

$$\theta_{q,l} = \beta_l \left[(1-c) m_3 \left(\operatorname{erf} \frac{\eta_{11}}{\sqrt{2}\sigma_1} - \operatorname{erf} \frac{\eta_{10}}{\sqrt{2}\sigma_1} \right) + c\left(1 - \frac{\eta_{1m_4}}{b}\right) \right] \quad (6.1.24)$$

and variables m_1- m_4 are defined as follows: $m_1 = 1$, if $l = 1$ and $q = 1$ and is zero otherwise, $m_2 = 1$, if $l = 0$ and $q = 1$ and is zero otherwise, $m_3 = 1$, if $l = 1$ and $q = 0$ and is zero otherwise, $m_4 = 0$, if $l = 0$ and $q = 0$ and is one otherwise.

This distribution (6.1.23) has the mean

$$\mathbf{E}\left[z_q|H_l\right] = \beta_l(1-c)\left[\sigma_l^2 \operatorname{erf}\left(\frac{\eta_{1m_1}}{\sqrt{2}\sigma_l} \right) - \right. \\ \left. - \sqrt{\frac{2}{\pi}}\sigma_l \eta_{1m_1} e^{-\frac{\eta_{1m_1}^2}{2\sigma_l^2}} \right] + \frac{m_2 c\beta_0}{3b}\left(\eta_{11}^3 - \eta_{10}^3\right) + \eta_{1q}^2 \theta_{q,l} \quad (6.1.25)$$

and the second moment

$$\mathbf{E}\left[z_q^2|H_l\right] = \beta_l(1-c)\left[3\sigma_l^4 \operatorname{erf}\left(\frac{\eta_{1m_1}}{\sqrt{2}\sigma_l} \right) - \right. \\ \left. - \sqrt{\frac{2}{\pi}}\sigma_l \eta_{1m_1} e^{-\frac{\eta_{1m_1}^2}{2\sigma_l^2}} \left(\eta_{1m_1}^2 + 3\sigma_l^2\right) \right] + \frac{m_2 c\beta_0}{5b}\left(\eta_{11}^5 - \eta_{10}^5\right) + \eta_{1q}^4 \theta_{q,l} \quad .(6.1.26)$$

The cross correlation between z_0 and z_1 is perfect if $z_1 < \eta_{10}^2$ and in this case $\mathbf{E}[z_0 z_1|H_l] = \mathbf{E}[z_0^2|H_l]$. This happens with a probability

$$\mathrm{P}\left(z_1 < \eta_0\right) = \int_0^{\eta_{10}^2} f_z\left(z_1|H_l\right) dz_1 = \beta_l(1-c) \operatorname{erf}\left(\frac{\eta_{10}}{\sqrt{2}\sigma_l} \right). \quad (6.1.27)$$

If $z_1 > \eta_{10}^2$, then $z_0 = \eta_{10}^2$ and hence $\mathbf{E}[z_0 z_1|H_l] = \eta_{10}^2 \mathbf{E}_{z1 > \eta_{10}^2}[z_1|H_l]$, where $\mathbf{E}_{z1 > \eta_{10}^2}[z_1|H_l]$ is the mean of z_1 above η_{10}^2. This happens with a probability $1 - \mathrm{P}(z_1 < \eta_{10}^2)$ and the cross correlation therefore is

$$\begin{aligned}\mathrm{E}\left[z_0 z_1|H_l\right] &= \mathrm{P}\left(z_1 < \eta_{10}^2\right)\mathrm{E}\left[z_0^2|H_l\right] + \\ &+ \left[1 - \mathrm{P}\left(z_1 < \eta_{10}^2\right)\right]\eta_{10}^2 \mathbf{E}_{z_1 > \eta_{10}^2}\left[z_1|H_l\right]\end{aligned}. \tag{6.1.28}$$

Examining (6.1.15) we see that to proceed we need the moments of the variable

$$w = \frac{1}{2\sigma_0^2} z_0 - \frac{1}{2\sigma_1^2} z_1 . \tag{6.1.29}$$

The mean on w is

$$\mathbf{E}\left[w|H_l\right] = \frac{\mathbf{E}\left[z_0|H_l\right]}{2\sigma_0^2} - \frac{\mathbf{E}\left[z_1|H_l\right]}{2\sigma_1^2} \tag{6.1.30}$$

and its second moment equals

$$\mathbf{E}\left[w^2|H_l\right] = \frac{\mathbf{E}\left[z_0^2|H_l\right]}{4\sigma_0^4} - \frac{2\mathbf{E}\left[z_0 z_1|H_l\right]}{4\sigma_0^2\sigma_1^2} + \frac{\mathbf{E}\left[z_1^2|H_l\right]}{4\sigma_1^4}. \tag{6.1.31}$$

The variance of w is equal to

$$\sigma_{H_l}^2 = \mathrm{E}\left[w^2|H_l\right] - \mathrm{E}^2\left[w|H_l\right]. \tag{6.1.32}$$

Let us now note that according to (6.1.15), the detector computes sample average of n IID random variables w. According to the central limit theorem [17, 40], the distribution of such a sum approaches Gaussian with mean $\mathbf{E}[w|H_l]$ (6.1.30) and variance

$$\frac{\sigma_{H_l}^2}{n}, l = 0,1 \tag{6.1.33}$$

when n increases, independent of the shape of the original distribution of the variables w. Therefore, we can evaluate the probability of false detection for large value of n

$$P_F = \int_{\lambda}^{+\infty} f_{\Lambda}\left(\Lambda \middle| H_0\right) dw = \frac{1}{2}\operatorname{erfc}\left\{\frac{\left(\lambda - \mathrm{E}\left[w \middle| H_0\right]\right)\sqrt{n}}{\sqrt{2}\sigma_{H_0}}\right\}. \qquad (6.1.34)$$

Accordingly, the probability of correct detection is

$$P_D = \int_{\lambda}^{+\infty} f_{\Lambda}\left(\Lambda \middle| H_1\right) dw = \frac{1}{2}\operatorname{erfc}\left\{\frac{\left(\lambda - \mathrm{E}\left[w \middle| H_1\right]\right)\sqrt{n}}{\sqrt{2}\sigma_{H_1}}\right\}. \qquad (6.1.35)$$

The threshold λ and required number of samples n to reach a given point P_D and P_F can be found by solving a system of equations formed from (6.1.34) and (6.1.35)

$$\begin{cases} \sqrt{2}\sigma_{H_0} \operatorname{erfc}^{-1}(2P_F) = \left(\lambda - \mathrm{E}\left[w \middle| H_0\right]\right)\sqrt{n} \\ \sqrt{2}\sigma_{H_1} \operatorname{erfc}^{-1}(2P_D) = \left(\lambda - \mathrm{E}\left[w \middle| H_1\right]\right)\sqrt{n} \end{cases}. \qquad (6.1.36)$$

Solving the system for n and λ we obtain that in order to reach the operating point (P_F, P_D), we need

$$\begin{cases} n = 2\left\{\dfrac{\sigma_{H_1} \operatorname{erfc}^{-1}(2P_D) - \sigma_{H_0} \operatorname{erfc}^{-1}(2P_F)}{\mathbf{E}\left[w \middle| H_0\right] - \mathbf{E}\left[w \middle| H_1\right]}\right\}^2 \\ \lambda = \dfrac{\sigma_{H_1} \operatorname{erfc}^{-1}(2P_D)\mathbf{E}\left[w \middle| H_0\right] - \sigma_{H_0} \operatorname{erfc}^{-1}(2P_F)\mathbf{E}\left[w \middle| H_1\right]}{\sigma_{H_1} \operatorname{erfc}^{-1}(2P_D) - \sigma_{H_0} \operatorname{erfc}^{-1}(2P_F)} \end{cases}. \qquad (6.1.37)$$

Equations (6.1.34) and (6.1.35) can also be used to express the theoretical ROC curve for the robust energy detector

$$P_D = \frac{1}{2}\operatorname{erfc}\left\{\frac{\sigma_{H_0}}{\sigma_{H_1}} \operatorname{erfc}^{-1}(2P_F) + \frac{\sqrt{n}\left(\mathrm{E}\left[w \middle| H_0\right] - \mathrm{E}\left[w \middle| H_1\right]\right)}{\sqrt{2}\sigma_{H_1}}\right\}. \qquad (6.1.38)$$

First, we investigate how many samples the detector should involve for our analysis to apply. In the simulation example we have used the following parameters to compute the probability of false detection P_F: $\sigma = 1$, $\sigma_s = 2$, $c = 0.01$ and $b = 100$. Figure 6.4 shows that with $n = 5$, the simulation and theory vaguely remember each other. The situation improves when we increase the number of samples. Already with $n = 30$, the theoretical curve and simulation dots are rather

close to each other. Here we note that $n = 30$ is much smaller than actual values of n found from (6.1.37) for cognitive radio applications.

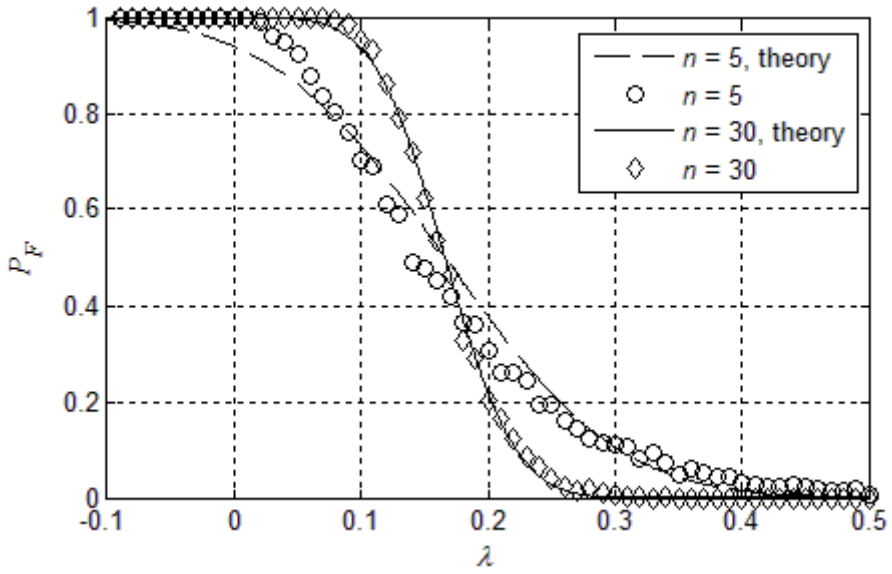

Fig. 6.4 Probability of false detection

Figure 6.5 presents the probability of missed detection $P_M = 1 - P_D$ as the function of SNR. Solid and dashed lines are theoretical results for $c = 10^{-3}$ and $c = 10^{-7}$, accordingly. Circles and squares are representing corresponding experimental results. A fast decrease of the curves can be observed as SNR increases, furthermore, the intensity of impulsive noise c does not influence the result much.

Figure 6.6 depicts the dependence of probability of false alarm on the number of samples n for the ordinary energy detector if there is no impulsive noise (dashed line). It also shows the curves corresponding to the ordinary energy detector (solid thin line) and the proposed robust detector (solid bold line) in the presence of impulsive noise with intensity $c = 0.001$. As shown, the proposed detector operates at those conditions almost as well as the ordinary energy detector in Gaussian noise. A small rise occurs in false detection probability in the robust detector when n increases. The reason is that we actually do not remove all impulsive noise but only the part above the intersection border η_1.

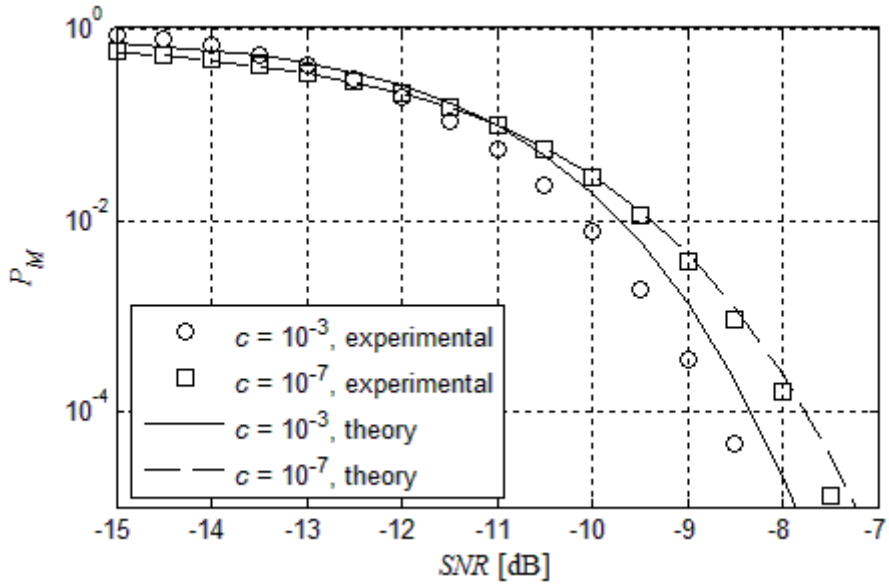

Fig. 6.5 Probability of missed detection as a function of SNR

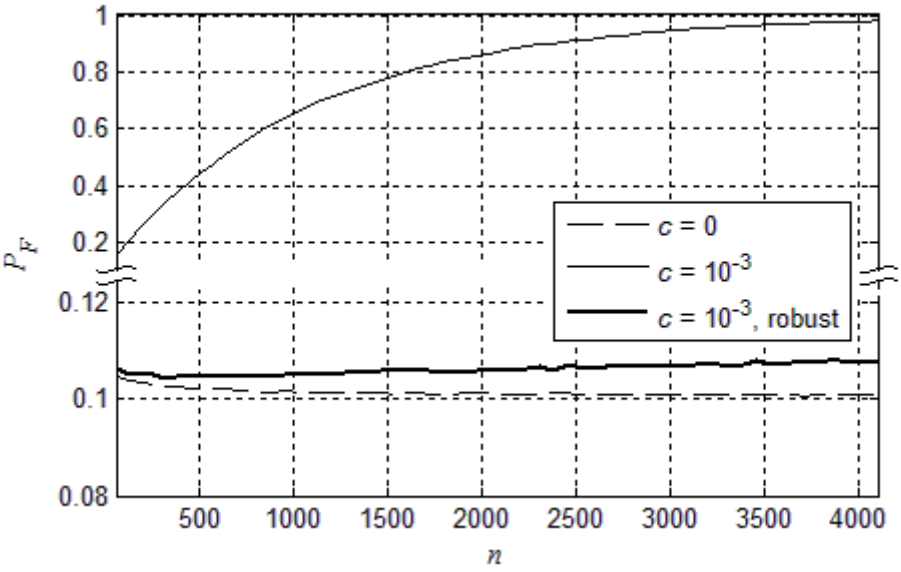

Fig. 6.6 Probability of false alarm as a function of n

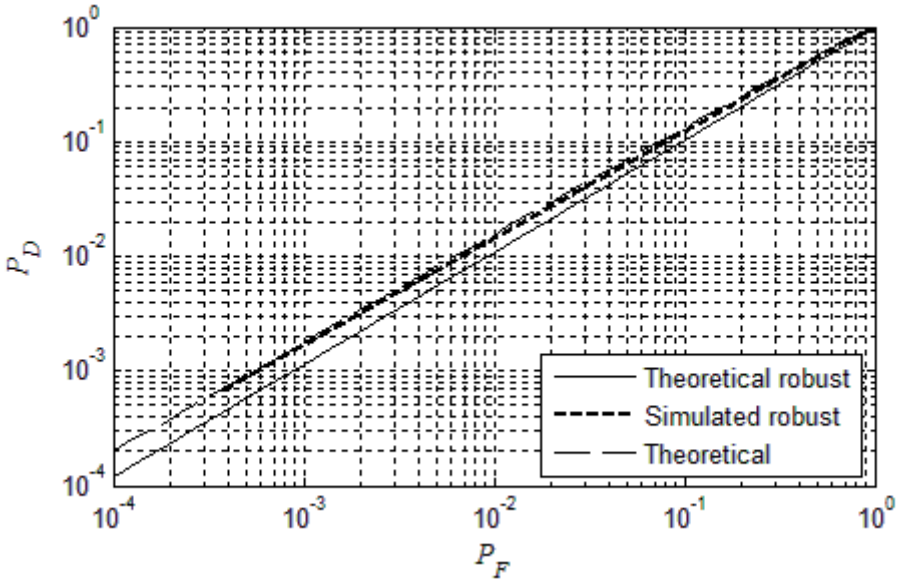

Fig. 6.7 Comparison of ROC for robust and regular energy detectors

To compare the performance of a regular energy detector and a derived robust detector, we have plotted their operating characteristics in Figure 6.7. Both lines are for SNR = -23dB and detector length n = 2080. In the case of a robust detector we assume impulsive noise to have parameters $c = 10^{-3}$ and b = 128. We can see that theoretical performance of our robust detector with impulsive noise is only slightly worse than the performance of a regular energy detector in Gaussian noise. Simulated results are showing even better performance – almost as good as the regular energy detector had in only Gaussian noise environment.

Several other robust energy detection methods are suggested in literature [10, 15], for example, so-called L_1 or so-called absolute value detector. Decision statistic for such detectors is computed as a sum of absolute values of samples

$$\Lambda = \sum_{k=1}^{n} |x_k| . \qquad (6.1.39)$$

As compared to a regular energy detector, there is no need to take square of outliers, thus not increasing their effect on the estimate. Neither do we take the received waveform into square, which, in turn, means that our sensitivity is lower than in the case of the energy detector. Both of those effects tend to cancel each other out and the robustness obtained is only slightly better than that of the regular energy detector. By combining advantages of the regular energy detector, in the means of sensitivity and L_1-norm detectors in the means of robustness, we obtain a so-called Huber's detector. This widely used popular detector has the following decision statistic:

$$\Lambda = \sum_{k=1}^{n} \rho(x_k), \tag{6.1.40}$$

where $\rho(\cdot)$ is Huber's distance function [11] (see Figure 6.8)

$$\rho(x) = \begin{cases} \dfrac{x^2}{2\sigma^2}, & for\ |x| \le k_\rho \sigma \\ \dfrac{k_\rho |x|}{\sigma} - \dfrac{k_\rho^2}{2}, & for\ |x| > k_\rho \sigma \end{cases} \tag{6.1.41}$$

and where the dependence $k_\rho = k_\rho(\varepsilon)$ is tabulated in [11] p. 87. As our noise model (3.3.8) can be viewed as ε-contaminated Gaussian noise (1.1), where contaminating impulsive noise is present, then for our case the probability of impulse c is equivalent to the contamination factor ε. Analysis of the last equation in Figure 6.8 shows that for the received waveform this detector works as an energy detector adding up squares of input samples. But for impulsive noise, Huber's detector works as an L_1 detector adding only absolute values of outliers instead of squares of them. Thus, on the one hand we have high sensitivity of an energy detector for a received waveform and on the other hand we have decreased the influence of impulsive outliers. But unlike our suggested robust detector the outliers are not removed, they are only suppressed. Thus, we can assume that robustness of Huber's detector, although better than energy detectors, is still inferior to our suggested robust energy detector.

In order to test this assumption, computer simulations were carried out to compare robustness of a regular energy detector (2.1.1) against both Huber's detector (6.1.40) and our derived robust energy detector (6.1.15). Figure 6.9 shows false alarm rate against the length of the detector when the probability of impulsive noise (or contamination factor ε) is $c = 10^{-3}$. The figure shows that Huber's detector is indeed somewhat more robust against impulsive noise than a regular energy detector but it is much inferior to robustness of our detector. Figure 6.10 depicts the results of another simulation where the length of the detector is fixed $n = 4160$ and probability of false detection P_F as the function of c is plotted on the graph. This figure indicates exactly the same – Huber's detector is slightly more robust than an energy detector but still much worse than our energy detector. Our detector's performance starts to decrease only when every hundredth sample is contaminated by impulsive noise.

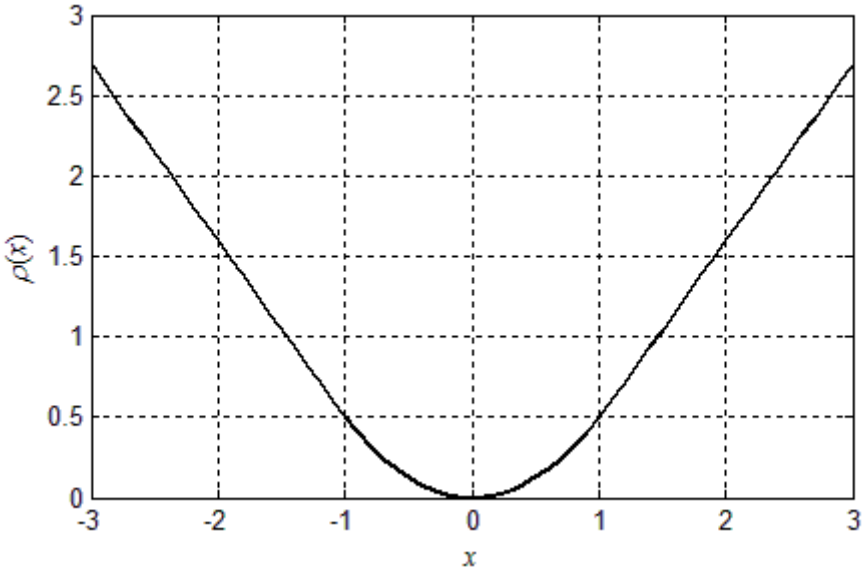

Fig. 6.8 Huber's distance function

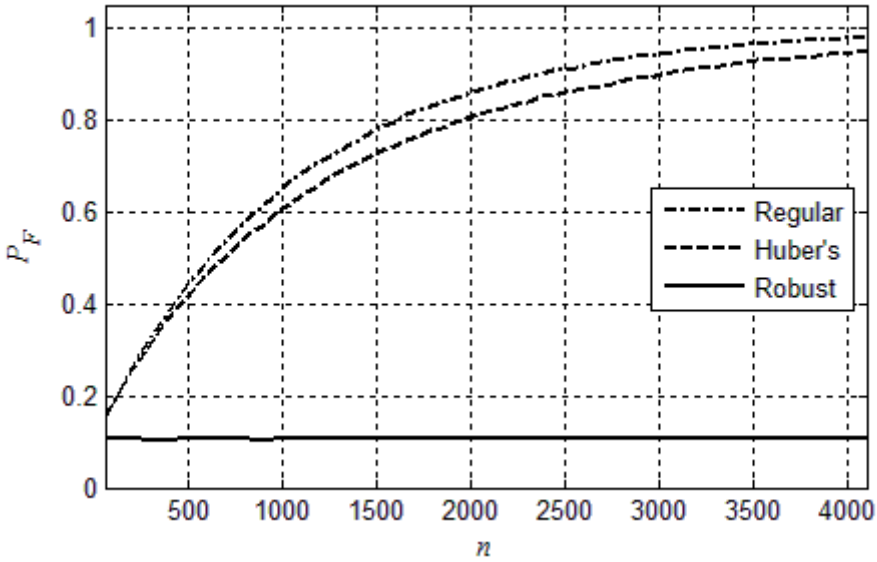

Fig. 6.9 Comparison of robustness of different energy detectors ($c = 10^{-3}$)

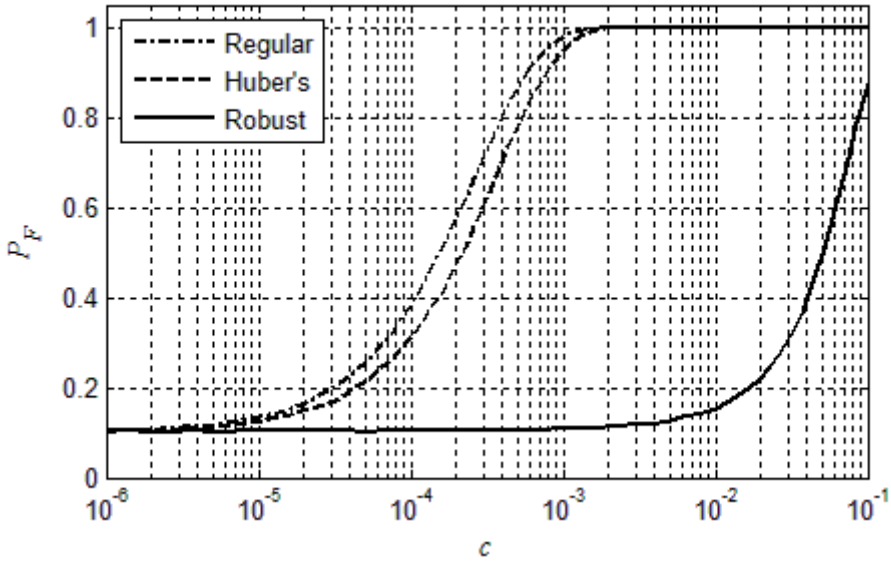

Fig. 6.10 Comparison of robustness of different energy detectors (n = 4160)

In this chapter we have derived a robust energy detector. Its sensitivity in the absence of impulsive noise is almost as good as that of regular energy detectors. When impulsive noise is present, our robust detector outperforms a regular energy detector in many orders of magnitude. Asymptotic analysis of detection performance was conducted and computer simulations have shown good fit with analytical expressions. Comparisons with other robust energy detection methods show that our solution works better than many other ones.

6.2 Robust Feature Detector

In the case of a robust feature detector we also have to solve the detection problem in the background of Gaussian and impulsive noise. As compared to the previous case of the energy detector, we have more information about the primary user signal. In fact, we assume that we have knowledge about periodicity in the primary user signal. For example, this can be carrier or pilot frequency, symbol rate or something similar. Due to this excess information we can now use a feature detector to ascertain the presence or absence of the primary user signal.

In this chapter we assume that detection is carried out through the use of cyclic spectrum $S_x^{\alpha}(f)$. For simplicity we use a single cycle detector, thus the primary signal is detected at one point (f,α) on the cycle-frequency plane. A single harmonic signal with known frequency is used as a model of the primary user signal. Decision threshold λ is based on the criterion of the constant false alarm rate (CFAR).

Gaussian noise itself is assumed to be uncorrelated here also but an added periodic signal causes samples of a received waveform to be periodically correlated. To calculate the cyclic spectrum of the received waveform, we need a relatively long input vector whereby correlation between signal elements must be preserved. Thus, when we eliminate the influence of impulsive noise, we must do it such that the correlation in the signal preserves. In other words, constructing an elimination algorithm we should consider correlation of the signal.

To start our derivation of the robust feature detector, we will find the robust estimator of the covariance matrix **C**. From there we will find threshold values η_p for removal of the impulsive noise component v_i and then by using the resulting limited waveform we estimate cyclic spectrum or the cyclic autocorrelation function (CAF) of the received waveform $x(t)$.

The algorithm for impulsive noise removal for a one-dimensional case was covered above in section 6.1. As here we have to deal with multidimensional noise and estimation of covariance matrix, we start with the ML estimator (4.3.49)

$$\hat{\mathbf{C}} = \frac{1}{n_1}\sum_{M_1}\mathbf{x}_k\mathbf{x}_k^T . \qquad (6.2.1)$$

The equation above states that we can estimate covariance on the received waveform x if we use only samples uncorrupted by the impulsive noise v_i. As demonstrated in Chapter 4, the border between the corrupted and the uncorrupted waveform was the p – dimensional hyper-rhombus. To test if vector $\mathbf{x}_k$ falls inside this shape and thus can be used to estimate covariance is relatively simple. But it

needs $2p$ comparisons to be done for each vector, thus computational load increases with dimension p. In order to give some numerical value to the performance of covariance estimating algorithms, we define a metric of estimation error e through matrix trace of squared difference between the actual covariance matrix $\mathbf{C}$ and our estimate of it as follows:

$$e = \frac{1}{p^2\sigma^4}\mathrm{tr}\left[\left(\mathbf{C}-\hat{\mathbf{C}}\right)\left(\mathbf{C}-\hat{\mathbf{C}}\right)^{\mathrm{T}}\right]. \qquad (6.2.2)$$

Error metric e in simple terms is the root mean average of difference between the element of a matrix and its estimate. Experimental results for the MLE estimator derived in section 4.3 are shown in Figure 6.11.

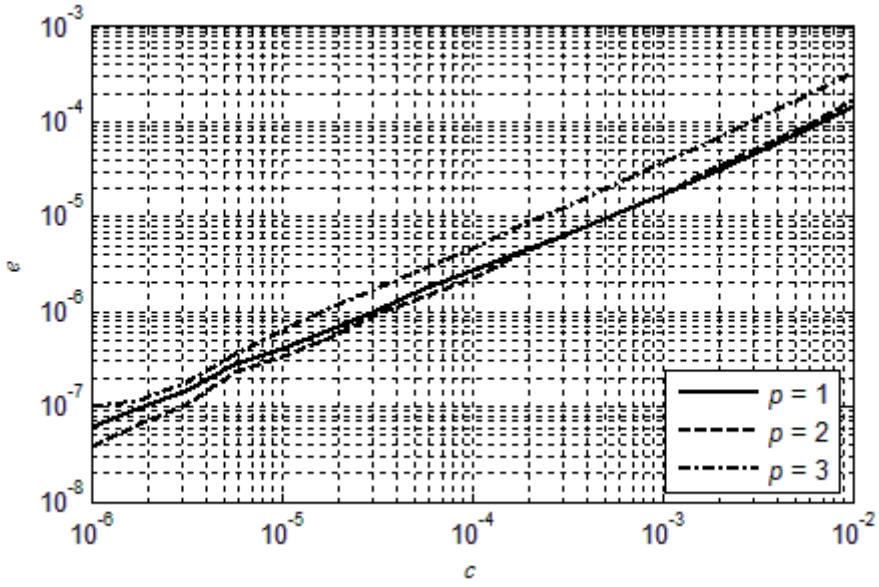

Fig. 6.11 Estimation error e as the function of impulse probability c and dimension p

Clearly, both one- and two-dimensional cases provide almost equal estimation accuracy. In the two-dimensional case we have to remove two samples if only one of them is corrupted by impulsive noise. For this reason, the estimation error of the two-dimensional result is slightly higher, around high values of c. In the three-dimensional case, similarly, we have to remove three samples already if only one of them is corrupted by impulsive noise. For this reason, $p = 3$ has even greater estimation error than in the previous cases. As a result, the estimation error increases with the number of dimensions p. Single noise impulse per realization causes removal of a larger number of samples and thus smaller estimation accuracy if p increases. This concept is illustrated in Figure 6.12. The figure depicts the intersection border for $p = 2$ and four possible two-dimensional realization vectors

$\mathbf{x}_1 ... \mathbf{x}_4$. Vector $\mathbf{x}_1$ is uncorrupted by impulsive noise and it can be used to estimate covariance in (6.2.1). All three other vectors have an impulsive noise component and thus they all are discarded from the estimation of covariance. A closer look at the image reveals that in the case of $\mathbf{x}_2$ only its first x_1 coordinate in inflicted by impulsive noise. Thus, throwing the second coordinate x_2 away is not a good idea because it causes loss of estimation accuracy. Similarly, only one of the two coordinates of vector $\mathbf{x}_3$ is corrupted by impulsive noise and the second one is actually appropriate for covariance estimation.

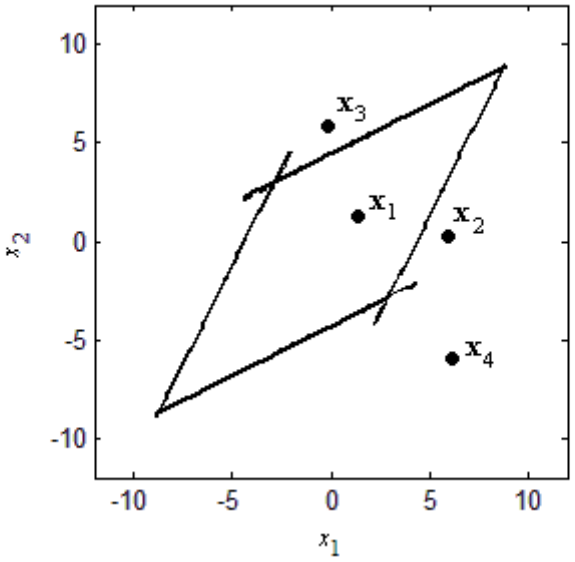

Fig. 6.12 Cause of estimation error increase along with dimension p

In summary, our derived ML estimator works well. Figure 6.11 shows that the estimation error is very small even at a high probability of impulse. On the other hand, as dimension p increases, we need more computational resources to test if the given vector $\mathbf{x}_k$ is suitable for the estimation of covariance or not. The second flaw of our estimator is in the fact that again if dimension p increases, one single noise impulse can cause discarding of the whole long $\mathbf{x}_k$. This, in turn, causes degradation in the estimation accuracy because due to only one noise pulse much of useful information is simply thrown away.

The estimator derived works as follows. It takes p samples from the input realization x forming a vector $\mathbf{x}_k$ with a length p. Then it compares the vector with the intersection border. When no impulsive noise is present, the vector falls inside the borders and it is used to estimate covariance. When one or more impulses are present, the whole vector is discarded because of no information about the exact location of impulsive noise inside this vector. For example, with the input

realization $x_1,x_2,x_3,x_4,...$ for $p = 2$, first, we form vector $\mathbf{x}_1 = \{x_1,x_2\}$ and compare it against the intersection border, the second vector would be $\mathbf{x}_2 = \{x_3,x_4\}$ and so on. If now, for example, x_2 is corrupted by impulsive noise, then our algorithm discards the whole vector $\mathbf{x}_1$ because it knows that this vector is corrupted by impulsive noise but it cannot identify the element. In order to remove this ambiguity, we must form three vectors out of the same realization. Those vectors will be $\mathbf{x}_1 = \{x_1,x_2\}$, $\mathbf{x}_2 = \{x_2,x_3\}$ and $\mathbf{x}_3 = \{x_3,x_4\}$. Now we compare all three vectors against the intersection border. Let us now continue with an example where sample x_2 was corrupted by impulsive noise. As now vectors $\mathbf{x}_1$ and $\mathbf{x}_2$ both indicate that at least one of their coordinates is corrupted by impulsive noise but vector $\mathbf{x}_3$ is uncorrupted, then we can pinpoint that sample x_2 is indeed the one we must remove. The approach described allows dealing with the problem of degradation of estimation accuracy. But now we have to do $2p^2$ comparisons to remove impulsive noise, instead of $2p$ comparisons we had to do with the original ML estimator. Thus, by solving one of our problems we enlarged another one.

Clearly, we need to do some approximations to simplify our estimator. Thus, let us take another look at the PDF of the sum of impulsive and Gaussian noise (Figure 6.13).

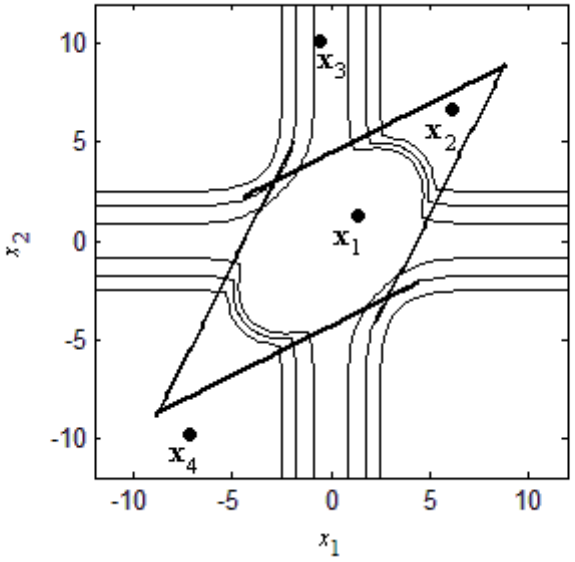

Fig. 6.13 2D PDF of the sum of impulsive and Gaussian noise

According to (3.3.29), the probability that the vector $\mathbf{x}_k$ is positioned inside the rhombus is in order of $(1-c)^p$, i.e. it is very high. As the PDF inside the rhombus is Gaussian, in our figure vector $\mathbf{x}_1$ is of much higher probability of appearance than vector $\mathbf{x}_2$. Impulsive noise appears seldom with a probability c. Thus, the

probability of vector $\mathbf{x}_3$ appearance is in the order of $c(1\text{-}c)^{p-1}/b$. As in our model, impulsive noise is uncorrelated and has a relatively low probability of appearance, the probability of vector $\mathbf{x}_3$ appearance is in the order of $(c/b)^p$, which in practical terms means that such an event is next to being impossible. In brief, the majority of noise samples have actually been gathered relatively close to the axis. For example, according to the properties of Gaussian noise, 99.7% of all samples lie within ±3σ from the origin. As we assumed limits of impulsive noise value b to be much larger than a standard deviation σ, the following simplification can be made. Thus, within the given range ±3σ we can approximate the intersection border as the hyper-plane parallel to the origin. In a two-dimensional case this means that the intersection border along the x_2 axis can be viewed to be parallel with the x_1 axis and vice versa.

In mathematical terms our simplification means ignoring information about correlation. In practical applications we usually lack such information anyway. Thus, such approximation is reasonable also from this point of view. Disregarding the dimension of the vector $\mathbf{x}_k$ and the correlation amongst its elements, we compare all its elements against the threshold (3.3.36)

$$\eta_1 = \sqrt{-2\sigma_l^2 \ln\left(\frac{c}{1-c}\frac{\sqrt{2\pi}\sigma_l}{2b}\right)}, \quad l = 0,1$$

and discard all the elements that will cross this threshold. In other words, element x_k is valid for the estimation of covariance if

$$\left(x_k < \eta_1\right) \wedge \left(x_k > -\eta_1\right). \tag{6.2.3}$$

Variable σ_l is defined in previous section (6.1.2). To obtain an estimate of Gaussian noise covariance, elements of x that do not pass the test should be discarded. But it should be taken into account that primary user signal may also be present. Discarding some samples of input realization causes changes in signal frequency and thus affects the probability of detection. Thus, if sample x_k does not pass the test, it cannot be discarded but its current value must be replaced with zero or the value of threshold η_1. Option 1 gives a slightly smaller estimation error, while the second one is compatible with other detectors and is easier to be implemented as saturation nonlinearity similar to (6.1.17).

Simulation results for the simplified decision rule (6.2.3) are presented in Figure 6.14. When comparing the results to those obtained by the exact rule in Figure 6.11, we can see that the performance is almost as good as it was before. But the number of operations required is highly reduced.

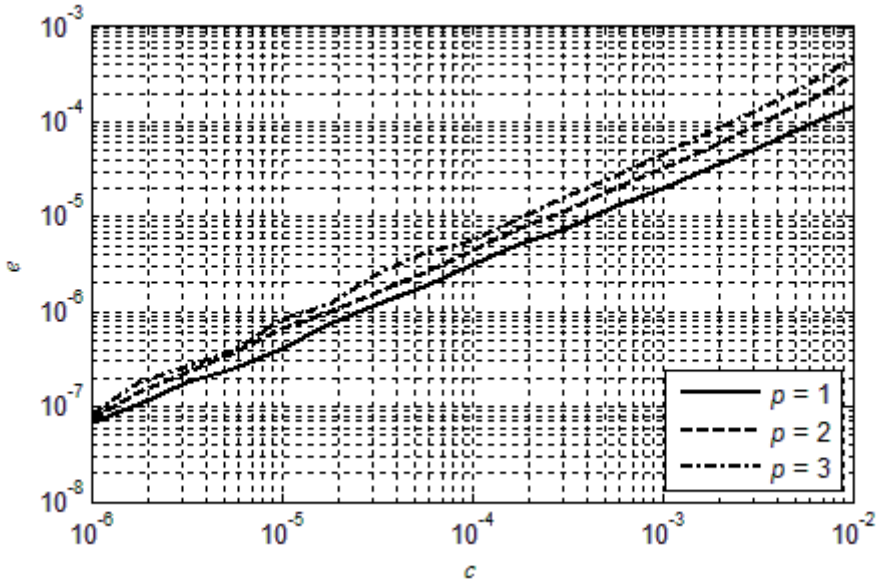

Fig. 6.14 Estimation error for the simplified decision rule

As mentioned in Chapter 2, the probability of the correct detection P_D for a cyclostationary detector is not analytically tractable. For this reason we start by finding an expression for the probability of false detection P_F and later find curves for P_D using simulations.

Figure 6.15 shows the schematics of a robust feature detector. The first node is a two-way comparator which compares input realization (6.2.3) with threshold $\pm\eta_{1l}$. This is followed by a spectral correlator to calculate the estimate of cyclic spectrum $S_x^{\alpha}(f)$, which is decision statistic for the given case. Decision Λ statistic is then compared against threshold λ and based on the result, decision Θ is made in favor of one of the two hypotheses H_l.

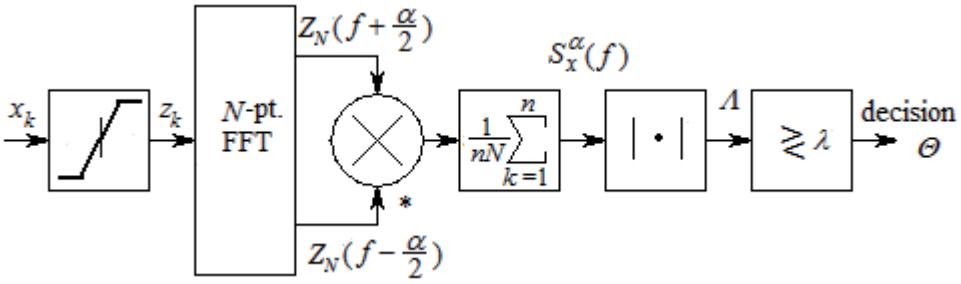

Fig. 6.15 Robust feature detector

If the received waveform is noise only (*l=0*), both Gaussian and impulsive noise are assumed to be white. PDF of the received waveform is then (3.3.8)

$$f_x(x) = \frac{c}{4b}\left[\operatorname{erf}\left(\frac{x+b}{\sqrt{2}\sigma}\right) - \operatorname{erf}\left(\frac{x-b}{\sqrt{2}\sigma}\right)\right] + \frac{1-c}{\sqrt{2\pi}\sigma} e^{-\frac{x^2}{2\sigma^2}} \quad (6.2.4)$$

A two-way comparator performs the following nonlinear operation with the input waveform *x*

$$z = \begin{cases} x, \; if \; |x| \le \eta_{1l} \\ 0, \; if \; |x| > \eta_{1l} \end{cases}. \quad (6.2.5)$$

This limited waveform is then used to calculate the estimate of SCF as

$$\hat{S}_x^{\alpha}(f) = \frac{1}{n}\frac{1}{N}\sum_{k=1}^{n} Z_N(k, f + \frac{\alpha}{2}) Z_N^*(k, f - \frac{\alpha}{2}), \quad (6.2.6)$$

our decision statistic will be as in (2.2.22)

$$\Lambda = \left|\hat{S}_x^{\alpha}(f)\right|.$$

PDF of the limited waveform is then approximately

$$f_z(z) = \begin{cases} \beta_1\left[\frac{c}{2b} + \frac{1-c}{\sqrt{2\pi}\sigma} e^{-\frac{x^2}{2\sigma^2}} + c\left(-\frac{\eta_{1l}}{b}\right)\delta(x)\right], & |x| \le \eta_{1l} \\ 0, & \text{otherwise} \end{cases} \quad (6.2.7)$$

As our waveform is limited symmetrically, the mean value of *z* is also zero. The variance of the limited waveform is

$$\sigma_z^2 = \frac{c\beta_1\eta_{1l}^3}{3b} + \beta_1(1-c)\sigma\left[\sigma \operatorname{erf}\left(\frac{\eta_{1l}}{\sqrt{2}\sigma}\right) - \sqrt{\frac{2}{\pi}}\eta_{1l} e^{-\frac{\eta_{1l}^2}{2\sigma^2}}\right]. \quad (6.2.8)$$

As the limiter acts most of the time in its linear region, we can fairly assume that its output *z* is also white noise. This means that after *N*–point FFT each frequency bin has an equal amount of input power. Thus, both real and imaginary parts of the FFT output have variance

$$\sigma_N^2 = \frac{N\sigma_z^2}{2}. \tag{6.2.9}$$

If N is sufficiently large, then the PDF of each frequency bin is due to the central limit theorem Gaussian and the output of the following multiplier follows the distribution described by the second kind zero-order Bessel function [28]. But again our interest is in noise variance here not in the actual shape of its PDF. If two variables X and Y are independent having zero mean, then the variance of their product can be found [29]

$$\mathbf{D}(XY) = \mathbf{D}X\mathbf{D}Y\,. \tag{6.2.10}$$

This means that noise variance at the output of the multiplier is

$$\frac{N^2\sigma_z^4}{2}. \tag{6.2.11}$$

Next, we average $2n$ times and normalize with nN, then the resulting PDF of both the imaginary and the real part at the output are Gaussian when n is sufficiently large. Variance of both the real and the imaginary part of the output PDF is

$$\sigma_0^2 = \frac{\sigma_z^4}{n}. \tag{6.2.12}$$

Non-multiplicativity property of the expected value states that the mean of the product of the two random variables is [30]

$$\mathbf{E}(XY) = \mathbf{E}X\mathbf{E}Y + \operatorname{cov}(X,Y). \tag{6.2.13}$$

As we assume our random variables to be independent and with zero mean and according to the last equation the mean of their product, thus also the output of the spectral correlator is zero.

The decision device compares the module of the SCF estimate (6.2.6) against the decision threshold λ. It is well known that in the case of random complex numbers whose real and imaginary components are Gaussian, the module of the complex number is Rayleigh-distributed. Thus, the decision statistic Λ (2.2.22) in the case of noise only follows the Rayleigh distribution

$$f(\Lambda|H_0) = \frac{n\Lambda}{\sigma_z^4} e^{-\frac{n\Lambda^2}{2\sigma_z^4}}, \quad \Lambda \geq 0 . \tag{6.2.14}$$

From the CDF of the Rayleigh distribution it is easy to derive the probability of false detection

$$P_F = e^{-\frac{n\lambda^2}{2\sigma_z^4}} \tag{6.2.15}$$

and from it the threshold value for the desired P_F

$$\lambda = \sigma_z^2 \sqrt{\frac{-2\ln P_F}{n}} . \tag{6.2.16}$$

As explained in section 2.2, there is no closed-form expression of correct detection P_D for a cyclostationary detector [30,31]. Therefore, we must use an approach where we calculate the threshold value (6.2.16) for a given false alarm probability and find ROC curves experimentally. However, in the same section it was demonstrated that in some specific cases it is possible to find an analytical expression for the probability of detection P_D. Necessary conditions were for pair $(\alpha, f) = (2f_s, 0)$ if FFT of the signal $s(t)$ is done coherently. Thus, next we adapt derivation from section 2.2 to be conforming to our robust detector.

As limiting takes into account the power of the received signal, the shape of the waveform can be considered unchanged. Also, in a robust detector the mean value of $X_N(k, f \pm \alpha/2)$ is determined by signal $s(t)$ and it can be expressed as (2.2.32)

$$\begin{aligned} \mathbf{E}\left[X_N\left(k, f + \frac{\alpha}{2} \right) \right] &= \frac{AN}{2}\left(\cos\varphi + j\sin\varphi\right) \\ \mathbf{E}\left[X_N\left(k, f - \frac{\alpha}{2} \right) \right] &= \frac{AN}{2}\left(\cos\varphi - j\sin\varphi\right) \end{aligned} .$$

As stated before, we can assume limited noise to be also white. Due to that variances of all spectrum bins are determined by the noise power σ_z^2(6.2.8) at the input and they are equal to

$$\mathbf{D}\left\{ \mathrm{Re}\left[X_N\left(k, f \pm \frac{\alpha}{2} \right) \right] \right\} = \mathbf{D}\left\{ \mathrm{Im}\left[X_N\left(k, f \pm \frac{\alpha}{2} \right) \right] \right\} = \frac{N\sigma_z^2}{2}$$

Thus, in our case output signals at the spectrum bins under interest are still Gaussian random processes with a mean determined by signal $s(t)$ (2.2.32) but variance is now determined by the limited sum of impulsive and Gaussian noise (6.2.7). The rest of the derivation is similar to that done for Gaussian noise only in section 2.2. Thus, under the given conditions our decision statistic Λ will also follow the Rice distribution $\Lambda \sim \mathbf{Ric}(\sigma_\Lambda, \psi)$ with the parameters

$$\sigma_\Lambda = \sqrt{\frac{A^2 N \sigma_z^2}{2n} + \frac{\sigma_z^4}{n}}, \quad \psi = \frac{NA^2}{4}. \tag{2.2.17}$$

The equation for the probability of correct detection P_D is then again the same (2.2.46)

$$P_D = 1 - F(\lambda) = Q_1\left(\frac{\psi}{\sigma_\Lambda}, \frac{\lambda}{\sigma_\Lambda}\right).$$

To calculate the necessary values of the number of samples n and threshold λ for a given operating point (P_F, P_D) at ROC, we face the same problem as in section 2.2. We need to know the inverse function of Marcum's Q function which can only be found through numerical iteration methods [32]. Thus, unfortunately we cannot give analytical expressions for values n and λ necessary to reach the operating point (P_F, P_D) at the ROC curve. But fortunately those values can be found through numerical methods.

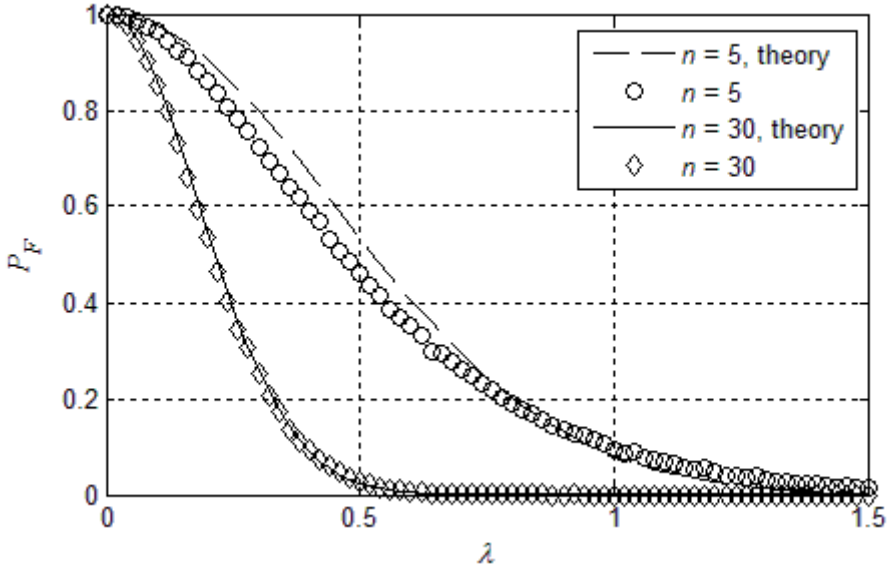

Fig. 6.16 Probability of false detection for a robust feature detector

As in the previous section regarding to the robust energy detector, we investigate here how many samples the detector should involve for our analysis to apply. In the simulation example we have used the following parameters to compute the probability of false detection P_F: $\sigma = 1$, $SNR = -17dB$, $c = 0.01$ and $b = 100$. Figure 6.16 shows that with $n = 5$, the simulation and theory vaguely remember each other. The situation improves when we increase the number of samples and already with $n = 30$ the theoretical curve and simulation dots are rather close to each other. Here we note that $n = 30$ is much smaller than the actual values of n used for cognitive radio applications.

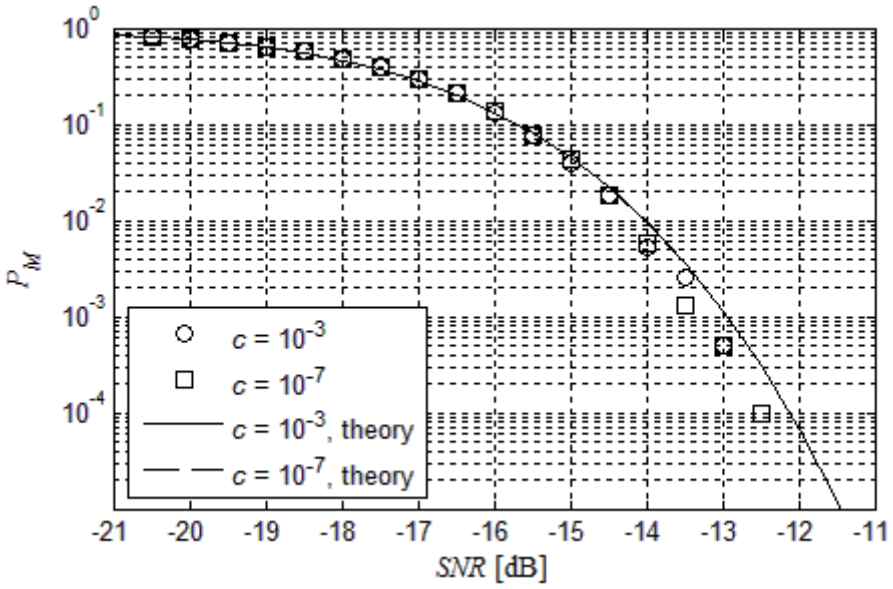

Fig. 6.17 Probability of missed detection as the function of SNR

Figure 6.17 presents the probability of missed detection $P_M = 1 - P_D$ as the function of SNR. Solid and dashed lines are theoretical results for $c = 10^{-3}$ and $c = 10^{-7}$ accordingly. Circles and squares are representing corresponding simulation results. A fast decrease of the curves occurs as the SNR increases. In addition, the intensity of impulsive noise c has only small influence on the results.

Figure 6.18 depicts the dependence of the probability of false alarm from the number of samples n for the ordinary cyclostationary detector if there is no impulsive noise (dashed line). It also shows the curves corresponding to the ordinary cyclostationary detector (solid thin line) and the proposed robust detector (solid bold line) in the presence of impulsive noise with intensity $c = 0.001$. The proposed detector operates at those conditions even slightly better than the ordinary cyclostationary detector in Gaussian noise. The reason of this is that the removal of impulsive noise contaminated samples also removes Gaussian noise value of this

sample. The second reason is that also some high valued Gaussian noise samples are removed by the comparator.

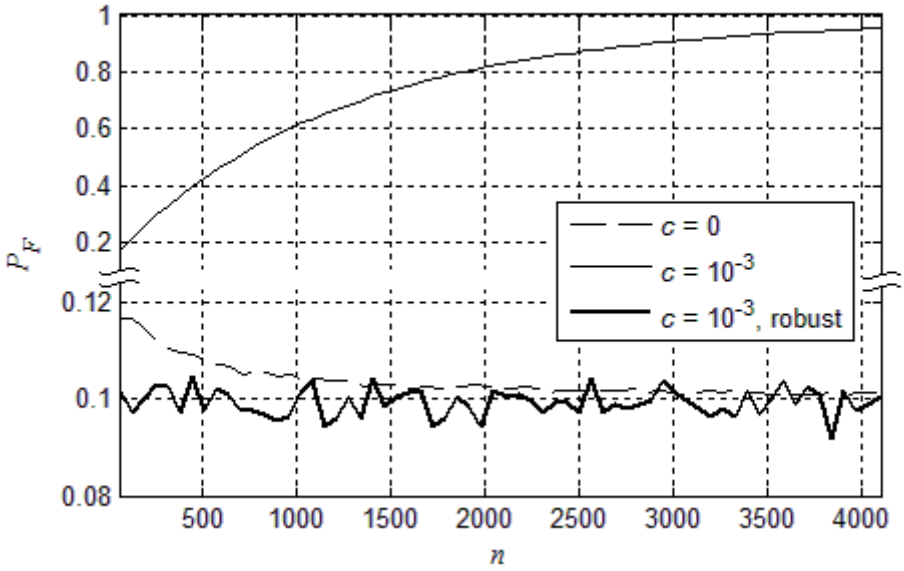

Fig. 6.18 Probability of false alarm as the function of n

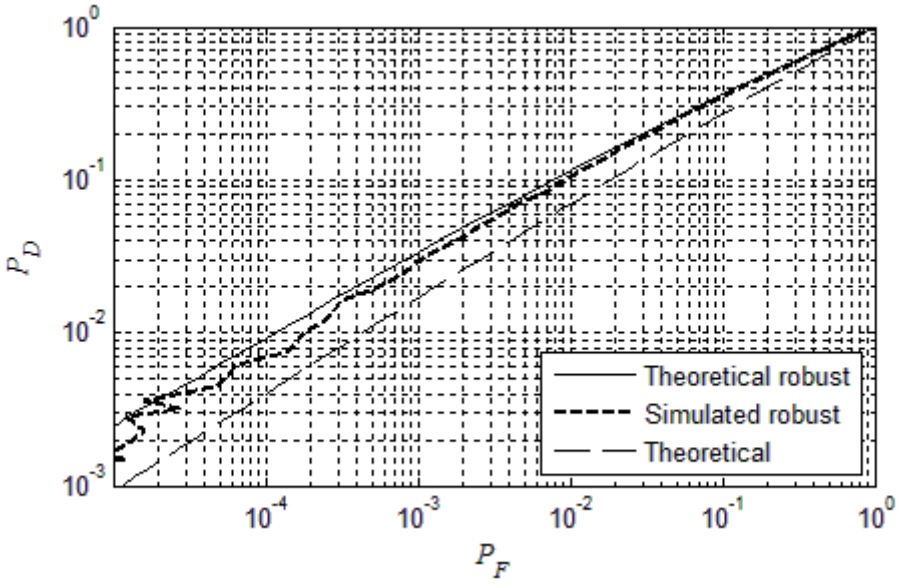

Fig. 6.19 Comparison of ROC for a robust and a regular cyclostationary detector

To compare the performance of a regular and a derived cyclostationary detector we have plotted their operating characteristics in Figure 6.19. Both lines are for SNR = -23dB, FFT length N = 65 and detector length n = 32. In the case of a robust detector we assume impulsive noise to have parameters $c = 10^{-3}$ and b = 128. Both theoretical and simulated performance of our robust detector with impulsive noise is slightly better than the performance of a regular detector in Gaussian noise.

Literature about other robust feature detectors is scarce. Still in [54] trimmed mean is suggested to guarantee robustness of a cyclic correlation estimator. Thus, before computing cyclic autocorrelation (or cyclic spectrum), a number of the largest values in the received waveform is eliminated. This method would work well in theory but compared to our solution it has two flaws. First, when no impulsive noise is present, trimmed mean still removes some part of the input waveform, thus decreasing performance in Gaussian noise only. When no impulsive noise is present, our robust detector passes all input samples – thus it has better performance in Gaussian noise. Second, a trimmed mean robust feature detector requires a large amount of computational resources. Finding one maximum value among a long vector is a time consuming task, which becomes even longer when the n_m largest values must be found.

In conclusion, we have derived a robust cyclostationary detector which works as well as a regular one in the Gaussian noise background. When impulsive noise is also acting in its input, the performance is still almost as good as without it. Knowing and taking into account the correlation between the elements of the received waveform, we can further increase the performance of our detector. It is shown that even without knowledge about the correlation a well working detector can still be built.

Asymptotic detection analysis and computer simulations were performed to test the accuracy of those analytical results. Simulations showed good match with theoretical results and slightly better performance than was predicted.

6.3 Known Primary Signal

Finally, we will describe the derivation of a robust detector for a case where the primary signal s is known accurately. This can be described as a matched filter case for our model.

The conditional probability density of the received waveform (6.1.1) being noise only can be written as

$$f_x(x|H_0) = \begin{cases} \beta_0 \max\left(\frac{1-c}{\sqrt{2\pi}\sigma} e^{\frac{-x^2}{2\sigma^2}}, \frac{c}{2b} \right), & |x| < b \\ 0, & \text{otherwise} \end{cases}, \quad (6.3.1)$$

and the conditional probability density of the received waveform being signal plus noise as

$$f_x(x|H_1) = \begin{cases} \beta_1 \max\left(\frac{1-c}{\sqrt{2\pi}\sigma} e^{\frac{-(x-s)^2}{2\sigma^2}}, \frac{c}{2b} \right), & |x| < b \\ 0, & \text{otherwise} \end{cases}. \quad (6.3.2)$$

With this approximation the signal to be detected appears as the mean value of the Gaussian process while the impulsive noise component is not affected by the presence or absence of the signal. This sets a restriction that a signal cannot change during the detection process. Fortunately, the matched filter is the fastest among the viewed detectors. This means that the time needed for detection is shorter than for any other detector. Thus, we can state that the primary signal cannot change much during detection.

The factor β_1 is used in the above equations to scale f_x to satisfy the requirements for the probability density function and can be found by solving

$$\int_{-b}^{b} f_x(x|H_i)dx = 1; \quad i = 0,1 \quad (6.3.3)$$

for β_1. However, the particular value of β_1 does not affect the resulting detector here and therefore the issue is not advanced further.

Instead, we proceed simplifying the expressions for probability densities $f_x(x|H_0)$ and $f_x(x|H_1)$. As the two differ just by the mean value of the Gaussian process, we concentrate only on $f_x(x|H_1)$ for the moment. An expression for $f_x(x|H_0)$ will follow by similar calculations. For $f_x(x|H_1)$ we have

$$f_x\left(x\middle|H_1\right)=\beta_1\max\left(\frac{1-c}{\sqrt{2\pi}\sigma}e^{\frac{-(x-s)^2}{2\sigma^2}},\frac{c}{2b}\right)=$$
$$=\frac{\beta_1(1-c)}{\sqrt{2\pi}\sigma}e^{-\frac{1}{2\sigma^2}\min\left[(x-s)^2,-2\sigma^2\ln\frac{c\sqrt{2\pi}\sigma}{(1-c)2b}\right]} \tag{6.3.4}$$

With this result and assuming that we have received n samples of waveform $x(t)$ that are statistically independent of each other, we can design the likelihood ratio test as follows. The log-likelihood ratio can be written as

$$\ln L=\ln\frac{\prod_{k=1}^{n}f_x(x|H_1)}{\prod_{k=1}^{n}f_x(x|H_0)}=$$
$$-\frac{1}{2\sigma^2}\sum_{k=1}^{n}\min\left[(x_k-s_k)^2,-2\sigma^2\ln\frac{c\sqrt{2\pi}\sigma}{(1-c)2b}\right]+ \tag{6.3.5}$$
$$+\frac{1}{2\sigma^2}\sum_{k=1}^{n}\min\left[x_k^2,-2\sigma^2\ln\frac{c\sqrt{2\pi}\sigma}{(1-c)2b}\right]$$

The hypothesis H_1 is selected if the log–likelihood ratio is greater than a threshold and the hypothesis H_0 otherwise. Cancellation of the common terms in the above equation results in the following detector. Select H_1 if

$$\sum_{k=1}^{n}\min\left[(x_k-s_k)^2,\eta_1^2\right]-\sum_{k=1}^{n}\min\left[x_k^2,\eta_1^2\right]>\lambda\ . \tag{6.3.6}$$

and H_0 otherwise. In the above, η1 is the intersection point (3.3.36)

$$\eta_1=\sqrt{-2\sigma^2\ln\frac{c\sqrt{2\pi}\sigma}{(1-c)2b}} \tag{6.3.7}$$

and λ is the threshold selected in accordance with the *a priori* probabilities and costs given to the different possible events [41]. The structure of the resulting robust detector is shown in Figure 6.20.

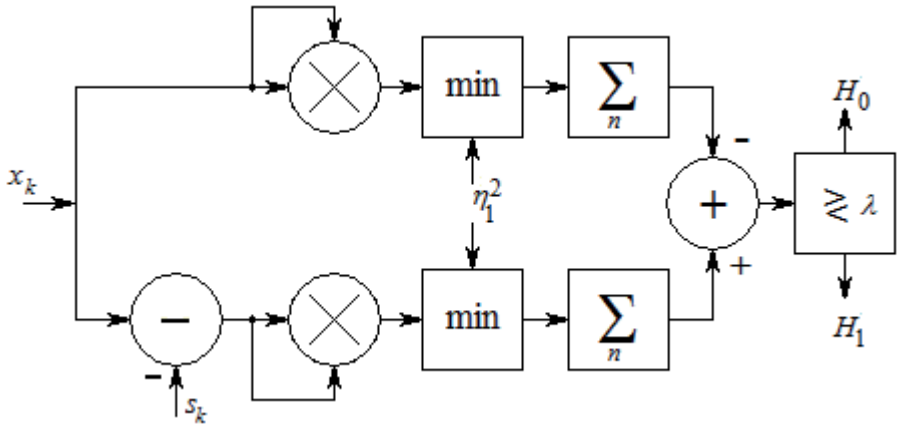

Fig. 6.20 Structure of a robust matched filter detector

We can analyze the performance of the derived detector by computing two arithmetic means and comparing their difference against the threshold

$$\frac{1}{n}\sum_{k=1}^{n}\min\left[(x_k - s_k)^2, \eta_1^2\right] - \frac{1}{n}\sum_{k=1}^{n}\min\left[x_k^2, \eta_1^2\right] > \lambda \qquad (6.3.8)$$

To perform our analysis, we assume that the signal s is small so that the intersection points of Gaussian and uniform distributions η_1 computed for the two sums above are close to each other. Again, we have two sums $q = 0; 1$ and two hypotheses $l = 0; 1$ we need to consider (6.1.17). In the case $q = 0$ and $l = 0$ the received signal comprises noise only and hence the PDF is

$$f_z(z_0|H_0) = \frac{\beta_1(1-c)}{\sqrt{2\pi z_0}\sigma} e^{-\frac{\left(\sqrt{z_0}-s\right)^2}{2\sigma^2}} \left[\Theta(z_0) - \Theta(z_0 - \eta_1^2)\right] + \\ + c\beta_1\left(1 - \frac{\eta_1}{b}\right)\delta(z_0 - \eta_1^2) \qquad (6.3.9)$$

Likewise, in the case $q = 1$ and $l = 0$ we have

$$f_z(z_1|H_0) = \frac{\beta_1(1-c)}{\sqrt{2\pi z_1}\sigma} e^{-\frac{z_1}{2\sigma^2}} \left[\Theta(z_1) - \Theta(z_1 - \eta_1^2)\right] + \\ + c\beta_1\left(1 - \frac{\eta_1}{b}\right)\delta(z_1 - \eta_1^2) \qquad (6.3.10)$$

In the case of H_1 the received signal x includes the signal component s in addition to the noise. It turns out that the problem is symmetric, thus

$$f_z(z_0|H_1) = f_z(z_1|H_0) \tag{6.3.11}$$

and

$$f_z(z_1|H_1) = f_z(z_0|H_0) \tag{6.3.12}$$

Next we need to find the moments of the distributions. The mean in case $q = 0$ and $l = 0$ equals

$$\begin{aligned}\mathbf{E}[z_0|H_0] = \frac{\beta_1(1-c)}{2\sqrt{2\pi}\sigma}\Bigg\{\sqrt{2\pi}\sigma\left(s^2+\sigma^2\right)\left[\operatorname{erf}\frac{\eta_1 - s}{\sqrt{2}\sigma} + \operatorname{erf}\frac{\eta_1 + s}{\sqrt{2}\sigma}\right] - \\ -2\sigma^2\left[(\eta_1+s)e^{-\frac{(\eta_1-s)^2}{2\sigma^2}} + (\eta_1-s)e^{-\frac{(\eta_1+s)^2}{2\sigma^2}}\right]\Bigg\} + \eta_1^2 c\beta_1\left(1-\frac{\eta_1}{b}\right)\end{aligned} \tag{6.3.13}$$

and the second moment equals

$$\begin{aligned}\mathbf{E}[z_0^2|H_0] = \frac{\beta_1(1-c)}{2\sqrt{2\pi}\sigma}\Big\{\sqrt{2\pi}\sigma\left(s^4+6s^2\sigma^2+3\sigma^4\right)\cdot \\ \cdot\left[\operatorname{erf}\frac{\eta_1 - s}{\sqrt{2}\sigma} + \operatorname{erf}\frac{\eta_1 + s}{\sqrt{2}\sigma}\right] + \\ +2\sigma^2 e^{-\frac{(\eta_1+s)^2}{2\sigma^2}}\left[-\eta_1^3 - \eta_1\left(s^2+3\sigma^2\right) + \eta_1^2 s + s^3 + 5s\sigma^2\right] - \\ -2\sigma^2 e^{-\frac{(\eta_1-s)^2}{2\sigma^2}}\left[\eta_1^3 + \eta_1\left(s^2+3\sigma^2\right) + \eta_1^2 s + s^3 + 5s\sigma^2\right]\Big\} + \\ +\eta_1^4 c\beta_1\left(1-\frac{\eta_1}{b}\right)\end{aligned} \tag{6.3.14}$$

In case $q = 1$ and $l = 0$, we have

$$\mathbf{E}\left[z_1|H_0\right] = \beta_1(1-c)\sigma^2 \operatorname{erf}\left(\frac{\eta_1}{\sqrt{2}\sigma}\right) - \\ -\frac{2\beta_1(1-c)}{\sqrt{2\pi}}\sigma\eta_1 e^{-\frac{\eta_1^2}{2\sigma^2}} + \eta_1^2 c\beta_1\left(1-\frac{\eta_1}{b}\right) \tag{6.3.15}$$

and

$$\mathbf{E}\left[z_1^2|H_0\right] = 3\beta_1(1-c)\sigma^4 \operatorname{erf}\left(\frac{\eta_1}{\sqrt{2}\sigma}\right) - \\ -\frac{2\beta_1(1-c)}{\sqrt{2\pi}}\sigma\eta_1 e^{-\frac{\eta_1^2}{2\sigma^2}}\left(\eta_1^2+3\sigma^2\right) + \eta_1^4 c\beta_1\left(1-\frac{\eta_1}{b}\right) . \tag{6.3.16}$$

Naturally it holds for the first and second order moments that $\mathbf{E}[z_0|H_1] = \mathbf{E}[z_1|H_0]$, $\mathbf{E}[z_1|H_1] = \mathbf{E}[z_0|H_0]$, $\mathbf{E}[z^2{}_0|H_1] = \mathbf{E}[z^2{}_1|H_0]$ and $\mathbf{E}[z^2{}_1|H_1] = \mathbf{E}[z^2{}_0|H_0]$: the noise is the same in both sums while the signal s only appears in either one of the sums. As we have assumed, the signal and noise to be independent, the cross correlation is

$$\mathbf{E}\left[z_0 z_1\right] = \mathbf{E}\left[z_1^2|H_0\right] \tag{6.3.17}$$

no matter which hypothesis we are looking for.

To proceed we need the moments of the variable

$$w = z_0 - z_1 . \tag{6.3.18}$$

The mean of w is

$$\mathrm{E}\left[w|H_l\right] = \mathrm{E}\left[z_0|H_l\right] - \mathrm{E}\left[z_1|H_l\right]. \tag{6.3.19}$$

Due to the symmetric nature of our detector, the expected values for the hypotheses are each other's opposites $\mathbf{E}[w|H_0] = -\mathbf{E}[w|H_1]$. Before we continue we must clarify the following. When there is no primary signal present, i.e. the hypothesis H_0 is valid, then the upper channel (in Fig. 6.20) $q = 1$ contains only noise v and lower channel $q = 0$ contains noise minus signal $v - s$. Due to this, $\mathbf{E}[z_0|H_0] > \mathbf{E}[z_1|H_0]$, which means that the expected value $\mathbf{E}[w|H_0]$ is positive. In an opposite case, when the primary signal s is present, the upper channel $q = 1$ contains noise plus signal $v + s$ and the lower channel $q = 0$ contains noise v only. In such a case, $\mathbf{E}[z_0|H_1] < \mathbf{E}[z_1|H_1]$, thus the expected value $\mathbf{E}[w|H_1]$ is negative. Thus, to put this together, the mean of decision statistic is positive when the

primary signal is absent and negative when it is present. This situation is illustrated in Figure 6.21. Such a reversal of usual polarity is caused by subtracting the known signal value *s* from the received waveform.

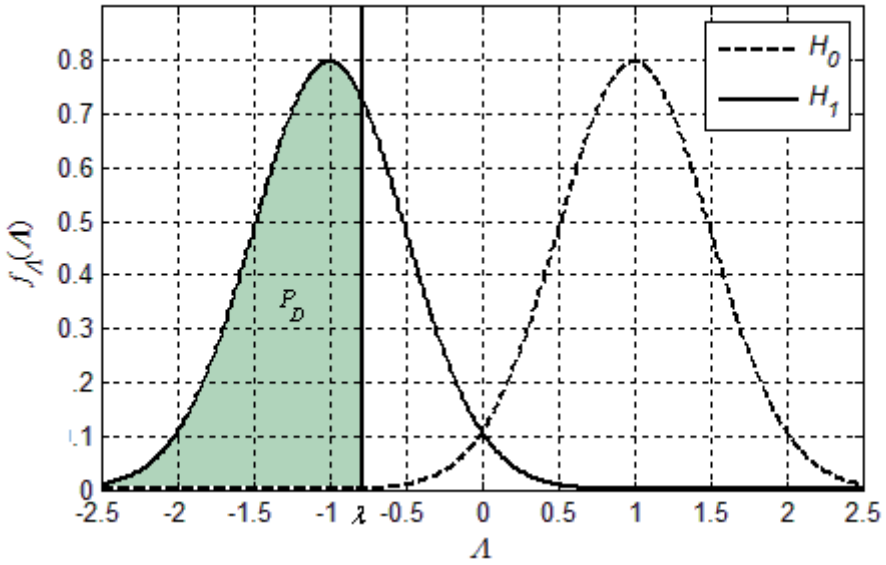

Fig. 6.21 Conditional PDFs for a robust matched filter

The second moment of variable *w* is

$$\mathrm{E}\left[w^2 \middle| H_l\right] = \mathrm{E}\left[z_0^2 \middle| H_l\right] - 2\mathrm{E}\left[z_0 z_1 \middle| H_l\right] + \mathrm{E}\left[z_1^2 \middle| H_l\right]. \qquad (6.3.20)$$

The variance equals

$$\sigma_{H_l}^2 = \mathrm{E}\left[w^2 \middle| H_l\right] - \mathrm{E}^2\left[w \middle| H_l\right]. \qquad (6.3.21)$$

Variances for both hypotheses are actually equal to $\sigma_{H_0} = \sigma_{H_1}$.

Now, according to (6.1.15), the detector computes a sample average of *n* IID random variables *w*. According to the central limit theorem [17, 40], the distribution of such a sum approaches Gaussian with mean **E**[*w*|*H*$_l$] (6.3.19) and variance (6.1.33)

$$\frac{\sigma_{H_l}^2}{n}, l = 0,1$$

when n increases, independent of the shape of the original distribution of the variables w. Due to reversed polarity, expressions for the values of probability of false and correct detection and thus also for the values of threshold and the number of required samples are

$$P_F = \int_{-\infty}^{\lambda} f_\Lambda\left(\Lambda \middle| H_0\right) dw = \frac{1}{2}\left[1 + \operatorname{erf}\left\{\frac{\left(\lambda - \mathbf{E}\left[w \middle| H_0\right]\right)\sqrt{n}}{\sqrt{2}\sigma_{H_0}}\right\}\right]. \quad (6.3.22)$$

The probability of correct detection correspondingly is

$$P_D = \int_{-\infty}^{\lambda} f_\Lambda\left(\Lambda \middle| H_1\right) dw = \frac{1}{2}\left[1 + \operatorname{erf}\left\{\frac{\left(\lambda - \mathbf{E}\left[w \middle| H_1\right]\right)\sqrt{n}}{\sqrt{2}\sigma_{H_1}}\right\}\right]. \quad (6.3.23)$$

The threshold λ and the required number of samples n to reach a given point P_D and P_F can be found by solving the system of equations formed from (6.3.22) and (6.3.23)

$$\begin{cases} \sqrt{2}\sigma_{H_0} \operatorname{erf}^{-1}(2P_F - 1) = \left(\lambda - \mathrm{E}\left[w \middle| H_0\right]\right)\sqrt{n} \\ \sqrt{2}\sigma_{H_1} \operatorname{erf}^{-1}(2P_D - 1) = \left(\lambda - \mathrm{E}\left[w \middle| H_1\right]\right)\sqrt{n} \end{cases}. \quad (6.3.24)$$

Taking into account that $\mathbf{E}[w|H_0] = -\mathbf{E}[w|H_1]$, $\sigma_{H_0} = \sigma_{H_1}$ and solving the system we obtain that in order to reach the operating point (P_F, P_D) values of n and λ must be

$$\begin{cases} n = \dfrac{\sigma_{H_1}^2}{2}\left\{\dfrac{\operatorname{erf}^{-1}(2P_F - 1) - \operatorname{erf}^{-1}(2P_D - 1)}{\mathbf{E}\left[w \middle| H_1\right]}\right\}^2 \\ \lambda = \dfrac{\mathbf{E}\left[w \middle| H_1\right]\left[\operatorname{erf}^{-1}(2P_F - 1) + \operatorname{erf}^{-1}(2P_D - 1)\right]}{\operatorname{erf}^{-1}(2P_F - 1) - \operatorname{erf}^{-1}(2P_D - 1)} \end{cases}. \quad (6.3.25)$$

Similarly to the previous chapters, we investigate how many samples the detector should involve for our analysis to apply. In the simulation example we have used the following parameters to compute the probability of false detection P_F: $\sigma = 1$, *SNR =-17dB*, $c = 0.01$ and $b = 100$. The graph in Figure 6.22 shows that with $n = 30$ the theoretical curve and simulation dots are closer to each other than in case $n = 5$. In order to obtain a better match, we need to increase the number of samples much above 30 because, as mentioned above with the FFT

energy detector, chi-square distributed variables are converging into Gaussian rather slowly.

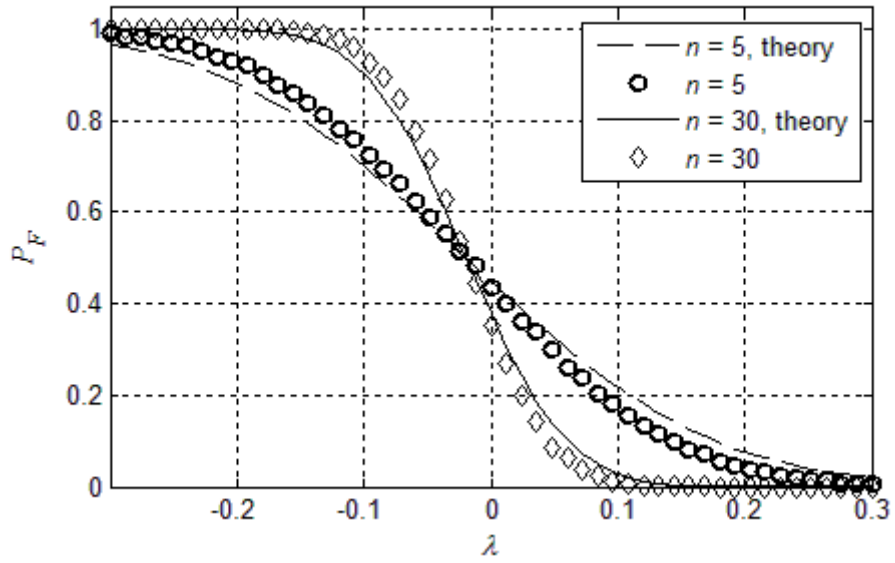

Fig. 6.22 Probability of false detection for a robust matched filter

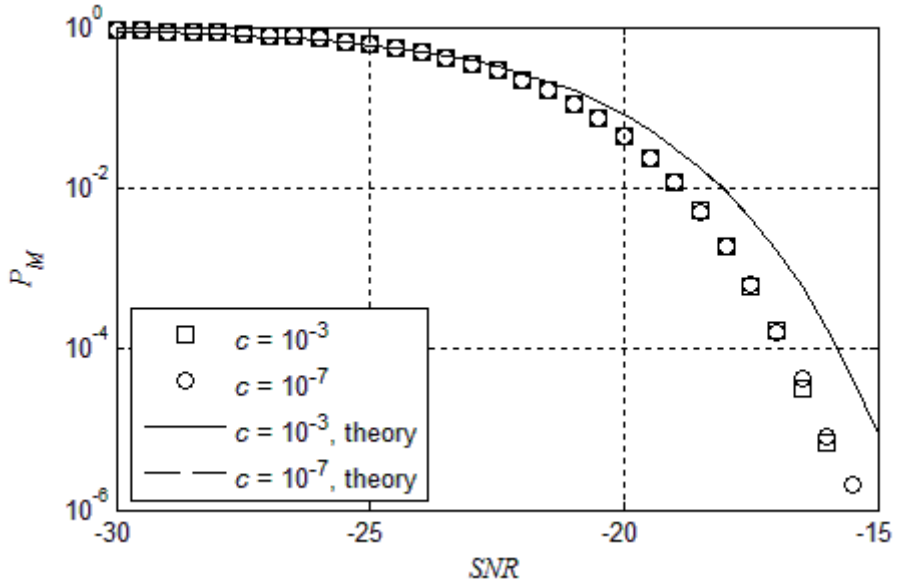

Fig. 6.23 Probability of missed detection as the function of SNR

Figure 6.23 presents the probability of missed detection $P_M = 1 - P_D$ as the function of SNR. Solid and dashed lines are theoretical results for $c = 10^{-3}$ and $c = 10^{-7}$ accordingly. Circles and squares represent simulation results. As compared to

previous robust detectors, curves are decreasing here even at lower SNR values than in previous cases. Also, the intensity of impulsive noise c has almost no influence on the results here.

Figure 6.24 depicts the dependence of the probability of false alarm on the number of samples n for the ordinary cyclostationary detector if there is no impulsive noise (dashed line). It also shows the curves corresponding to the ordinary cyclostationary detector (solid thin line) and the proposed robust detector (solid bold line) in the presence of impulsive noise with intensity $c = 0.001$. It seems that the proposed detector operates at those conditions even better than the ordinary matched filter in Gaussian noise. In fact, it is the effect caused by the small difference between the theoretical model and experimental results. A smaller value of the decision threshold λ should be used in order to achieve the desired *a priori* probability of false detection.

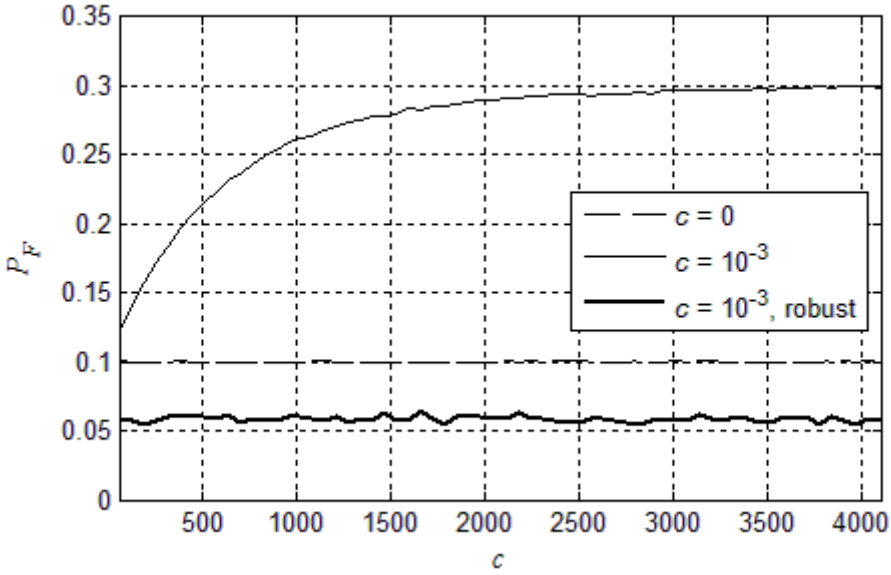

Fig. 6.24 Probability of false alarm as the function of n

To compare the performance of a regular and the derived robust matched filter, their operating characteristics are plotted in Figure 6.25. Both lines are for SNR = -23dB and detector length $n = 2080$. In the case of a robust detector we assume impulsive noise to have parameters $c = 10^{-3}$ and $b = 128$. The theoretical performance of our robust detector with impulsive noise is worse than the performance of the regular energy detector in Gaussian noise. But simulated results are showing much better performance, i.e. almost as good as with a regular energy detector in only the Gaussian noise environment.

For comparison Huber sense Neyman-Pearson detector was used, based on the minimum distance between the signal and observations presented in [68]. As in this article a detectable signal *s* is assumed to be known, we view it as a case of a known primary signal.

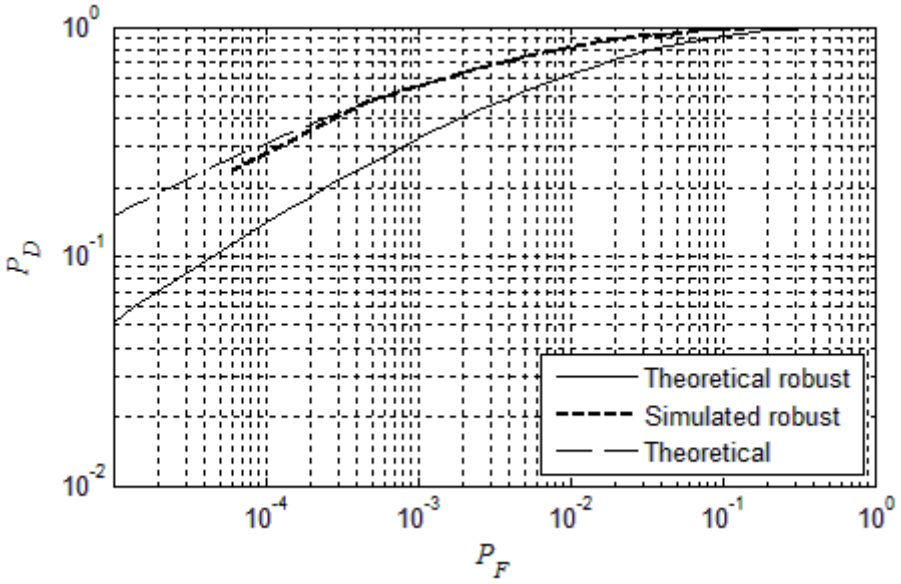

Fig. 6.25 Comparison of ROC for a robust and a regular matched filter

As we want to test the robustness of the proposed detector against our noise model, the detector proposed for ε-contaminated Gaussian noise is most suitable here. The reason of this choice is demonstrated by the comparison of the PDF of ε-contaminated Gaussian noise (1.1)

$$f_v(v) = \frac{1-\varepsilon}{\sqrt{2\pi}\sigma} e^{-\frac{v^2}{2\sigma^2}} + \varepsilon f(v)$$

With the PDF of the sum of Gaussian and impulsive noise (3.3.8) used in our work

$$f_v(v) = \frac{1-c}{\sqrt{2\pi}\sigma} e^{-\frac{v^2}{2\sigma^2}} + \frac{c}{4b}\left[\operatorname{erf}\left(\frac{v+b}{\sqrt{2}\sigma}\right) - \operatorname{erf}\left(\frac{v-b}{\sqrt{2}\sigma}\right)\right].$$

The comparison shows that our noise is actually a special case of ε-contaminated Gaussian noise where the probability of impulse *c* acts as a contamination factor ε. For such distributions a Huber's detector with the distance function (6.1.41)

$$\rho(x) = \begin{cases} \dfrac{x^2}{2\sigma^2}, & for\ |x| \le k_\rho \sigma \\ \dfrac{k_\rho |x|}{\sigma} - \dfrac{k_\rho^2}{2}, & for\ |x| > k_\rho \sigma \end{cases}$$

is used, where the dependence $k_\rho = k_\rho(\varepsilon)$ is tabulated in [11] p. 87. The detection rule proposed in [68] is to compare the decision statistic

$$\Lambda = \sum_{k=1}^{n} \rho(x_k) - \sum_{k=1}^{n} \rho(x_k - s_k) \qquad (6.3.26)$$

Against the threshold λ. When the threshold λ is exceeded, the decision is made in favor of hypothesis H_1 and if it is not, then in favor of H_0. The value of the threshold is

$$\lambda = \Phi^{-1}(1 - P_F)\sqrt{\frac{(1-\varepsilon)[2\Phi(k_\rho) - 1]E_s}{\sigma^2}} - \frac{(1-\varepsilon)[2\Phi(k_\rho) - 1]E_s}{2\sigma^2}, \qquad (6.3.27)$$

where P_F is the desired false detection probability, $\Phi(\cdot)$ is the standard Gaussian CDF and E_s is the energy of signal s.

When comparing this proposed Huber's detector with our robust detector for the known primary signal (6.3.8), the difference basically is in the used distance function.

To test the influence of such a difference on the performance, we carried out computer simulations. Simulations compared the robustness of the regular matched filter against both Huber's detector (6.3.26) and our derived robust energy detector (6.3.8). Figure 6.26 shows the false alarm rate against the length of the detector when the probability of impulsive noise is $c = 10^{-3}$.

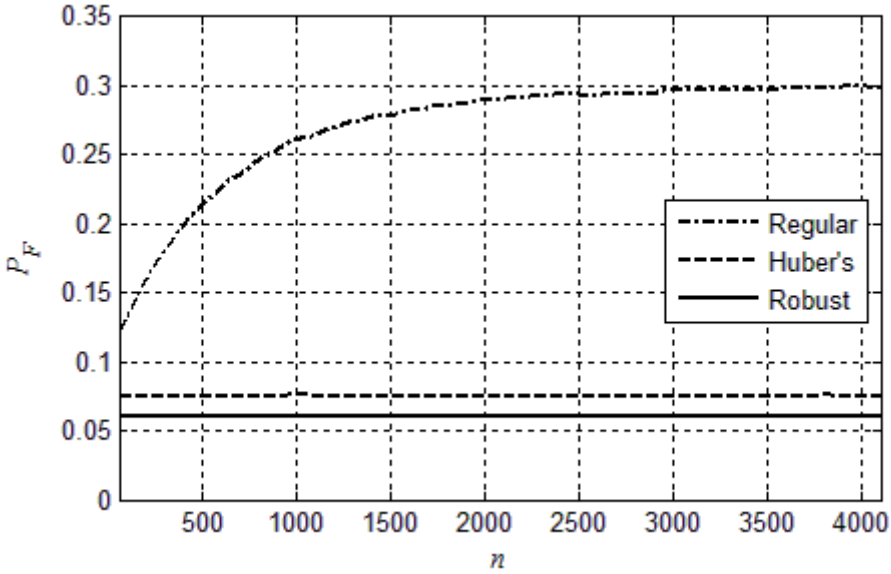

Fig. 6.26 Comparison of robustness of different matched filters ($c = 10^{-3}$)

Results in Figure 6.26 show that at a relatively low probability of impulses, both Huber's detector and our robust detector perform well.

Figure 6.27 depicts the results of another simulation where the length of the detector was fixed $n = 4160$ and the probability of false detection P_F as the function of c was plotted on the graph. This figure shows that in the region of low c both detectors work equally well, but when c increases over 10^{-2}, our detector starts to outperform Huber's detector proposed in [68]. Also, taking into account that our detector's computational complexity is somewhat smaller, we can conclude that the robust matched filter proposed in this thesis is more efficient with less effort.

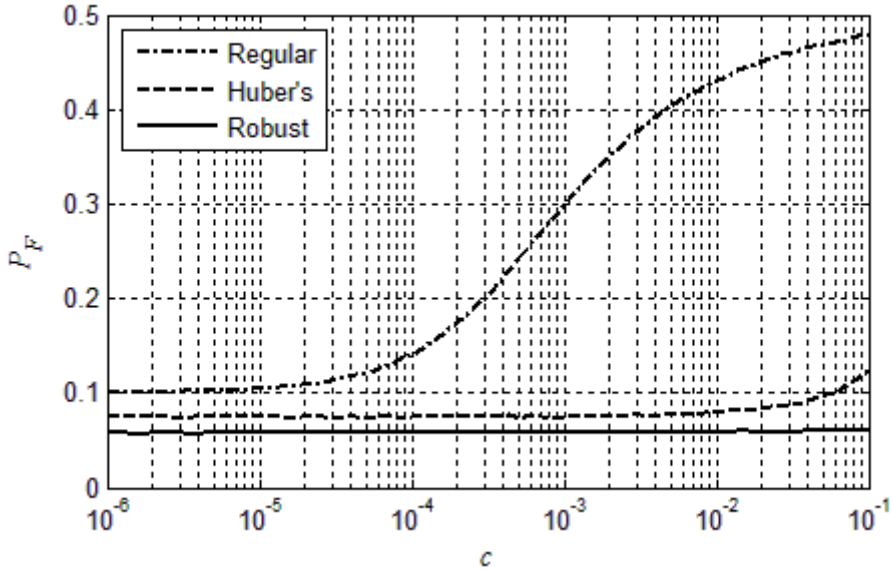

Fig. 6.27 Comparison of robustness of different matched filters (n =4160)

In this chapter we have derived the robust matched filter. Its sensitivity in the absence of impulsive noise is almost as good as that of a regular energy detector. When impulsive noise is present, the performance of our robust matched filter is the same as without impulses present. Asymptotic analysis of detection performance was conducted and computer simulations show a good compliance with analytical expressions. We demonstrated that our solution works slightly better than the Huber sense Neyman-Pearson detector based on the minimum distance between the signal and observations proposed in [68].

6.4 Conclusions

In the current chapter we derived robust analogues to three main types of detectors used to determine the presence or absence of the primary user signal at cognitive radio applications. Robustness here means that all derived detectors perform well both in only Gaussian and in the sum of Gaussian and impulsive noise. Thus their sensitivity to impulsive interference is very low.

Asymptotic analysis of detection performance was carried out for all three types. Computer simulations gave test results satisfactorily close to analytical results, indicating thus that the derived detectors are working as predicted. The derived detectors and other robust detectors proposed in literature were compared. The results showed that our solutions outperformed other proposed ones in robustness.

To compare those three derived robust detectors it is best to compare their ROC curves, as shown in Figure 6.28. All the curves in this figure are derived for the signal-to-noise ratio -23dB and impulse probability $c = 10^{-3}$. The result is very similar to that between the three types of regular detectors in Figure 2.16.

An advantage of the robust energy detector is that it needs almost no preliminary data in order to perform detection. However, a disadvantage of such a lack of information is poorer performance than with other detection methods, as illustrated in Figure 6.28.

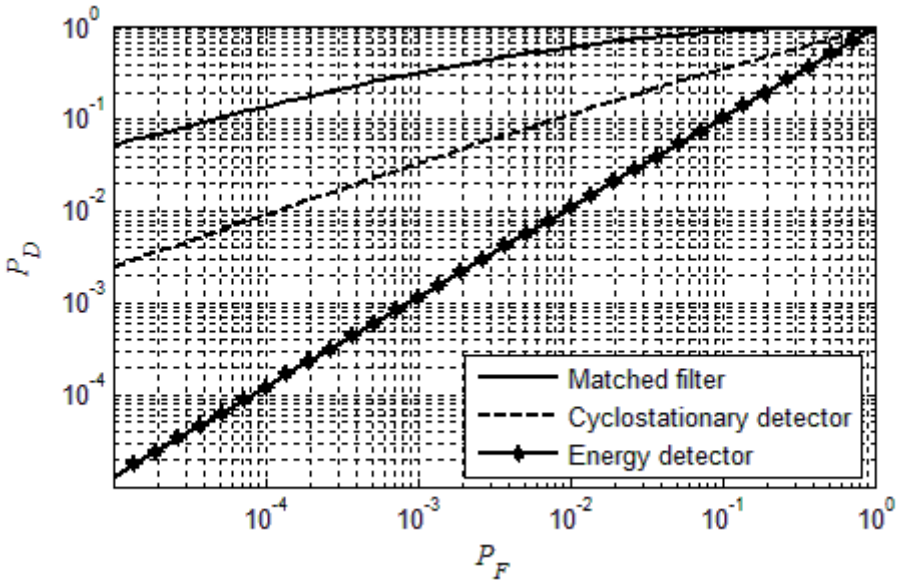

Fig. 6.28 Comparison of the performance of presented detectors (SNR =-23dB, c = 10^{-3})

A robust feature detector needs more preliminary information about the primary signal. In order to perform detection, we need to know some or all periodicities in the primary signal. Much better performance than that of an energy detector is an advantage in this case, as shown in Figure 6.28.

A matched filter detector has shown the best performance. This superiority in performance is only obtained through detailed information about the primary signal, including its shape and timing information.

In conclusion, the task of the current thesis to derive robust analogues to three most widely used detectors for cognitive radio was completed successfully. The results obtained are of substantial practical interest as the need for opportunistic spectrum sharing in urban areas is increasing daily.

7 Sensitivity of the Detectors to the Errors in Parameter Estimates

All robust detectors derived in the previous chapters need some *a priori* information about the parameters of input noise and signal. Such information is essential to their proper work. In our analysis in the previous chapters the assumption was that we know the values of all needed parameters exactly, which is not the actual case. In real life scenarios, we must estimate necessary parameters from input realization. All the results presented in this chapter are the result of author's own work.

To characterize the input noise, we want to know the variance of the Gaussian noise component σ^2 and the probabilities of impulses c. Estimators for both were derived in Chapter 4. ML estimators for variance of the Gaussian noise component is (4.3.6) and for the probability of impulse are (4.3.27)

$$\hat{\sigma}^2 = \frac{1}{n_1}\sum_{M_1} v_k^2 \qquad \hat{c} = \frac{n_2}{n}$$

Also, maximum amplitude of noise pulse b is required, but we assume that this parameter is determined by the receiver architecture. Because of this the value of b is known and we do not need to estimate it.

In addition, it is necessary to know some parameters of the primary signal. How much and what kind of information we need depends strongly on the used detector type. In the case of a robust energy detector we only need to know primary signal power σ_s^2, the estimate of which was derived in sixth chapter (6.1.14)

$$\hat{\sigma}_s^2 = \frac{1}{n_1}\sum_{M_1} x_k^2 - \hat{\sigma}^2 .$$

For robust feature detector we need to have knowledge about periodicity in primary user signal. For example, this can be carrier or pilot frequency, symbol rate or something else similar. For an unknown signal, those values also must be estimated from the cyclic spectrum but in the current thesis we assume that we already know those necessary parameters of the signal under interest. It was shown in the second part of Chapter 6 that our feature detector performance is better if we know the correlation between the elements of the received waveform. For this reason we also derived the ML estimator of the covariance matrix of input realization (4.3.49)

$$\hat{\mathbf{C}} = \frac{1}{n_1}\sum_{M_1} \mathbf{v}_k \mathbf{v}_k^T .$$

To build a robust matched filter detector, we need to know detailed information about the primary signal, including its shape and timing information. In practice, this information is usually too complex to estimate and it must be known. In all cases we need to estimate the variance of the Gaussian noise component σ^2 and the probability of noise impulses c. In addition, for some scenarios we need to estimate the power of the primary signal σ_s^2 or the covariance $\mathbf{C}$ between the elements of the received waveform. Other parameters needed are here assumed to be known *a priori*.

As we need to estimate some necessary parameters and this process is never 100% accurate, there will be errors in parameter estimates. Focus in this chapter is on the influence of those errors on the work of our robust detectors. The Monte Carlo method is used for this purpose here. The model of the detector for a predetermined set of variables is generated and then the model is tested for input waveform parameters that differ from those used in the model derivation. Results are depicted on graphs and are analyzed to obtain information about the behavior of previously proposed robust detectors.

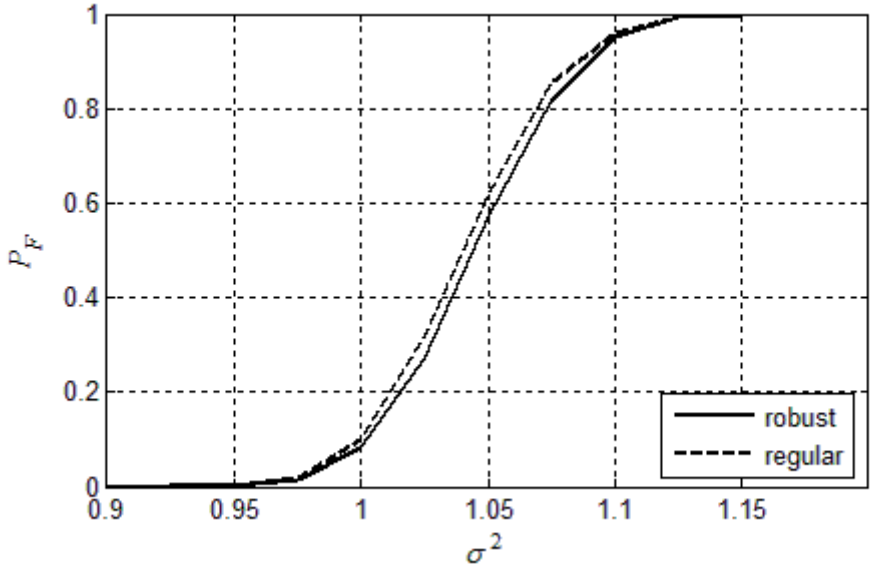

Fig. 7.1 Energy detector against noise power uncertainty

First, the robust energy detector (6.1.15) is dealt with. The situation in Figure 7.1 is as follows. A robust energy detector with the length n = 2080 is tuned for the parameter values: c = 10^{-3}, b = 128, σ^2 = 1, SNR = -10dB and *a priori* false detection probability is set to P_F = 0.1. The thick line in the figure illustrates the influence of noise power uncertainty. When the noise power has its assumed value 1, also the probability of false detection has its desired value 0.1. But if the actual value of noise power differs from its estimated value, then a dramatic change

occurs in the false detection probability. Even a difference of 5% in the value of noise power causes an increase of P_F by 0.5. Thus, our robust energy detector is very sensitive to uncertainty of noise power. The influence of noise power uncertainty on the ROC curve of thee robust energy detector is shown in Figure 7.2. Merely a 10% uncertainty has a clearly visible effect. When the actual noise power is higher than that estimated, the ROC curve slides toward the lower right corner of the graph, indicating loss of performance. On the other hand, when the actual noise power is smaller than that estimated, the threshold will be crossed very rarely and our detector stops working. Dashed line in Figure 7.1 shows the influence of noise power uncertainty for the regular energy detector. Both curves are overlapping showing that high sensitivity is the property of the energy detector, it is not just caused by the robustness of our detector.

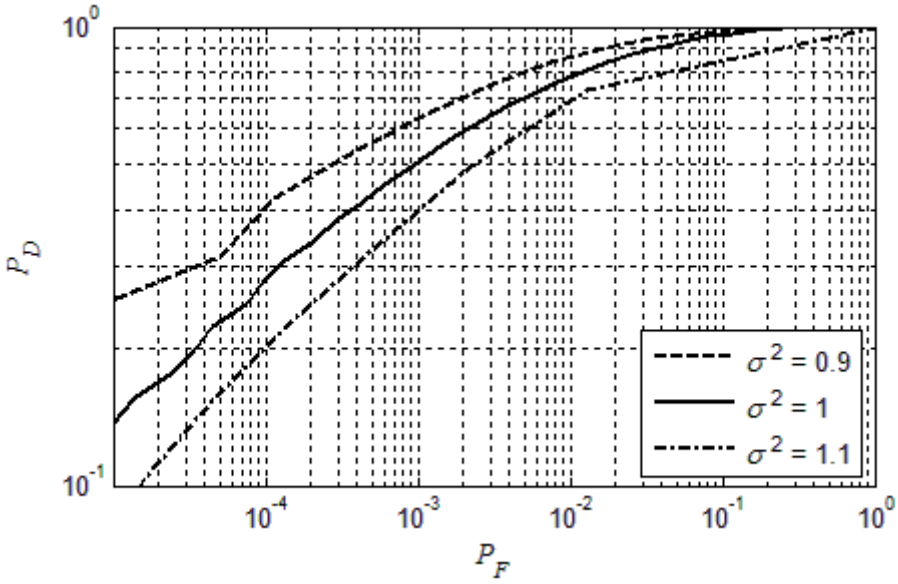

Fig. 7.2 Influence of noise power uncertainty on the ROC curve of the robust energy detector

In the derivation of the robust energy detector we modeled the primary signal also as the Gaussian random process with the variance σ_s^2 equal to the signal power. Due to this assumption, our model has symmetry between the power of the noise and that of the signal. When the signal-to-noise ratio is low, the dependence on the accuracy of noise power estimation is strong, as shown in Figure 7.1. If the signal is small, then also the influence of the precision of its estimate is small and can be discarded. In the opposite case, when the signal-to- noise ratio is large, then the dependence of the accuracy of the signal power estimation is the same as the dependence on the accuracy of noise power estimation at small SNR and vice versa. As the value of SNR is unknown in advance, in a general case both the signal and the noise power must be estimated as accurately as possible.

Next, we investigate the sensitivity of the robust energy detector to the precision of the estimate of impulse probability c (4.3.27). All the parameters of the detector are the same as previously, but now we change the actual value of impulse probability and measure its effect on false alarm probability. Results are depicted in Figure 7.3.

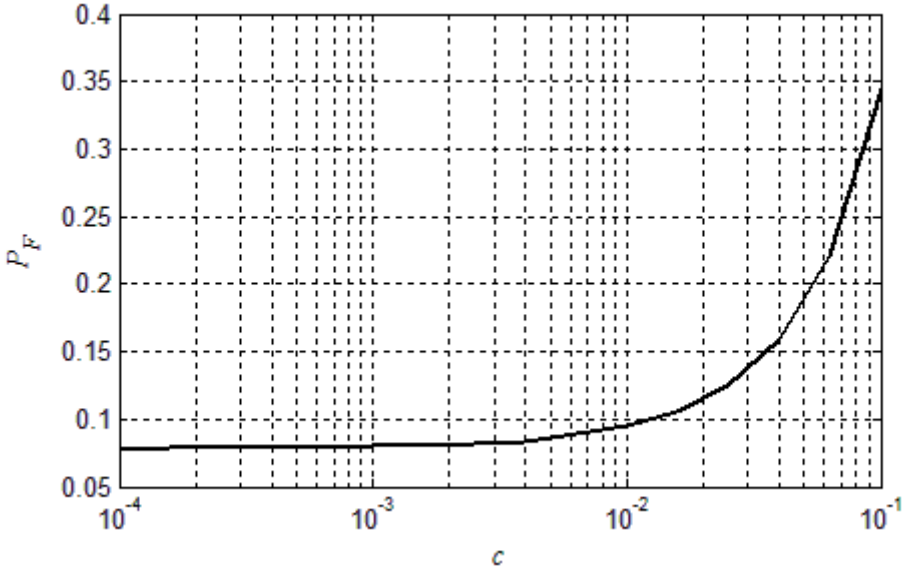

Fig. 7.3 Robust energy detector against uncertainty of impulse probability

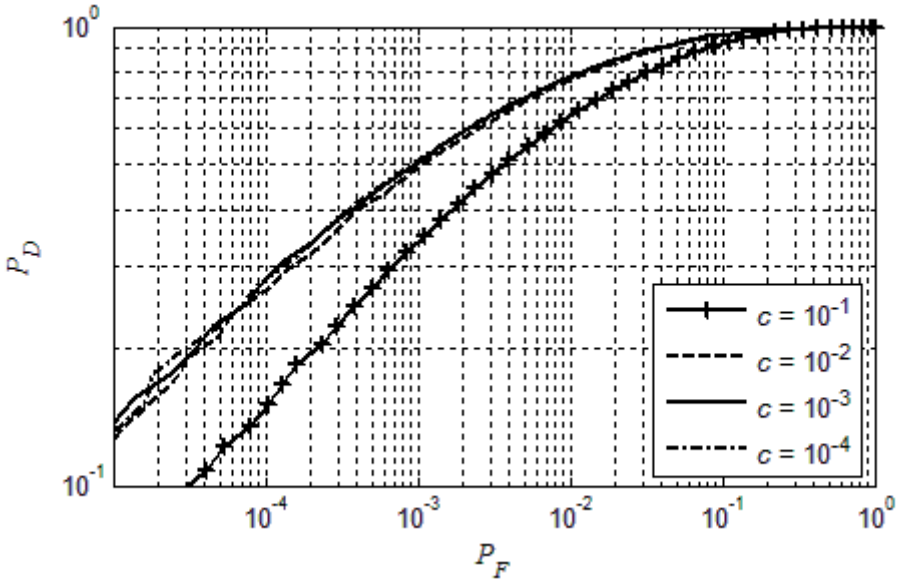

Fig. 7.4 ROC curve of robust energy detector against impulse probability uncertainty

Results in Figure 7.3 show that sensitivity to impulse probability uncertainty is smaller and its influence is asymmetric in nature. When the actual impulse probability is higher than estimated, then its sensitivity is strong. In the opposite case, when the actual probability is smaller than estimated, there is almost no influence. This claim can be reassured when comparing ROC curves in Figure 7.4. For the values of $c = 10^{-2}$, 10^{-3} and 10^{-4}, curves are practically overlapping, only unrealistically high probability $c = 0.1$ causes visible degradation of detector performance. In conclusion, the estimation of impulse probability does not have to be as accurate as the estimation of noise variance or signal power and we even may bias the shift towards low values of c.

Next, we consider a robust feature detector in Figure 6.15. As we used the CFAR approach here, we need no information about the primary signal power. It is necessary to have only information about one or more cyclic frequencies. But this information is assumed to be known previously and thus no estimation is needed. Thus, here our interest is in the influence of noise parameters σ^2 and c.

Graphs in Figures 7.5 and 7.6 show clearly that the robust feature detector is less sensitive to noise variance uncertainty than the robust energy detector. The model of the robust feature detector is tuned to exactly the same parameters as the robust energy detector before, the only difference is in the signal-to-noise ratio that is -23dB. This time the actual noise power must be more than twice of the estimated value to achieve the same 0.5 increase in false detection probability that was obtained with only 5% of uncertainty in the case of the robust energy detector.

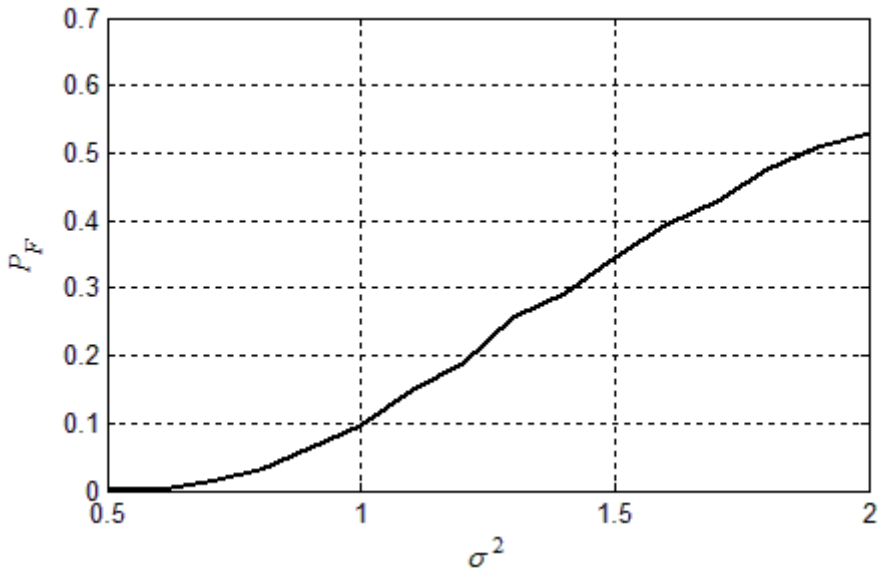

Fig. 7.5 Robust feature detector against noise power uncertainty

Simulated ROC curves for different noise variance uncertainty are depicted in Figure 7.6 for the robust feature detector. To show the difference clearly, the uncertainties used are much greater than those in Figure 7.2. When the actual noise variance is larger than that estimated, then the decision threshold is crossed much more often than assumed. For that reason, the corresponding ROC curve in Figure 7.6 is so short. In order to lengthen this curve, we need to increace the simulation time dramatically. As the feature detector uses the FFT in its implementation, then on the one hand, smaller noise variance than the estimated results will decrease the number of false detection, on the other hand, correct detection probability remains almost the same. For that reason the corresponding curve shows better performance in the figure. But if we had used proper threshold level for the given value of noise variance, then even better performance would have been available.

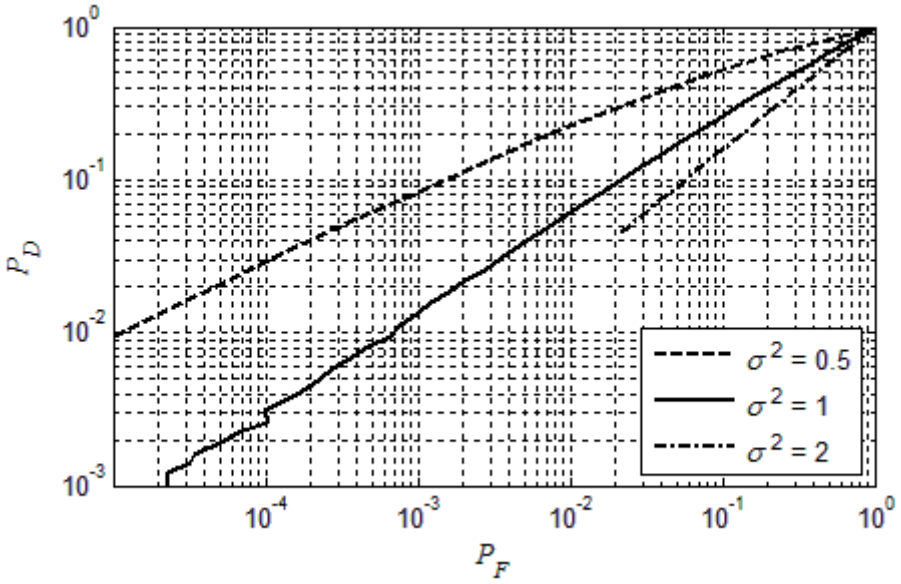

Fig. 7.6 Influence of noise power uncertainty on the ROC curve of the robust feature detector

Now we will consider the influence of the uncertainty of impulse probability on the robust feature detector. The graph in Figure 7.7 and ROC curves in Figure 7.8 can answer that question. Two differences between Figures 7.3 and 7.7 can be noticed. First, similarly to variance, much smaller influence of impulse probability uncertainty occurs here than with the robust energy detector. Another difference is in the behavior of the curves. When the actual impulse probability increases, the curve in Figure 7.3 is increased but the curve in the second figure shows a small decrease instead. The effect in the figure is caused by the difference in the treatment of an impulsive noise by the robust feature detector. As the robust energy detector limits impulses, replacing them with the threshold value η_{1l}, the feature detector replaces impulses with 0. This means that when impulse probability rises, more noise samples are removed and false detection probability decreases slightly.

But this does not mean better performance of the detector, as also a useful signal hidden in the noise is removed together with impulsive noise. This is clearly seen in Figure 7.8 where again ROC curves for $c = 10^{-2}$, 10^{-3} and 10^{-4} are practically overlapping and only the case $c = 0.1$ has somewhat poorer performance. Thus, in general, the robust feature detector is less sensitive to noise parameter uncertainty than observed in the case of the robust energy detector.

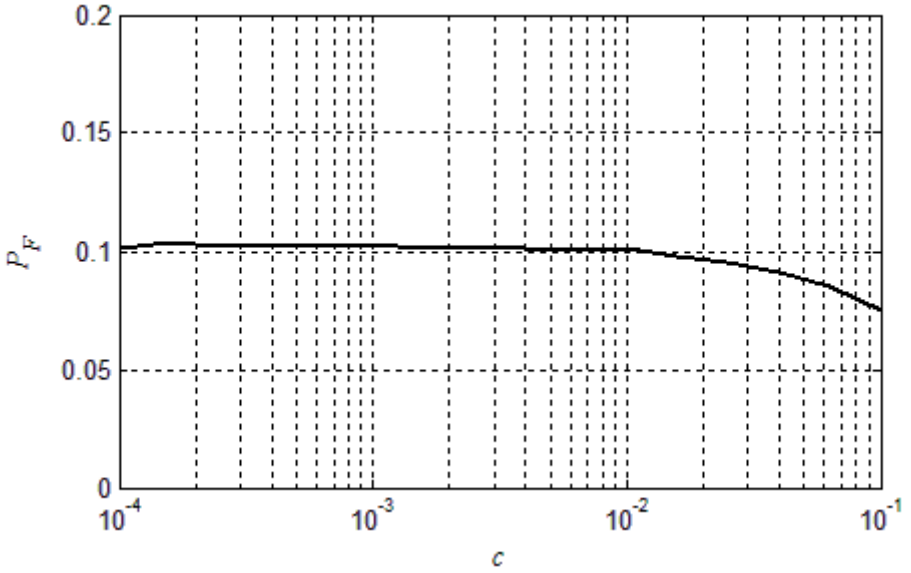

Fig. 7.7 Robust feature detector against uncertainty of impulse probability

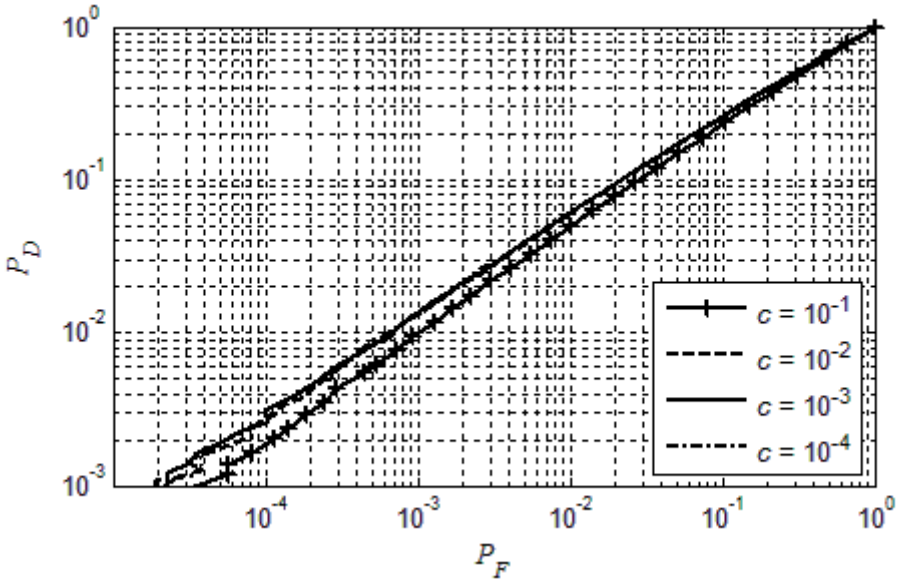

Fig. 7.8 ROC curve of the robust feature detector against impulse probability uncertainty

Finally, we will discuss the robust matched filter or the known primary signal case. Here we assume that we have complete information about the primary signal. Thus again, only things that must be estimated are noise parameters as was the case with the robust feature detector.

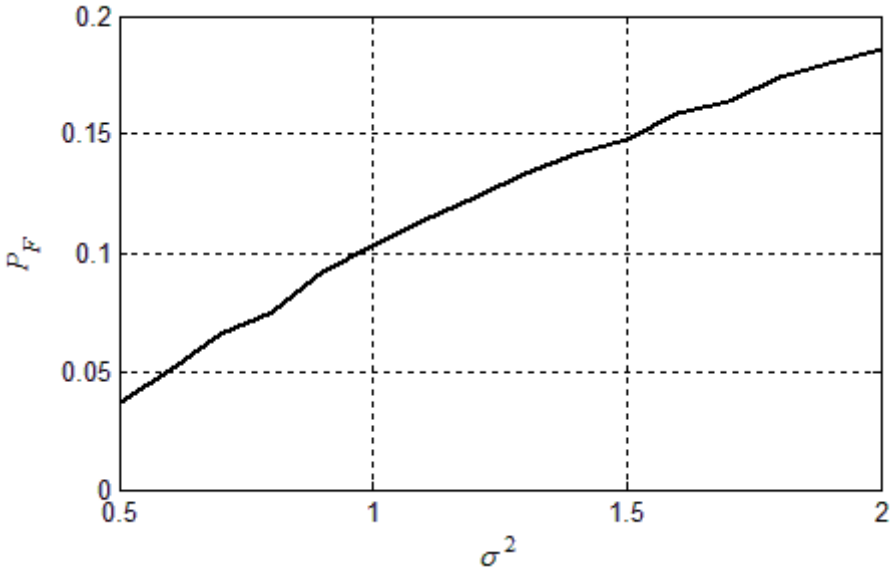

Fig. 7.9 Robust matched filter against noise power uncertainty

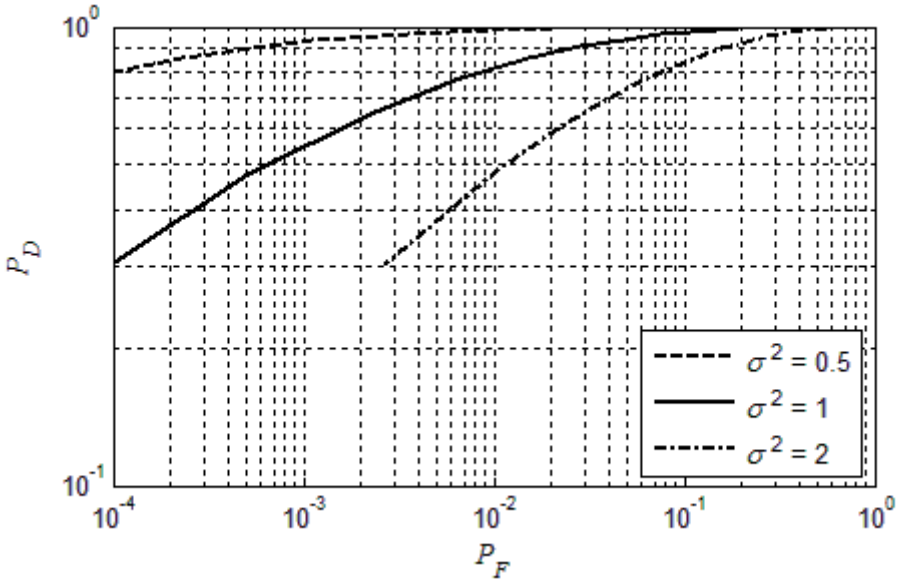

Fig. 7.10 Influence of noise power uncertainty on the ROC curve of the robust matched filter

Matched filter is tuned to exactly the same parameters as the two previous detectors; the only difference here is again in the signal-to-noise ratio, which is -23dB. Compared to the previous detectors, the robust matched filter has the lowest sensitivity to noise variance uncertainty, as shown clearly in Figure 7.9. The influence of uncertainty of impulse probability on our robust matched filter is shown in Figure 7.11. It is approximately the same as on the robust feature detector. But as here we also limit noise impulses instead of removing them, the actual value of c causes false detection probability to increase slightly. A similar fact can be identified also in Figure 7.12 where only the ROC curve visibly different from the other ones corresponds to the value $c = 0.1$.

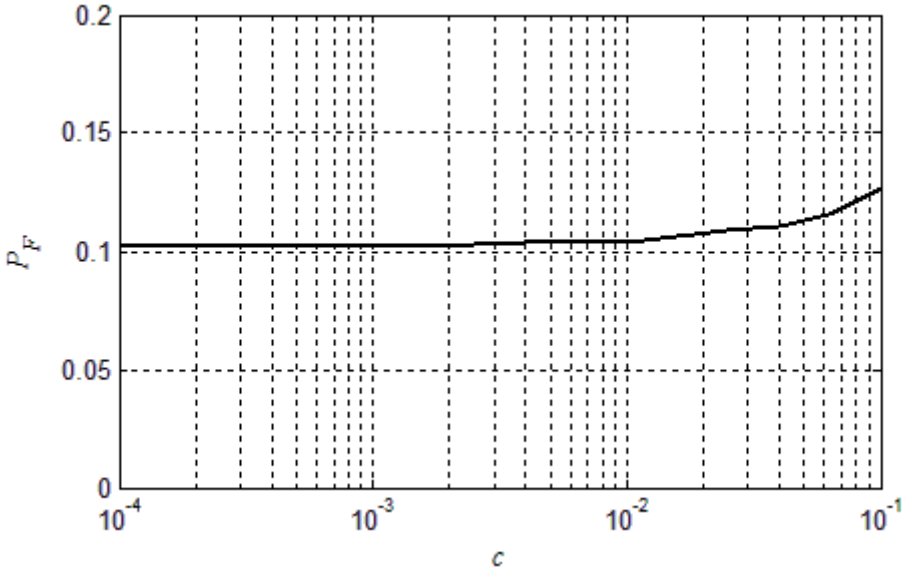

Fig. 7.11 Robust matched filter against uncertainty of impulse probability

In conclusion, all the robust detectors proposed are sensitive to the estimation error of the Gaussian noise variance σ^2. A robust energy detector is the most sensitive; an error of a few percent only can cause very large changes in false detection probability there. The robust feature detector has lower sensitivity to an estimation error and the robust matched filter, in turn, has the lowest sensitivity to such an error.

Regarding to sensitivity to the estimation error of the impulse probability c, this is smaller than in all three detectors. When comparing detectors against each other, the robust energy detector is the most sensitive to estimation errors. The robust feature detector and the matched filter have both the same low sensitivity. The dependence on the accuracy of the impulse probability estimation rises when the

probability of impulses is unrealistically high, above 0.01. In the region of lower impulse probability almost no dependence on estimation errors exists.

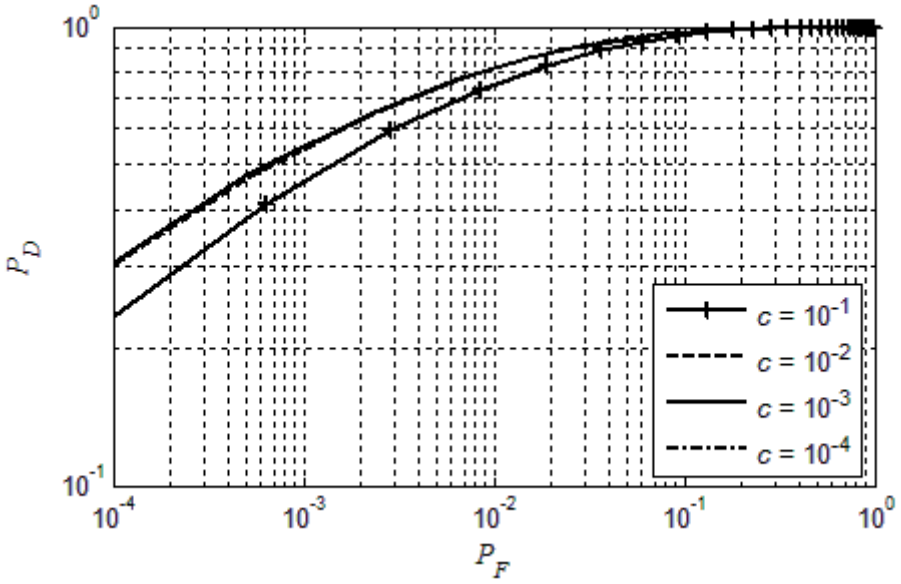

Fig. 7.12 ROC curve of the matched filter against impulse probability uncertainty

In conclusion, the estimation of the variance of the Gaussian component σ^2 must be done much more precisely than the estimation of the probability of impulse c. This is very favorable because most of the input samples contain Gaussian noise and only a few comprise impulsive noise. For that reason, the estimation of Gaussian noise variance is faster and more accurate than the estimate of impulse probability.

Furthermore, the sensitivity of our robust detectors to Gaussian noise variance uncertainty does not exceed that of regular detectors. On other hand, the sensitivity of our detectors to uncertainty of impulse probability is low, except in the areas of large values of c. This means that our detectors are indeed robust against impulses while for Gaussian noise they work as well as regular detectors.

8 Conclusion of the Thesis

The objective of the current thesis was to work out a set of three robust detectors for cognitive radio. This objective has been achieved successfully. We have an algorithm for each detector to be practically implemented. Theoretical analytical performance of those detectors was verified by computer simulation experiments.

An additional condition was that in the case of Gaussian background noise only their performance must be almost as good as that of regular detectors. However, when impulsive noise is added to the scene, they must continue working at the same performance level. This additional condition was also fulfilled for all three detectors, as proved by both analytical and simulated results. Thus, all three derived detectors are suitable for use in cognitive radio, selection of the detector depends mainly on the information about the primary signal available *a priori*.

The main contributions of the thesis are:

1. Introduction of a new model for impulsive noise. Impulsive noise was modeled explicitly by a uniform distribution. We allow impulses to occur only with certain probability and preserve the usual Gaussian noise component for most of the time.

The uniform distribution is selected because of its maximum entropy property, i.e. nothing is assumed to be known about the origin of the impulses. This noise model takes into account that the impulses that disturb the detection based on Gaussian assumption occur only with certain probability c. As such, the noise model is more intuitively satisfying than other popular models for impulsive noise.

2. Introduction of the robust energy detector. In the current thesis we derived a robust energy detector analogue for use in cognitive radio. In the merely Gaussian noise background the derived detector works almost as well as the regular energy detector. When the impulsive noise component appears, our robust detector continues to work as before without impulsive noise in its input. Asymptotic noise analysis was carried out and comparison of achieved analytical results showed good accordance with simulation results. Comparison with other robust energy detectors showed superiority of our model. The robust energy detector is suitable for applications where almost nothing is known about the primary user signal.

3. Introduction of the robust feature detector. We derived a robust cyclostationary detector analogue for use in cognitive radio. In the merely Gaussian noise background, the derived detector works almost as well as a regular cyclostationary detector. When an impulsive noise component appears, our robust detector continues to work almost as well as without impulsive noise in its input.

Asymptotic noise analysis was carried out and comparison of achieved analytical results showed good accordance with simulation results. It was shown that if we know the correlation between input waveform samples, then we can achieve even better performance but our detector still works quite well without such knowledge.

The robust feature detector achieves much better performance than the previously introduced robust energy detector if we have some preliminary information about the periodicity of the primary signal. Thus, such kind of detector is suitable for applications where some information about the primary user signal is available.

4. Introduction of the robust matched filter. We also derived a robust detector for a known primary signal – or a robust matched filter. In the merely Gaussian noise background, the derived detector works almost as well as a regular matched filter. When an impulsive noise component appears, our robust detector continues to work almost as well as without impulsive noise in its input. Asymptotic noise analysis was carried out and comparison of achieved analytical results showed good accordance with simulation results. Comparison with other robust matched filters showed advantages of our model against those compared. A robust detector for a known primary signal demands exact knowledge about the primary signal, on the other hand, it offers far superior performance than the other two detector types.

In conclusion, the task of the current thesis – to derive robust analogues to three most widely used detectors for cognitive radio was completed successfully. The results obtained are of great practical interest, as the need for opportunistic spectrum sharing in urban areas is increasing daily.

8.1 Directions for Further Research

During work with this thesis, many new questions and problems arose. Some topics briefly described below provide for future research.

In this research, it appeared that there is no known analytical solution for the PDF of the output noise of a cyclostationary detector in the presence of the primary signal. Output noise PDF can only be derived when a noise only acts at a detector's input. Thus, a common solution for this type of a detector is to fix the decision threshold for a constant false detection rate and then find the probability of correct detection through computer simulation. The core of the problem is in the fact that the joint PDF of the product of two noncentral Gaussian variables has no known analytical solution. When those multiplicands were independent, then moments of resulting variable and a solution could be found by help of the central limit theorem. But as the cyclostationary detector finds a signal through its inside

correlation, this is not the case. Thus, solving this problem would be of high practical value.

In the current thesis we only analyzed a single-cycle feature detector. In the future work also multi-cycle detectors should be studied.

Chapters 5 and 7 are based mostly on computer simulations. The author believes that in most cases, also analytical expressions can be derived for the performance of regular detectors in impulsive noise and the influence of noise parameters uncertainty on the derived robust detectors.

This thesis focused on binary hypothesis. The detector had to make one out of two decisions – the primary signal is present or absent. Another possibility, so-called three-way detectors, exists. When the detector cannot make a decision in favor of absence or presence of the primary signal, then it says, "I do not yet" and collects more data to make a decision later. Such an approach used with robust detectors would be interesting to study.

One of the most interesting problems to solve in future is to derive recursive algorithms for noise parameter estimation. In brief, the problem is as follows. In order to correctly estimate noise parameters we need to know intersection between the Gaussian and the impulsive noise. But in order to calculate this threshold we need to know estimates of noise parameters. Thus, there must be some initial estimate of noise parameter values and recursive algorithm that moves towards actual values themselves.

References

[1] FCC, BSpectrum Policy Task Force report,“ ET Docket 02-155, Nov. 2002.

[2] Estonian technical surveillance authority. “The Estonian radio frequency allocation plan.” Internet: http://www.tja.ee/index.php?id=11822, [Dec. 6, 2012].

[3] J. Mitolla and G. Q. MaGuire, Jr. “Cognitive Radio: Making Software Radios More Personal.” *IEEE Pers. Commun*, vol. 6, pp. 13–18, Aug. 1999.

[4] R. Sathyanarayana, M. Raustia, T. Hänninen and M. Jokinen. „CRAMNET opportunistic cognitive radio for manet with adaptive phy and dynamic routing capability.“ Internet: http://www.cwc.oulu.fi/home/files/news/CRAMNET_1.pdf, [Dec. 6, 2012].

[5] S. Haykin, "Cognitive Radio: Brain-empowered Wireless Communications", *IEEE Journal on Selected Areas of Communications*, vol. 23, pp. 201–220, Feb. 2005.

[6] J. Ma, G. Y. Li and B. H. Juang. “Signal Processing in Cognitive Radio.” *Proceedings of the IEEE*, vol 97, pp. 805-823, May 2009.

[7] C. R. Stevenson, G. Chouinard, Z. Lei, W. Hu, S. J. Shellhammer and W. Caldwell. “IEEE 802.22: The First Cognitive Radio Wireless Regional Area Network Standard.” *IEEE Communications Magazine*, vol. 47, pp. 130-138, Jan. 2009.

[8] S. Haykin, D. J. Thomson and J. H. Reed. “Spectrum Sensing for Cognitive Radio.” *Proceedings of the IEEE*, vol. 97, pp. 849-877, May 2009.

[9] Z. Quan, H.V. Poor, and A.H. Sayed, “Collaborative Wideband Sensing for Cognitive Radios.” *IEEE Signal Processing Magazine*, vol. 25, pp. 60–73, Nov. 2008.

[10] D. Pham, A. Zoubir, R. Bricic, and Y. Leung, “A Nonlinear M-Estimation Approach to Robust Asynchronous Multiuser Detection in Non-Gaussian Noise.” *IEEE Transactions on Signal Processing*, vol. 55, pp. 1624–1633, May 2007.

[11] P.J. Huber. *Robust Statistics.* John Wiley & Sons, 2005.

[12] K.L. Blackard, T.S. Rappaport, and C.W. Bostian, “Measurements and Models of Radio Frequency Impulsive Noise for Indoor Wireless Communications.” *IEEE Journal on Selected Areas in Communication*, vol. 11, pp. 991–1001, Sep. 1993.

[13] Q. Shan, S. Bhatti, I.A. Glover, R. Atkinson, I.E. Portugues,P.J. Moore, and R. Rutherford. "Characteristics of impulsive noise in electricity substations," in *Proc. 17th European Signal Processing Conference,* 2009, pp. 2136 -2140.

[14] G. Zhang, X. Wang, Y.-C. Liang and J. Liu. „Fast and Robust Spectrum Sensing via Kolmogorov-Smirnov Test." *IEEE Transactions On Communications*, vol. 58,pp. 3410 - 3416, Dec. 2010

[15] F. Moghimi, A. Nasri, and R. Schober. „*Lp*–Norm Spectrum Sensing for Cognitive Radio Networks Impaired by Non–Gaussian Noise," in *Proc. IEEE GLOBECOM*, 2009, pp. 901-906.

[16] W. Lin and Q. Zhang. „A Design of Energy Detector in Cognitive Radio under Noise Uncertainty," in *Proc. ICCS,* 2008, pp. 213- 217.

[17] A. Jõgi. *Tõenäosusteooria I*. Tallinn: TTÜ kirjastus, 2000.

[18] F. F. Digham, M.-S. Alouini and M. K. Simon. "On the Energy Detection of Unknown Signals Over Fading Channels." *IEEE Transactions on Communications*, vol. 55, pp. 3575-3579, Jan. 2007.

[19] D. Cabric, A. Tkachenko and R. W. Brodersen. "Experimental Study of Spectrum Sensing based on Energy Detection and Network Cooperation." *TAPAS '06 Proceedings of the first international workshop on Technology and policy for accessing spectrum,* 2006.

[20] A.Sahai, N.Hoven and R. Tandra. "Some Fundamental Limits on Cognitive Radio", in *Proceedings Allerton Conference on Communications, Control and Computing*, 2004.

[21] D. Hanson, J. Antoni, G. Brown and R. Emslie." Cyclostationarity for ship detection using passive sonar: progress towards a detection and identification framework." In *Proc. of Acoustics 2009*, 2009, pp. 1-8.

[22] D. Cabric and R.W. Brodersen. „Cognitive Radio Spectrum-Sharing Technology" in *Wireless Technologies: Circuits, Systems, and Devices*. K. Iniewski, CRC press, 2007, pp.131-157

[23] W.A.Gardner, *Introduction to Random Processes with Applications to Signals and Systems*. New York: Macmillan, 1985.

[24] W.A. Gardner, A. Napolitanob and L. Paurac. "Cyclostationarity: Half a century of research." *Journal of Signal Processing*, vol. 86, pp. 639–697, Apr. 2006.

[25] N. Wiener. *The Fourier Integral and Certain of its Applications.* London, Cambridge University Press, 1933.

[26] W.A. Gardner and C. M. Spooner. “Cyclic spectral analysis for signal detection and modulation recognition.” in *Proc. MILCOM 88*, 1988, pp. 419 – 424.

[27] J. Lunden, V. Koivunen, A. Huttunen and H. V.Poor. “Spectrum Sensing in Cognitive Radios Based on Multiple Cyclic Frequencies.” In *Proc. CrownCom 2007*, 2007, pp. 37 – 43.

[28] A. G. Glen, L. M. Leemis and J. H. Drew. “Computing the Distribution of the Product of Two Continuous Random Variables.” *Computational Statistics & Data Analysis*, vol. 44, pp. 1-14, Jan. 2004.

[29] L. A. Goodman. "The Variance of the Product of K Random Variables." *Journal of the American Statistical Association*, vol. 297, pp. 54-60. Mar.1962,

[30] R.Ware and F. Lad. “Approximating the Distribution for Sums of Products of Normal Variables.” Internet: http://www.math.canterbury.ac.nz/research/ucdms2003n15.pdf, [Dec. 6, 2012].

[31] S. Enserink and D. Cochrun. “On Detection of Cyclostationary Signals,” in *Proc. ICASSP-95,* 1995, pp. 2004-2007.

[32] R. T. Short. “Computation of Rice and Noncentral Chi-Squared Probabilities.” Internet: http://www.phaselockedsystems.com/NoncentralChiSquared.pdf, Apr. 27, 2012 [Dec. 1, 2012].

[33] Y. Zeng and Y. C. Liang. “Maximum-Minimum Eigenvalue Detection for Cognitive Radio.” in *Proc. IEEE PIMRC*, 2007, pp. 1-5.

[34] Y. Zeng and Y. C. Liang. “Covariance Based Signal Detections for Cognitive Radio, in *Proc. IEEE DYSPAN*, 2007, pp. 202–207.

[35] Y. Zeng, C. L. Koh, and Y. C. Liang. “Maximum eigenvalue detection: Theory and application.” in *Proc. IEEE ICC*, 2008, pp. 4160–4164.

[36] J. Parsons, *The Mobile Radio Propagation Channel*. New York: Wiley, 2000.

[37] J. Myung, “Tutorial on maximum likelihood estimation.” *Journal of Mathematical Psychology*, vol. 47, pp. 90–100, 2003.

[38] P.S. Dwyer. “Some Applications of Matrix Derivatives in Multivariate Analysis.” *Journal of the American Statistical Association*, vol. 62, pp. 607-625, Jun. 1967.

[39] K. B. Petersen and M. S. Pedersen. (2008, November 14) *The Matrix Cookbook*. [On-line]. Available: http://orion.uwaterloo.ca/~hwolkowi/matrixcookbook.pdf, [Dec. 6, 2012].

[40] A. Papoulis and S.U. Pillai. *Probability, Random Variables and Stochastic Processes*. McGraw Hill, 2002.

[41] H. L. van Trees, *Detection, Estimation and Modulation Theory*. John Wiley and sons, 1968.

[42] T. A. Schonhoff and A. A. Giordano. *Detection and Estimation Theory and Its Applications*. New Jersey: Prentice Hall, 2006, pp. 300-304.

[43] A. Hjorungnes. *Complex-Valued Matrix Derivatives. With Applications in Signal Processing and Communications*. Cambridge University press, 2011.

[44] I. Tammeraid. *Tõenäosusteooria ja matemaatiline statistika*. Tallinn : TTÜ Kirjastus, 2004.

[45] T. Trump, “A Robust Detector for Uniformly distributed noise” in *Proc. ICASSP,* 2010, pp. 3870-3873.

[46] J. Myung, “Tutorial on maximum likelihood estimation.” *Journal of Mathematical Psychology*, vol. 47, pp. 90–100, 2003.

[47] W.A.Gardner, *Introduction to Random Processes with Applications to Signals and Systems*. New York: Macmillan, 1985.

[48] K. Po and J.-I Takada. Signal Detection Method based on Cyclostationarity for Cognitive Radio. Technical Report of IEICE. Internet: http://www.ap.ide.titech.ac.jp/publications/Archive/IEICE_TRSR(0703Kimtho)pdf , [Dec. 6, 2012].

[49] A. V. Dandawatk and G. B. Giannakis. “Statistical Tests for Presence of Cyclostationarity.” *IEEE transactions on signal processing*, vol. 42, pp. 2355 - 2369, Sep.1994.

[50] V. Bunyakovsky. **“**Sur quelques inegalités concernant les intégrales aux différences finies”. *Mem. Acad. Sci. St. Petersbourg* 7 (1): 9 1859.

[51] J. O. Smith, *Spectral Audio Signal Processing*. [On-line]. Available: http://ccrma.stanford.edu/~jos/sasp/ [Dec. 6, 2012].

[52] P.A. Bromiley. "Products and Convolutions of Gaussian Distributions." Internet: http://www.tina-vision.net/docs/memos/2003-003.pdf, Nov. 27, 2003 [Dec. 6, 2012].

[53] H. Wang, G. Noh, D. Kim, S. Kim and D.Hong. "Advanced Sensing Techniques of Energy Detection in Cognitive Radios." *Journal of Communications and Networks*, vol. 12, pp 19-29, Feb. 2010.

[54] T. E. Biedka, L. Mili and J. H. Reed. "Robust Estimation of Cyclic Correlation in Contaminated Gaussian Noise," in *Proc. Signals, Systems and Computers*, 1995, pp. 511 – 515.

[55] J. Lehtomäki. "Analysis of Energy Based Signal Detection." Ph.D. thesis, University of Oulu, Findland, 2005.

[56] Y.T. Chan, H.C. So, Q. Yuan and R. Inkol. "Optimum Detection of Spread Spectrum Signals," in *Proc. Wireless 98*, 1998. pp.1-9.

[57] A. M. Zoubir, V. Koivunen, Y. Chakhchoukh and M. Muma. "Robust Estimation in Signal Processing". *IEEE Signal Processing Magazine*, vol. 29, pp 61.-80, Jul. 2012.

[58] I.Tammeraid. *Matemaatiline analüüs I*. Tallinn: TTÜ kirjastus, 2001.

[59] S. B. Pope. "Algorithms for Ellipsoids." Internet: http://tcg.mae.cornell.edu/pubs/Pope_FDA_08.pdf, Feb. 01, 2008 [Dec. 6, 2012].

[60] M. Väljas. *Analüütiline Geomeetria*. Tallinn: TTÜ kirjastus, 2012.

[61] S. R. Das**. "**Quantitative Methods for Finance. Cholesky Decomposition." Internet: http://algo.scu.edu/~sanjivdas/q115/node91.html, Feb. 11, 2010 [Dec. 6, 2012].

[62] W. *A.* Gardner and C.M. Spooner. "Signal Interception: Performance Advantages of Cyclic-Feature Detectors". IEEE Transactions on Communications, vol. 40, pp. 149-159, Jan. 1992.

[63] H. Hu. (2009) "Cyclostationary Approach to Signal Detection and Classification in Cognitive Radio Systems." [On-line]. Available: http://cdn.intechopen.com/pdfs/8832/InTechCyclostationary_approach_to_signal_detection_and_classification_in_cognitive_radio_systems.pdf [Dec. 2, 2012].

[64] M. E. Castro. “Cyclostationary Detection for OFDM in Cognitive Radio Systems.” MS thesis, University of Nebraska, USA, 2011.

[65] S. A. Bhatti, Q. Shan, I. A. Glover, R. Atkinson, I. E. Portugues, P. J. Moore and R. Rutherford. „Impulsive noise modelling and prediction of its impact on the performance of WLAN receiver,“ in *Proc. EUSIPCO, 2009*, pp. 1680-1684.

[66] D. Erdogmus, R. Agrawal and J. C. Principe. „A Mutual Information Extension to The Matched Filter“. *Signal Processing,* vol 85. Pp.927-935.May. 2005.

[67] G. Shevlyakov and K. Kim. „Minimax robust detection of a known signal in a general class of noises,“ in *proc ICASSP’05,* 2005, pp. 721-724.

[68] G. Shevlyakov, K. Lee, V. Shin and K. Kim. “Robust Minimum Distance Neyman-Pearson Detection of A Weak Signal in Non-Gaussian Noise,“ in *proc* EUSIPCO 2009,2009, pp. 1012-1016

[69] G. Shevlyakov and K. Kim.“ Robust Minimax Detection of a Weak Signal in Noise With a Bounded Variance and Density Value at the Center of Symmetry,“ *IEEE Transactions on Information Theory*, vol. 52,pp. 1206-1211, Mar. 2006

[70] D. G. Khairnar, S. N. Merchant and U. B. Desai. „Radar Signal Detection In Non-Gaussian Noise Using RBF Neural Network,“ *Journal of Computers*, vol 3, pp.32-39, Jan. 2008.

[71] S. Haykin and M. Moher. Modern Wireless Communications, Prentice Hall, 2005, pp 70 -71.

Author’s Publications

[72] T. Trump and I. Müürsepp. “An Energy Detector for Spectrum Sensing in Impulsive Noise Environment,” in *Proc. PIMRC,* 2011, pp 467 – 471.

[73] T. Trump and I. Müürsepp. “Robust Spectrum Sensing for Cognitive Radio,” in *Proc. EUSIPCO,* 2011, pp 1224 – 1228.

[74] J. Berdnikova, T. Ruuben, I. Müürsepp, E. Lossmann. „Resolution and Doppler Tolerance of Cognitive System Waveforms.“ *Electronics and Electrical Engineering*, vol.103(7), pp. 101 – 104, May 2010

Abstract

The thesis handles detectors in cognitive radio. The main goal of the research is to derive robust analogues to three main detector types proposed for use in cognitive radio applications. Those three are: an energy detector, a cyclostationary detector and a matched filter.

License based radio spectrum allocation is unsuitable for increasing demand for excess bandwidth for mobile users. Frequency channels dedicated for mobile users or wireless access are under heavy load while at same time many licensed frequency bands are highly underutilized. Cognitive radio technology can offer a helping hand here allowing dynamic spectrum access. Licensed or so called primary user can still use its dedicated radio resources. But when they happen to be free, then secondary users are allowed to use this idle resource opportunistically for their own purposes.

Correct detection of presence or absence of the primary user is very important for cognitive radio. There are many well known solutions for this detection problem but they all share the same problem. Those solutions are not meant to work in the presence of impulsive background noise. Due to the man-made impulsive noise component present today, such detectors would perform badly, thus degrading the performance of whole cognitive radio system.

Three robust detectors are derived in the current work in order to solve the problems described. All of them were found to work well both with and without the presence of the impulsive noise component.

A new improved model for impulsive noise is proposed. Joint probability density function is derived for the sum of Gaussian and proposed impulsive noise. Based on the derived PDFs, Maximum Likelihood Estimators are derived for noise parameters.

Robust detectors are derived and their asymptotic performance is presented. Analytical results are compared with computer simulations, showing good agreement between the two. Finally, our solutions are compared with the other robust detectors proposed in order to demonstrate superiority of our work.

Kokkuvõte

Käesolev doktoritöö käsitleb kognitiivses raadios kasutust leidvaid detektoreid. Töö põhieesmärgiks on välja töötada impulssmürade suhtes robustsed analoogid kolmele enimkasutatavale detektoritüübile, milleks on energiadetektor, tsüklostatsionaarne detektor ja sobitatud filter.

Seoses mobiilsideseadmete järjest suuremahulisema kasutamisega osutub senini rakendust leidnud raadioeetri litsentsipõhine jagamine ebaefektiivseks. Mobiilside jaoks eraldatud sageduskanalid töötavad suurel koormusel, kuid samas leidub ohtralt muuks otstarbeks eraldatud kanaleid, mille reaalne kasutatavus on väga madal. Lahendus seisneb kognitiivse raadio tehnoloogias, mis võimaldab raadioeetri dünaamilist jagamist kasutajate vahel. Raadiosagedusloa omanik, nn primaarne kasutaja, saaks ka sellisel juhul alati kasutada talle eraldatud kanaleid. Kuid juhul, kui viimane neid ise parajasti ei kasuta, oleks avatud võimalus kõigile teistele, sekundaarsetele kasutajatele vaba ressursi oportunistlikuks kasutamiseks.

Kognitiivse raadio juures on väga oluliseks aspektiks võimekus õigesti tuvastada primaarse kasutaja signaali olemasolu või puudumist. Selle ülesande lahendamiseks on välja töötatud mitmeid tehnilisi lahendusi. Varasemate lahenduste puudus seisneb selles, et nende väljatöötamisel aluseks võetud müramudel ei vasta tänapäeval tihti enam tegelikkusele. Inimtekkeliste impulssmürade mõjul ei tööta sellised lahendused enam korrektselt, mistõttu nende kasutamine tooks kaasa kognitiivse raadiosüsteemi töö kvaliteedi märkimisväärse languse.

Ülaltoodud põhjustel on käesolevas töös välja töötatud kolm robustse detektori tüüpi. Kõik kolm töötavad ühtemoodi hästi, olenemata sellest, kas taustamürad sisaldavad impulsskomponenti või mitte.

Töös on kirjeldatud enamlevinumaid detektoritüüpe ja nende sooritust nii Gaussi- kui impulssmüra korral.

Töös esitatakse uus ja parem impulssmürade mudel seni kasutusesolevate asemel. Seejärel uuritakse impulss- ja Gaussi müra ühist jaotusseadust nii ühe- kui mitme-mõõtmelisel juhul. Saadud jaotustiheduste põhjal leitakse maksimaalse tõepärasuse hinnangud müra parameetrite jaoks.

Uurimistulemusena esitatakse kolm robustset detektorit, leitakse nende asümptootiline sooritus ja võrreldakse saadud analüütilisi avaldisi arvuti-simulatsioonide tulemustega. Teoreetiliste ja simuleeritud tulemuste kokkulangevus on kõikidel juhtudel hea. Lisaks võrreldakse töös meie detektoreid varem väljapakutud robustsete detektoritega demonstreerimaks veel kord, et meie tulemused on varasemast paremad.

APPENDIX 1

PUBLICATIONS

PUBLICATION 1

T. Trump and I. Müürsepp. “An Energy Detector for Spectrum Sensing in Impulsive Noise Environment,” in *Proc. PIMRC,* 2011, pp 467 – 471.

An Energy Detector for Spectrum Sensing in Impulsive Noise Environment

Tõnu Trump and Ivo Müürsepp
Department of Radio and Telecommunication Engineering
Tallinn University of Technology
Tallinn, Estonia
Email: tonu.trump@lr.ttu.ee, ivom@lr.ttu.ee

***Abstract*—In this paper we propose a robust energy detector for spectrum sensing in cognitive radio systems. The detector is derived by modelling the noise process as consisting of two components, Gaussian noise and impulsive noise. The impulsive noise is modelled using a uniform distribution that appears with a certain probability. A convenient approximation using the max operator is then applied to the resulting probability density function to gain mathematical tractability. The performance of the proposed detector is analysed theoretically and the results of the theoretical analysis are verified in our simulation study.**

***Index Terms*—Cognitive radio, spectrum sensing, robust detection**

I. Introduction

Cognitive radio is a promising new technology that provides a way for opportunistic and efficient reuse of radio spectrum resources. The key enabler to this technology is reliable detection of spectral holes which could be used by the secondary users. In the literature there are several detectors proposed for this purpose [1], [2], most popular of them probably being the energy detector. The popularity is partly because of simplicity of the energy detector but also because it does not need any assumptions on the waveforms emitted by primary users.

Spectrum sensing for cognitive radio has to work with several impairments like fading, shadowing, and presence of noise. Usually the noise is assumed to be white and Gaussian but in real life situations this does not need to be the case. In particular one has to consider the presence of impulsive noise, both man-made and natural. Non-Gaussian ambient noise is a major impairment to signal processing techniques that are based on a Gaussian assumption [3]. To cope with the impulsive noise one needs to build some robustness [4] into the detector. For measurement results concentrating on impulsive noise see e.g. [5], [6] and references therein. A robust detection algorithm for spectrum sensing in cognitive radio applications based on L_p norm has recently been proposed in [7].

In this paper we will develop an energy–like detector that is not sensitive to impulsive noise. The derivation is based on modelling the impulsive component of the noise explicitly by a uniform distribution and preserving the Gaussian noise component as usual. The uniform probability density function (PDF) have been used to model heavy tail noise before in e.g. [8]. In the analysis part of the paper we derive the formulae for probabilities of detection, P_D, and false alarm, P_F, of the proposed detector but also for the time required to reach a given P_D and P_F level with certain signal and noise powers.

II. System model

We consider the problem of detecting the presence of primary users in a given frequency band without any prior knowledge of primary transmissions. The detection problem we need to solve is [2], [9]

$$\begin{aligned} H_0 &: x(t) = v(t) \\ H_1 &: x(t) = s(t) + v(t), \end{aligned} \tag{1}$$

i.e. the received waveform $x(t)$ may be noise $v(t)$ only or it may consist of a sum of signal of interest $s(t)$ and noise $v(t)$ and the variable t denotes discrete time. The detector has to decide which of the hypotheses is more likely given the received waveform $x(t)$. We assume that the noise $v(t)$ comprises a weighted sum of zero mean additive white Gaussian noise process and an additional impulsive noise component. The impulsive noise component is assumed not to be present most of the time but appear with certain probability c so that the impulsive component obeys the probability density function

$$f_i(x) = \frac{c}{b-a} + (1-c)\delta(x), \tag{2}$$

with $0 < c < 1$ and a and b being the lower and upper limits on the values that the impulsive noise can take and $\delta(\cdot)$ denotes the Dirac delta function. In practice a and b may for instance be the smallest and largest numbers that can be represented at the output of analogue to digital (A/D) converter. We assume that $b = -a$. The uniform distribution is selected because of its maximum entropy property i.e. there is nothing assumed to be known about the origin of the impulses. For instance the impulses may be due to failures of the A/D converter or some interferences that are not well modelled by a Gaussian noise process.

Thus the noise $v(t)$ is a sum of two components

$$v(t) = v_g(t) + v_i(t). \tag{3}$$

The noise model obtained this way is intuitively very satisfying as most of the time the noise is Gaussian and in addition to that there are relatively rare impulses. It is believed that this model represents the actual situation rather accurately.

978-1-4577-1348-4/11/$26.00 ©2011 IEEE

The PDF of $v(t)$ can be found as convolution of the probability densities of its additive components.

$$\begin{aligned} p(x) &= \int_{-\infty}^{\infty} \frac{1-c}{\sqrt{2\pi}\sigma} e^{-\frac{\tau^2}{2\sigma^2}} \left[\frac{c}{b-a} \left(u(\tau - x - a) \right.\right. \\ &\quad \left.\left. - u(\tau - x - b) \right) + (1-c)\delta(\tau - x) \right] d\tau \\ &= \frac{1-c}{\sqrt{2\pi}\sigma} e^{-\frac{x^2}{2\sigma^2}} \\ &\quad + \frac{c}{2(b-a)} \left[\mathrm{erf}\left(\frac{x+b-s}{\sqrt{2}\sigma} \right) \right. \\ &\quad \left. - \mathrm{erf}\left(\frac{x+a-s}{\sqrt{2}\sigma} \right) \right], \end{aligned} \tag{4}$$

where $u(t)$ is the unit step function and $\mathrm{erf}(x)$ is the error function

$$\mathrm{erf}(x) = \frac{2}{\sqrt{\pi}} \int_0^x e^{-x^2} dx.$$

Unfortunately this PDF is not convenient for designing a detector and to continue we invoke some approximations. First we assume that $b-a$ is much larger that σ and also much larger than $|s|$. This is a reasonable assumption if we think of a and b being the limits of the dynamic range that is available for the waveform. Then the impulsive noise can take any value inside these limits and in fact it is distinguishable from the Gaussian noise component only if it takes on large values as compared to the rest of the waveform components. In this case the difference of the error functions is approximately constant in the range of $[a, b]$.

$$\frac{1}{2} \left(\mathrm{erf}(\frac{x+b-s}{\sqrt{2}\sigma}) - \mathrm{erf}(\frac{x+a-s}{\sqrt{2}\sigma}) \right) \approx 1.$$

Second, let us approximate the sum of two remaining probability density functions, Gaussian and uniform, for any given value of x by the one that has the largest absolute value. In addition we assume again that the data is collected via an A/D converter operating in the range $a < x(t) < b$ so that the Gaussian probability density function with infinite support gets limited into the interval $[a, b]$. Another interpretation of changing the summation with picking the one with largest absolute value would be that if impulses are present, they replace the original samples as it would in fact be in case of A/D converter failures.

The approximation is illustrated in Fig. 1 with $c = 0.3$, $b = -a = 50$ and $\sigma = 5$. Note that we have selected the difference between b and σ to be relatively small and the probability of impulses unrealistically high to make the differences between the curves clearly visible. It can be seen that the approximation is very close to the true probability density function. The differences appear in the area where the Gaussian PDF goes over to the uniform tail and at the ends of the interval $[a, b]$. The larger is the difference between the standard deviations of signal and the Gaussian noise from one side and the impulsive noise interval $b-a$ from the other side, the better is the invoked approximation. The main benefit from the approximation is that it leads to tractable mathematics.

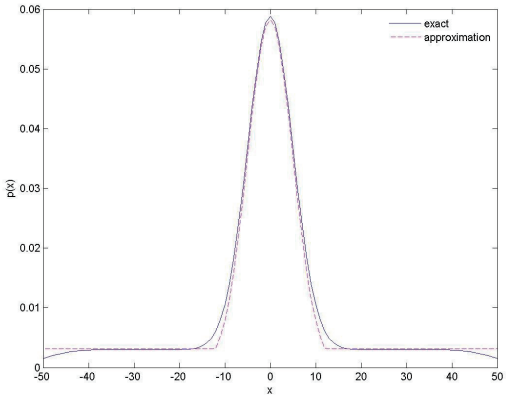

Fig. 1. Comparison of exact PDF and the approximation used in this paper for $a = -50$, $b = 50$, $c = 0.3$ and $\sigma = 5$.

The noise $v(t)$ is thus modelled as consisting of two components with the largest component determining the outcome entirely at each time instant

$$|v(t)| = \max[|v_g(t)|, |v_i(t)|]. \tag{5}$$

III. Likelihood Ratio

Let us now continue with derivation of an energy–like detector using the noise model just derived. The conditional probability density of the received waveform being noise only can with these approximations be written as

$$p(x|H_0) = \begin{cases} \beta_0 \max\left(\frac{1-c}{\sqrt{2\pi}\sigma_n} e^{-\frac{|x|^2}{2\sigma_n^2}}, \frac{c}{b-a} \right) & a < x < b \\ 0, & \text{otherwise} \end{cases} \tag{6}$$

and the conditional probablility density of the received waveform being signal plus noise as

$$p(x|H_1) = \beta_1 \max\left(\frac{1-c}{\sqrt{2\pi(\sigma_n^2+\sigma_s^2)}} e^{-\frac{|x|^2}{2(\sigma_n^2+\sigma_s^2)}}, \frac{c}{b-a} \right) \tag{7}$$

if $a < x < b$ and 0 otherwise. Let us denote the variances appearing in the expressions for the two hypotheses as

$$\sigma_l^2 = \begin{cases} \sigma_n^2 & l = 0 \\ \sigma_n^2 + \sigma_s^2 & l = 1 \end{cases}.$$

With this notation we can express the densities above as

$$p(x|H_l) = \begin{cases} \beta_l \max\left(\frac{1-c}{\sqrt{2\pi}\sigma_l} e^{-\frac{|x|^2}{2\sigma_l^2}}, \frac{c}{b-a} \right) & a < x < b \\ 0, & \text{otherwise} \end{cases}. \tag{8}$$

The normalization factors β_l can be found by solving

$$\int_a^b p(x|H_l) dx = 1 \tag{9}$$

for β_l. This results in

$$\beta_l = \left[(1-c)\mathrm{erf}\left(\sqrt{\frac{\eta_l}{2\sigma_l^2}}\right) + c\left(1 - \frac{2\sqrt{\eta_l}}{b-a}\right)\right]^{-1} \quad (10)$$

and

$$\eta_l = -2\sigma_l^2 \ln\left(\frac{c}{1-c}\frac{\sqrt{2\pi\sigma_l^2}}{b-a}\right) \quad (11)$$

is the intersection point of the Gaussian and uniform distributions.

We can give to PDF-s of x in the interval $a \leq x \leq b$ a more convenient form for future derivation as

$$\begin{aligned} p(x|H_l) &= \frac{\beta_l(1-c)}{\sqrt{2\pi\sigma_l^2}} \max\left[e^{-\frac{|x|^2}{2\sigma_l^2}}, e^{\ln\left(\frac{c}{1-c}\frac{\sqrt{2\pi\sigma_n^2}}{b-a}\right)}\right] \\ &= \frac{\beta_l(1-c)}{\sqrt{2\pi\sigma_l^2}} \\ &\quad e^{-\frac{1}{2\sigma_l^2}\min\left(|x|^2, -2\sigma_l^2\ln\left(\frac{c}{1-c}\frac{\sqrt{2\pi\sigma_l^2}}{b-a}\right)\right)}. \end{aligned} \quad (12)$$

PDFs of $y = x^2$ are then $p(y) = \frac{p(x)}{\frac{dy}{dx}}$ and hence

$$p(y|H_l) = \frac{\beta_l(1-c)}{\sqrt{2\pi y\sigma_l^2}} e^{-\frac{1}{2\sigma_l^2}\min(y,\eta_l)}. \quad (13)$$

Suppose that we have made N observations of the variable y and we have collected these observations into a vector $\mathbf{y}$. Also assume that the observations at different time instances are statistically independent of each other. Then the joint probability density function is a product of the individual probability densities

$$p(\mathbf{y} \mid H_l) = \textstyle\prod_{n=1}^{N} p(y_n \mid H_l), \quad l = 0, 1. \quad (14)$$

The likelihood ratio for the above hypothesis reads

$$L(y) = \prod_{n=1}^{N} \frac{\beta_1}{\beta_0}\sqrt{\frac{\sigma_0^2}{\sigma_1^2}} \frac{e^{-\frac{1}{2\sigma_1^2}\min(y_n,\eta_1)}}{e^{-\frac{1}{2\sigma_0^2}\min(y_n,\eta_0)}} \quad (15)$$

Taking the logarithm of both sides of (15) and simplifying we readily obtain the log-likelihood ratio

$$\begin{aligned} l(y) &= \frac{N}{2}\ln\left(\frac{\beta_1^2\sigma_0^2}{\beta_0^2\sigma_1^2}\right) \\ &\quad -\frac{1}{2\sigma_1^2}\sum_{n=1}^{N}\min(y_n,\eta_1) + \frac{1}{2\sigma_0^2}\sum_{n=1}^{N}\min(y_n,\eta_0) \end{aligned} \quad (16)$$

Our detector thus needs to decide in favour of H_1 if the log–likelihood ratio is larger than a threshold. Otherwise the hypothesis H_0 is selected.

IV. Assymptotic analysis for large N

The detector derived in the previous Section computes if

$$\frac{1}{2\sigma_0^2}\frac{1}{N}\sum_{n=1}^{N}\min(y_n,\eta_0) - \frac{1}{2\sigma_1^2}\frac{1}{N}\sum_{n=1}^{N}\min(y_n,\eta_1) > \gamma \quad (17)$$

where

$$\gamma = \frac{l(y)}{N} - \frac{1}{2}\ln\left(\frac{\beta_1^2\sigma_0^2}{\beta_0^2\sigma_1^2}\right)$$

We thus need to find a difference between weighted arithmetical means of saturated variables and compare the result to a threshold in order to perform the detection.

Let us concentrate on the variables under the summations in (17) and define a new variable z_k as

$$z_k = h(y) = \min(y, \eta_k), \ k = 0, 1. \quad (18)$$

The function $h(y)$ is a saturation nonlinearity. The probability density function of the output of $z_k = h(y)$ is given by [10]

$$p_z(z_k) = \left.\frac{p_y(y)}{\frac{dz_k}{dy}}\right|_{y=h_i^{-1}(z_k)}. \quad (19)$$

We need to investigate probability density functions in four different cases, two sums in (17), $k = 0, 1$ and two hypothesis $l = 0, 1$. Substituting the probability density functions of y from (13) into above in those four cases and combining the results we can reach a common expression covering all the cases as

$$\begin{aligned} p(z_k|H_l) &= \frac{\beta_l(1-c)}{\sqrt{2\pi\sigma_l^2 z_k}} e^{-\frac{z_k}{2\sigma_l^2}}\Pi(0,\eta_{m_1}) \\ &\quad + m_2\frac{\beta_0 c}{2b\sqrt{z_k}}\Pi(\eta_0,\eta_1) + \delta(z_k-\eta_k)\theta_{k,l}, \end{aligned} \quad (20)$$

where $\Pi(c,d)$ is one between c and d and is zero otherwise, $\theta_{k,l} = \beta_l(1-c)m_3\left[\mathrm{erf}\left(\sqrt{\frac{\eta_1}{2\sigma_1^2}}\right) - \mathrm{erf}\left(\sqrt{\frac{\eta_0}{2\sigma_1^2}}\right)\right] + \beta_l c\left(1 - \frac{\sqrt{\eta_{m_4}}}{b}\right)$, $m_1 = 1$, if $l = 1$ and $k = 1$ and is zero otherwise, $m_2 = 1$, if $l = 0$ and $k = 1$ and is zero otherwise and $m_3 = 1$, if $l = 1$ and $k = 0$ and is zero otherwise, $m_4 = 0$, if $l = 0$ and $k = 0$ and is one otherwise.

This distribution has mean

$$\begin{aligned} E[z_k|H_l] &= \beta_l(1-c)\left[\sigma_l^2\mathrm{erf}\left(\sqrt{\frac{\eta_{m_1}}{2\sigma_l^2}}\right)\right. \\ &\quad \left. -\sqrt{\frac{2\sigma_l^2\eta_{m_1}}{\pi}}e^{-\frac{\eta_{m_1}}{2\sigma_l^2}}\right] \\ &\quad + \frac{\beta_0 c}{3b}(\eta_1^{\frac{3}{2}} - \eta_0^{\frac{3}{2}})m_2 + \eta_k\theta_{k,l} \end{aligned} \quad (21)$$

and second moment

$$\begin{aligned} E[z_k^2|H_l] &= \beta_l(1-c)\left[3\sigma_l^4\mathrm{erf}\left(\sqrt{\frac{\eta_{m_1}}{2\sigma_l^2}}\right)\right. \\ &\quad \left. -\sqrt{\frac{2\sigma_l^2\eta_{m_1}}{\pi}}e^{-\frac{\eta_{m_1}}{2\sigma_l^2}}(\eta_{m_1} + 3\sigma_l^2)\right] \\ &\quad + \frac{\beta_0 c}{5b}(\eta_1^{\frac{5}{2}} - \eta_0^{\frac{5}{2}})m_2 + \eta_k^2\theta_{k,l}. \end{aligned} \quad (22)$$

The crosscorrelation between z_0 and z_1 is perfect if $z_1 < \eta_0$ and in this case $E[z_0 z_1|H_l] = E[z_0^2|H_l]$. This happens with probability

$$P(z_1 < \eta_0) = \int_0^{\eta_0} p_z(z_1|H_l)dz_1 = \beta_l(1-c)\text{erf}\left(\sqrt{\frac{\eta_0}{2\sigma_l^2}}\right). \quad (23)$$

If $z_1 > \eta_0$, $z_0 = \eta_0$ and hence $E[z_0 z_1] = \eta_0 E_{z_1>\eta_0}[z_1]$, where $E_{z_1>\eta_0}[z_1]$ is the mean of z_1 above η_0. This happens with probability $1 - P(z_1 < \eta_0)$ and the cross-correlation is therefore

$$\begin{aligned} E[z_0 z_1|H_l] &= P(z_1 < \eta_0)E[z_0^2|H_l] \quad (24) \\ &\quad +[1 - P(z_1 < \eta_0)]\eta_0 E_{z_1>\eta_0}[z_1|H_l] \end{aligned}$$

Examining (17) we see that to proceed we need the moments of the variable

$$w = \frac{1}{2\sigma_0^2} z_0 - \frac{1}{2\sigma_1^2} z_1. \quad (25)$$

The mean of w is

$$E[w|H_l] = \frac{E[z_0|H_l]}{2\sigma_0^2} - \frac{E[z_1|H_l]}{2\sigma_1^2} \quad (26)$$

the second moment is

$$E[w^2|H_l] = \frac{E[z_0^2|H_l]}{4\sigma_0^4} - \frac{2E[z_0 z_1|H_l]}{4\sigma_0^2\sigma_1^2} + \frac{E[z_1^2|H_l]}{4\sigma_1^4} \quad (27)$$

The variance equals

$$\sigma_{H_l}^2 = E[w^2|H_l] - E^2[w|H_l] \quad (28)$$

Let us now note that according to (17), the detector computes a sample average of N i.i.d. random variables w. According to the central limit theorem [10] the distribution of such a sum approaches Gaussian with mean $E[w|H_l]$ and variance $\frac{\sigma_{H_l}^2}{N}$, $l = 0, 1$ when N increases, independent of the shape of the original distribution of the variables w. We can therefore for large N evaluate the probability of correct detection as

$$\begin{aligned} P_D &= \int_\gamma^\infty p_w(w \mid H_1)dw \quad (29) \\ &= \frac{N}{\sqrt{2\pi}\sigma_{H_1}} \int_\gamma^\infty \exp\left(-\frac{(w - E[w \mid H_1])^2 N}{2\sigma_{H_1}^2}\right) dw \\ &= \frac{1}{2}\text{erfc}\left(\frac{(\gamma - E[w \mid H_1])\sqrt{N}}{\sqrt{2}\sigma_{H_1}}\right), \end{aligned}$$

The probability of false alarm is correspondingly

$$\begin{aligned} P_F &= \int_\gamma^\infty p_w(w \mid H_0)dw \quad (30) \\ &= \frac{N}{\sqrt{2\pi}\sigma_{H_0}} \int_\gamma^\infty \exp\left(-\frac{(w - E[w \mid H_0])^2 N}{2\sigma_{H_0}^2}\right) dw \\ &= \frac{1}{2}\text{erfc}\left(\frac{(\gamma - E[w \mid H_0])\sqrt{N}}{\sqrt{2}\sigma_{H_0}}\right). \end{aligned}$$

The receiver operating characteristic (ROC) of the proposed detector is shown in Fig. 2. The characteristic is computed for

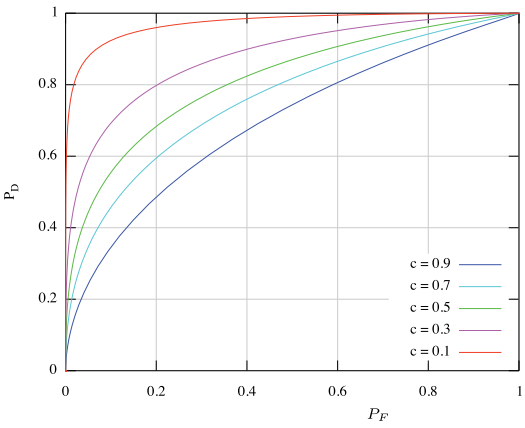

Fig. 2. Receiver operating characteristic.

$\sigma_s^2 = 0.3$, $\sigma_v^2 = 1$, $b = -a = 100$ and $N = 1000$. The blue line corresponds to probability of impulses $c = 0.9$, cyan to $c = 0.7$, green to 0.5, magenta to $c = 0.3$ and red to $c = 0.1$. It should be noted that the parameters have been selected to make the curves clearly observable. If required, the ROC curves can be moved toward the upper left corner by increasing N so that the detector becomes more resistant to impulsive noise for the price of increasing the detection time.

The threshold γ and the number of samples N that are required to reach given P_F and P_D can be found by solving system of equations formed by (27) and (28)

$$\begin{cases} \sqrt{2}\sigma_{H_0}\ \text{erfc}^{-1}(2P_F) = [\gamma - E(\omega|H_0)]\sqrt{N} \\ \sqrt{2}\sigma_{H_1}\ \text{erfc}^{-1}(2P_D) = [\gamma - E(\omega|H_1)]\sqrt{N} \end{cases}. \quad (31)$$

Solving the system for N and γ we obtain that in order to reach the operating point (P_F, P_D) we need

$$\begin{cases} N = 2\left[\frac{\sigma_{H_1}\ \text{erfc}^{-1}(2P_D) - \sigma_{H_0}\ \text{erfc}^{-1}(2P_F)}{E(\omega|H_0) - E(\omega|H_1)}\right]^2 \\ \gamma = \frac{\sigma_{H_1}\ \text{erfc}^{-1}(2P_D)E(\omega|H_0) - \sigma_{H_0}\ \text{erfc}^{-1}(2P_F)E(\omega|H_1)}{\sigma_{H_1}\ \text{erfc}^{-1}(2P_D) - \sigma_{H_0}\ \text{erfc}^{-1}(2P_F)} \end{cases}. \quad (32)$$

V. Simulation results

First we investigate how many samples should the detector involve for our analysis to apply. In the simulation example we have used the following parameters to compute the probability of detection $P_D(\gamma)$: $\sigma_n = 1, \sigma_s = 2, c = 0.01$ and $b = -a = 100$. In Fig. 3 one can see that with $N = 5$, the simulation and theory vaguely resemble each other. The situation improves if we increase the number of samples to 15 and already with $N = 30$ the theoretical curve and simulation dots are rather close to each other. The simulation points are averages over 1 million independent trials. We note that $N = 30$ is much smaller than N found from (32) for signal

to noise ratios required for proper operation of the detector in cognitive radio applications. A similar result can be obtained for the probability of false alarm P_F.

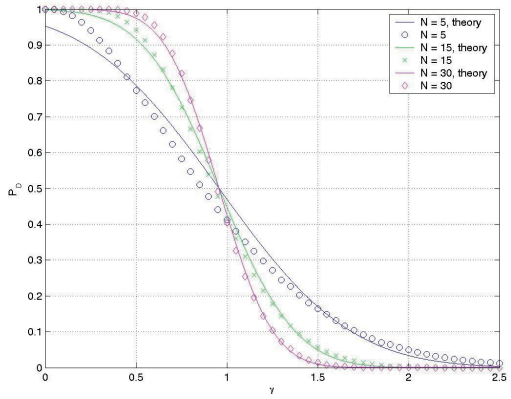

Fig. 3. Probability of detection.

Fig. 4 depicts the dependence of the probability of false alarm from the number of samples N for ordinary energy detector if there is no impulsive noise (black dashed line). It also shows the curves corresponding to the ordinary energy detector (blue line) and the proposed robust detector (magenta line) in the presence of impulsive noise with intensity $c = 0.001$. For comparison we show the results of the robust L_p norm detector with $p = 1$ (red line) and $p = 1.5$ (green line) of [7] in the same noise. The proposed detector operates in these conditions almost as well as the ordinary energy detector in Gaussian noise and outperforms all the others.

In Fig. 5 we present the probability of missed detection $P_m = 1 - P_D$ as the function of SNR. The blue and red lines are the theoretical results with $c = 10^{-3}$ and

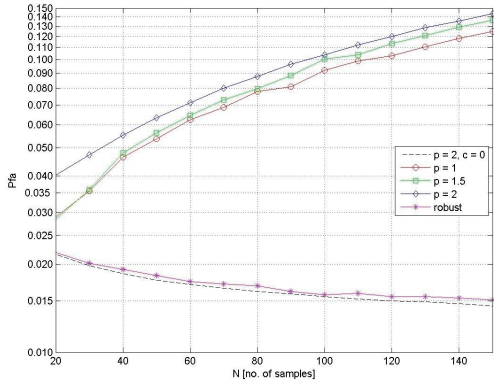

Fig. 4. Probability of false alarm as function of N.

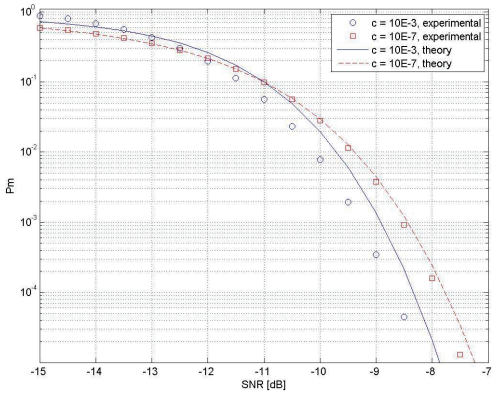

Fig. 5. Probability of missed detection as function of SNR.

$c = 10^{-7}$ respectively and the circles and diamonds represent the corresponding simulation results. One can observe a fast decrease of the curves as SNR increases. One can also observe that the intensity of impulsive noise c does not influence the result much.

VI. Conclusions

In this paper we proposed a robust energy detector for cognitive radio applications. Error analysis of the algorithm was carried out and the number of samples required for given performance was analysed. It was shown that the proposed algorithm outperforms the ordinary energy detector in the presence of impulsive noise.

References

[1] S. Haykin, D. Thomson, and J. Reed, "Spectrum sensing for cognitive radio," *Proc. IEEE*, vol. 97, pp. 849–877, May 2009.

[2] Z. Quan, H. Poor, and A. Sayed, "Collaborative wideband sensing for cognitive radios," *IEEE Signal Processing Magazine*, vol. 25, pp. 60–73, November 2008.

[3] D. Pham, A. Zoubir, R. Bricic, and Y. Leung, "A nonlinear m-estimation approach to robust asynchronous multiuser detection in non-gaussian noise," *IEEE Transactions on Signal Processing*, vol. 55, pp. 1624–1633, May 2007.

[4] P. J. Huber, *Robust Statistics*. John Wiley and sons, 2004.

[5] K. Blackard, T. Rappaport, and C. Bostian, "Measurements and modles of radio frequency impulsive noise for indoor wireless communications," *IEEE Journal on Seleted Areas in Communication*, vol. 11, pp. 991–1001, September 1993.

[6] Q. Shan, S. Bhatti, I. Glover, R. Atkinson, I. Portugues, P. Moore, and R. Rutherford, "Characteristics of impulsive noise in electricity substations," in *Proc. European Signal Processing Conference*, Glasgow, Scotland, 2009, pp. 2136–2140.

[7] F. Moghimi, A. Nasri, and R. Schober, "l_p-norm spectrum sensing for cognitive radio networks impaired by non-gaussian noise," in *IEEE Global Telecommunications Conference (Globecom)*, Honolulu, Hawaii, 2008.

[8] T. Trump, "A robust detector for uniformly distributed noise," in *Proc. ICASSP*, 2010, pp. 3870–3873.

[9] D. Ramirez, J. Via, I. Santamaria, R. Lopez-Valcarce, and L. Scharf, "Multiantenna spectrum sensing: Detection of spatial correlation among time-series with unknown spectra," in *Proc. ICASSP*, 2010, pp. 2954–2957.

[10] A. Papoulis and P. S.U, *Probability, Random Variables and Stochastic Processes*. McGraw Hill, 2002.

PUBLICATION II

T. Trump and I. Müürsepp. “Robust Spectrum Sensing for Cognitive Radio,” in *Proc. EUSIPCO,* 2011, pp 1224 – 1228.

ROBUST SPECTRUM SENSING FOR COGNITIVE RADIO

Tõnu Trump and Ivo Müürsepp

Department of Radio and Telecommunication Engineering
Tallinn University of Technology, Tallinn, Estonia
Email: tonu.trump@lr.ttu.ee, ivom@lr.ttu.ee

ABSTRACT

This paper studies spectrum sensing in the context of cognitive radio. The proposed detector is robust with respect to disturbing impulses, that are in practice present in many cases in addition to the Gaussian noise. The presence of impulsive noise deteriorates the performance of the detectors derived using Gaussian assumption. In the paper we model the noise explicitly consisting of two components and derive the proper detector. Asymptotic analysis of the detector is then presented and formulae for probabilities of correct detection and fault alarm are derived. The theoretical findings are verified in our simulation study.

1. INTRODUCTION

Traditionally the spectral bands required for work by any radio equipment are licensed to the users and cannot be utilized by anybody else even if the licensed users do not use the spectrum at the given location and time by themselves. This leaves a large amount of radio spectrum unused in practice. Recently the cognitive radio paradigm has emerged that can overcome this problem by allowing unlicensed users opportunistically access the spectrum, given that they do not interfere with the primary users. In order to do so the secondary users need first to detect if the primary users are using the spectrum or not. Because of radio effects like shadowing and fading the signal of the primary user may be rather weak at the position of the secondary user. This leaves the secondary user with the requirement of detecting a potentially weak primary user signal in unknown noise. For instance IEEE 802.22 suggests that the cognitive radio needs to detect the primary signals that have power level as low as -22 dB below the noise level [1].

In the literature there are several detectors proposed for this purpose [2, 3], most popular of them probably being the energy detector. The popularity is partly because of simplicity of the energy detector but also because it does not need any assumptions on the waveforms emitted by primary users.

The noise is usually assumed to be white and Gaussian but in real life situations this does not need to be the case. In particular one has to consider the presence of impulsive noise, both man-made and natural. Non-Gaussian ambient noise is a major impairment to signal processing techniques that are based on a Gaussian assumption [4]. The examples of the impulsive noise include man–made noise like car ignition, emissions from the microwave ovens or natural impulsive noise due to e.g. lightning. For measurement results concentrating on impulsive noise see e.g. [5, 6] and references therein.

In this paper we will develop an energy–like detector that is not sensitive to impulsive noise. The derivation is based on modelling the impulsive component of the noise explicitly by a uniform distribution. We allow the impulses to occur only with certain probability and preserve the usual Gaussian noise component for most of the time. This results in an intuitively rather satisfying noise model.

In the analysis part of the paper we derive the formulae for probabilities of detection, P_D, and fault alarm, P_F, of the proposed detector but also for the time required to reach a given P_D and P_F level with certain signal and noise powers. Finally we present some simulation results. The simulation results are consistent with our theoretical findings.

2. ROBUST DETECTOR

We consider the problem of detecting the presence of primary users in a given frequency band without any prior knowledge of primary transmissions. The detection problem we need to solve is [3, 7]

$$\begin{aligned} H_0 &: x(t) = v(t) \\ H_1 &: x(t) = \alpha(t)s(t) + v(t), \end{aligned} \tag{1}$$

i.e. the received waveform $x(t)$ may be noise $v(t)$ only or it may consist of a sum of signal of interest $s(t)$ and noise $v(t)$ and the variable t denotes discrete time. The signal of interest, $s(t)$, is assumed to be passed through a slow Rayleigh fading channel with attenuation $\alpha(t)$. The detector has to decide which of the hypotheses is more likely given the received waveform $x(t)$. We assume that the noise $v(t)$ comprises a sum of zero mean additive white Gaussian noise $v_g(t)$ process and an additional impulsive noise component $v_i(t)$. The impulsive noise component is assumed not to be present most of the time but appear with certain probability c so that the impulsive component obeys the probability density function (PDF)

$$f_i(x) = \frac{c}{b-a} + (1-c)\delta(x), \tag{2}$$

with $0 < c < 1$ and a and b being the lower and upper limits on the values that the noise can take. In practice a and b may for instance represent the smallest and largest numbers that can be represented at the output of analogue to digital (A/D) converter that is included at the input of the processing system. Note that we have limited also the Gaussian noise component to lay between a and b resulting in a minor deviation from Gaussianity. The deviation is, however, small because we assume that $b-a$ is much larger than the standard deviation of the Gaussian noise. The uniform distribution is selected because of its maximum entropy property i.e. there is nothing assumed to be known about the origin of the impulses. This noise model takes into account that most of the time the noise is Gaussian and that the impulses that disturb the detection based on Gaussian assumption occur only with

certain probability c. As such, the noise model is more intuitively satisfying than other popular models for impulsive noise like Laplacian.

The noise $v(t)$ is modelled as consisting of two components with the largest component determining the outcome entirely at each time instant [10]

$$v(t) = v_g(t) + v_i(t) \approx \max[v_g(t), v_i(t)]. \tag{3}$$

Let us denote the variances of primary user signal and noise as σ_s^2 and σ_n^2. Let us also denote a common variance as

$$\sigma_l^2 = \begin{cases} \sigma_n^2 & l = 0 \\ \sigma_n^2 + \sigma_s^2 & l = 1 \end{cases}.$$

With this notation we can express the conditional PDF-s corresponding to our two hypotheses for $l = 0, 1$ as

$$p(x|H_l) = \begin{cases} \beta_l \max\left(\frac{1-c}{\sqrt{2\pi\sigma_l}} e^{-\frac{|x|^2}{2\sigma_l^2}}, \frac{c}{b-a}\right) & a < x < b \\ 0, & \text{otherwise} \end{cases} \tag{4}$$

The normalization factors β_l can be found by solving $\int_a^b p(x|H_l)dx = 1$ for β_l. This results in

$$\beta_l = \left[(1-c)\mathrm{erf}\left(\sqrt{\frac{\eta_l}{2\sigma_l^2}}\right) + c\left(1 - \frac{2\sqrt{\eta_l}}{b-a}\right)\right]^{-1} \tag{5}$$

where $\mathrm{erf}(x) = \frac{2}{\sqrt{\pi}} \int_0^x \exp(-t^2)dt$ and

$$\eta_l = -2\sigma_l^2 \ln\left(\frac{c}{1-c}\frac{\sqrt{2\pi\sigma_l^2}}{b-a}\right) \tag{6}$$

is the intersection point of the Gaussian and uniform distributions.

We can give to PDF-s of x in the interval $a \le x \le b$ a more convenient form for future derivation

$$\begin{aligned} p(x|H_l) &= \beta_l \max\left(\frac{1-c}{\sqrt{2\pi\sigma_l^2}} e^{-\frac{|x|^2}{2\sigma_l^2}}, \frac{c}{b-a}\right) \\ &= \frac{\beta_l(1-c)}{\sqrt{2\pi\sigma_l^2}} e^{-\frac{1}{2\sigma_l^2}\min\left(|x|^2, \eta_l\right)}. \end{aligned}$$

PDFs of $y = x^2$ are then $p(y) = \frac{p(x)}{\frac{dy}{dx}}$ and hence

$$p(y|H_l) = \frac{\beta_l(1-c)}{\sqrt{2\pi y\sigma_l^2}} e^{-\frac{1}{2\sigma_l^2}\min(y, \eta_l)}. \tag{7}$$

Suppose that we have made N observations of the variable y and we have collected these observations into a vector $\mathbf{y}$. Also assume that the observations at different time instances are statistically independent of each other. Then the joint probability density function is a product of the individual probability densities

$$p(\mathbf{y} \mid H_l) = \prod_{n=1}^N p(y_n \mid H_l), \quad l = 0, 1. \tag{8}$$

The likelihood ratio for the above hypothesis reads

$$L(y) = \prod_{n=1}^N \frac{\beta_1}{\beta_0}\sqrt{\frac{\sigma_0^2}{\sigma_1^2}} \frac{e^{-\frac{1}{2\sigma_1^2}\min(y_n, \eta_1)}}{e^{-\frac{1}{2\sigma_0^2}\min(y_n, \eta_0)}} \tag{9}$$

Taking the logarithm of both sides of (9) and simplifying we readily obtain the log-likelihood ratio

$$\begin{aligned} \ln L &= \frac{N}{2}\ln\left(\frac{\beta_1^2\sigma_0^2}{\beta_0^2\sigma_1^2}\right) \\ &\quad -\frac{1}{2\sigma_1^2}\sum_{n=1}^N \min(y_n, \eta_1) + \frac{1}{2\sigma_0^2}\sum_{n=1}^N \min(y_n, \eta_0) \end{aligned} \tag{10}$$

Our detector thus needs to decide in favour of H_1 if the log–likelihood ratio is larger than a threshold. Otherwise the hypothesis H_0 is selected.

If there is no impulsive noise i.e. $c \to 0$ we have

$$\begin{aligned} \lim_{c\to 0} \eta_l &= -2\sigma_l^2 \ln(0) = \infty \\ \lim_{c\to 0} \beta_l &= 1 \\ \lim_{c\to 0} \frac{N}{2}\ln\left(\frac{\beta_1^2\sigma_0^2}{\beta_0^2\sigma_1^2}\right) &= \frac{N}{2}\ln\left(\frac{\sigma_0^2}{\sigma_1^2}\right) \end{aligned}$$

and the test reduces to an ordinary energy detector

$$\frac{1}{N}\sum_{n=1}^N y_n > \frac{\sigma_0^2\sigma_1^2}{\sigma_1^2 - \sigma_0^2}\ln\left(\frac{\sigma_0^2}{\sigma_1^2}\right). \tag{11}$$

3. ESTIMATION OF UNKNOWN PARAMETERS

Parameters η_0 and η_1 are dependent on the Gaussian noise variance σ_n, signal variance σ_s and the impulse probability c. Those parameters may not be known in advance and if they are not, they must be estimated from the input signal. In some applications it is known for certain that during some times the primary user is silent and during some other times it is working. The question is about all the other times. For those applications we derive the maximum likelihood estimators for σ_n, σ_s and c below. For other applications we can use the techniques outlined in e.g. [8]. In [9] it is shown that if we can observe a length N noise only realization then the maximum likelihood estimator of noise variance is

$$\hat{\sigma}_n = \frac{1}{N_1}\sum_{i\in M_1} x^2(i). \tag{12}$$

Here M_1 is a set that contains all signal samples that satisfy $x^2 < -2\sigma_n^2\left(\ln\sigma_n + \ln\frac{c\sqrt{2\pi}}{(1-c)(b-a)}\right)$ and N_1 is the number of elements in set M_1. Let M_2 and N_2 denote the complementary set. If signal of interest $s(t)$ is also present then the log–likelihood function can be written as

$$\begin{aligned} \ln L &= \sum_{n=0}^{N-1}\left[\ln\frac{\beta_1(1-c)}{\sqrt{2\pi}}\right. \\ &\quad \left. -\ln\sqrt{\sigma_n^2 + \sigma_s^2} - \frac{1}{(\sigma_n^2 + \sigma_s^2)}\min(x^2, \eta_1)\right] \end{aligned} \tag{13}$$

Derivative of the log-likelihood function respect to σ_s equals

$$\frac{\partial}{\partial \sigma_s}\ln L = -\frac{N\sigma_s}{\sigma_n^2+\sigma_s^2} - \\ -\frac{\sigma_s}{(\sigma_n^2+\sigma_s^2)^2}\sum_{M_1} x^2 + \sum_{M_2}\frac{\sigma_s}{\sigma_n^2+\sigma_s^2}. \quad (14)$$

Equating (14) to zero results in

$$\sigma_s^2 = \frac{1}{N_1}\sum_{i\in M_1} x^2(i) - \hat{\sigma}_n^2. \quad (15)$$

In order to obtain estimate for c let us compute the derivative of log-likelihood with respect to c

$$\frac{\partial}{\partial c}\ln L = \frac{cN - N_2}{c(c-1)}. \quad (16)$$

Setting above to zero we get an estimate

$$\hat{c} = \frac{N_2}{N}. \quad (17)$$

4. PERFORMANCE ANALYSIS

In this Section we perform the asymptotic analysis of the detector in case of large N. We first note that the detector computes if

$$\frac{1}{2\sigma_0^2}\frac{1}{N}\sum_{n=1}^{N}\min(y_n,\eta_0) - \frac{1}{2\sigma_1^2}\frac{1}{N}\sum_{n=1}^{N}\min(y_n,\eta_1) > \gamma \quad (18)$$

where

$$\gamma = \frac{\ln L}{N} - \frac{1}{2}\ln\left(\frac{\beta_1^2\sigma_0^2}{\beta_0^2\sigma_1^2}\right)$$

We thus need to find a difference between weighted arithmetical means of saturated variables and compare the result to a threshold in order to perform the detection.

Let us concentrate on the variables under the summations in (18) and define a new variable z_k as

$$z_k = h(y) = \min(y,\eta_k),\ k = 0,1. \quad (19)$$

The function $h(y)$ is a saturation nonlinearity. The probability density function of the output of $z_k = h(y)$ is given by [10].

$$p_z(z_k) = \left.\frac{p_y(y)}{\frac{dz_k}{dy}}\right|_{y=h_i^{-1}(z_k)}. \quad (20)$$

For sake of simplicity let us assume that $b = -a$. We need to investigate PDF-s in four different cases, two sums in (18), $k = 0,1$ and two hypothesis $l = 0,1$. Substituting (7) into above in those four cases we get the following four PDF-s:

$$p(z_0|H_0) = \frac{\beta_0(1-c)}{\sqrt{2\pi z_0\sigma_0^2}}e^{-\frac{z_0}{2\sigma_0^2}}\Pi(0,\eta_0) \quad (21)$$
$$+c\beta_0\left(1-\frac{\sqrt{\eta_0}}{b}\right)\delta(z_0-\eta_0)$$

if $l = 0$ and $k = 0$,

$$p(z_1|H_0) = \frac{\beta_0(1-c)}{\sqrt{2\pi z_1\sigma_0^2}}e^{-\frac{z_1}{2\sigma_0^2}}\Pi(0,\eta_0) \quad (22)$$
$$+\frac{c\beta_0}{2b\sqrt{z_1}}\Pi(\eta_0,\eta_1) + c\beta_0\left(1-\frac{\sqrt{\eta_1}}{b}\right)\delta(z_1-\eta_1)$$

if $l = 0$ and $k = 1$,

$$p(z_0|H_1) = \frac{\beta_1(1-c)}{\sqrt{2\pi z_0\sigma_1^2}}e^{-\frac{z_0}{2\sigma_1^2}}\Pi(0,\eta_0) \quad (23)$$
$$+\left[\beta_1(1-c)\left(\mathrm{erf}\sqrt{\frac{\eta_1}{2\sigma_1^2}} - \mathrm{erf}\sqrt{\frac{\eta_0}{2\sigma_1^2}}\right)\right.$$
$$\left.+\beta_1 c\left(1-\frac{\sqrt{\eta_1}}{b}\right)\right]\delta(z_0-\eta_0)$$

if $l = 1$ and $k = 0$ and

$$p(z_1|H_1) = \frac{\beta_1(1-c)}{\sqrt{2\pi z_1\sigma_1^2}}e^{-\frac{z_1}{2\sigma_1^2}}\Pi(0,\eta_1) \quad (24)$$
$$+\frac{\beta_1 c(b-\sqrt{\eta_1})}{b}\delta(z_1-\eta_1)$$

if $l = 1$ and $k = 1$. The function $\Pi(c,d)$ equals one between c and d and is zero otherwise. The cases are illustrated in Figure 1.

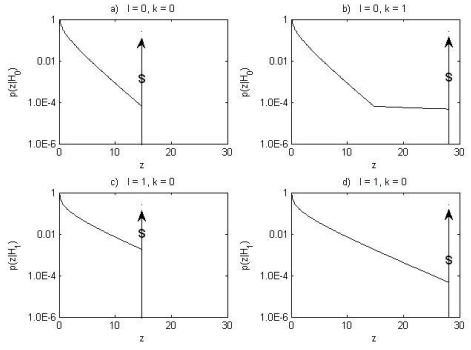

Figure 1: Probability density functions of the four cases.

Combining the results we can reach a common expression covering all the cases as

$$p(z_k|H_l) = \frac{\beta_l(1-c)}{\sqrt{2\pi\sigma_l^2 z_k}}e^{-\frac{z_k}{2\sigma_l^2}}\Pi(0,\eta_{m_1}) \quad (25)$$
$$+m_2\frac{\beta_0 c}{2b\sqrt{z_k}}\Pi(\eta_0,\eta_1) + \delta(z_k-\eta_k)\theta_{k,l},$$

where $\theta_{k,l} = \beta_l(1-c)m_3\left[\mathrm{erf}\left(\sqrt{\frac{\eta_1}{2\sigma_l^2}}\right) - \mathrm{erf}\left(\sqrt{\frac{\eta_0}{2\sigma_l^2}}\right)\right]$ $+\beta_l c\left(1-\frac{\sqrt{\eta_{m_4}}}{b}\right)$, $m_1 = 1$, if $l = 1$ and $k = 1$ and is zero

otherwise, $m_2 = 1$, if $l = 0$ and $k = 1$ and is zero otherwise and $m_3 = 1$, if $l = 1$ and $k = 0$ and is zero otherwise, $m_4 = 0$, if $l = 0$ and $k = 0$ and is one otherwise.

This distribution has mean

$$E[z_k|H_l] = \beta_l(1-c)\left[\sigma_l^2 \text{erf}\left(\sqrt{\frac{\eta_{m_1}}{2\sigma_l^2}}\right) - \sqrt{\frac{2\sigma_l^2\eta_{m_1}}{\pi}} e^{-\frac{\eta_{m_1}}{2\sigma_l^2}}\right] + \frac{\beta_0 c}{3b}(\eta_1^{\frac{3}{2}} - \eta_0^{\frac{3}{2}})m_2 + \eta_k\theta_{k,l} \quad (26)$$

and second moment

$$E[z_k^2|H_l] = \beta_l(1-c)\left[3\sigma_l^4 \text{erf}\left(\sqrt{\frac{\eta_{m_1}}{2\sigma_l^2}}\right) - \sqrt{\frac{2\sigma_l^2\eta_{m_1}}{\pi}} e^{-\frac{\eta_{m_1}}{2\sigma_l^2}}(\eta_{m_1} + 3\sigma_l^2)\right] + \frac{\beta_0 c}{5b}(\eta_1^{\frac{5}{2}} - \eta_0^{\frac{5}{2}})m_2 + \eta_k^2\theta_{k,l}. \quad (27)$$

The crosscorrelation between z_0 and z_1 is perfect if $z_1 < \eta_0$ and in this case $E[z_0 z_1|H_l] = E[z_0^2|H_l]$. This happens with probability

$$P(z_1 < \eta_0) = \int_0^{\eta_0} p_z(z_1|H_l)dz_1 = \beta_l(1-c)\text{erf}\left(\sqrt{\frac{\eta_0}{2\sigma_l^2}}\right). \quad (28)$$

If $z_1 > \eta_0$, $z_0 = \eta_0$ and hence $E[z_0 z_1] = \eta_0 E_{z_1>\eta_0}[z_1]$, where $E_{z_1>\eta_0}[z_1]$ is the mean of z_1 above η_0. This happens with probability $1 - P(z_1 < \eta_0)$ and the cross-correlation is therefore

$$E[z_0 z_1|H_l] = P(z_1 < \eta_0)E[z_0^2|H_l] + [1 - P(z_1 < \eta_0)]\eta_0 E_{z_1>\eta_0}[z_1|H_l]. \quad (29)$$

Examining (18) we see that to proceed we need the moments of the variable

$$w = \frac{1}{2\sigma_0^2}z_0 - \frac{1}{2\sigma_1^2}z_1. \quad (30)$$

The mean of w is

$$E[w|H_l] = \frac{E[z_0|H_l]}{2\sigma_0^2} - \frac{E[z_1|H_l]}{2\sigma_1^2} \quad (31)$$

and its second moment equals

$$E[w^2|H_l] = \frac{E[z_0^2|H_l]}{4\sigma_0^4} - \frac{2E[z_0 z_1|H_l]}{4\sigma_0^2\sigma_1^2} + \frac{E[z_1^2|H_l]}{4\sigma_1^4}. \quad (32)$$

The variance is equal to

$$\sigma_{H_l}^2 = E[w^2|H_l] - E^2[w|H_l]. \quad (33)$$

Let us now note that according to (18), the detector computes a sample average of N i.i.d. random variables w. According to the central limit theorem [10] the distribution of such a sum approaches Gaussian with mean $E[w|H_l]$ and variance $\frac{\sigma_{H_l}^2}{N}$, $l = 0, 1$ when N increases, independent of the shape of the original distribution of the variables w. We can therefore for large N evaluate the probability of correct detection as

$$P_D = \int_\gamma^\infty p_w(w \mid H_1)dw = \frac{1}{2}\text{erfc}\left(\frac{(\gamma - E[w \mid H_1])\sqrt{N}}{\sqrt{2}\sigma_{H_1}}\right), \quad (34)$$

The probability of fault alarm is correspondingly

$$P_F = \int_\gamma^\infty p_w(w \mid H_0)dw = \frac{1}{2}\text{erfc}\left(\frac{(\gamma - E[w \mid H_0])\sqrt{N}}{\sqrt{2}\sigma_{H_0}}\right). \quad (35)$$

The threshold γ and the number of samples N that are required to reach given P_F and P_D can be found by solving system of equations formed by (34) and (35)

$$\begin{cases} \sqrt{2}\sigma_{H_0}\ \text{erfc}^{-1}(2P_F) = [\gamma - E(w|H_0)]\sqrt{N} \\ \sqrt{2}\sigma_{H_1}\ \text{erfc}^{-1}(2P_D) = [\gamma - E(w|H_1)]\sqrt{N} \end{cases}. \quad (36)$$

Solving the system for N and γ we obtain that in order to reach the operating point (P_F, P_D) we need

$$\begin{cases} N = 2\left[\frac{\sigma_{H_1}\ \text{erfc}^{-1}(2P_D) - \sigma_{H_0}\ \text{erfc}^{-1}(2P_F)}{E(w|H_0) - E(w|H_1)}\right]^2 \\ \gamma = \frac{\sigma_{H_1}\ \text{erfc}^{-1}(2P_D)E(w|H_0) - \sigma_{H_0}\ \text{erfc}^{-1}(2P_F)E(w|H_1)}{\sigma_{H_1}\ \text{erfc}^{-1}(2P_D) - \sigma_{H_0}\ \text{erfc}^{-1}(2P_F)} \end{cases}. \quad (37)$$

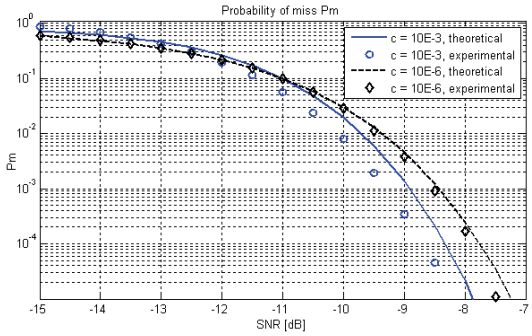

Figure 2: Probability of missed detection as function of SNR.

5. SIMULATION RESULTS

In Figure 2 we present the probability of missed detection $P_m = 1 - P_D$ as the function of SNR. The blue and black lines are the theoretical results with $c = 10^{-3}$ and $c = 10^{-6}$ respectively and the circles and diamonds represent the corresponding simulation results. One can observe a fast decrease of the curves as SNR increases. One can also observe that the intensity of impulsive noise c does not influence the result much.

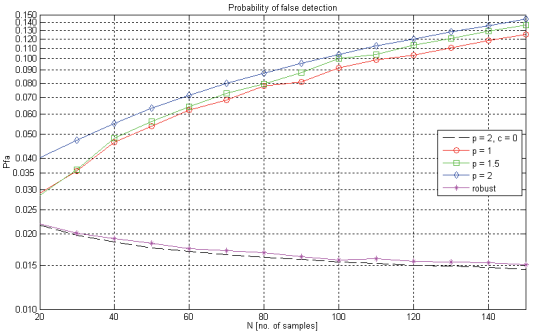

Figure 3: Probability of fault alarm as function of N.

Figure 3 depicts the dependence of the probability of fault alarm from the number of samples N for ordinary energy detector if there is no impulsive noise (black dashed line). It also shows the curves corresponding to the ordinary energy detector (blue line) and the proposed robust detector (magenta line) in the presence of impulsive noise with intensity $c = 0.001$. For comparison we show the results of the robust L_p norm detector with $p = 1$ (red line) and $p = 1.5$ (green line) of [11] in the same noise. The proposed detector operates in these conditions almost as well as the ordinary energy detector in Gaussian noise and outperforms all the others.

Finally we investigate how many samples should the detector involve for our analysis to apply. In the simulation example we have used the following parameters to compute the probability of miss $P_m(\gamma) = 1 - P_D(\gamma) : \sigma_n = 1, \sigma_s = 2, c = 0.01$ and $b = -a = 100$. In Figure 4 one can see that with $N = 5$, the simulation and theory vaguely remember each other. The situation improves if we increase the number of samples to 15 and already with $N = 30$ the theoretical curve and simulation dots are rather close to each other. We note that $N = 30$ is much smaller than N found from (37) for cognitive radio applications. A similar result can be obtained for the probability of fault alarm P_F.

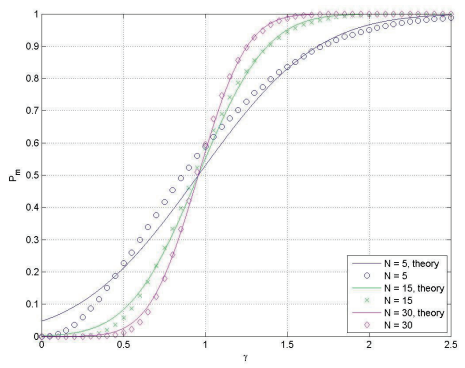

Figure 4: Probability of miss.

6. CONCLUSIONS

In this paper we proposed a robust energy detector for spectrum sensing in cognitive radio applications. The derivation of our detector is based on a noise model that explicitly includes two components – clipped Gaussian distribution and impulses with uniform distribution. Error analysis of the algorithm was carried out. It was shown that the proposed algorithm outperforms the existing similar algorithms in the presence of impulsive noise.

REFERENCES

[1] C. R. Stevenson et. al., "Ieee 802.22: The first cognitive radio wireless regional area network standard," *IEEE Communications Magazine* , pp. 130–138, January 2009.

[2] S. Haykin, D.J. Thomson, and J.H. Reed, "Spectrum sensing for cognitive radio," *Proc. IEEE*, vol. 97, pp. 849–877, May 2009.

[3] Z. Quan, H.V. Poor, and A.H. Sayed, "Collaborative wideband sensing for cognitive radios," *IEEE Signal Processing Magazine*, vol. 25, pp. 60–73, November 2008.

[4] D. Pham, A. Zoubir, R. Bricic, and Y. Leung, "A nonlinear m-estimation approach to robust asynchronous multiuser detection in non-gaussian noise," *IEEE Transactions on Signal Processing*, vol. 55, pp. 1624–1633, May 2007.

[5] K.L. Blackard, T.S. Rappaport, and C.W. Bostian, "Measurements and modles of radio frequency impulsive noise for indoor wireless communications," *IEEE Journal on Seleted Areas in Communication*, vol. 11, pp. 991–1001, September 1993.

[6] Q. Shan, S. Bhatti, I.A. Glover, R. Atkinson, I.E. Portugues, P.J. Moore, and R. Rutherford, "Characteristics of impulsive noise in electricity substations," in *Proc. European Signal Processing Conference*, Glasgow, Scotland, 2009, pp. 2136–2140.

[7] D. Ramirez, J. Via, I. Santamaria, R. Lopez-Valcarce, and L.L. Scharf, "Multiantenna spectrum sensing: Detection of spatial correlation among time-series with unknown spectra," in *Proc. ICASSP*, 2010, pp. 2954–2957.

[8] G. Zhang, X. Wang, Y. Liang, and J. Liu, "Fast and robust spectrum sensing via kolmogorov-smirnov test," *IEEE Transactions on Communications*, vol. 58, pp. 3410–3416, December 2010.

[9] T. Trump, "A robust detector for impulsive noise environment," in *Forty-First Asilomar Conf. on Signals, Systems, and Computers*, Pacific Grove, CA, USA, 2007, pp. 730–734.

[10] A. Papoulis and Pillai S.U, *Probability, Random Variables and Stochastic Processes*, McGraw Hill, 2002.

[11] F. Moghimi, A. Nasri, and R. Schober, "l_p-norm spectrum sensing for cognitive radio networks impaired by non-gaussian noise," in *IEEE Global Telecommunications Conference (Globecom)*, Honolulu, Hawaii, 2008.

PUBLICATION III

J. Berdnikova, T. Ruuben, I. Müürsepp, E. Lossmann. „Resolution and Doppler Tolerance of Cognitive System Waveforms.“ *Electronics and Electrical Engineering*, vol.103(7), pp. 101 – 104, May 2010

ELECTRONICS AND ELECTRICAL ENGINEERING
ISSN 1392 – 1215 2010. No. 7(103)
ELEKTRONIKA IR ELEKTROTECHNIKA

TELECOMMUNICATIONS ENGINEERING
T 180
TELEKOMUNIKACIJŲ INŽINERIJA

Resolution and Doppler Tolerance of Cognitive System Waveforms

J. Berdnikova, T. Ruuben, I. Müürsepp, E. Lossmann
Department of Radio and Communication Engineering, Tallinn University of Technology,
Ehitajate tee 5, 19086 Tallinn, Estonia, phone: +3726202350,
e-mails: juliad@lr.ttu.ee, ivom@lr.ttu.ee, truuben@lr.ttu.ee, eriklos@lr.ttu.ee

Introduction

The environment is constantly changing in case of mobile systems and often there is lack of preliminary information about the environment and objects. This complicates the use of adaptation techniques because initial values of system parameters are unclear. In this case additional information must be acquired in real time about the environment. This implies the use of cognitive signal processing [1]. Cognitivity allows the data acquisition system to adapt to particular objects and environment, therefore increasing object detection probability and measurement accuracy (distance to objects and resolution).

A cognitive signal processing algorithm in data acquisition system can be divided into the following tasks: intelligent signal processing; taking into account the information gained about the environment to choose the parameters of a sounding signal to be radiated; continuous acquisition and storage of information about the environment for basic adaptation of the sounding system [1].

Cognitive radar is an actual research topic in radar system engineering. Nevertheless, the cognition concepts could be applied for sonars. To apply the cognitive principle to the data acquisition systems three main stages should be implemented:

- the transmitter should adjust the necessary parameters in an intelligent manner, taking into account size of the target, range and target velocity based on the received information
- the system should include the feedback from the receiver to the transmitter
- intelligent signal processing should be implemented to gather all necessary information for the transmitter adjustment.

Moreover, other relevant information on the environment could be gathered by other sensors working cooperatively with the acquisition system. The cognitive system decision is based on signals gathered on the outside environment on the fly as opposed to knowledge-based (KB) systems [1] where the signal-processing is based on prior information.

According to the location of transmitters and receivers, cognitive monostatic and bistatic sonars can be divided into following categories: monostatic, bistatic/multistatic, hybrid multistatic [2]. Every sonar application has different optimum performance characteristics. For one system, it could be range resolution, for the other Doppler tolerance or even a digital beam steering. Rather than optimizing waveforms for a single design criterion, the intelligent system should be able to synthesize waveforms that provide a smooth tradeoff between competing design criteria [3].

Firstly, this paper discusses possible criterions for some sonar applications and proposes general solution. Secondly, the structure of the flexible MATLAB model will be presented. This model allows us include the intelligent module for the future system development. Finally, modeling of the Doppler effect and estimated resolution of the real system with given sounding waveforms would provide the input for the intelligent signal processing in the prototype.

Sonar applications and possible solutions

Next, we take a closer look at the specific applications and possible feedback solution concerning the digital system, which could change the digital waveform and appropriate reception. The performance should be improved by other adjustments as the frequency and bandwidth of the real system are difficult to change.

The goal of the hydrographic application is to measure the bottom profile with maximum resolution and accuracy within a given range. The environmental effects and feedback values will be:

- in the case of the decreased signal-to-noise ratio (SNR) the output power of the system could be increased by the variable gain control at the transmitter or by the use of phase-manipulated signals [4]. Moreover, this leaves the range resolution value unchanged
- in the case of limited detectability due to the unwanted reflections from fish, other biologic objects, air bubbles, dust and dirt, target reflection registration

could be improved by multiple reflection registration, filtering and tracking or beam steering

- in the case of decreased bottom scattering strength it would be necessary to choose different algorithm for received signal processing; to select different waveform; to use digital beam steering, and to change frequency.

Imaging applications like Sidescan or Forward Looking Sonars (FLS), used for large area efficient sea floor imaging, require higher SNR values at the reception. In this case adaptation could be accomplished as follows:

- increase in SNR by using variable output power or by changing signal length or type
- fading, reverberation and the Doppler effect could be eliminated by proper waveform selection
- sensitivity to the ship motion could be in some extent decreased by beamforming.

In general, the efficient SNR increase and resolution are achievable through appropriate waveform design. However, selected waveforms have different Doppler tolerance at the same range resolution. To study the Doppler tolerance and range resolution of the specific waveforms the MATLAB model was created. Furthermore, this allows us implement additional signal processing algorithms, beamforming and possible feedback values of the cognitive system. The flexible model of the cognition system and later the prototype should include digital signal generation, reception with digital beamforming and optimal filtering. Future development will include the intelligent feedback decision making based on tracking and processing information.

The research showed that previously studied binary phase coded waveforms [4] (Barker and nested Barker codes [5]) are efficient for hydrographic applications, but at the same time Doppler tolerance of those signals is limited. Desirable SNR increase would decrease the Doppler tolerance significantly. Fig. 1 illustrates the maximum target velocities for phase manipulated signals Barker and nested Barker codes. Here, element length corresponds to 4, 8, 16 and 32 carrier signal periods per element and sonar frequency is 250 kHz.

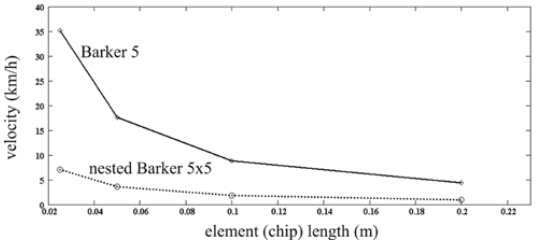

Fig. 1. The maximum target velocities for Barker code signals with 5 and 25 elements

In spite of the fact that phase manipulated codes are more Doppler intolerant, they allow for increasing the system resolution and application distance range could be increased significantly at the same transmitted power level. Thus, for Doppler tolerant cognitive applications further waveform research would be needed [3, 6, 7].

Digital beamforming is the most suitable approach to phased array antenna pattern control. Therefore, it is necessary to model signal reception at the critical target or vessel velocities to determine the properties of the specific waveforms. At the same time we can simulate real system performance in the presence of the Doppler effect.

Wideband beamforming in sonar systems

The beam pattern of the sensor array is typically calculated using harmonic vibrations of infinite duration at a constant magnitude in the case of an electrical scanning, but it is possible to use digital signal processing technology and spread spectrum scanning signals. Derived from the characteristics of this type of signal, the sensor array is not able to use classical phase compensation for the purpose of beam steering. Wideband beamforming algorithm should be used to achieve a high resolution in all partial directions.

The choice of wideband beamforming algorithm in sonar system depends on exact situation, type and length of the probe signal and available hardware. We observed that the general behavioral model is the same and still related to the duration of the shortest element of the signal regarding the dynamics of the scanning signals in the sensor array studied in the previous work [4]. Some differences appeared when using very long nested codes (the average amplitude of the output signal of the sensor array remained somewhat higher for large angles than when using traditional signals), but the choice of scanning signals is not an essential factor with respect to the dynamics. The choice of scanning signal is rather determined by the operating range of sonar and the correlation features of the signal (included the Doppler shift). Comparison of theoretical results suggests that both FDFIB (Frequency-Domain Frequency-Invariant Beamformer) and Block-phase algorithms are realizable and provide very good results. It is also essential that in the case of FDFIB algorithm the amplitude weights only determine the shape of the beam pattern. The level of the side lobes and the beam patterns of any shape can be constructed independent of the frequency. In principle, this method is an alternative to the adaptive methods of forming beam patterns and can be considered the most accurate variant. FDFIB algorithm is based on the properties of the Fourier transform. When switching to a complex envelope, we can find the output signal M from sensor n at time l using the equation

$$\overset{0}{M}_{l,n} = \sum_{p=0}^{KV-1}\sum_{k=0}^{KH-1} A(l - k\tau_e - round\left(fs \cdot n \cdot d \cdot \sin\beta_\gamma / c\right), k + \\ +(p \cdot KH)) \cdot \exp\left(-j\left(\left|\phi_p - \phi_k\right| + \left(\omega_0 \cdot \frac{n \cdot d \cdot \sin\beta_\gamma}{c}\right)\right)\right), \quad (1)$$

where KH – the number of internal components; KV – the number of external components; A – element function; τ_e – signal initial delay; d – distance between sensors; c – wave speed; ω_0 – support (centre) frequency; fs – sampling frequency; β_γ – partial direction; ϕ_p – phase of p-th external component $\phi_p \in \{0°,180°\}$; ϕ_k – phase of k-th internal component $\phi_k \in \{0°,180°\}$.

For time delay compensation in frequency domain we will use the weight

$$\theta(n,q) = \frac{2\pi q}{(L-1)} \cdot round\left(\frac{n \cdot d \cdot fs \cdot \cos(\beta_\gamma)}{c} \right), \quad (2)$$

where q – sampled frequency; L – signal length [4].

By taking the inverse Fourier transform with respect to frequency q, the output electrical signals in each channel are now synchronous. These formulas are modeled in MATLAB environment and sensor output signal and corresponding ambiguity function in case of 5-element Barker code and 5-element sensor array are shown in Fig. 2 and Fig. 3.

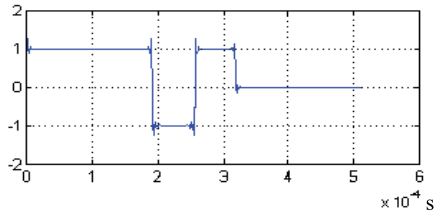

Fig. 2. Sensor output after FDFIB compensation

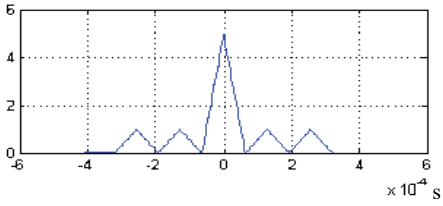

Fig. 3. Vertical cut of the ambiguity function of the optimal filter after FDFIB compensation

As mentioned before, the Barker codes are very intolerant to the Doppler shift. Fig. 4 and Fig. 5 illustrate the matched filter output when objects move towards the sonar system (9 km/h and 20 km/h).

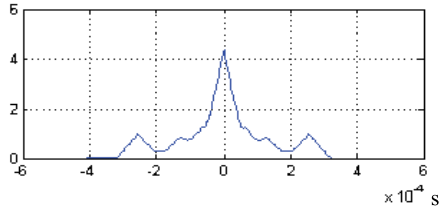

Fig. 4. Receiver output with Barker code waveform affected by the Doppler shift (9 km/h)

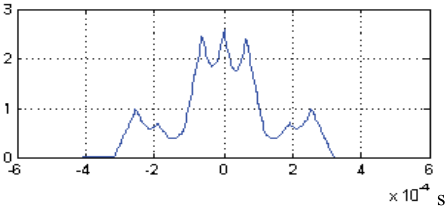

Fig. 5. Vertical cut of the ambiguity function affected by the Doppler shift (20 km/h)

Here vertical cut of the ambiguity function depends only on code and the Doppler shift and modeling results reveal that the Doppler shift can be disregarded when the speed of the object is below 9 km/h. Then vertical cut of the ambiguity function is quite similar to its original. In practice we can obtain sufficient results with speed up to 4.5 km/h as shown in Fig. 6.

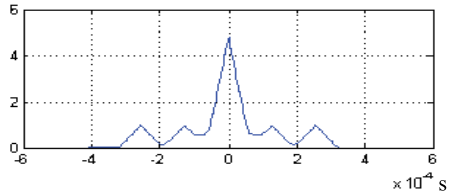

Fig. 6. Receiver output with Barker code waveform affected by the Doppler shift (4.5 km/h)

Obviously, these results are valid for a certain situation. Here we used carrier frequency 250 kHz and 16 signal periods inside one Barker code element. The situation is different when we use longer codes, for example nested code with 5x5 elements. Corresponding ambiguity functions with and without the Doppler shift equal to speed 9 km/h are shown in Fig. 7 and Fig. 8.

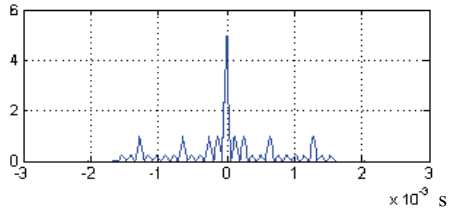

Fig. 7. Optimal filter output of nested Barker without the Doppler shift

As it can be seen from Fig. 8, speed 9 km/h is too high for 5x5 nested codes. Here the Doppler shift can be disregarded if the speed of the object is below 1.7 km/h (Fig. 9).

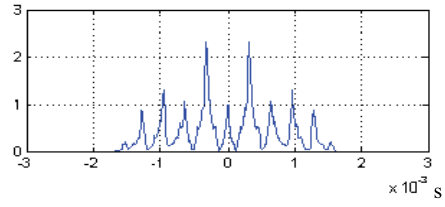

Fig. 8. Optimal filter output of nested Barker affected by the Doppler shift (9 km/h)

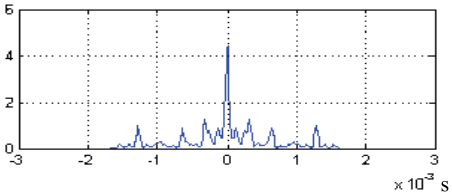

Fig. 9. Receiver output with Barker code waveform affected by the Doppler shift (1.7 km/h)

The question arises: how the Doppler shift will affect the FDFIB beamforming algorithm? It is clear that it has no effect when the signal arrives at the array from the normal direction. In this case the vertical cut of the ambiguity function depends only from code and from the Doppler shift as mentioned before. In the opposite case we can see additional distortions at the output of the matched filter when classical phased array or block-phase algorithm is used. However, FDBIB algorithm is invariant to the scanning signals [4], and the Doppler shift will not affect the FDFIB beamforming algorithm.

Conclusions

The cognitive radar principles could be successfully extended to other data acquisition systems. This paper considers the problems of intelligent sonar system as an illustrative case. It is possible to implement cognitive sonar application with digital signal generation, processing and feedback from the receiver to the transmitter. Intelligence should provide a smooth tradeoff between different criterions. Therefore, one of the main feedback components will be waveform selection, which gives desirable SNR, Doppler tolerance and range resolution. Optimal filtering with digital beamforming facilitates receiver adaptation and also digital beam steering if necessary. The cognitive system basic functions were modeled in MATLAB environment. Discussed model showed that the Doppler tolerance of the system is determined by waveform, and the Doppler shift will not affect the proposed beamforming algorithms. Only low-speed target applications are suitable because the binary phase coded waveforms are relatively sensitive to the Doppler effect. Future research should include waveform design, intelligent signal processing, and feedback modeling and implementing.

References

1. **Gini F., Rangaswamy M.** Knowledge Based Radar Detection, Tracking and Classification. – John Wiley, 2008.
2. **Wenhua Li Genshe Chen, Blasch E. Lynch R.** Cognitive MIMO Sonar Based Robust Target Detection for Harbor and Maritime Surveillance Applications // Aerospace conference, IEEE. – 2009.
3. **Haykin S., Xue Y., Davidson T. N.** Optimal Waveform Design For Cognitive Radar // 42nd Asilomar Conference on Signals, Systems and Computers, IEEE. – 2008.
4. **Ruuben T., Derkats J.** Some Methods of Signal Processing and Beamforming in a Hydrographic Applications // Electronics and Electrical Engineering. Kaunas: Technologija, 2008. – No. 6(86). – P. 27–31.
5. **Richards M. A.** Fundamentals of radar signal processing. – New York: McGraw–Hill, 2005. – 513 p.
6. **Wang B., Wang J., Song X., Han Y.** Optimal Adaptive Waveform Selection Based on ADP in Cognitive Radar // WRI World Congress on Computer Science and Information, IEEE. – 2009.
7. **Goodman N. A., Venkata P. R., Neifeld M. A.** Adaptive Waveform Design and Sequential Hypothesis Testing for Target Recognition With Active Sensors // IEEE Journal of Selected Topics in Signal Processing, Institute of Electrical and Electronics Engineers. – 2007.

Received 2010 02 26

J. Berdnikova, T. Ruuben, I. Müürsepp, E. Lossmann. Resolution and Doppler Tolerance of Cognitive System Waveforms // Electronics and Electrical Engineering. – Kaunas: Technologija, 2010. – No. 7(103). – P. 101–104.

Modern intelligent data acquisition systems use spread-spectrum waveforms and sensor systems with varying parameters according to the state of environment and objects to be tracked. Cognitivity allows the system to adapt to particular objects and environment, therefore increasing object detection probability and measurement accuracy (distance to objects, speed and resolution). This paper discusses the possible future development of a cognitive system with dynamic spread-spectrum waveform design. The active data acquisition system modeling results will provide information about the suitability of proposed waveforms and reception algorithms concerning Doppler tolerance and noisy environment. The devised methods could be implemented in sounding equipment prototypes for further studies. Theoretical and experimental results will be compared and evaluated. Ill. 9, bibl. 7 (in English; abstracts in English, Russian and Lithuanian).

Ю. Бердникова, Т. Рубен, И. Муурсепп, Э. Лоссманн. Резолюция и доплеровская толерантность в когнитивной системе // Электроника и электротехника. – Каунас: Технология, 2010. – № 7(103). – С. 101–104.

Рассматривается использование принципов когнитивности в современных интеллектуальных сонарных системах, что позволяет оптимально согласовывать параметры сигналов и систем датчиков с заданными погрешностями измерения в реальном времени. Результаты моделирования представленных методов, экспериментальная проверка которых будет проведена в дальнейшем, иллюстрируют пригодность к использованию предлагаемых сигналов и алгоритмов приема. Ил. 9, библ. 7 (на английском языке; рефераты на английском, русском и литовском яз.).

J. Berdnikova, T. Ruuben, I. Müürsepp, E. Lossmann. Doplerinis priartėjimas ir rezoliucijos kognityvinėse sistemose // Elektronika ir elektrotechnika. – Kaunas: Technologija, 2010. – Nr. 7(103). – P. 101–104.

Aprašomos intelektualios kognityvinės sistemos, kurios leidžia suderinti jutiklių signalų parametrus ir užtikrina matavimo paklaidas realiu laiku. Pateikiami modeliavimo metodai ir jų eksperimentiniai rezultatai patvirtino, kad pasiūlyti algoritmai tinka intelektualioms sistemoms, kuriose leidžiama naudoti doplerinio priartėjimo teoriją. Il. 9, bibl. 7 (anglų kalba; santraukos anglų, rusų ir lietuvių k.).

PUBLICATION IV

T. Trump, I. Müürsepp. „Detection Speed of Responsive Communication Jamming Detectors.“ Presented at the 2nd International Conference on Circuits, Systems, Communications, Computers and Applications ,Dubrovnik, Croatia June 25-27, 2013

Detection Speed of Responsive Communication Jamming Detectors

TÕNU TRUMP
Tallinn University of Technology
Department of Radio
and Communication Engineering
Ehitajate tee 5, 19086 Tallinn
Estonia
tonu.trump@lr.ttu.ee

IVO MÜÜRSEPP
Tallinn University of Technology
Department of Radio
and Communication Engineering
Ehitajate tee 5, 19086 Tallinn
Estonia
ivom@lr.ttu.ee

Abstract: This paper studies the detectors that can be used in responsive communication jamming systems against radio–controlled improvised explosive devices. The roadside improvised explosive devices is a major treat, encountered in many war zones, in nowadays warfare. The device consists of an improvised bomb that can be detonated remotely via a wireless control device. In this paper we study detectors that can be potentially used to discover the radio signals that control the bombs. The most important requirement of the detector is that detection of the control signals needs to be faster than the reaction time of the bomb is, so that the control signal could effectively be disrupted by jamming. We examine four types of detectors in this paper with focus on their detection speed.

Key–Words: Detector, Responsive Communication Jamming

1 Introduction

Roadside improvised explosive devices have become one of the most important threats in today's asymmetric warfare. These devices are inexpensive, easy to build or acquire, and difficult to trace and can be triggered from long distances, keeping the operator safe from any detonation or exposure to targeted military forces. In many cases is the device simply explosive material that is integrated with a handheld wireless radio or device that will trigger upon receipt of a signal from a second wireless handheld device [1].

Thanks to the availability of cheap radio circuits many of the road side bombs are nowadays radio controlled meaning that they are detonated remotely via some radio communication links. Such bombs have become a real danger in several war zones e.g. Afganistan. In order to protect vehicles against such radio controlled bombs, vehicle mounted barrage jammers have been used for some time. These jamming systems jam continuously in all the relevant bands thus avoiding the control signals reach the bomb and explode it. Using such barrage jammers leads however in a rather high energy consumption as all potential frequency bands need to be jammed.

More recently the concept of responsive communication jamming [2] has been proposed to deal with the problem. The responsive communication jamming system regularly analyses the spectrum and only if a potential bomb controlling signal is discovered in some of the bands, the jamming of this band is performed. This strategy has clear benefits in the amount of consumed energy. On the other hand the responsive system becomes more complex.

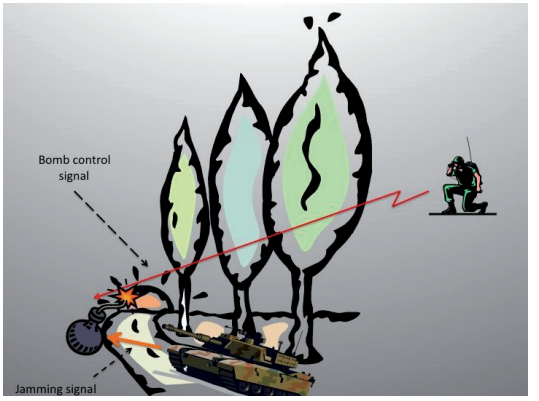

Figure 1: Road side explosive device jamming.

The road side explosive device jamming situation is depicted in Figure 1.

As discussed in [3], there are several jamming strategies which can be used against the improvized explosive devices. However, if responsive communication jamming is used the detector has to find the bomb triggering signal faster than the triggering time of the bomb is. In addition, the detection has to occur

in multiple potential frequency bands simultaneously.

Responsive jamming is closely related to the concept of cognitive radio [4] which has recently gained a lot of attention. In cognitive radio systems secondary users attempt to detect if the primary (or licensed) user is present and occupy the band of interest only if it is not, allowing thus opportunistic spectrum access. In responsive jamming system on the other hand the jammer attempts to sense the bomb control signals and reacts by jamming it if it finds one.

The key challenge of both cognitive radio and responsive communication jamming is fast and reliable spectrum sensing. In this paper we are going to examine several potential detection approaches. We will investigate the detection times that are necessary to reach a given probability of detection and probability of false alarm rate with the varying detection strategies. The detectors considered are energy detector, matched filter, cyclostationarity based feature detector and detector based on eigenvalue spread of the received signal covariance matrix.

We assume that the signal has been divided into frequency bands before executing the detector algorithms on the partial signals. The division can be accomplished using discrete Fourier transform or any other filter bank algorithm. The requirement being that the division algorithm should not introduce any considerable delay.

As the responsive communication jamming system is responsive for human lives we want the probability of missed detection to be as small as possible. This often implies a relatively large probability of false alarm. However, jamming a frequency band without a real threat in this band is a small price to pay for not jamming the actual bomb steering signal in most of the cases.

The problem we address is the typical detection problem

$$\begin{aligned} H_0: &\quad x(n) = v(n) \\ H_1: &\quad x(n) = s(n) + v(n), \end{aligned} \tag{1}$$

where $x(n)$ is the received waveform, $s(n)$ is the signal, presence of what we want to detect, and $v(n)$ is the noise. We thus wish to determine whether the received waveform consists of noise only or is there also a signal component present.

The italic, bold face lower case and bold face upper case letters will be used for scalars, column vectors and matrices respectively. The superscript $*$ denotes complex conjugate, the superscript H denotes Hermitian transposition of a matrix and the operator $E[\cdot]$ marks mathematical expectation.

2 Energy Detector

Energy detector or radiometer is the simplest possible detector as it does not need any information about the transmitted signal other than the band occupied by the signal. It compares the energy of the received signal to the energy of presumed white noise energy in the band of interest. If the energy of the incoming signal is significantly larger than the presumed energy of the thermal noise, the energy detector decides in favour of signal being present.

Energy detector, finds a sum of N samples of the incoming waveform and compares it with a threshold γ [5]

$$T(x) = \sum_{n=1}^{N} |x(n)|^2 > \gamma? \tag{2}$$

It can be shown [6] that the probability of false alarm P_f (there is no signal but the detector decides in favour of signal being present) of energy detector is

$$P_f = Q\left(\frac{\gamma - N\sigma_v^2}{\sigma_v^2\sqrt{2N}}\right). \tag{3}$$

The probability of detection P_d (there is signal and the detector detects it) is

$$P_d = Q\left(\frac{\gamma - N\sigma_v^2 - Np_s}{\sigma_v\sqrt{2N\sigma_v^2 + 4Np_s}}\right). \tag{4}$$

The probability of missed detection (there is signal but the detector does not find it) is given by

$$P_{md} = 1 - P_d. \tag{5}$$

Here

$$Q(z) = \frac{1}{2\pi}\int_z^\infty e^{-\frac{\lambda^2}{2}} d\lambda, \tag{6}$$

σ_v^2 is the noise power, p_s is signal power, γ is the threshold of the detector and N is the number of samples. We have assumed that the samples are statistically independent of each other.

The Receiver Operating Characteristic (ROC) for the case when both the signal and noise powers equal unity are shown in Figure 2. In the lower left corner the threshold equals $\gamma = \infty$, and in this case nothing will be detected but the probability of false alarm equals zero. In the upper right corner the threshold is $\gamma = 0$, then the detection always occurs and the probability of false alarm equals unity. In practice we of course want to be in some intermediate point on the ROC curve dependent on what false alarm and missed detection would cost us. In the responsive commnication jamming detection application we would like to make sure that the probability of missed detection is

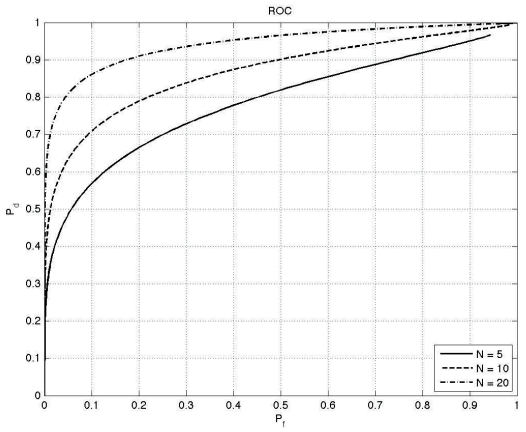

Figure 2: Receiver Operating Characteristic of energy detector.

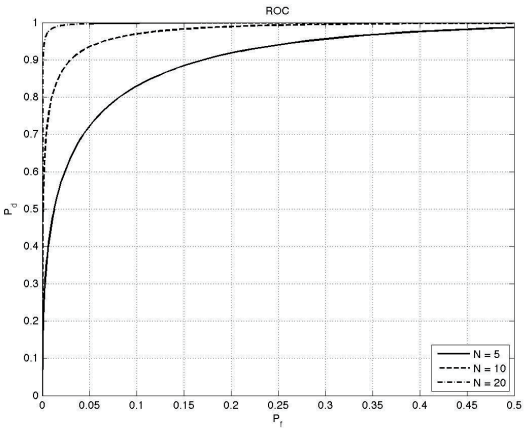

Figure 3: Receiver Operating Characteristic of matched filter.

small and do not care that much about the probability of false alarm. Therefore we select an operating point close to the upper right corner of ROC curve.

Solving the system of equations that consists of equations (3) ja (4) we get that the number of samples required for given probability of detection and probability of false alarm is

$$N = 2\frac{[Q^{-1}(P_f) - \sqrt{1+2SNR}Q^{-1}(P_d)]^2}{SNR^2} \quad (7)$$

samples, where $SNR = \frac{p_s}{\sigma_v^2}$ and that for achieving this we need to set the threshold at

$$\gamma = [N + \sqrt{2N}Q^{-1}(P_f)]\sigma_v^2 \quad (8)$$

To exemplify this we consider the requirement to reach the probability of missed detection and probability of false alarm levels $P_{md} = P_f = 10^{-6}$ for all the detectors. With energy detector it is required to process 338 samples to reach this operating point in the condition where both signal and noise have unity power.

As mentioned earlier, the samples should be statistically independent and for that the sampling frequency should be no faster than $f_D \leq 2B$, where B is the bandwith of the filter forming the channel.

3 Matched filter

The matched filter is optimal detector of signals in white Gaussian noise. The drawback being that the detector needs a large amount of information about the signal it attempts to detect. Most likely we do not have all this information about a hostile bomb control device, however, the performance of matched filter would serve the limit of possibility.

The matched filter correlates the image of the transmitted signal $s(n)$ with the received signal $x(n)$ and compares the result with a threshold.

$$T(x) = \sum_{n=1}^{N} x(n)s^*(n) > \gamma? \quad (9)$$

Under both hypothesis, the test statistic is normally distributed. The probability of false alarm is

$$P_f = Q\left(\frac{\gamma}{\sigma_v\sqrt{Np_s}}\right) \quad (10)$$

and the probability of detection is

$$P_d = Q\left(\frac{\gamma - Np_s}{\sigma_v\sqrt{Np_s}}\right). \quad (11)$$

The ROC for matched filter is shown in Figure 3. Comparing Figure 3 with Figure 2 one can see that the curves have been moved towards the upper left corner of the figure indicating the better (P_d, P_f) performance of the matched filter detector as compared to the energy detector. This is natural as the matched filter detector makes use of considerably more information about the detected signal then the energy detector.

The number of samples to reach operating point (P_d, P_f) is

$$N = \frac{\left[Q^{-1}(P_f) - Q^{-1}(P_d)\right]^2}{SNR}. \quad (12)$$

This will be achieved if the threshold is

$$\gamma = \frac{\sigma_v Q^{-1}(P_f)\left[Q^{-1}(P_f) - Q^{-1}(P_d)\right]}{\sqrt{SNR}}. \quad (13)$$

With matched filter one requires 91 samples to reach the $P_{md} = P_f = 10^{-6}$ with both signal and noise having unity power.

4 Feature detector

Feature detector can be viewed as compromise between energy detector and matched filter. In one hand it needs less information about signal under interest than matched filter. In other hand it has better sensitivity than energy detector. Feature detector uses information about periodicities in signal for detection. Those periodicities can be for example carrier- or pilot frequencies, data rates and so on.

The feature detector correlates received signal $x(n)$ with frequency shifted version of itself resulting in spectral correlation function (SCF)

$$\hat{S}_x^{\alpha}(f) = \frac{1}{NK}\sum_{n=1}^{N} X_K\left(n, f + \frac{\alpha}{2}\right) X_K^*\left(n, f - \frac{\alpha}{2}\right). \quad (14)$$

Here $X_K(n,f)$ is the K point FFT around sample n and α is amount of frequency shift. If signal has no periodical features, for example white noise, then correlation between its spectrum and frequency shifted spectrum is always zero. In other hand when signal has some periodical features then there is strong correlation for a fixed values of α. Those correlation peaks can be used to detect presence of signal of interest. Because function (13) is a complex function then decision statistic is module of this SCF and it is compared against given threshold

$$T(x) = |\hat{S}_x^{\alpha}(f)| > \gamma? \quad (15)$$

It can be shown that the probability of false alarm of feature detector is

$$P_f = e^{-\frac{N\gamma^2}{2\sigma_v^4}}. \quad (16)$$

Unlike for previous two detection methods there is no closed-form expression of correct detection P_d for cyclostationary detector [7], [8]. However there are some specific cases when it is possible to find analytical expression for probability of detection P_d. For example when pair (α, f) = ($2f_s$,0), where f_s is signal frequency, and if FFT is done coherently , then

$$P_d = Q_1\left(\frac{\psi}{\sigma_T}, \frac{\gamma}{\sigma_T}\right), \quad (17)$$

where values of scale- and placement parameters are

$$\sigma_T = \sqrt{\frac{p_s K \sigma_v^2}{N} + \frac{\sigma_v^4}{N}}, \quad (18)$$

$$\psi = \frac{K p_s}{2} \quad (19)$$

and $Q_1(\cdot)$ is the Marcum Q function

$$Q_1(a,b) = \int_b^{\infty} x \exp\left(-\frac{x^2 + a^2}{2}\right) I_0(ax) dx. \quad (20)$$

Here $I_0(\cdot)$ denotes the modified Bessel function of order 0.

Marcum Q function is not elementary function and its inverse can only be found trough some approximations or numerical calculations. So we cannot calculate the number of samples required for given probability of detection in case of feature detector. Numerical simulation methods must be used here instead.

The ROC curve for feature detector is shown in Figure 3. As it could be expected the performance of feature detector lies between those of energy detector and matched filter. Curves displayed in figure 3 are calculated numerically. Value of P_f is changed from 0 to 1 and corresponding values of P_d are calculated numerically with equation (18).

In order to find the number of samples N required for given probability of detection $P_d = 1 - 10^{-6}$ and probability of false alarm $P_f = 10^{-6}$ when both signal and noise have unity power we must use numerical simulation of (16). For given conditions equation (16) becomes

$$P_d = Q_1\left(\frac{K}{s\sqrt{K+1}}N, \sqrt{\frac{-2\ln P_f}{K+1}}\right). \quad (21)$$

Now we just have to calculate values of P_d numerically for each value of N until we found N that gives us desired value of $P_d = 1 - 10^{-6}$. As it can be seen our result here depends also on length of FFT. For example if we use K = 8 point FFT transform then to achieve desired value of detection P_d we need to average over N = 23 samples resulting that KN = 184 samples is required to process to reach given operating point at ROC curve. When we compare this result with energy detector and matched filter we see again that performance of feature detector lies between those two.

5 Eigenvalue detector

It was recently proposed to use the eigenvalues of the covariance matrix of the received signal for detection purposes [9]. It turns out that the ratio of maximum

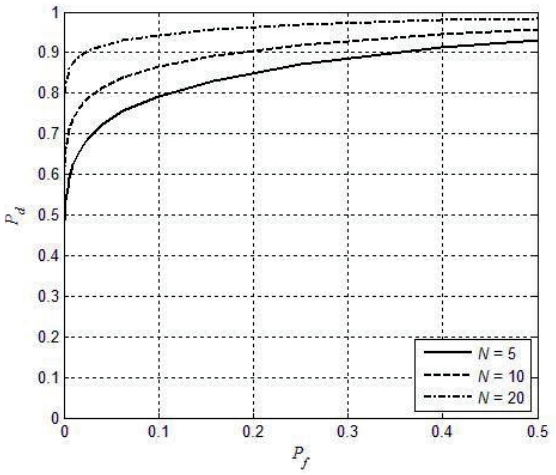

Figure 4: Receiver Operating Characteristic of feature detector.

and minimum eigenvalue can be used to detect the signal. This is based on the fact that the eigenvectors of the sample covariance matrix correspond to principal components of the data and the eigenvalues to the variance explained by the principal components. The eigenvectors of the covariance matrix provide thus an orthonormal eigen basis for the space of the observed data. In this basis, the largest eigenvalues correspond to the principal-components that are associated with most of the covariability among a number of observed data. The first principal component has the largest possible variance (that is, accounts for as much of the variability in the data as possible), and each succeeding component in turn has the highest variance possible under the constraint that it is orthogonal to the preceding components. In other words if there is no signal present the eigenvalues of the covariance matrix tend to be approximately equal to each other. On the other hand, if the signal is present, the energy of it is contained in the largest eigenvalue.

Let us assume that the M vector of the signal received is

$$\mathbf{x}(n) = \mathbf{s}(n) + \mathbf{v}(n) \tag{22}$$

The different entries in the vector can be signals at different antennas in an array or they can be obtained due to oversampling. The covariance matrix of the received signal is

$$\mathbf{R}_x = E\left[\mathbf{x}(n)\mathbf{x}^H(n)\right] \tag{23}$$

The method thus examines the eigenvalues of the received signal covariance matrix λ_i. The algorithm consists of the following steps:

1. Compute the sample covariance matrix of the received signal

$$\hat{\mathbf{R}}_x(N) = \frac{1}{N}\sum_{n=1}^{N-1}\mathbf{x}(n)\mathbf{x}^H(n), \tag{24}$$

   where N is the number of collected snapshots.

2. Compute the maximum and minimum eigenvalue λ_{max} and λ_{min} of the matrix $\hat{\mathbf{R}}_x(N)$.

3. Decide that the signal exists if

$$T(x) = \lambda_{max}/\lambda_{min} > \gamma, \tag{25}$$

   where γ is the threshold of the test.

It is demonstrated in [9] that based on the theory of random matrices [10] one can obtain the following approximate expressions for the probability of false alarm and probability of detection

$$P_f \approx 1 - F_1\left(\frac{\gamma(\sqrt{N}-\sqrt{ML})^2 - \mu}{\nu}\right), \tag{26}$$

$$P_d \approx 1 - F_1\left(\frac{\gamma N + N(\gamma\rho_{min} - \rho_{max})/\sigma_v^2 - \mu}{\nu}\right), \tag{27}$$

where γ is the detection threshold, $\mu = (\sqrt{N-1}+\sqrt{ML})^2$, $\nu = (\sqrt{N-1}+\sqrt{ML})(\frac{1}{\sqrt{N-1}}+\frac{1}{\sqrt{ML}})^{\frac{1}{3}}$, L is the smoothing factor, ρ is an eigenvalue of the signal covariance matrix $\mathbf{R}_s$ and $F_1(\cdot)$ is the cumulative Tracy–Widom distribution of the first order [10].

As the analysis of the detector provided in [9] is rather evolved and uses approximations that make it difficult to use the results for computing the ROC curves we provide herein simulation results instead of the theoretical curves. In addition, as the smallest eigenvalue of the received signal covariance matrix can be rather small and thereby cause problems in computing the ratio of maximum and minimum eigenvalue we have replaced the ratio with difference of the eigenvalues of normalised covariance matrix in our simulations as a practical approach.

The ROC curves of the detector for the case when both the signal and noise powers equal unity and one uses four element array to receive the signal are shown in Figure 5.

Our simulations show that in order to reach the operating point $P_{md} = P_f = 10^{-6}$ one needs 75 samples, which is less than the matched filter requires. One should note, however, that the eigenvalue based detector uses four antennas to achieve this result compared to the single antenna of matched filter.

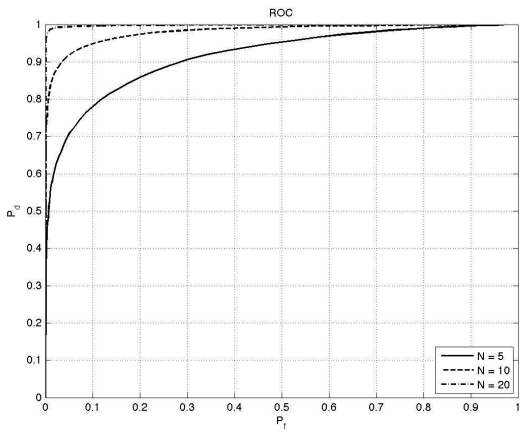

Figure 5: Receiver Operating Characteristic of the received signal covariance matrix eigenvalue based detector.

6 Conclusions

In this paper we have investigated four detectors in an attempt to ascertain their detection speed. The comparison is meant for clear what detector suits best for discovery of roadside explosive device control signals in war zones. We have compared the energy detector, the matched filter detector, the cyclostationarity based feature detector and eigenvalue based detector. The detectors require different amount of information about the signals they attempt to detect.

Energy detector is simplest but it is also the slowest detecor among the studied ones and we cannot recommend it by that reason. The matched filter detector requires information about the waveform of the bomb control signal. Vehicles on the road usually do not have this information and we cannot recommend the matched filter by that reason. It turns out that the eigenvalue based detector can provide fastest detection time but it needs several antennas or oversampling. The cyclostationarity based feature detector comes next in our comparison and it can do with single antenna. Our recommendation is therefore to use one of the two detectors in the responsive communication jamming systems.

References:

[1] M. C. Pesci, "Systems Engineering in Counter Radio- Controlled Improvised Explosive Device Electronic Warfare," *Johns Hopkins APL Technical Digest,* Vol. 31, No. 1, 2012

[2] J. Mietzner, A. Meusling, P. Loos and G. Bauch "Responsive Communications Jamming Against Radio Controlled Improvised Explosive Devices" *IEEE Communications Magazine*. October 2012, pp. 38–46.

[3] K. Wilgucki, R. Urban, G. Baranowski, P. Grdzki, and P. Skarzynski "Selected aspects of effective RCIED jamming," In Proc. *Communications and Information Systems Conference (MCC),* Gdansk, October 2012.

[4] S. Haykin, D.J. Thomson, and J.H. Reed, "Spectrum sensing for cognitive radio," *P*roc. IEEE, vol. 97, pp. 849–877, May 2009.

[5] Z. Quan, H.V. Poor, and A.H. Sayed, "Collaborative wideband sensing for cognitive radios," *I*EEE Signal Processing Magazine, vol. 25, pp. 60–73, November 2008.

[6] S. M. Kay, *Fundamentals of Statistical Signal Processing, Detection Theory,* Prenctice Hall, 1998.

[7] R.Ware and F. Lad, "Approximating the Distribution for Sums of Products of Normal Variables." Internet: http://www.math.canterbury.ac.nz/research/ucdms2003n15.pdf, [Dec. 6, 2012].

[8] S. Enserink and D. Cochrun, "On Detection of Cyclostationary Signals," in Proc. ICASSP-95, 1995, pp. 2004-2007.

[9] Y. Zeng, Y-C Liang, "Eigenvalue-based spectrum sensing algorithms for cognitive radio," *IEEE Transactions on Communications,* vol. 57, no. 6, June 2009, pp 1784–1793.

[10] C. A. Tracy, H. Widom, "The distribution of the largest eigenvalue in the Gaussian ensembles," in *Calogero–Moser–Sutherland Models,*, J. van Diejen and L. Vinet ed., Springler, 2000, pp. 461–472.

APPENDIX 2

ELULOOKIRJELDUS

1. Isikuandmed

Ees- ja perekonnanimi	Ivo Müürsepp
Sünniaeg ja -koht	06.09.1980, Keila
Kodakondsus	Eesti

2. Kontaktandmed

Aadress	TTÜ Raadio- ja sidetehnika instituut, Ehitajate tee 5, 19086 Tallinn
Telefon	(+372) 6202355
E-posti aadress	ivom@lr.ttu.ee

3. Hariduskäik

Õppeasutus (nimetus lõpetamise ajal)	Lõpetamise aeg	Haridus (eriala/kraad)
Tallinna Tehnikaülikool		doktorant
Tallinna Tehnikaülikool	2004	MSc
Tallinna Tehnikaülikool	2002	BSc (Cum Laude)
Keila Gümnaasium	1998	Keskharidus

4. Keelteoskus

Keel	Tase
Eesti	Kõrgtase
Inglise	Kõrgtase
Soome	Kesktase

5. Täiendusõpe

Õppimise aeg	Täiendusõppe läbiviija nimetus
2010	Kaitseliidu kool

6. Teenistuskäik

Töötamise aeg	Tööandja nimetus	Ametikoht
2012-2015	Tallinna Tehnikaülikool, Raadio- ja sidetehnika instituut, Raadiotehnika õppetool	Telekommunikatsiooniteenuste assistent

2007-2012	Tallinna Tehnikaülikool, Raadio- ja sidetehnika instituut, Raadiotehnika õppetool	Assistent
2002-2007	Tallinna Tehnikaülikool, Infotehnoloogia teaduskond, Raadio- ja sidetehnika instituut	Assistent
2002	Tallinna Tehnikaülikool, Raadio- ja sidetehnika instituut, Signaalitöötluse õppetool	Insener
2001	Tallinna Tehnikaülikool, Raadio- ja sidetehnika instituut, MAI keskus	GPRS koolituskursuse koostaja
1998	AL Electronic AS	abitööline

7. Teadustegevus

Osalemine projektides:

Teema: Telekommunikatsioonitehnika alased uuringud
Organisatsioon: TTÜ Infotehnoloogia teaduskond, RSTI
Osalus: Täitja
Ajavahemik: 01.01.2003- 31.12.2007
Annotatsioon:

Keerulistesignaalide kasutamine objektide kauguse, asukoha ja kiiruse hindamiseks radar- ja sonarseadmete abil; ökoloogiliselt ohutute sonarite ja radarite väljatöötlus.

Teema: Raadiojuhtimisega seadmete häirimine
Organisatsioon: TTÜ Infotehnoloogia teaduskond, RSTI
Osalus: Põhitäitja
Ajavahemik: 14.11.2007 – 30.11.2010

Annotatsioon:

Projekti eesmärgiks oli monitooringu ja häireseadmete väljatöötamine Eesti kaitseministeeriumile.

Teema: Inim-masin liidese kasutusvõimaluste uurimine eesmärgiga suurendada otsustusprotsesside kiirust tänapäevases linnalahingu keskkonnas.
Organisatsioon: TTÜ Infotehnoloogia teaduskond, RSTI
Osalus: Põhitäitja
Ajavahemik: 01.04.2010- 30.09.2012

Annotatsioon:

Euroopa kaitseagentuuri tellimusel teostatud uurimustöö infohankesüsteemide ja automaatsete otsustusalgoritmide kasutamiseks tänapäevase linnalahingu keskkonnas.

Juhendatud lõputööd

Allan Gern, SAR radar. K2007, BSc, hindele „3“ – hea.

Toomas Vahter, ESTCube-1 pikosatelliidi saatja võimsusvõimendi ja vastuvõtja madala-müralise eelvõimendi prototüüpide disainimine. K 2011, MSc, hindele „5“ – suurepärane.

Endrik Kriisa, FM ringhäälingu sagedushaldus. K2012, MSc, hindele „4“ – väga hea.

Konstantin Aleksejev, Radar Power Amplifier With Short Switch Off Time. S2012, MSc, hindele „5“ – suurepärane.

Konverentsi- ja seminariettekanded

Ivo Müürsepp. Complex amplitude-phase manipulated probe signals. Üheksas Balti elektroonikakonverents. Tallinna Tehnikaülikool, Tallinn, Eesti, 3.-6. oktoober 2004.

Ivo Müürsepp. Software Defined Radar. Info -ja kommunikatsioonitehnoloogia doktorikooli IKTDK teine aastakonverents. Viinistu, Eesti, 11.-12. mai 2007.

Ivo Müürsepp. Software Radar. 12. rahvusvaheline teaduskonverents ELECTRONICS’ 2008. Kaunas, Leedu 20.-22. mai 2008.

Andres Taklaja, Urve Madar, Ivo Müürsepp, Toomas Ruuben and Julia Berednikova. Software Defined Short-Range Naval Surveillance Radar. NATO RTO sümpoosium „NATO RTO SET-136 Software Defined Radar“. Lissabon, Portugal, 22.-26. juuni 2009.

Ivo Müürsepp. Robust Energy Detector for Cognitive Radio. Info- ja kommunikatsioonitehnoloogia doktorikooli IKTDK neljas aastakonverents. Essu, Eesti, 27. november 2010.

Ivo Müürsepp. Cognitive radio. IEEE augustiseminar. Pedase, Eesti, 20. august 2011.

Tõnu Trump and Ivo Müürsepp. Robust spectrum sensing for Cognitive Radio. 19th European Signal Processing Conference EUSIPCO2011, Barcelona, Hispaania, 29. August – 2. september 2011 [73].

Tõnu Trump and Ivo Müürsepp. An Energy Detector for Spectrum Sensing in Impulsive Noise Environment. 22nd Annual IEEE International Symposium on Personal, Indoor and Mobile Radio Communications. Toronto, Kanada, September 11-14, 2011[72].

8. Artiklid

Artiklite nimekiri on ära toodud ingliskeelse CV juures.

9. Autasud

2003, TTÜ arengufond, AS Elion Ettevõtted stipendium.

2010, Jaan Poska nimeline stipendium silmapaistva ühiskondliku tegevuse eest Eesti ja Tallinna arengu heaks.

10. Kaitstud lõputööd

2004, Amplituud-faasmoduleeritud sondeerivad signaalid ja nende optimaalne töötlemine,MSc, Tallinna Tehnikaülikool, Infotehnoloogia teaduskond, juhendaja professor Ilmar Arro.

2002, Lähiseireradar, BSc, Tallinna Tehnikaülikool, Infotehnoloogia teaduskond, juhendaja professor Ilmar Arro.

11. Teadustöö põhisuunad

1. Infohankesüsteemid, radarid ja sonarid.
2. digitaalne signaalitöötlus.
3. Kognitiivne raadio.

APPENDIX 3

CURRICULUM VITAE

1. Personal data

Name	Ivo Müürsepp
Date and place of birth	06.09.1980, Keila

2. Contact information

Address	Department of Radio and Communication Engineering, Ehitajate Street 5, 19086 Tallinn
Phone	(+372) 6202355
E-mail	ivom@lr.ttu.ee

3. Education

Educational institution	Graduation year	Education (field of study/degree)
Tallinn University of Technology		PhD student
Tallinn University of Technology	2004	MSc
Tallinn University of Technology	2002	BSc (Cum Laude)
Keila Gymnasium	1998	Subprofessional

4. Language skills

Language	Level
Estonian	Fluent
English	Fluent
Finnish	Average

5. Special Courses

Period	Educational or other organisation
2010	Estonian Defense League School

6. Professional Employment

Period	Organisation	Position
2012-2015	Tallinn University of Technology, Department of Radio and Communication Engineering, Chair of Radio Engineering.	Teaching assistant
2007-2012	Tallinn University of Technology, Department of Radio and Communication Engineering, Chair of Radio Engineering.	Teaching assistant
2002-2007	Tallinn University of Technology, Department of Radio and Communication Engineering, Chair of Radio Engineering.	Teaching assistant
2002	Tallinn University of Technology, Department of Radio and Communication Engineering, Chair of Signal Processing.	Engineer
2001	Tallinn University of Technology, Department of Radio and Communication Engineering, MAI center.	Contractual employee
1998	AL Electronic AS	Assistant worker

7. Scientific work

Projects:

Project: Research in Telecommunications Technology
Oranization: Faculty of Information Technology, Department of Radio and Communication Engineering.
Participation: Researcher
Duration: 01.01.2003- 31.12.2007
Abstract:

Design of wideband equipment for telecommunication systems, applications of complex signalst to the estimation of distance, position and velocity of an object by means of radar and sonar equipment. Development of ecologically safe sonars.

Project: Monitoring, jamming and neutralizing of radio-controlled systems.
Oranization: Faculty of Information Technology, Department of Radio and Communication Engineering.
Participation: Researcher
Duration: 14.11.2007 – 30.11.2010
Abstract:

Objective of project was to develop monitoring and jamming devices for Estonian ministry of defence.

Project: Capability study to investigate the essential man-machine relationship for improved decision making in urban military environment
Oranization: Faculty of Information Technology, Department of Radio and Communication Engineering.
Participation: Researcher
Duration: 01.04.2010- 30.09.2012
Abstract:

Study for European Defence agency to investigate the essential man-machine relationship for improved decision making in urban military environment.

Supervised theses

Allan Gern, SAR radar. spring 2007, BSc, "C" – average.

Toomas Vahter, Design of Power Amplifier and Low Noise Amplifier prototypes for picosatellite ESTCube-1 spring 2011, MSc, "A" – excellent.

Endrik Kriisa, Spectrum management in FM broadcasting. spring 2012, MSc, "B" – good.

Konstantin Aleksejev, Radar Power Amplifier with Short Switch off Time. autumn 2012, MSc, "A" – excellent.

Conference and Seminar presentations

Ivo Müürsepp. Complex amplitude-phase manipulated probe signals. 9th Biennial Baltic Electronics Conference BEC2004. Tallinn University of Technology, Tallinn, Estonia, October 3-6, 2004.

Ivo Müürsepp, Software Defined Radar." Second Annual Conference of the Doctoral School in ICT. Viinistu, Estonia, May 11-12, 2007.

Ivo Müürsepp. Software Radar. 12th international conference ELECTRONICS' 2008. Kaunas, Lithuania, May 20-22, 2008.

Andres Taklaja, Urve Madar, Ivo Müürsepp, Toomas Ruuben and Julia Berednikova. Software Defined Short-Range Naval Surveillance Radar. NATO

RTO symposium „NATO RTO SET-136 Software Defined Radar“. Lisbon, Portugal, June 22-26, 2009.

Ivo Müürsepp. Robust Energy Detector for Cognitive Radio. 4th annual Conference of the Doctoral School in ICT. Essu, Estonia, November 27, 2010.

Ivo Müürsepp. Cognitive radio. Annual IEEE Estonia Section seminar. Pedase, Estonia, August 20, 2011.

Tõnu Trump and Ivo Müürsepp. Robust spectrum sensing for Cognitive Radio. 19th European Signal Processing Conference EUSIPCO2011, Barcelona, Spain, August 29-September 2, 2011 [73].

Tõnu Trump and Ivo Müürsepp. An Energy Detector for Spectrum Sensing in Impulsive Noise Environment. 22nd Annual IEEE International Symposium on Personal, Indoor and Mobile Radio Communications. Toronto, Canada, September 11-14, 2011[72].

8. Publications

[1] Müürsepp, I. (2011). Usaldusväärsus ja veakindlus infohankesüsteemides. A & A: Arvutid ja Andmetöötlus, 2, 28 - 46.

[2]Trump, T; Müürsepp, I (2011). An Energy Detector for Spectrum Sensing in Impulsive Noise Environment. *In: IEEE 22nd International Symposium on Personal, Indoor and Mobile Radio Communications (PIMRC 2011): Toronto, Canada, 11-14 september 2011.* IEEE, 2011, 467 - 471.

[3] Trump, T.; Müürsepp, I. (2011). Robust Spectrum Sensing for Cognitive Radio. *In: Proceedings of the 19th European Signal Processing Conference (EUSIPCO 2011): European Signal Processing Conference (EUSIPCO2011), Barcelona, 29.08-02.09.2011.* EURASIP, 2011, 1224 - 1228.

[4] Müürsepp, I. (2011). Intelligentne raadio toob kiire võrguühenduse kaugeimassegi metsatallu.

[5] Müürsepp, I. (2010). Robust Energy Detector for Cognitive Radio. Info- ja kommunikatsioonitehnoloogia doktorikooli IKTDK neljanda aastakonverentsi artiklite kogumik (113 - 116).Infotrükk OÜ

[6] Müürsepp, I.; Berdnikova, J.; Ruuben, T.; Madar, U. (2010). Probe Signals with Nonrectangular Envelope. Electronics and Electrical Engineering, 101(5), 99 - 102.

[7] Berdnikova, J.; Ruuben, T.; Müürsepp, I.; Lossmann, E. (2010). Resolution and Doppler Tolerance of Cognitive System Waveforms. Electronics and Electrical Engineering, 103(7), 101 - 104.

[8] Ruuben, T.; Berdnikova, J.; Müürsepp, I.; Madar, U. (2010). Optimal Waveform Selection for Software Defined Data Acquisition System. *In: EuCap2010 conference proceedings: EuCap2010 : The 4th European Conference on Antennas and Propagation - Barcelona, Spain 12-16 April 2010* . Barcelona: IEEE, 2010, 1 - 5.

[9] Taklaja, A.; Madar, U.; Müürsepp, I.; Ruuben, T.; Berdnikova, J. (2009). Software Defined Short-Range Naval Surveillance Radar. *In: Software Defined Radar : Proceeding of the NATO Research & Technology Organisation (RTO): SET-136 Specialists Meeting on "Software Defined Radar", Lissabon (Portugal), June 23-25, 2009.* North Atlantic Treaty Organization, 2009, (SET-136).

[10] Müürsepp, I. (2008). Keskkonnasäästlik radar. Keskkonnatehnika, 7, 37 - 39.

[11] Müürsepp, I. (2008). Software Radar. Elektronika ir elektrotechnika = Electronics and electrical engineering, 4 (84), 59 - 62.

[12] Müürsepp, I. (2007). Software Defined Radar. Info- ja kommunikatsioonitehnoloogia doktorikooli IKTDK teise aastakonverentsi artiklite kogumik : 11.-12. mai 2007, Viinistu Kunstimuuseum (101 - 103). Tallinn: Tallinna Tehnikaülikooli Kirjastus

[13] Müürsepp, I. (2005). Sharc-arhitektuuriga signaaliprotsessorite rakendamine infohankesüsteemides. A & A: Arvutid ja Andmetöötlus, 4, 38 - 45.

[14] Müürsepp, Ivo (2005). Faasmanipuleeritud sondeerivate signaalide vastuvõtja optimeerimine. XII rahvusvahelise telekommunikatsioonipäeva materjalid (48 - 58).Tallinna Tehnikaülikooli Kirjastus

[15] Müürsepp, I. (2004). Complex amplitude-phase manipulated probe signals. *In: BEC2004 : proceedings of the 9th biennial Baltic Electronics Conference : 9th Bal biennial Baltic Electronics Conference BEC 2004, October 3-6, 2004, Tallinn, Estonia.* Tallinn: Tallinna Tehnikaülikooli Kirjastus, 2004, 287 - 290.

[16] Arro, I.; Müürsepp, I. (2003). Invariant detection of a signal with a random phase. Elektronika ir elektrotechnika = Electronics and electrical engineering, 3, 23 - 26.

[17] Müürsepp, I. (2003). Juhusliku algfaasiga impulss-signaali optimaalne vastuvõtt ja häirekindlus. X rahvusvahelise telekommunikatsioonipäeva materjalid (90 - 97).Tallinna Tehnikaülikooli Kirjastus

[18] Müürsepp, I (2013). Sensitivity of Robust Energy Detector to the Errors in Parameter Estimates. Presented at the the Second IEEE International Workshop on Emerging COgnitive Radio Applications and aLgorithms (IEEE CORAL 2013), Madrid, Spain.

9. Honours and Awards

2003, TUT Development Fund, AS Elion Enterprices Scholarship.

2010, Jaan Poska Scholarship for spectacular public activity for development of Estonia and Tallinn.

10. Defended theses

2004, Amplitude-Phase Manipulated Probe Signals and Optimal Processing of Them, MSc, Tallinn University of Technology, Faculty of Information Technology, supervisor professor Ilmar Arro.

2002, Short Range Surveillance Radar, BSc, Tallinn University of Technology, Faculty of Information Technology, supervisor professor Ilmar Arro.

10. Main areas of scientific work/Current research topics

1. Information gathering systems, radars, sonars
2. Digital signal processing
3. Cognitive radio

DISSERTATIONS DEFENDED AT TALLINN UNIVERSITY OF TECHNOLOGY ON *INFORMATICS AND SYSTEM ENGINEERING*

1. **Lea Elmik**. Informational Modelling of a Communication Office. 1992.

2. **Kalle Tammemäe**. Control Intensive Digital System Synthesis. 1997.

3. **Eerik Lossmann**. Complex Signal Classification Algorithms, Based on the Third-Order Statistical Models. 1999.

4. **Kaido Kikkas**. Using the Internet in Rehabilitation of People with Mobility Impairments – Case Studies and Views from Estonia. 1999.

5. **Nazmun Nahar**. Global Electronic Commerce Process: Business-to-Business. 1999.

6. **Jevgeni Riipulk**. Microwave Radiometry for Medical Applications. 2000.

7. **Alar Kuusik**. Compact Smart Home Systems: Design and Verification of Cost Effective Hardware Solutions. 2001.

8. **Jaan Raik**. Hierarchical Test Generation for Digital Circuits Represented by Decision Diagrams. 2001.

9. **Andri Riid**. Transparent Fuzzy Systems: Model and Control. 2002.

10. **Marina Brik**. Investigation and Development of Test Generation Methods for Control Part of Digital Systems. 2002.

11. **Raul Land**. Synchronous Approximation and Processing of Sampled Data Signals. 2002.

12. **Ants Ronk**. An Extended Block-Adaptive Fourier Analyser for Analysis and Reproduction of Periodic Components of Band-Limited Discrete-Time Signals. 2002.

13. **Toivo Paavle**. System Level Modeling of the Phase Locked Loops: Behavioral Analysis and Parameterization. 2003.

14. **Irina Astrova**. On Integration of Object-Oriented Applications with Relational Databases. 2003.

15. **Kuldar Taveter**. A Multi-Perspective Methodology for Agent-Oriented Business Modelling and Simulation. 2004.

16. **Taivo Kangilaski**. Eesti Energia käiduhaldussüsteem. 2004.

17. **Artur Jutman**. Selected Issues of Modeling, Verification and Testing of Digital Systems. 2004.

18. **Ander Tenno**. Simulation and Estimation of Electro-Chemical Processes in Maintenance-Free Batteries with Fixed Electrolyte. 2004.

19. **Oleg Korolkov**. Formation of Diffusion Welded Al Contacts to Semiconductor Silicon. 2004.

20. **Risto Vaarandi**. Tools and Techniques for Event Log Analysis. 2005.

21. **Marko Koort**. Transmitter Power Control in Wireless Communication Systems. 2005.

22. **Raul Savimaa**. Modelling Emergent Behaviour of Organizations. Time-Aware, UML and Agent Based Approach. 2005.

23. **Raido Kurel**. Investigation of Electrical Characteristics of SiC Based Complementary JBS Structures. 2005.

24. **Rainer Taniloo**. Ökonoomsete negatiivse diferentsiaaltakistusega astmete ja elementide disainimine ja optimeerimine. 2005.

25. **Pauli Lallo.** Adaptive Secure Data Transmission Method for OSI Level I. 2005.

26. **Deniss Kumlander**. Some Practical Algorithms to Solve the Maximum Clique Problem. 2005.

27. **Tarmo Veskioja**. Stable Marriage Problem and College Admission. 2005.

28. **Elena Fomina**. Low Power Finite State Machine Synthesis. 2005.

29. **Eero Ivask**. Digital Test in WEB-Based Environment 2006.

30. **Виктор Войтович**. Разработка технологий выращивания из жидкой фазы эпитаксиальных структур арсенида галлия с высоковольтным p-n переходом и изготовления диодов на их основе. 2006.

31. **Tanel Alumäe**. Methods for Estonian Large Vocabulary Speech Recognition. 2006.

32. **Erki Eessaar**. Relational and Object-Relational Database Management Systems as Platforms for Managing Softwareengineering Artefacts. 2006.

33. **Rauno Gordon**. Modelling of Cardiac Dynamics and Intracardiac Bio-impedance. 2007.

34. **Madis Listak**. A Task-Oriented Design of a Biologically Inspired Underwater Robot. 2007.

35. **Elmet Orasson**. Hybrid Built-in Self-Test. Methods and Tools for Analysis and Optimization of BIST. 2007.

36. **Eduard Petlenkov**. Neural Networks Based Identification and Control of Nonlinear Systems: ANARX Model Based Approach. 2007.

37. **Toomas Kirt**. Concept Formation in Exploratory Data Analysis: Case Studies of Linguistic and Banking Data. 2007.

38. **Juhan-Peep Ernits**. Two State Space Reduction Techniques for Explicit State Model Checking. 2007.

39. **Innar Liiv**. Pattern Discovery Using Seriation and Matrix Reordering: A Unified View, Extensions and an Application to Inventory Management. 2008.

40. **Andrei Pokatilov**. Development of National Standard for Voltage Unit Based on Solid-State References. 2008.

41. **Karin Lindroos**. Mapping Social Structures by Formal Non-Linear Information Processing Methods: Case Studies of Estonian Islands Environments. 2008.

42. **Maksim Jenihhin**. Simulation-Based Hardware Verification with High-Level Decision Diagrams. 2008.

43. **Ando Saabas**. Logics for Low-Level Code and Proof-Preserving Program Transformations. 2008.

44. **Ilja Tšahhirov**. Security Protocols Analysis in the Computational Model – Dependency Flow Graphs-Based Approach. 2008.

45. **Toomas Ruuben**. Wideband Digital Beamforming in Sonar Systems. 2009.

46. **Sergei Devadze**. Fault Simulation of Digital Systems. 2009.

47. **Andrei Krivošei**. Model Based Method for Adaptive Decomposition of the Thoracic Bio-Impedance Variations into Cardiac and Respiratory Components. 2009.

48. **Vineeth Govind**. DfT-Based External Test and Diagnosis of Mesh-like Networks on Chips. 2009.

49. **Andres Kull**. Model-Based Testing of Reactive Systems. 2009.

50. **Ants Torim**. Formal Concepts in the Theory of Monotone Systems. 2009.

51. **Erika Matsak**. Discovering Logical Constructs from Estonian Children Language. 2009.

52. **Paul Annus**. Multichannel Bioimpedance Spectroscopy: Instrumentation Methods and Design Principles. 2009.

53. **Maris Tõnso**. Computer Algebra Tools for Modelling, Analysis and Synthesis for Nonlinear Control Systems. 2010.

54. **Aivo Jürgenson**. Efficient Semantics of Parallel and Serial Models of Attack Trees. 2010.

55. **Erkki Joasoon**. The Tactile Feedback Device for Multi-Touch User Interfaces. 2010.

56. **Jürgo-Sören Preden**. Enhancing Situation – Awareness Cognition and Reasoning of Ad-Hoc Network Agents. 2010.

57. **Pavel Grigorenko**. Higher-Order Attribute Semantics of Flat Languages. 2010.

58. **Anna Rannaste**. Hierarcical Test Pattern Generation and Untestability Identification Techniques for Synchronous Sequential Circuits. 2010.

59. **Sergei Strik**. Battery Charging and Full-Featured Battery Charger Integrated Circuit for Portable Applications. 2011.

60. **Rain Ottis**. A Systematic Approach to Offensive Volunteer Cyber Militia. 2011.

61. **Natalja Sleptšuk**. Investigation of the Intermediate Layer in the Metal-Silicon Carbide Contact Obtained by Diffusion Welding. 2011.

62. **Martin Jaanus**. The Interactive Learning Environment for Mobile Laboratories. 2011.

63. **Argo Kasemaa**. Analog Front End Components for Bio-Impedance Measurement: Current Source Design and Implementation. 2011.

64. **Kenneth Geers**. Strategic Cyber Security: Evaluating Nation-State Cyber Attack Mitigation Strategies. 2011.

65. **Riina Maigre**. Composition of Web Services on Large Service Models. 2011.

66. **Helena Kruus**. Optimization of Built-in Self-Test in Digital Systems. 2011.

67. **Gunnar Piho**. Archetypes Based Techniques for Development of Domains, Requirements and Sofware. 2011.

68. **Juri Gavšin**. Intrinsic Robot Safety Through Reversibility of Actions. 2011.

69. **Dmitri Mihhailov**. Hardware Implementation of Recursive Sorting Algorithms Using Tree-like Structures and HFSM Models. 2012.

70. **Anton Tšertov**. System Modeling for Processor-Centric Test Automation. 2012.

71. **Sergei Kostin**. Self-Diagnosis in Digital Systems. 2012.

72. **Mihkel Tagel**. System-Level Design of Timing-Sensitive Network-on-Chip Based Dependable Systems. 2012.

73. **Juri Belikov**. Polynomial Methods for Nonlinear Control Systems. 2012.

74. **Kristina Vassiljeva**. Restricted Connectivity Neural Networks based Identification for Control. 2012.

75. **Tarmo Robal**. Towards Adaptive Web – Analysing and Recommending Web Users` Behaviour. 2012.

76. **Anton Karputkin**. Formal Verification and Error Correction on High-Level Decision Diagrams. 2012.

77. **Vadim Kimlaychuk**. Simulations in Multi-Agent Communication System. 2012.

78. **Taavi Viilukas**. Constraints Solving Based Hierarchical Test Generation for Synchronous Sequential Circuits. 2012.

79. **Marko Kääramees**. A Symbolic Approach to Model-based Online Testing. 2012.

80. **Enar Reilent**. Whiteboard Architecture for the Multi-agent Sensor Systems. 2012.

81. **Jaan Ojarand**. Wideband Excitation Signals for Fast Impedance Spectroscopy of Biological Objects. 2012.

82. **Igor Aleksejev**. FPGA-based Embedded Virtual Instrumentation. 2013.

83. **Juri Mihhailov**. Accurate Flexible Current Measurement Method and its Realization in Power and Battery Management Integrated Circuits for Portable Applications. 2013.

84. **Tõnis Saar**. The Piezo-Electric Impedance Spectroscopy: Solutions and Applications. 2013.

85. **Ermo Täks**. An Automated Legal Content Capture and Visualisation Method. 2013.

86. **Uljana Reinsalu**. Fault Simulation and Code Coverage Analysis of RTL Designs Using High-Level Decision Diagrams. 2013.

87. **Anton Tšepurov**. Hardware Modeling for Design Verification and Debug. 2013.